SUBPHTHALOCYANINES, PHTHALOCYANINES AND AZULENOCYANINES: YELLOW, RED- AND NEAR-IR-ABSORBING DYES FOR MOLECULAR PHOTOVOLTAICS

TESIS DOCTORAL

MİNE İNCE

Madrid, 2012

UNIVERSIDAD AUTONOMA
DE MADRID

FACULTAD DE CIENCIAS

DEPARTAMENTO DE QUÍMICA ORGÁNICA

SUBPHTHALOCYANINES, PHTHALOCYANINES AND AZULENOCYANINES: RED- AND NIR-ABSORBING DYES FOR MOLECULAR PHOTOVOLTAICS

MEMORIA

presentada por

MİNE İNCE

Para optar al grado de

DOCTOR EN CIENCIAS QUÍMICAS

Madrid, 20 de Julio de 2012

I dedicate this work to my family and

Kasım

El presente trabajo ha sido realizado en el Departamento de Química Orgánica de la Universidad Autónoma de Madrid bajo la dirección de los Profesores Tomás Torres Cebada y Mª Victoria Martínez-Díaz, a quienes deseo expresar mi más sincero agradecimiento.

Durante el desarrollo de este trabajo se han realizado estancias predoctorales en los seguientes centros de investigacion:

- Institute for Molecules and Materials, Radboud University Nijmegen, Nijmegen, The Netherlands, bajo la direccion del Prof. Alan Rowan y el Dr. Paul H.J. Kouwer.
- Department of Organic Chemistry, University of Zaragoza, Zaragoza, Spain, bajo la direccion del Prof. Joaquin Barbera.
- Laboratory of Photonics and Interfaces (LPI) Institute of Chemical Science and Engineering, Faculty of Basic Science Ecole Polytechnique Federale de Lausanne, Switzerland, bajo la direccion del Prof. Michael Grätzel y el Dr. Md. K. Nazeeruddin.
- Molecular Materials and Nanosystems Departments of Applied Physics and Chemical Engineering & Chemistry Eindhoven University of Technology, Eindhoven, The Netherlands, bajo la direccion del Prof. René Janssen y el Dr. Martijn Wienk.
- Department of Chemistry, Graduate School of Science, Kyoto University, Kyoto, Japan, bajo la direccion del Prof. Atsuhiro Osuka.

La obtención de dendrones de oligotiofeno ha sido llevada a cabo en colaboración con el Dr. Amaresh Mishra y el Prof. Peter Bäuerle en la Ulm Universität, Ulm, Germany.

Los estudios fotofísicos han llevado a cabo en colaboración con el grupo del Prof. Dirk M. Guldi en la Erlangen-Nürnberg Universität, Germany.

Un dendrimero mesogeno fue preparado en el grupo del Prof. Deshenaux en la Université de Neuchâtel, Institut de Chimie, Switzerland.

El Prof. Christian G. Claessens ha participado activamente en diferentes aspectos relacionados con la preparación y estudios en subftalocianinas.

A todos, mi más sincero agradecimiento.

Asi mismo, agradezco al Departamento de Química Orgánica el haberme permitido utilizar todos los medidos técnicos de que dispone para la realización de esta Tesis Doctoral.

A todos vosotros, ¡¡Gracias!!

Parte del trabajo descrito en esta memoria ha servido como contribución a los siguientes artículos.

- "Liquid crystalline phthalocyanine-fullerene dyads" M. Ince, M.V. Martínez-Díaz, J. Barbera , T. Torres, *J. Mater. Chem.* **2011**, *21*, 1531.
- "Phthalocyanines: colorful macroheterocyclic sensitizers for dye-sensitized solar cells" M. V. Martínez-Díaz, M. Ince, T. Torres, *Monatsh. Chem.* **2011**, *142*, 699.
- "Molecular Engineering of Zinc Phthalocyanines with Phosphinic Acid Anchoring Groups" I. López-Duarte, M. Wang, R. Humphry-Baker, M. Ince, M. V. Martínez-Díaz, M. K. Nazeeruddin, T. Torres, M. Grätzel, T. Torres, *Angew. Chem. Int. Ed.* **2012***, 51,* 1895*.*
- ''Immobilizing NIR Absorbing Azulenocyanines onto Single Wall Carbon Nanotubes – From Charge Transfer to Photovoltaics" M. Ince, J. Bartelmess, D. Kiessling, K. Dirian, M. V. Martínez-Díaz, T. Torres, D. M. Guldi, *Chem. Sci*. **2012**, *3*, 1472.
- ''Non-covalent versus covalent donor-acceptor systems based on near-infrared absorbing azulenocyanines and C_{60} fullerene derivatives'' M. Ince, A. Hausmann, M. V. Martínez-Díaz, D. M. Guldi, T. Torres, *Chem. Commun.* **2012***, 48,* 4058.
- "Convergent synthesis of novel Near-Infrared absorbing "push-pull" bisthiophene-substituted Zn(II)Phthalocyanines and their application in Dye Sensitized Solar Cells" M. Ince, F. Cardinali, J. H. Yum, M. V. Martínez-Díaz, M. K. Nazeeruddin, M. Grätzel, T. Torres, *Chem. Eur. J.* **2012**, *18*, 6343.
- "Towards artificial photosynthesis: Supramolecular, donor–acceptor, porphyrin and phthalocyanine/carbon nanostructure ensembles" G. Bottari, O. Trukhina, M. Ince, T. Torres, *Coord. Chem. Rev.* **2012.** DOI:10.1016/j.ccr.2012.03.011

Abreviations y Acronyms

A	Aceptor
AIBN	Azo-bis-isobutyronitrile
BHJ	Bulkheterojunction
CHENO	3α, 7α-dihydroxy-5β-cholic acid
CR	Charge Recombination
CS	Charge Separated
CT	Charge Transfer
CV	Cyclic Voltammetry
D	Donor
DBU	Diazabicyclo[5.4.0]undec-7-ene
o-DCB	o-Dichlorobenzene
DCC	*N,N'*-Dicyclohexylcarbodiimide
DIPEA	*N,N*-Diisopropylethylamine
DMAC	*N*,*N*-Dimethylacetamide
DMAE	*N*,*N*-Dimethylaminoethanol
DMAP	4-Dimethylaminopyridine
DMF	*N*,*N*-Dimethylformamide
DMSO	Dimethylsulfoxide
DPV	Differential Pulse Voltammetry
DSSC	Dye Sensitized Solar Cells
DSC	Differential Scanning Calorimetry
EBL	Exciton Blocking Layer
EQE	External Quantum Efficiency
ERD	Energy Relay Dyes

FF	Fill factor
FRET	Förster Resonance Energy Transfer
HOMO	Highest Occupaid Molecular Orbital
IBX	2-Iodoxybenzoic acid
IPCE	Incident photon to current conversion efficiency
IR	Infrarred spectroscopy
ITO	Indinium Tin Oxide
ISC	Intersystem Crossing
Isc	Short-circuit current
Ka	Association constant
LC	Liquid Crystal
LUMO	Lowest Unoccupied Molecular Orbital
MALDI	Matrix-Assisted Laser Desorption Ionization
NBS	N-Bromosuccinimide
NIR	Near Infrared
OFET	Organic Field Effect Transistor
OLED	Organic Light-Emitting Diode
PEDOT	Poly(3,4-ethylenedioxythiophene)
PDT	Photodynamic Therapy
PET	Photoinduced Electron Transfer
SDBS	Sodium dodecyl benzene sulphonate
SWNT	Single Wall Nanotube
TGA	Thermal gravimetric analysis
TLC	Thin Layer Chromatography
TOF	Time Of Flight
UV-Vis	Ultraviolet/Visible
Voc	Open-circuit voltage

Table of Contents

Chapter 1. Donor-Acceptor Sytems Based on Phthalocyanines and Azulenocyanines

1.1. Phthalocyanine-Oligothiophene Derivatives for Bulk Heterojunctions

1.2. Azulenocyanine-SWNTs and Azulenocyanine-C_{60} dyads

Chapter 2. Porphyrinoids for Dye Sensitized Solar Cells

Resumen

El principal objetivo de esta Tesis Doctoral es la síntesis de nuevas ftalocianinas y análogos con determinadas propiedades electrónicas para su utilización como componentes foto- y electroactivos en fotovoltaica molecular, más concretamente en dipositivos de heterounión masiva (BHJ) y para células solares sensibilizadas por colorante (DSSCs). Basados en la amplia experiencia de nuestro grupo, adquirida durante los diez últimos años, el diseño molecular de nuevas ftalocianinas se ha enfocado:

1) a la preparación de derivados con absorción en las regiones del rojo y del infrarrojo cercano (NIR) donde el flujo solar de fotones tiene máxima intensidad, y

2) al control de la organización de las moléculas en el estado sólido con objeto de mejorar la morfología de los sistemas.

En este sentido se han sintetizado ftalocianinas portadoras de sustituyentes periféricos con carácter dador o aceptor de tipo **a** y **b,** con absorción en el rojo, que han sido empleadas en la preparación de dipositivos de heterounión masiva

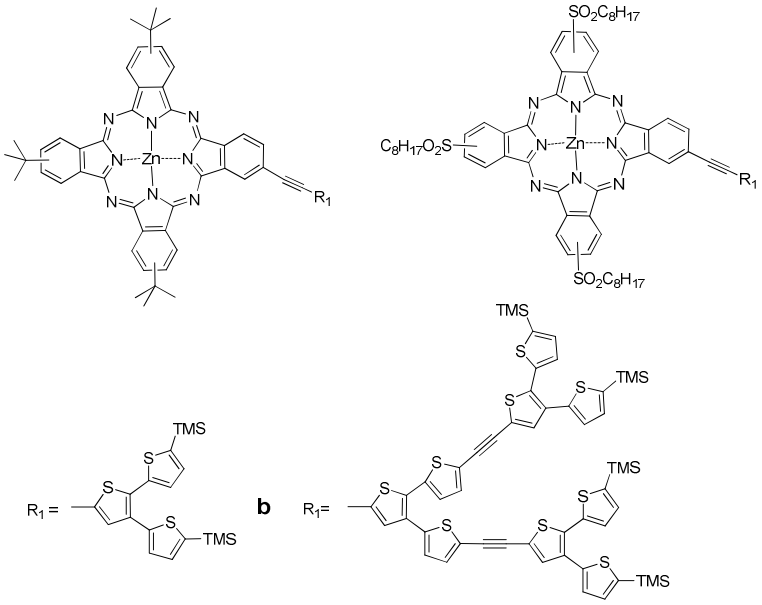

También se han preparado carboxiftalocianinas con sustituyentes fuertemente dadores de electrones y conjugación extendida de tipo **c** y **d** para células solares sensibilizadas por colorante.

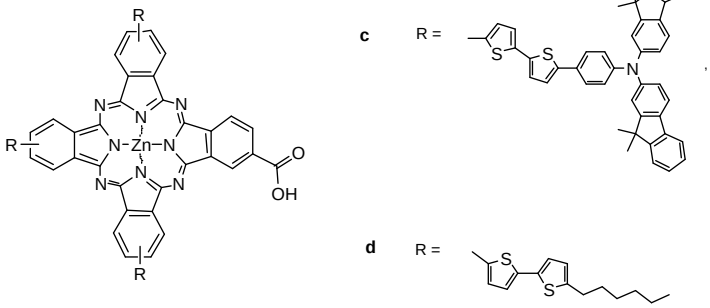

Por otra parte, y para el mismo propósito anterior, se han sintetizado análogos de ftalocianina, como las azulenocianinas (**e**), cuya absorción se extiende de 400 a 1000 nm, y subftalocianinas (**f**) que absorben fuertemente en la región entre 550 y 600 nm, funcionalizadas con grupos carboxilo, para su anclaje a óxido de titanio.

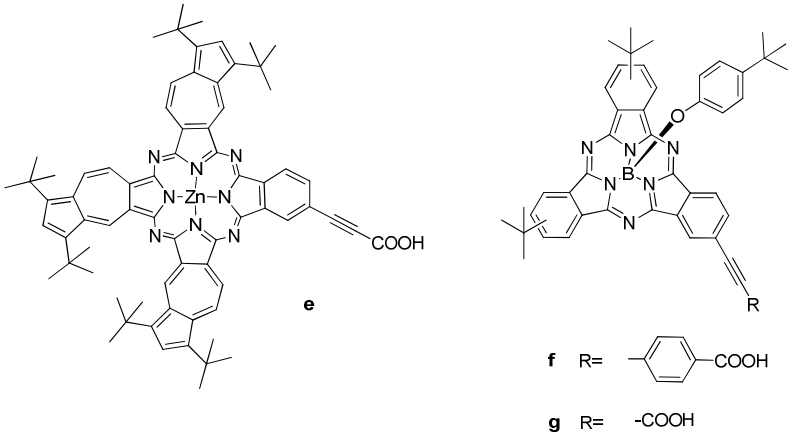

Asimismo, y dado que nanoestructuras de carbono como fullereno C_{60} y nanotubos de pared simple (SWNTs) son los aceptores más frecuentemente empleados en células solares, se han preparado una serie de sistemas dador-aceptor, tanto covalentes (**h**) como supramoleculares (**i**), en los que estas subestructuras se han acoplado a derivados de azulenocianina, de carácter dador, con el ánimo de estudiar procesos de transferencia electrónica fotoinducida.

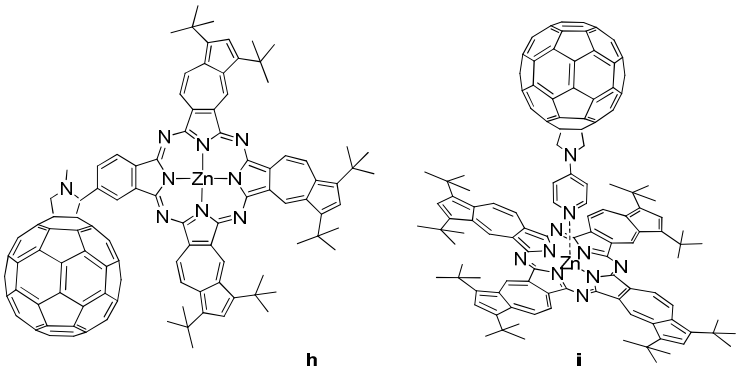

h **i**

Se ha estudiado la organización a nivel supramolecular en fases liquido-cristalinas de tipo columnar de una serie de sistemas multicomponente ftalocianina-fullereno (Pc-C_{60}), como **j**, con el objeto de incrementar la movilidad de los transportadores de carga a lo largo del eje de apilamiento, un hecho que puede ser de interés en el campo de la fotovoltaica molecular, dado que el control de la nanoestructura de la capa activa es un aspecto fundamental para el desarrollo de dispositivos eficientes.

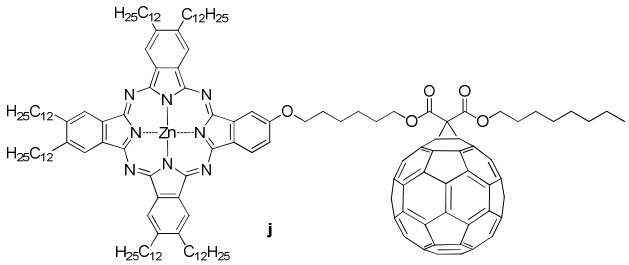

j

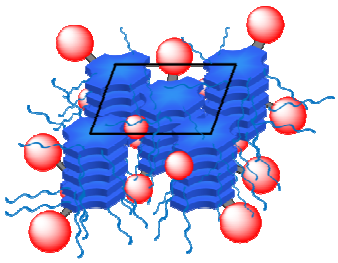

Finalmente, algunas de las ftalocianinas y análogos de ftalocianina preparados en esta tesis han sido evaluados como componentes activos en células solares.

Introduction

Natural and Artificial Photosynthesis

Photosynthesis is the process in which plants and some bacteria use the energy from sunlight to produce sugar that serves as the energy source. In this process, luminous energy is efficiently transformed into chemical energy by cascades of energy and electron transfer occurring between well-arranged organic pigments.[1] Figure 1 shows the structure of a representative photosynthetic reaction center in bacteria Rb. Sphaeroides.

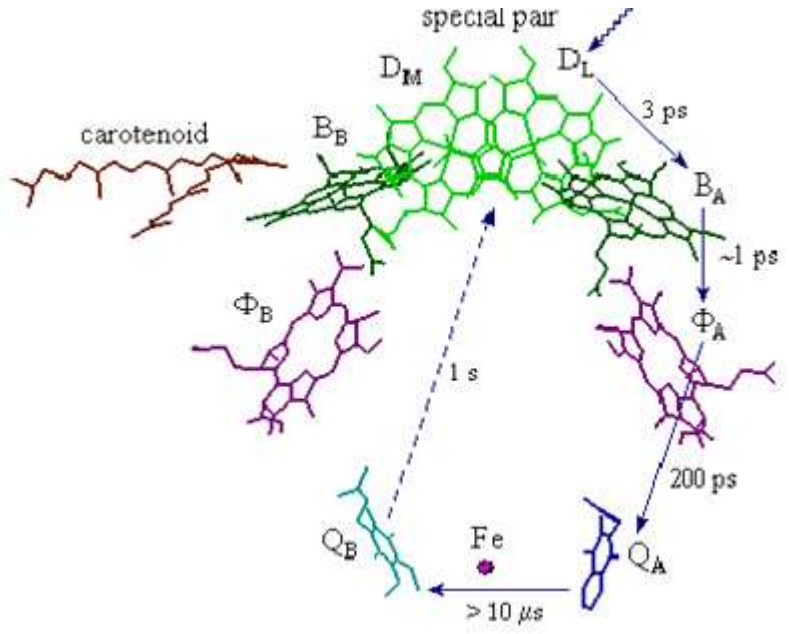

Figure 1. Scheme of a photosynthetic reaction center.

In the first step, light is absorbed by a special pair of the bacteriochlorophyll dimer (DM-DL), which is a non-covalent dimer of chlorophyll molecules strongly

[1] a) G. Gingras, in *The Photosynthetic Bacteria* (Eds.: R. K. Clayton, W. R. Sistrom), Elsevier, Amsterdam, **1988**. b) M. Pessarakli, *Handbook of Photosynthesis*, Ed. 2, Taylor & Francis, Boca Raton, **2005**. c) G. Renger, *Primary Processes of Photosynthesis: Principles and Apparatus,* RSC Publishing Cambridge, **2008**. d) T. B. Buchner, N. H. Ewingen, *Photosynthesis: Theory and Applications in Energy, Biotechnology and Nanotechnology*, Nova Science Publishers, New York, **2009**.

coupled electronically, generating its singlet excited state ^{1}(DM-DL)*.[2] In a second step, an electron transfer occurs from ^{1}(DM-DL)* to the bacteriopheopytin Φ_A through chlorophyll B_A to generate the $DL^{\cdot+}$-$\Phi_A^{\cdot-}$ radical pair. The electron can be transferred through the membrane from $\Phi_A^{\cdot-}$ to quinone A (QA) and then to quinone B (QB), yielding the $DL^{\cdot+}$-$\Phi_B^{\cdot-}$ radical pair. As a whole, a sequence of fast and efficient electron transfer processes, moving an electron away from the special pair, ultimately results in a spatially and electronically well-isolated radical couple.

The excitation of the photosynthetic reaction center by another photon finally induces the reduction of semiquinone $QB^{\cdot-}$ to QB^{2-}, which captures two protons from the cytoplasmic medium to yield QBH_2. This mechanism is responsible for the generation of a proton gradient between both sides of the cytoplasmic membrane. The energy collected by the crossing of protons through the membrane to compensate this gradient is employed for the synthesis of molecules (ATP, NADPH) that store the energy that is used to drive the subsequent biochemical reactions.

1. Donor-Acceptor Systems for Artificial Photosynthesis

Photosynthesis is the most successful process for the conversion and storage of solar energy. The concepts of photosynthesis are attractive to researchers in their efforts to create artificial systems capable of transforming solar energy into chemical energy. The key process in natural photosynthesis is photo-induced charge separation. Photo-induced electron transfer in organic molecules, therefore, has attracted attention of several research groups. Within the aim to systematically build suitable artificial solar energy conversion devices and mimic the analogous natural systems, a great variety of synthetic donor-acceptor ensembles has been designed, synthesized and photophysically studied.[3]

---

[2] a) G. Feher, J. P. Allen, M. Y. Okamura, D. C. Rees, *Nature*, **1989**, *339*, 111. b) M. R. Wasielewski, *Chem. Rev*. **1992**, *92*, 435. c) *The Photosynthetic Reaction Center* (Eds: J. Deisenhoifer, J. R. Norries), Academic Press, New York, **1993**. d) R. E. Blankenship, *Molecular Mechanisms of Photosynthesis*, Blackwell Science, Chichester, **2002**. e) V. Balzani, A. Credi, M. Venturi, *ChemSusChem*. **2008**, *1*, 26.

[3] a) V. Balzani, F. Scandola, *Supramolecular Photochemistry*, Ellis Horwood, Chichester, **1991**. b) S. Spesier, *Chem. Rev*. **1996**, *96*, 1953. c) *Electron Transfer in Chemistry Vol. I-V* (Ed.: V. Balzani), Wiley-VCH, Weinheim, **2001**. d) D. Gust, T. A. Moore, A. L. Moore, *Acc. Chem. Res.* **2009**, *42*, 1890. e) J. S. Park, E. Karnas, K. Ohkubo, P. Chen, K. M. Kadish, S. Fukuzumi, C. W. Bielawski, R. W. Hudnall, V. M. Lynch, J. L. Sessler, *Science* **2010**, *329,* 1324. f) Y. Pellegrin, F. Odobel, *Coord. Chem. Rev*. **2011**, *255*, 2578.

In their most simple version, these systems can be presented as A-(L)-D dyads (Figure 2), where A is the electron acceptor and D is the electron donor component connected by means of a spacer L through covalent or non-covalent interactions.

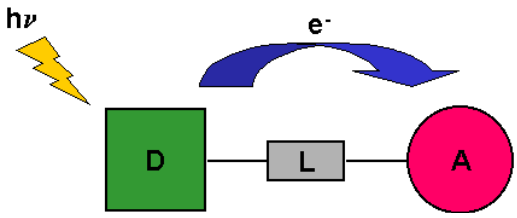

Figure 2. Model of dyad molecule for photoinduced electron transfer.

Photoexcitation of the donor or acceptor units can result in photoinduced electron or energy transfer. In the electron transfer process, upon photoexcitation, the electron travels from the donor to the acceptor, creating a charge separated pair involving a radical cation ($D^{\cdot+}$) and a radical anion ($A^{\cdot-}$).[4] In the case of energy transfer, the energy of the excited state is transferred to the acceptor, leaving the donor molecule in the ground state and the acceptor molecule in the excited state. On the other hand, once a molecule is excited by the absorption of a photon, it can return to the ground state by many pathways, such as internal conversion, intersystem crossing, fluorescence, and phosphorescence. Therefore, the rates of the energy/electron transfer should be faster than those of the deactivation processes in order to achieve efficient energy or electron transfer.

Within this context, for the construction of efficient artificial photoactive devices some major requirements should be met:[5]

- The light must be captured efficiently by antenna molecules leading to excited states

[4] a) J. S. Connoly, J. R. Bolton, *in Photoinduced Electron Transfer* (Eds.: M.A. Fox, M. Chanon), Elsevier, Amsterdam, **1988**.

[5] a) M. E. El-Khouly, O. Ito, P. M. Smith, F. D'Souza, *J. Photochem. Photobiol. C.* **2004**, *5,* 79. b) D. Wrobel, A. Graja, *Coord. Chem. Rev.* **2011**, *255,* 2555.

- The light absorption of chromophores must result in transfer of an electron to the acceptor
- The electron transfer must be directional
- The lifetime of the excited states must be long enough for electron transfer

A basic description of the photoinduced charge transfer between donor and acceptor is shown in Figure 3.

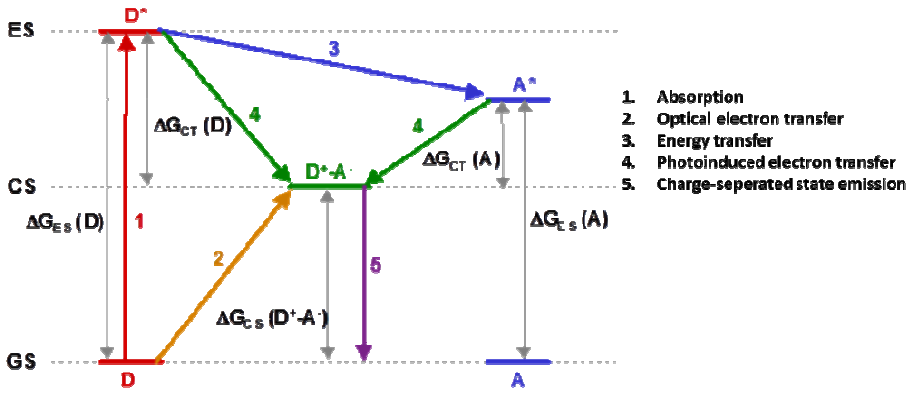

Figure 3. Photophysical processes occurring between D-A upon excitation of donor.

Several electroactive molecules including ferrocene,[6] aniline derivatives,[7] tetrathiafulvalene (TTF),[8] aromatic oligomers[9] and porphyrins[10] have been studied as electron donor partners. Among the acceptor moieties employed for the preparation of D-A ensembles, quinone,[11] perylenebisimide,[12] tetracyano-*p*-quinodimethane[13] and

---

6 a) F. Hauke, A. Hirsch, S. G. Liu, L. Echegoyen, A. Swartz, C. Luo, D. M. Guldi, *ChemPhysChem.* **2002**, *3*, 195. b) Y. Araki, Y. Yasumura, O. Ito, *J. Phys. Chem. B,* **2005**, *109*, 9843.

7 R. M. Williams, J. M. Zwier, J. W. Verhoeven, *J. Am. Chem. Soc*. **1995**, *117*, 4093.

8 a) L. Sanchez, I. Perez, N. Martin, D. M. Guldi, *Chem. Eur. J.* **2003**, *11*, 21640. b) Y. Takano, M. A. Herranz, N. Martin, S. G. Radhakrishnan, D. M. Guldi, T. Tsuchiya, S. Nagase, T. Akasaka, *J. Am. Chem. Soc.* **2010**, *132*, 8048.

9 a) M. Fujitsiko, O. Ito, T. Yamashiro, Y. Aso, T. Otsubo, *J. Phys. Chem. A.* **2000**, *104*, 4876. b) D. M. Guldi, A. Swartz, C. Luo, R. Gomez, J. L. Segura, N. Martin, *J. Am. Chem. Soc*. **2002**, *124*, 10875.

10 a) A. Harriman, Y. Kubo, J. L. Sessler, *J. Am. Chem. Soc.* **1992**, *114*, 388. b) *Handbook of Porphyrin Science* (Eds.: K. Kadish, K. M. Smith, R. Guilard), World Scientific Press, Singapur, **2010-2012**, Vols. *10-20*. c) F. D'Souza, O. Ito, *Chem. Soc. Rev.* **2012,** *41*, 86. d) D. M. Guldi, *Chem. Soc. Rev*. **2002**, *31*, 22.

11 a) J. L. Sessler, M. R. Johnson, T. Lin, S. E. Creager, *J. Am. Chem. Soc.* **1988**, *110*, 3659. b) K. Okamoto, S. Fukuzumi, *J. Phys, Chem. B.* **2005**, *109*, 7713.

12 a) A. Prodi, C. Chiorboli, F. Scandola, E. Lengo, E. Alessio, R. Dobrawa, F. Würthner, *J. Am. Chem. Soc.* **2005**, *127*, 1454. b) X. W. Zhan, Z. A. Tan, B. Domercq, Z. An, X. Zhang, S. Barlow, Y. Li, D. Zhu, B. Kippelen, S. R. Marder, *J. Am. Chem. Soc.* **2007**, *129*, 7246.

members of the carbon nanostructures family such as C_{60} fullerene and carbon nanotubes hold a privileged position.[14] In particular, C_{60} fullerene, possesses excellent electron acceptor properties, which coupled with its small reorganization energy and ability for promoting ultrafast charge separation with slow charge recombination features, can give rise, when implemented in D-A systems, to the formation of very stable radical ion pair species.[15]

The preparation and study of D-A hybrids involving phthalocyanines (Pcs) and carbon nanostructures represents nowadays an important field of research.

Pcs[16] are macroheterocyclic compounds constituted by four isoindole units linked by nitrogen atoms at the *meso* position. They are planar 18 π-electron aromatic compounds with a considerable large π-delocalized surface that accounts for their unique optical properties and the strong tendency of phthalocyanines to form π-stacked aggregates. The electronic absorption spectrum of phthalocyanines shows two main bands, the Q-band and the Soret or B-band. The Q-Band, associated to π-π* HOMO-LUMO transition, is usually found in the region of 620-700 nm (Figure 4) and is responsible for the deep green or blue color of these compounds. These bands can be easily tuned by the careful choice of the metal atom in the macrocycles cavity and by placing adequate substituents at the macrocycles peripheral and axial positions. Moreover, Pcs are thermally and chemically stable compounds and present rich redox chemistry, thus representing perfect light-harvesting systems and ideal components for donor-aceptor systems.

---

13 a) J. Gomez, C. Seoane, J. L. Segura, *Chem. Soc. Rev.* **2007**, *36*, 1305.

14 a) *Carbon Nanotubes and Related Structures: Synthesis, Characterization, Functionalization, and Applications* (Eds.: D. M. Guldi, N. Martin), Wiley, Weinheim, **2010**.

15 a) S. Fukuzumi, D. M. Guldi, *In Electron Transfer in Chemistry* (Ed.: V. Balzani), Wiley-VCH, New York, **2001**. b) D. M. Guldi, B. M. Illescas, M. Wielopolski, N. Martin, *Chem. Soc. Rev.* **2009**, *38*, 1587.

16 a) *Phthalocyanines. Properties and Applications* (Eds. C. C. Leznoff, A. B. P. Lever), VCH Publishers (LSK) Ltd., Cambridge, **1996**, Vols. *1-4.* b) *Phthalocyanine Materials. Synthesis, Structure and Function* (Ed. N. B. McKeown), Cambridge University Press, Cambridge, **1998**. c) G. de la Torre, C. G. Claessens, T. Torres, *Chem. Commun*. **2007**, 2000. d) C. G. Claessens, U. Hahn, T. Torres, *Chem. Record*. **2008**, *8*, 75. e) Y. Rio, M. S. Rodríguez-Morgade, T. Torres, *Org. Biomol. Chem.* **2008**, *6*, 1877. f) J. Mack, N. Kobayashi, *Chem. Rev.* **2011**, *111*, 281.

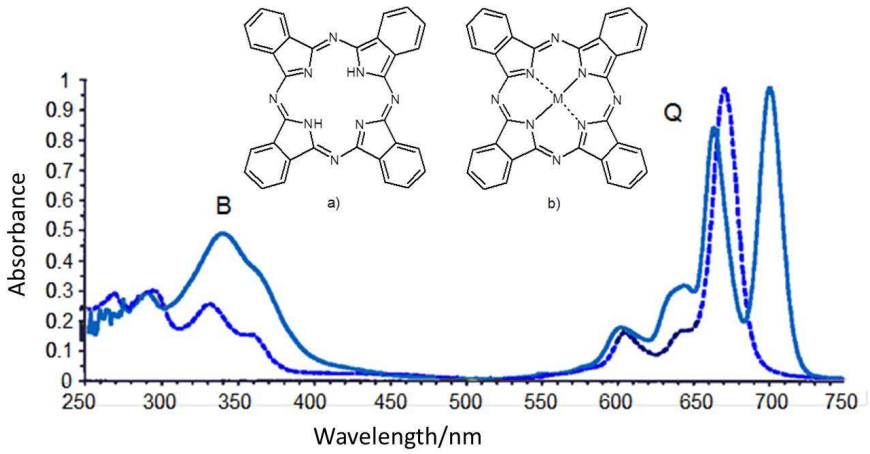

Figure 4. UV-visible spectra of metal-free Pc (solid line) and metallophthalocyanine (dashed line).

1.1. Phthalocyanine-C_{60} and Phthalocyanine-SWNTs Dyads

The unique physicochemical properties of Pcs have prompted the incorporation of these macrocycles in a large number of D-A systems where their role is i) to harvest light efficiently and ii) once photoexcited, to act as an electron donor for an acceptor moiety.[17] A schematic picture for the photoinduced charge transfer from phthalocyanine to fullerene is shown in Figure 5.

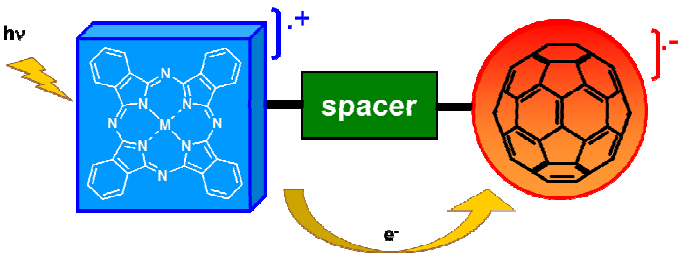

Figure 5. Photoinduced charge (electron) transfer from photoexcited phthalocyanine to fullerene.

[17] a) G. Bottari, G. de la Torre, D. M. Guldi, T. Torres, *Chem. Rev.* **2010**, *110*, 6768. b) G. de la Torre, G. Bottari, U. Hahn, T. Torres, *Struct. Bonding*, **2010**, *135*, 1. c) G. Bottari, J. A. Suanzes, O. Trukhina, T. Torres, *J. Phys. Chem. Lett*. **2011**, *2*, 905.

Up to date, a large variety of covalent and supramolecular systems based on Pcs and carbon nanostructures have been described and the photophysical properties of some of them studied both in solution and in solid state in order to understand the interesting electron and energy transfer properties and thus mimic natural photosynthetic systems.[5,17,18] When comparing these two constructing approaches (covalent *vs* supramolecular), the use of supramolecular interactions for the preparation of systems based on Pcs and carbon nanostructures present some advantages over the covalent synthesis. This strategy, in fact, allows to obtaining, thermodynamically reversible assemblies, whose stability can be influenced by the careful choice of the supramolecular interactions used, as well as by some external conditions such as temperature or solvent polarity. In addition, noncovalent systems have the advantage of producing efficient and long-lived photoinduced charge separation processes, thus representing an attractive alternative to their covalently linked counterparts.

The first report on a donor-acceptor system containing covalently linked Pc and C_{60} was reported in 1995 by Hanack (Figure 6).[19] However, photoinduced electron transfer was not studied in this kind of dyads until ZnPc-C_{60} and H_2Pc-C_{60} were synthesized by our group in 2002 and studied in collaboration with D. M. Guldi.[20] It was demonstrated that the initial photoexcitation is followed by an ultrafast electron transfer largely because of the strong electronic coupling between the electron donor (Pc) and the electron acceptor (C_{60}) generating surprisingly long-lived radical ion pairs $Pc^{\cdot+}$-$C_{60}^{\cdot-}$ with lifetimes of several nanoseconds.

---

5 a) M. E. El-Khouly, O. Ito, P. M. Smith, F. D'Souza, *J. Photochem. Photobiol. C.* **2004**, *5,* 79. b) D. Wrobel, A. Graja, *Coord. Chem. Rev.* **2011**, *255,* 2555.

18 a) F. D`Souza, O. Ito, *Coord. Chem. Rev.* **2005**, *249*, 1410. b) D. M. Guldi, A. Gouloumis, P. Vázquez, T. Torres, V. Georgakilas, M. Prato, *J. Am. Chem. Soc.* **2005**, *127*, 5811. c) F. D'Souza, O. Ito, *Chem. Commun.* **2009**, 4913.

19 T. G. Linssen, K. Durr, M. Hanack, A. Hirsch, *Chem. Commun*. **1995**, 2056.

20 a) A. Gouloumis, S. G. Liu, A. Sastre, P. Vázquez, L. Echegoyen, T. Torres, *Chem. Eur. J*. **2000**, *6*, 3600, b) D. M. Guldi, A. Gouloumis, P. Vázquez, T. Torres, *Chem. Commun.* **2002**, 2056. c) D. M. Guldi, I. Zilbermann, A. Gouloumis, P. Vázquez, T. Torres, *J. Phys. Chem. B.* **2004**, *108,* 18485.

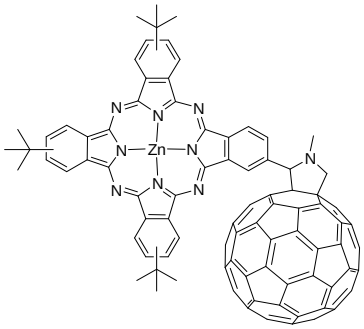

	lifetimes (τ) of $Pc^{\cdot+}$- $C_{60}^{\cdot-}$ (THF) (ns)
H_2Pc-C_{60}	4.6
ZnPc-C_{60}	2.9
CuPc-C_{60}	7.8

Figure 6. Molecular structure of first Pc-C_{60} dyads reported by Torres et al.

The nature of the spacer is very crucial in order to control the distance, orientation, and electron coupling in the covalently linked donor-acceptor systems. With the aim of studying the influence of the nature of the spacer between Pc and C_{60}, a series of ZnPc-C_{60} conjugates were synthesized and their photoinduced electron transfer behaviour was studied in different solvents (Figure 7).[21] Upon photoexcitation of ZnPc-C_{60} conjugates, electron transfer takes place from the generated singlet excited state of ZnPc to yield the formation of a radical ion pair. The bands at 520 nm and 840 nm were attributed to the one-electron oxidized ZnPc radical cation and the band at 1000 nm matched the absorption of the one-electron-reduced fullerene radical anion. In general, the lifetimes of charge separated states tend to be shorter if the system lacking any spacer at all, whereas longer lifetime was found in the system that carried the triple-bond spacer. In other words, the general trend is that the lifetime increases with distance and with spacers that provide a more effective electronic conjugation.

[21] a) M. Quintiliani, A. Kahnt, T. Wölfle, W. Hieringer, P. Vazquez, A. Görling, D. M. Guldi, T. Torres, *Chem. Eur. J.* **2008**, *14*, 3765. b) A. Kahnt, D. M. Guldi, A. de la Escosura, M. V. Martínez-Díaz, T. Torres, *J. Mater. Chem*. **2008**, *18*, 77.

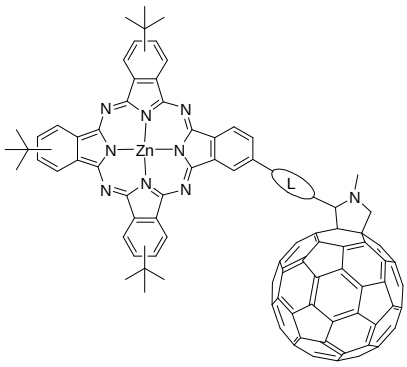

		lifetimes (τ) of $Pc^{\cdot+}$-$C_{60}^{\cdot-}$(ps) Toluene	THF
L=	C≡C	154	13 000
	HC=CH	120	14 000
	CH_2CH_2	131	10 000
	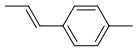	35 000	
	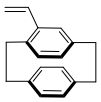	458 000	2 400

Figure 7. Molecular structure of Pc-C_{60} dyads incorporating different spacers.

On the other hand, the highest lifetime of the radical ion pair state was obtained for ZnPc-paracyclopropan-C_{60} dyad. This can be explained by the fact that the cyclophane linker helps to suppress the charge recombination when compared to the phenylene viniylene linker. Also, in all cases, the lifetime increased with decreasing polarity of the solvents.

Supramolecular donor-acceptor (D-A) Pc/C_{60} systems have been assembled by non-covalent interactions such as hydrogen bonding[22] and metal-ligand coordination.[23] The construction of D-A ensembles by ammonium ion-crown ether interactions leads to systems that provides strong enough binding and weak enough formation for reversible assembled/disassembled dyads. The first report on Pc/C_{60} fullerene pseudorotaxane systems assembled *via* alkylammonium/crown ether supramolecular interactions appeared (Figure 8) in 2002.[24] The supramolecular complexes consist of a C_{60} derivative bearing a secondary dibenzylammonium moiety which is treaded into the

[22] a) J. L. Sessler, J. Jayawickramarajah, A. Gouloumis, G. D. Pantos, T. Torres, D. M. Guldi, *Tetrahedron,* **2006***, 62*, 2123. b) T. Torres, A. Gouloumis, D. Sanchez-Garcia, J. Jayawickramarajah, W. Seitz, D. M. Guldi, J. L. Sessler, *Chem. Commun*. **2007**, 292.

[23] a) M. E. El-Khouly, L. M. Rogers, M. E. Zandler, G. Suresh, M. Fujitsuka, O. Ito, F. D'Souza, *ChemPhysChem*. **2003**, *4*, 474. b) M. E. El-Khouly, Y. Araki, O. Ito, S. Gadde, M. E. Zandler, F. D'Souza, *J. Porphyrins Phthalocyanines* **2006**, *10*, 1156. c) F. D'Souza, E. Maligaspe, K. Ohkubo, M. E. Zandler, N. K. Subbaiyan, S. Fukuzumi, *J. Am. Chem. Soc.* **2009**, *131*, 8787. d) M. S. Rodriguez-Morgade, M. E. Plonska-Brzezinska, A. J. Athans, E. Carbonell, G. de Miguel, D. M. Guldi, L. Echegoyen, T. Torres, *J. Am. Chem. Soc.* **2009**, *131*, 10484.

[24] a) M. V. Martínez-Díaz, N. S. Fender, M. S. Rodriguez-Morgade, M. Gomez-Lopez, F. Diederich, L. Echegoyen, J. F. Stoddart, T. Torres, *J. Mater. Chem.* **2002***, 12*, 2095. b) D. M. Guldi, J. Ramey, M. V. Martínez-Díaz, A. de la Escosura, T. Torres, T. Da Ros, M. Prato, *Chem. Commun.* **2002***,* 2774.

dibenzo-24-crown-8 cavity of a Pc macrocycle. The two components C_{60} salt and Pc moiety self-assembled in chloroform solutions in a 1:1 stoichiometry and with a high K_a (1.53×10^4 M^{-1}) as inferred by ^1H NMR experiments. However, electrochemical and UV-Vis studies failed to reveal any ground state electronic communication between the Pc and the C_{60} units. The lack of ground state electronic interactions could be due to the distance between the two-electroactive units, which can adopt several conformations within the complex as revealed by molecular modeling studies.

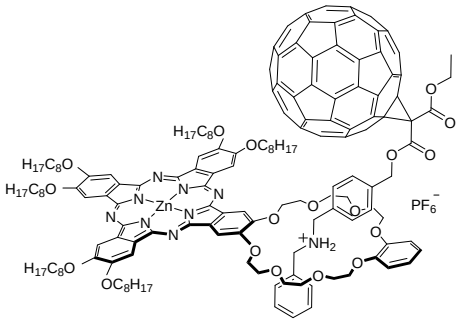

Figure 8. Molecular structure of one example of noncovalent Pc/C_{60} dyad.

Photophysical studies revealed a progressive, nonlinear quenching of the Zn(II)Pc fluorescence upon addition of the fullerene derivative. The fate of the photogenerated Pc excited-state was unveiled by transient absorption measurements, which showed the formation of a microsecond-lived radical ion pair state (1.5 μs) because of an efficient intracomplex electron transfer mechanism. It is worth mentioning that these supramolecular ensembles present a stabilization of more than two orders of magnitude of their radical ion pair state lifetimes with respect to covalently linked Zn (II) Pc-C_{60} conjugates.

Similarly to C_{60}, carbon nanotubes (SWNTs) also present a high affinity for electrons, which, once accepted, can be transported along their 1-D tubular structure. Furthermore, the electrical and thermal conductivity, mechanical strenght, and good chemical stability of SWNT are promising features that stimulate their integration into

electronic devices.[25] However, CNTs are difficult to handle because of the strong Van der Waals forces causing bundling and formation of aggregates, which hinders their solubility in organic solvents and diminishes the special mechanical and electrical properties of the individual tubes. With the aim of increasing the solubility of nanotubes and achieving stable dispersions, it is necessary to functionalize them.

There are two general approaches for the functionalization of carbon nanotubes [26] (i) the use of noncovalent, π-π interactions between appropriately functionalized molecules and the nanotube wall, or (ii) by covalent attachment of organic molecules to the carbon nanotube open edges or side walls. While the covalent approach leads to more thermodynamically stable structures, the noncovalent functionalization presents the advantage that the electronic structure of the nanotube remains almost unaffected. Some functionalization possibilities for SWNTs are shown in Figure 9: Covalent functionalization by attaching functional groups to the nanotube ends or defect sites (A), covalent functionalization through sidewall functionalization (B), noncovalent functionalization with surfactants (C), noncovalent functionalization, for example, wrapping nanotubes by polymers (D), functionalization from inside (endohedral) by filling nanotubes with different nonoparticles (E).[27]

[25] a) D. M. Guldi, G. M. A. Rahman, V. Sgobba, N. A. Kotov, D. Bonifazi, M. Prato, *J. Am. Chem. Soc*. **2006**, *128*, 2315. b) D. R. Rolison, J. W. Long, J. C. Lytle, A. E. Fischer, C. P. Rhodes, T. M. McEvoy, M. E. Bourg, A. M. Lubers, *Chem. Soc. Rev*. **2009**, *38*, 226. c) *Chemistry of Nanocarbons* (Eds.: T. Akasaka, F. Wudl, S. Nagase), Wiley- Blackwell, London, **2010**.

[26] a) J. Chen, M. A. Hamon, H. Hu, Y. Chen, A. M. Rao, P. C. Eklund, R. C. Haddon, *Science*, **1998**, *282*, 95. b) S. Banerjee, T. Hemraj-Benny, S. S. Wong, *Adv. Mater*. **2005**, *17*, 17. c) D. Tasis, N. Tagmatarchis, A. Bianco, M. Prato, *Chem. Rev*. **2006**, *106*, 1105.

[27] A. Hirsch, *Angew. Chem. Int. Ed. Engl*. **2002**, *41*, 1853.

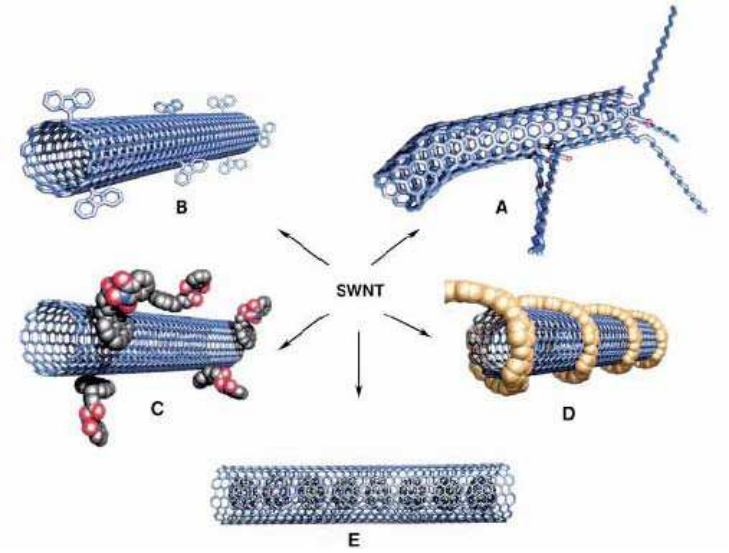

Figure 9. Most common functionalization patterns of CNTs.

Up to date, a variety of supramolecular assemblies based on phthalocyanines or porphyrins (Pors) and SWNTs have been reported either by direct immobilization of the macrocycles cores onto the SWNT sidewalls or by means of pyrene/SWNT supramolecular interaction, taking advantage of the strong π-π interactions of pyrene to the SWNT sidewalls.[28] These systems will be explained in more detail in chapter 1.2.

On the other hand, effective covalent functionalization of carbon nanotubes with Pors or Pcs has been achieved by producing carboxylic acid groups on the surface of nanotubes through acid treatment followed by the esterification of acid groups with functional group appended Pcs or Pors.[29] Another approach, the 1,3 dipolar cycloaddition of azomethine ylides which has met a wide acceptance in the field of

[28] a) R. J. Chen, Y. Zhang, D. Wang, H. Dai, *J. Am. Chem. Soc*. **2001**, *123*, 3838. b) F. D'Souza, R. Chitta, A. S. D. Sandanayaka, N. K. Subbaiyan, L. D'Souza, Y. Araki, O. Ito, *J. Am. Chem. Soc.* **2007**, 129, 15865. c) S. Kyatskaya, J. Ramon, G. Mascaros, L. Bogani, F. Hennrich, M. Kappes, W. Wernsdorfer, M. Ruben, *J. Am. Soc.* **2009**, *131*, 15143. d) E. Maligaspe, A. S. D. Sandanayaka, T. Hasobe, O. Ito, F. D'Souza, *J. Am. Chem. Soc.* **2010**, *132*, 8158. e) J. Bartelmess, B. Ballesteros, G. de la Torre, D. Kiessling, S. Campidelli, M. Prato, T. Torres, D. M. Guldi, *J. Am. Chem. Soc.* **2010**, *132*, 16202. f) J. Bartelmess, A. R. M. Soares, M. V. Martinez-Diaz, M. G. P. M. S. Neves, A. C. Tomé, J. A. S. Cavaleiro, T. Torres, D. M. Guldi, *Chem. Commun*. **2011**, *47*, 3490. g) J. Bartelmess, C. Ehli, J. J. Cid, M. Garcia-Iglesias, P. Vazquez, T. Torres, D. M. Guldi, *Chem. Sci*. **2011**, *2*, 652.

[29] a) G. de la Torre, W. Blau, T. Torres, *Nanotechnology* **2003**, *14*, 765. b) H. B. Xu, H. Z. Chen, M. M. Shi, R. Bai, M. Wang, *Mater. Chem. Phys*. **2005**, *94*, 342. c) Z. Yang, H. Pu, J. Yuan, D. Wan, Y. Liu, *Chem. Phys. Lett.* **2008**, *465*, 73. d) N. He, Y. Chen, J. Bai, J. Wang, W. J. Blau, J. Zhu, *J. Phys. Chem. C.* **2009**, *113*, 13029.

fullerenes, affords easy attachment of pyrrolidine rings with various functional groups.[30] This method was used for the covalent attachment of Pcs on SWNT following two routes depicted in Figure 10.[31] The first one is a stepwise approach consisting in the initial functionalization of SWNTs by reaction of N-octyl glycine and formyl benzoic acid, followed by esterification with a hydroxy-functionalized Pc. The second approach involved the cyloaddition reaction of N-octylglicine and formyl Pc. Thermogravimetric analyse showed that largely functionalized (30 wt. %) nanohybrid system was obtained by the first method. The occurring of electron transfer from photoexcited Pcs to the nanotube framework in these ZnPc-SWNT ensembles was observed in transient absorption experiments and these studies confirmed the absorption of the one-electron oxidized ZnPc cation and the concomitant bleaching of the van Hove singularities typical from SWNTs. Charge-separation (*i.e.*, 2.0×10^{10} s^{-1}) and charge-recombination (*i.e.*, 1.5×10^{6} s^{-1}) dynamics revealed a notable stabilization of the radical ion pair product in DMF.

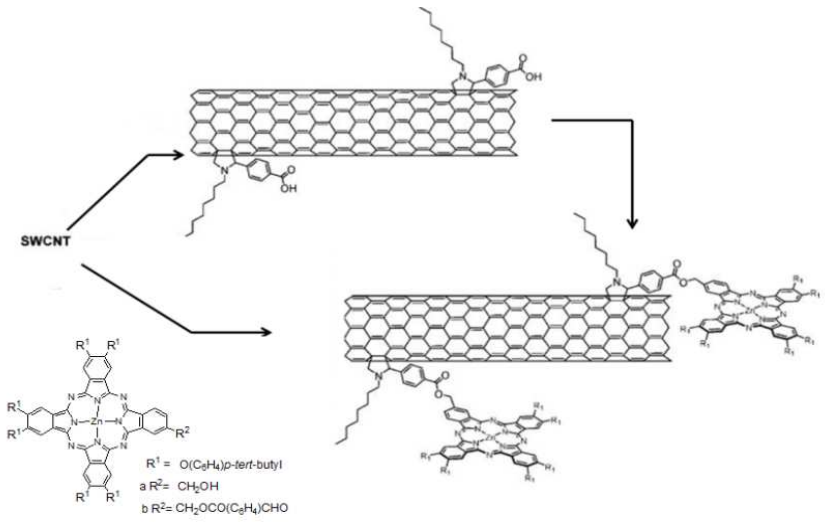

Figure 10. Synthesis of a covalently linked Pc/SWNT ensamble by a 1,3–dipolar cycloaddition reaction.

[30] a) S. Campidelli, C. Sooambar, E. L. Diz, C. Ehli, D. M. Guldi, M. Prato, *J. Am. Chem. Soc.* **2006**, *128*, 12544. b) B. Ballesteros, S. Campidelli, G. de la Torre, C. Ehli, D. M. Guldi, M. Prato, T. Torres, *Chem. Commun*. **2007**, 2950. c) S. Campidelli, B. Ballesteros, A. Filoramo, D. Diaz Diaz, G. de la Torre, T. Torres, G. M. A. Rahman, C. Ehli, D. Kiessling, F. Werner, V. Sgobba, D. M. Guldi, C. Cioffi, M. Prato, J. P. Bourgoin, *J. Am. Chem. Soc.* **2008**, *130*, 11503.

[31] B. Ballesteros, G. de la Torre, C. Ehli, G. M. A. Rahman, F. Agullo-Rueda, D. M. Guldi, T. Torres, *J. Am. Chem. Soc.* **2007**, *129*, 5061.

2. Organic Solar Cells

Solar power has a high potential of becoming the energy source of the future, since the earth receives about 100.000 terawatt of light at its surface every hour, which is enough to meet humanity's demand for a year.[32] This point has been addressed over the last decades by the development of photovoltaics, which convert sunlight into electrical energy. Photovoltaic have a number of considerable advantages in terms of reliability and sustainability, and environmentally friendly.

The first crystalline silicon solar cell was developed at Bell Laboratories in 1954. [33] Since then, photovoltaic cells have been extensively studied. Although laboratory cell efficiencies have reached 24%, production cell efficiencies are still in the range of 12–18%.[34] Even so, at present there is a significant amount of photovoltaic installed by inorganic-semiconductor based technology, the materials and production cost of this technology limits the economically competition with conventional fossil-fuel energy conversion systems. In this regard, organic photovoltaic (OPV) have attracted significant attention as a lower cost alternative to their inorganic relatives. Organic materials fulfill many requirements for solar cells, such as strong optical absorption, easy manufacturing in thin film, low cost synthesis, chemical tailoring to alter their properties, etc. [35] Organic solar cells are categorized into three types; planar heterojunction, bulk heterojunction (BHJ) and dye sensitized solar cells (DSSC).

Planar heterojunction solar cells consist of an organic hole-conducting donor and an organic electron-conducting acceptor material sandwiched in between two electrodes (Figure 11a). The first breakthrough in planar heterojunction solar cells was achieved by Tang in 1986.[36] This cell consists of a combination of p-type copper phthalocyanine and n-type perylenetetracaboxylic acid bisbenzimidazole into a p–n heterojunction giving rise to 1% conversion efficiency. Since then, a wide variety of

---

32 Q. Schiermeier, J. Tollefson, T. Scully, A. Witze, O. Morton, *Nature*, **2008**, *454*, 816.

33 D. M. Chapin, C. S. Fuller, G. L. Pearson, *J. Appl. Phys*. **1954**, *25*, 676.

34 M. A. Green, K. Emery, D. L. King, S. Igari, W. Warta, *Prog. Photovoltaics*, **2005**, *13*, 49.

35 a) S. E. Shaheen, C. J. Brabec, N. S. Sariciftci, F. Padinger, T. Fromherz, J. C. Hummelen, *Appl. Phys. Lett.* **2001**, *78*, 841. b) K. Schulze, C. Uhrich, R. Schüppel, K. Leo, M. Pfeiffer, E. Brier, E. Reinold, P. Bauerle, *Adv. Mater*. **2006**, *18*, 2872. c) N. S. Lewis, *Science.* **2007**, *315*, 798. d) P. M. Beajuge, J. M. J. Frechet, *J. Am. Soc.* **2011**,*133*, 20009.

36 C. W. Tang, *Appl. Phys. Lett.* **1986**, 48, 183.

donor and acceptor materials has been tested in the Tang type planar solar cells.[37] The conversion efficiency of planar devices is mainly limited by charge generation at the donor acceptor interface.

Bulk heterojunction solar cells (BHJ), are formed by depositing donor and acceptor together in an interpenetrating network (Figure 11b). The interface between donor and acceptor provides the continuous pathway in each material from the interface to the electrodes, thus, the photon-to-electron conversion efficiency is dramatically increased.[38] Therefore, the bulk heterojunction concept is the most promising for OPV.

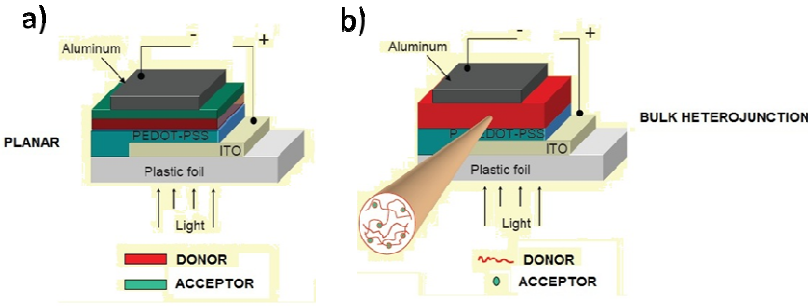

Figure 11. Schematic representation of a) planar and b) bulk heterojunction solar cells.

In addition to simple BHJ, another type, called tandem solar cells, have gained a lot of attention. They consist on the combination of two active layers (one on top of the other) forming a multilayer. Their advantage is that a combination of absorbing molecules can allow for a large spectral coverage with efficient absorption, which would be difficult to obtain with a single heterojunction (Figure 12).[39]

---

37 a) N. S. Sariciftci, D. Braun, C. Zhang, V. I. Srdanov, A. J. Heeger, G. Stucky, F, Wudl, *Appl. Phys. Lett*. **1993**, *62*, 585. b) R. H. Friends, S. C. Moratti, A. B Holmes, *Nature.* **1995**, *78*, 451. c) A. J. Breeze, A. Salomon, D. S. Ginley, B. A. Gregg, H. Tillmann, H. H. Hoerhold, *Appl. Phys. Lett.* **2002**, *81*, 3085. d) F. Yang, S. R. Forrest, *ACS .Nano*, **2008**, *2,* 1022.

38 a) G. Yu, J. Gao, J. C. Hummelen, F. Wudl, A. J. Heeger, *Science*. **1995**, *270*, 1789. b) P. Schilinsky, P. Waldauf, C. Brabec, *J. Appl. Phys. Lett.* **2002**, *81*, 3885. c) H. Hoppe, N. S. Sariciftci, *J. Mater. Chem*. **2004**, *19*, 1924. d) S. Gunes, H. Neugebaues, N. S. Sariciftci, *Chem. Rev*. **2007**, *107*, 1324.

39 a) J. Y. Kim, K. Lee, N. E. Coates, D. Moses, T. Q. Nguyen, M. Dante, A. J. Heeger, *Science*, **2007**, *317*, 222. b) J. Peet, M. L. Senatore, A. J. Heeger, G. C. Bazan, *Adv. Mater*. **2009**, *21*, 1521. c) M. Riede, C. Uhrich, J. Widmer, R. Timmreck, D. Wynands, G. Schwartz, W. M. Gnehr, D. Hildebrandt, A. Weiss, J. Hwang, S. Sundarraj, P. Erk, M. Pfeiffer, K. Leo, *Adv. Funct. Mater.* **2011**, *21*, 3019.

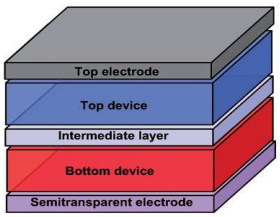

Figure 12. Schematic representation of organic tandem solar cell.

2.1. Optimization of Organic Solar Cells

In contrast to inorganic solar cells, absorption of photons from either the donor or the acceptor leads to formation of electron-hole pairs, the so-called excitons, with a binding energy of about 0.5 eV.[40] These excitons cannot dissociate by thermal energy at room temperature, therefore, they have to diffuse to dissociation sites where charge separation occurs. The exciton diffusion length, that is, the distance the exciton can travel before reaching the interface, is limited (5-10 nm).[41] In the case where the layer thickness of the absorption material is much longer than exciton diffusion length, by-processes (*i.e.* fluorescence, non-radiative decay) occur resulting in losing the energy of the exciton. The exciton is separated when the charge carrier moves from the LUMO of donor to the LUMO of acceptor if the potential difference between the ionization potential of donor and the electron affinity of acceptor is larger than the exciton binding energy. Energetically, the LUMO of acceptor should lie below the LUMO of donor with minimum energy difference of 0.3 eV to affect the exciton splitting and charge dissociation.[42]

The separated charges are then transported within the organic semiconductor to the respective electrodes. Figure 13 shows the operating principles of organic solar

[40] a) R. N. Marks, J. J. M. Halls, D. D. C. Bradley, R. H. Friend, A. B. Holmes, *J. Phys. Condens. Matter.* **1994**, *6*, 1379. b) P. B. Miranda, D. Moses, A. Heeger, *J. Phys. Rev. B*. **2001**, *64*, 81201.

[41] a) J. J. M. Halls, K. Pichler, R. H. Friend, S. C. Moratti, A. B. Holmes, *Appl. Phys. Lett*. **1996**, *68*, 3120. b) D. E. Markov, E. Amsterdam, P. W. M. Blom, A. B. Sieval, J. C. Hummelen*, J. Phys. Chem. A.* **2005**, *109*, 5266. c) D. E. Markov, C. Tanase, P. W. M. Blom, J. Wildeman, *Phys. Rev. B.* **2005**, *72*, 045217.

[42] a) C. J. Brabec, C. Winder, N. S. Sariciftci, J. C. Hummelen, A. Dhanabalan, P. A. van Hal, R. A. J. Janssen, *Adv. Funct. Mater.* **2002**, *12*, 709. b) M. C. Scharber, D. Wuhlbacher, M. Koppe, P. Denk, C. Waldauf, A. J. Heeger, C. L. Brabec, *Adv. Mater*. **2006**, *18*, 789.

cells. There are, four important processes in the operation of OPVs.[43] 1. Exciton formation 2. Exciton diffusion 3. Charge dissociation 4. Charge transport.

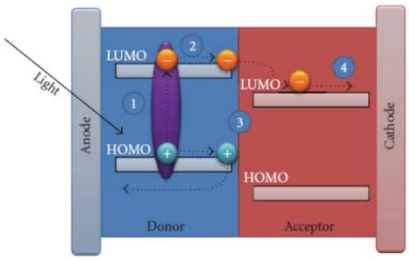

1. Exciton generation
2. Exciton diffusion
3. Charge dissociation
4. Charge transport

Figure 13. Operating principles of OPVs.

2.1.1. Characteristic Parameters of Solar Cells

The current density-voltage curve (J-V-curve) of an illuminated solar cell can be characterized by a number of parameters (Figure 14).

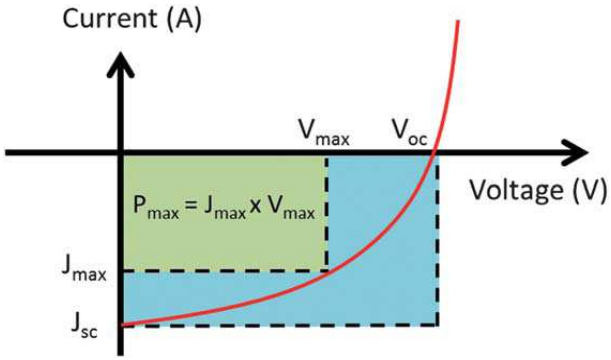

Figure 14. Current-Voltage (J-V) characteristics of an organic solar cell.

Open circuit voltage: Voc is the maximum possible voltage delivered by a solar cell and measured when no current is flowing. For organic heterojunction devices, the Voc

[43] a) C. J. Brabec, A. Cravino, D. Meissner, N. S. Sariciftci, T. Fromherz, M. T. Rispens, L. Sanchez, J. C. Hummelen, *Adv. Funct. Mater*. **2001**, *11*, 374. b) B. C. Thompson, J. M. Fréchet, *Angew. Chem. Int. Ed. Engl*. **2008**, *47*, 58. c) T. M. Clarke, J. R. Durrant, *Chem. Rev.* **2010**, *110*, 6736. d) C. W. Schlenker, M. E. Thompson, *Chem.Commun*. **2011**, *47*, 3702. e) A. Mishra, P. Bäuerle, *Angew. Chem. Int, Ed*. **2012**, *51*, 2020.

is determined by the band gap between HOMO of the donor and LUMO of the acceptor. The difference between the LUMO of the donor and the acceptor should be minimized to maximize the open-circuit voltage.

Short circuit current: Jsc is the current that flows when there is no external field applied. The Jsc depend on the efficiencies of the light absorption of active layer, exciton diffusion, and dissociation at the donor-acceptor interface, charge transport in active layer and charge collection on the electrodes.

The power conversion efficiency defines how much energy the solar cell can extract out of the sun's light and calculated by the formula; where, Voc is open circuit voltage, Jsc is the short circuit current, FF is the fill factor. Pin is the incident light power, which is standardized at 100 Vm^{-2} for solar cell testing with a spectral intensity distribution matching that of the sun on the earth's surface at the incident angle of 45º, which is called AM. 1.5 spectrum.

$$\eta_p = \frac{P_{max}}{P_{in}} = \frac{FFJ_{sc}V_{oc}}{P_{in}}$$

2.2. Active Organic Molecules for Solar Cells

The organic molecules used in the active layer of organic solar cells can be classified as polymer or small molecules, depending on their size. Polymers are mostly deposited in wet solution processes such as spin coating, screen printing, allowing flexible, ultrathin, and low-cost devices. On the other hand, small molecules are mainly deposited by vacuum deposition techniques since they show limited solubility in common solvents.

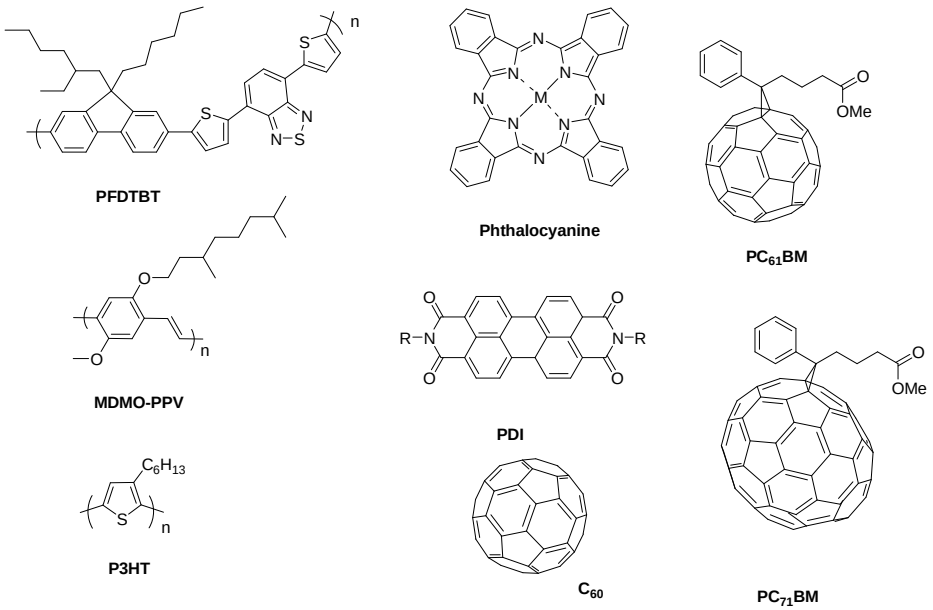

Figure 15. Examples of donor and acceptor materials used in organic solar cells.

The molecular structures of some of the donor and acceptor materials are shown Figure 15. In contrast to the wide range of donor materials, the preferred acceptor material in organic solar cells is fullerene C_{60} and its soluble derivative [6,6]-phenyl-C61-butyric acid methyl ester (PCBM). Their success is related to their high electron mobility and high exciton diffusion length, as well as to the fact that exciton dissociation at donor-fullerene interfaces is highly efficient and ultrafast. However, the low absorption of C_{60} derivatives limits their potential. The use of C_{70} derivatives, instead of C_{60} allows higher absorption in the range of 380–700 nm significantly stronger over a wider range of the visible spectrum than C_{60}.[44]

Among polymers, poly(3-hexylthiophene) (P3HT) is the most intensely studied donor material. Power conversion efficiencies of about 5% have been achieved in P3HT/PCBM–based solar cells.[45]

---

[44] a) M. M. Wienk, J. M. Kroon, W. J. H. Verhees, J. Knol, J. C. Hummelen, P. A. van Hal, R. A. J. Janssen, *Angew. Chem. Int. Ed.* **2003**, *42*, 3371. b) S. Pfuetzner, J. Meiss, A. Petrich, M. Riede, K. Leo, *Appl. Phys. Lett.* **2009,** *94*, 223307.

[45] a) C. J. Brabec, N. S. Sariciftci, J. C. Hummelen, *Adv. Funct. Mater.* **2001**, *11*, 15. b) G. Li, Y. Yao, H. Yang, V. Shrotriya, G. Yang, Y. Yang, *Adv. Funct. Mater*. **2007**, *17*, 1636. c) M. H. Chen, J. Hou, Z. Hong,

In terms of enhancing the power conversion efficiency of BHJs, the design of new donor molecules with broad absorption and better charge transport properties is one of the most pursuit goals. Efficiencies of up to 7.4%[46] based on the polymer poly(dithienogermole-thienopyrrolodione) (PDTG-TPD) and 6.7%[47] based on the small molecule, namely, 5,5′-bis {(4-(7-hexylthiophen-2-yl)thiophen-2-yl)-[1,2,5]thiadiazolo [3,4-c]pyridine }-3,3′-di-2-ethylhexylsilylene- 2,2′-bithiophene, ($DTS(PTTh)_2$) have been recently achieved.

2.3. Phthalocyanines and Subphthalocyanines in Organic Solar Cells

Pcs are preferred photosensitizers for utilizing them as active component in solar cells.[48] Apart from their unique electronic properties, and chemical structure they show an extended photo response at 600-800 nm, where the photons flux is maximum. This means that only extremely thin films are necessary to absorb a substantial fraction of the solar photons. Pc-based solar cells can be prepared either by vacuum evaporation or solution processing techniques. Due to the strong interactions between ring systems, unsubstituted Pcs are practically insoluble in common organic solvents. Therefore, solar cells based on them cannot be easily prepared by solution processes. However, they have been successfully used as the active layer in vacuum-deposited small molecule solar cells. Conversely, solution-processing techniques are frequently used with chemically modified Pcs. The introduction of suitable substituents either in peripheral or in the axial position of the macrocycle, besides allowing modulating its electronic properties, increases the solubility of these compounds in organic solvents.

After the first reports of planar solar cells based on phthalocyanines and perylenebisimide derivatives, device performance was significantly increased by combination of planar and bulk heterojunction solar cells or stacking of different cells in

G. Yang, S. Sista, L. M. Chen, Y. Yang, *Adv. Mater*. **2009**, *21*, 4238. d) M. T. Dang, L. Hirsch, G. Wantz, *Adv. Mater*. **2011**, *23*, 3597.

46 C. E. Small, S. Chen, J. Subbiah, C. M. Amb, S. W. Tsang, T. H. Lai, J. R. Reynolds, F. So, *Nat. Photonics* **2012**, *6*, 115.

47 Y. Sun, G. C. Welch, W. L. Leong, C. J. Takacs, G. C. Bazan, A. J. Heeger, *Nat. Materials*. **2012**, *11*, 44.

48 a) M. V. Martínez-Díaz, T. Torres, *in Handbook of Porphyrin Science* (Eds.: K. Kadish, K. M. Smith, R. Guilard), World Scientific Press, Singapur, **2010**, Vol. 10, Chapter 45, pp 141-181. b) M. V. Martínez-Díaz, G. de la Torre, T. Torres, *Chem. Commun*. **2010**, *46*, 7090. c) M. G. Walter, A. B. Rudine, C. C. Wamser, *J. Porphyrins Phthalocyanines* **2010***, 14*, 759. d) H. Imahori, T. Umeyama, K. Kurotobi, Y. Takano, *Chem. Commun.* **2012**, *48,* 4032.

the tandem concept. For instance, a hybrid planar-mixed molecular heterojunction cell, sandwiching a mixed layer in between pure donor and acceptor layers, using CuPc and C_{60} gave the highest efficiency of 5%.[49] Particularly, tandem solar cells, (two hybrid planar-mixed molecular heterojunction cells stacked in series) consisting of CuPc/CuPc:C_{60} (1:1) / C_{60} as active layers provided increase efficiencies of up to 5.7%, which was about 15% higher than that of a single cell (Figure 16).[50]

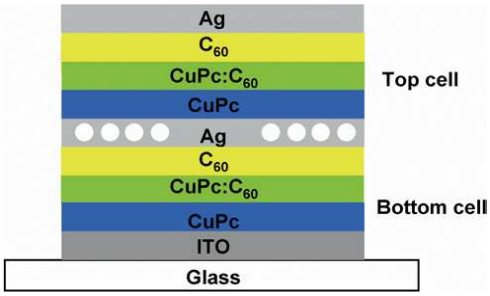

Figure 16. Schematic structure of the tandem organic solar cell realized by Forrest et al.

The Pcs derivatives mostly used for vacuum-deposited small-molecule solar cells are Cu and Zn complex that have similar absorption properties. The power conversion efficiency of a solar cell shows the importance of obtaining simultaneously a high Jsc and Voc. Therefore, researchers have concentrated their efforts on improving the limited open-circuit voltage. This clearly shows that there is still room for improvement of efficiency by modification of Pc structures.

Subphthalocyanines (SubPcs)[51] are lower homologues of Pcs comprising of a 14-π electron non-planar aromatic macrocycle consisting of three diiminoisoindole units *N*-fused around a central boron atom. In contrast with their related congeners, the planar Pcs, SubPcs possess a peculiar conical structure, which provides them with relatively high solubility and low tendency to aggregate (Figure 17). The important photochemical advantage of this class of compounds is based on their strong light

[49] J. Xue, B. P. Rand, S. Uchida, S. R. Forrest, *Adv. Mater*. **2005,** *17*, 68.
[50] J. Xue, S. Uchida, B. P. Rand, S. R. Forrest, *Appl. Phys. Lett.* **2004**, *85*, 23.
[51] a) A. Meller, A. Ossko, *Monatsh. Chem.* **1972**, *103*, 150. b) B. del Rey, U. Keller, T. Torres, G. Rojo, F. Agullo-Lopez, S. Nonell, C. Marti, S. Brasselet, I. Ledoux, J. Zyss, *J. Am. Chem. Soc*. **1998**, *120*, 12808. c) C. G. Claessens, T. Torres, *Chem. Eur. J.* **2000**, *6*, 2168. d) C. G. Claessens, D. González-Rodríguez, T. Torres, *Chem. Rev.* **2002**, *102*, 835. e) T. Torres, *Angew. Chem. Int. Ed.* **2006**, *45*, 2834.

absorption properties in the visible region (500-700 nm) which makes them to be an effective light harvesting material in the concept of artificial photosynthetic systems.[52]

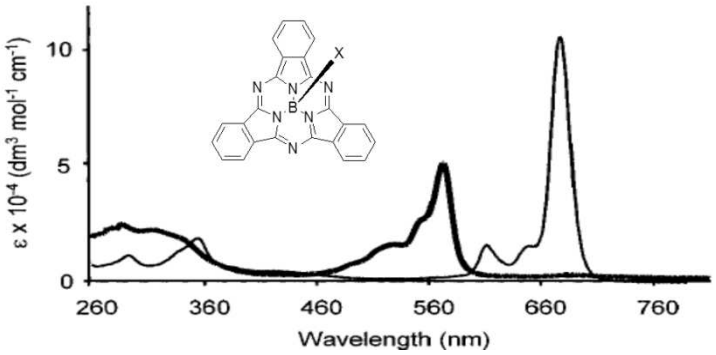

Figure 17. Chemical structure of SubPc and its UV-vis spectrum of (thick line) compared to the one of nickel phthalocyanine (thin line).

Additionally, their electronically rich π-conjugated system, and lower oxidation potential render them an excellent material for the production of solution processed small molecule OPVs.[53] In this regard, SubPcs appeared as an alternative active layer component in photovoltaic devices due to the high Voc values obtained by their introduction. The HOMO level of SubPc is -5.6 eV, and is shifted by approximately 400 meV compared to CuPc (HOMO: -5.2 eV), which leads to an increase of the Voc of nearly one volt.

Gommans *et al.* have reported efficient organic photovoltaic cells with a power conversion efficiency of 3% by using vacuum-deposited SubPc film as the electron

[52] a) D. González-Rodríguez, T. Torres, D. M. Guldi, J. Rivera, L. Echegoyen, *Org. Lett.* **2002**, *4*, 335. b) C. G. Claessens, T. Torres, *Chem Commun.* **2004**, *7*, 1298. c) D. Rodriguez, T. Torres, D. M. Guldi, J. Rivera, M. A. Herranz, L. Echegoyen, *J. Am. Chem. Soc*, **2004**, *126*, 6301. d) D. González-Rodríguez, C. G. Claessens, T. Torres, S. Liu, L. Echegoyen, N. Vila, S. Nonell, *Chem. Eur. J.* **2005***, 11,* 3881. e) R. S. Iglesias, C. G. Claessens, T. Torres, G. M. Rahman, D. M. Guldi, *Chem Commun.* **2005**, *28*, 2113. f) A. Medina, C. G. Claessens, G. M. A. Rahman, A. M. Lamsabhi, O. Mó, M. Yáñez, D. M. Guldi, T. Torres, *Chem. Commun.* **2008**, 1759. g) D. González-Rodríguez, E. Carbonell, G. De Miguel Rojas, C. Atienza Castellanos, D. M. Guldi, T. Torres, *J. Am. Chem. Soc.* **2010**, *132*, 16488.

[53] a) K. L. Mutolo, E. I. Mayo, B. P. Rand, S. R. Forrest, M. E, Thompson, *J. Am. Chem. Soc.* **2006,** *128*, 8108. b) C. E. Mauldin, C. Piliego, D. Poulsen, D. A. Unruh, C. Woo, B. Ma, J. L. Mynar, J. M. J. Fréchet, *Appl. Mater. Interfaces*, **2010**, *2*, 2833. c) E. B. Isaacs, S. Sharifzadeh, B. Ma, J. B. Neaton, *J. Phys. Chem. Lett.* **2011**, *2*, 2531.

donor and fullerene C_{60} as the electron acceptor.[54] More recently, cells with a power conversion efficiency of 3.7 % have been demonstrated by vacuum thermal evaporation of a uniform mixture of SubPc:C_{60} containing 80 wt.% C_{60} (Figure 18). The optimized performance was found to be originated from an improvement in the charge transport due to the formation of nanocrystalline domains of SubPc which likely exist through the depth of the mixture forming pathways for hole transport.[55]

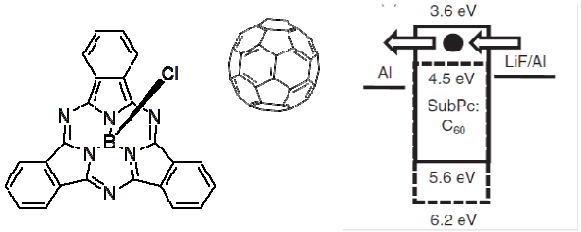

Figure 18. Molecular orbital energy level diagram for a SubPc:C_{60} mixture showing (a) electron transport along the lowest unoccupied molecular orbital (LUMO) of C_{60}.

However, in contrast to Pcs, SubPcs do not absorb light at wavelengths above 600 nm, thus limiting their photon harvesting capabilities, and in turn limiting the maximum obtainable Jsc. In this regard, subnaphthalocyanine (SubNc) is fulfilling this gap. While maintaining a high Voc, this macrocycle exhibit a broadening absorption compared to SubPcs. Consequently, a power conversion efficiency of 2.5%[56] in vacuum deposited and 1.5% in solution-processed PHJ were obtained in SubNc/C_{60} solar cells.[57] Further improvement of device performance has been achieved by using a combination of SubPcs and SubNcs in the tandem concept, producing efficiency of 5.15%.[58]

In another interesting example, Verreet *et al.* demonstrated that a fluorinated fused subphthalocyanine dimer (FSubPc Dimer) proved to be an exceptional novel

---

54 H. Gommans, D. Cheyns, T. Aernouts, C. Girotto, J. Poortmans, P. Heremans, *Adv. Funct. Mater*. **2007**, *17*, 2653.

55 R. Pandey, A. A. Gunawan, K. A. Mkhoyan, R. J. Holmes, *Adv. Funct. Mater.* **2012**, *22*, 617.

56 B. Verreet, S. Schols, D. Cheyns, B. P. Rand, H. Gommans, T. Aernouts, P. Heremans, J. Genoe, *J. Mater. Chem.* **2009**, *19*, 5295.

57 B. Ma, C. H. Woo, Y. Miyamoto, J. M. J. Fréchet, *Chem. Mater.* **2009***, 21*, 1413.

58 D. Cheyns, B. P. Rand, P. Heremans, *Appl. Phys. Lett.* **2010**, *97*, 033301.

acceptor material with complementary absorption to the SubPc donor material.[59] Compared to an optimized solar cell with C_{60} as an acceptor, this leads to an enhancement of 60% photocurrent due to contribution to the photocurrent of the low-bandgap FsubPc Dimer, while preserving the high open circuit voltage characteristic of SubPc-based devices. The best FFs were achieved by introducing a C_{60} interlayer in between FSubPc Dimer and bathocuproine (BCP), leading to a 4% efficient cell, which is quite high for cells with another acceptor than fullerene (Figure 19).

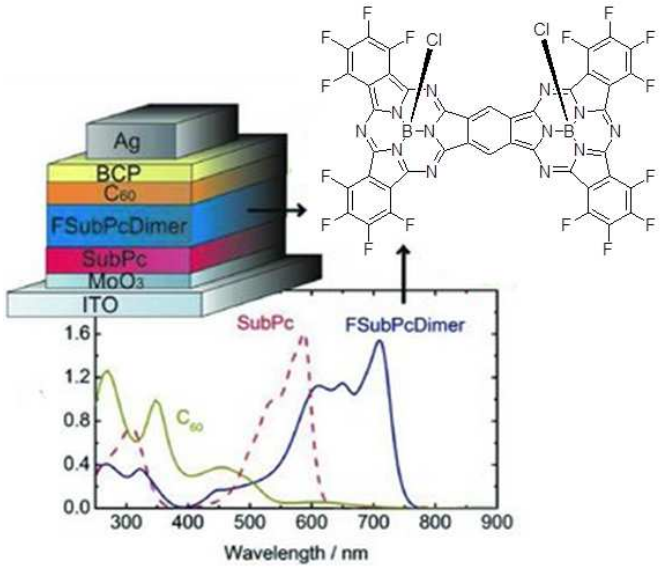

Figure 19. Planar solar cell based on FSubPc dimer.

In the case of solution-processed bulk heterojunction solar cells, there are only a few examples of soluble Pc derivatives blended with soluble acceptor materials to form a BHJ active layer.[60] In one example, SiPc has been used as the third component at the P3HT/PCBM interface to improve the light-harvesting efficiency. This device

[59] B. Verreet, B. P. Rand, D. Cheyns, A. Hadipour, T. Aernouts, P. Heremans, A. Medina, C. G. Claessens, T. Torres, *Adv. Energy Mater*. **2011**, *1*, 565.

[60] a) Q. Wang, Y. Li, X. Yan, M. Rathi, M. Ropp, D. Galipeau, J. Jiang, *Appl. Phys. Lett.* **2008**, *93*, 073303. b) F. Silvestri, I. Lopez-Duarte, W. Seitz, L. Beverina, M. V. Martinez-Diaz, T. J. Marks, D. M. Guldi, G. A. Pagani, T. Torres, *Chem. Commun*. **2009**, 4500. c) M. K. R. Fischer, I. Lopez-Duarte, M. M. Wienk, M. V. Martinez-Diaz, R. A. J. Janssen, P. Bauerle, T. Torres, *J. Am. Chem. Soc.* **2009**, *131*, 8669. d) A. Varotto, C-Y. Nam, I. Radivojevic, J. P. C. Tome, J. A. S. Cavaleiro, C. T. Black, C. M. Drain, *J. Am. Chem. Soc*. **2010**, *132,* 2552. e) A. Sánchez-Díaz, R. Pacios, U. Muñecas, T. Torres, E. Palomares, *Organic Electronics* **2011***, 12,* 329.

leads to substantial increased the short-circuit current density and hence improved the overall power conversion efficiency by 20%, compared to the P3HT/PCBM control device (Figure 20). These findings suggest that SiPc molecules serve not only as a light-harvesting photosensitizer but also as an energy funnel for P3HT excitons at the P3HT/PCBM interface. The key point for this success is also related to the use of a Pc dye with much reduced tendency to form aggregates due to the axial substituents.[61]

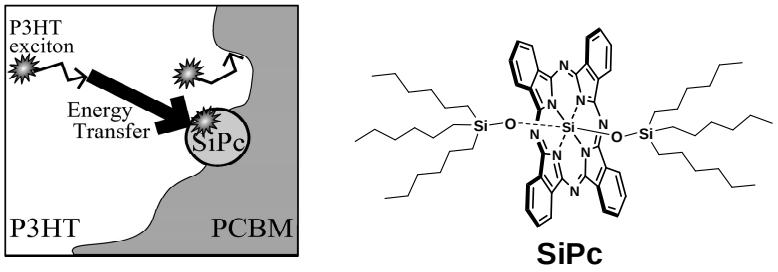

Figure 20. Schematic representation of a SiPc sensitized P3HT/PCBM solar cell.

2.4. Dye-Sensitized Solar Cells

Dye sensitized nanocrystalline TiO_2 solar cells, also known as Grätzel cells, combine semiconductor nanoparticules, on which an organic dye is adsorbed, and a redox electrolyte, to generate electricity from light.[62] In these devices, absorption of light by the dye sensitizer (S) generates an excited state (S*) which may either undergo the desired charge injection process (with rate k_1), or relax back to the ground state either by fluorescence or by non-radiative decay processes (with rate k_7). In order for charge injection to be successful, k_1 must be greater than k_7. Once the charge has been injected into the metal oxide conduction band, it may also undergo one of several fates, namely diffusion through the semiconducting metal oxide to the electrode (at rate k_2),

[61] S. Honda, T. Nogami, H. Ohkita, H. Benten, S. Ito, *Appl. Mater. Interfaces*, **2009**, *1*, 804.

[62] a) B. C. O'Regan, M. Grätzel, *Nature,* **1991**, *353*, 737. b) A. Hagfeldt, M. Grätzel, *Chem. Rev.* **1995**, *95*, 49. c) A. Hagfeldt, M. Grätzel, *Acc. Chem. Res*. **2000**, *33*, 269. d) M. Grätzel, *J. Photochem. Photobiol. C*, **2003**, *4*, 145. e) M. Grätzel, *J. Photochem. Photobiol. A,* **2004**, *164*, 3. f) M. Grätzel, *Inorg. Chem.* **2005**, *44*, 6841. g) N. Robertson, *Angew. Chem. Int. Ed.* **2006**, *45*, 2338. h) N. Robertson, *Angew. Chem. Int. Ed*. **2008**, *47*, 1012. i) B. C. O´Regan, J. R. Durrant, *Acc. Chem. Res*. **2009**, *42*, 1799. j) H. J. Snaith, *Adv. Funct. Mater*. **2010**, *20*, 13. k) A. Listorti, B. O`Regan, J. R. Durrant, *Chem. Mater*. **2011**, *23*, 3381.

recombination with the dye cation (k_6), or reduction of the redox couple I_3^-/I^- (at rate k_5) giving rise to a dark current. In order for a DSSC to operate efficiently, k_2 must be faster than both k_5 and k_6, as these undesirable competing processes reduce the number of electrons taking part in the operational cycle, thereby reducing both the short-circuit current density (J_{SC}) and the open-circuit voltage (V_{OC}). Provided k_5 and k_6 are slower than k_2 and k_3, the oxidised dye will be reduced by the redox couple I_3^-/I^-. The circuit is completed by hole migration from I_3^-/I^- to the cathode in a process with rate k_4 (Figure 21).

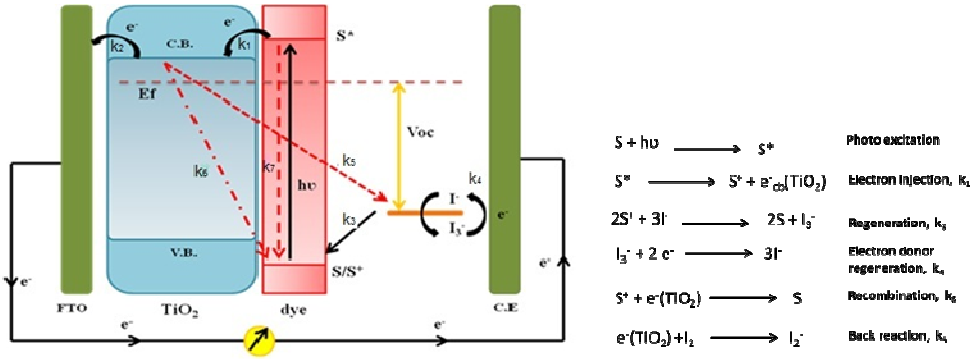

Figure 21. Schematic diagram of DSSCs. Electron-transfer processes are indicated with black arrows. Unwanted back-reactions are indicated with red arrows. k_1 =charge injection from the excited state of the dye into the metal oxide conduction band, k_2 = diffusion of electrons through metal oxide, k_3 = regeneration of dye, k_4 = hole migration from redox couple to cathode, k_5= reduction of redox couple I_3^-/I^- by electrons from the metal oxide conduction band, k_6 = recombination of dye cation with electrons from the metal oxide conduction band, k_7 = relaxation of excited state of the dye to its ground state.

2.4.1. Factors Affecting DSSC Efficiency

As can been seen from the above, the efficiency of a DSSC depends on a complex interplay of factors. Apart from the rates of the injection and regeneration steps with respect to the recombination and dark current processes, the nature of the metal oxide layer, the choice of electrolyte, and the dye sensitizer affecting DSSC efficiency.

Titanium dioxide (anatase) is the most common metal oxide used in DSSC devices, although other oxides such as zinc oxide (ZnO)[63] and tin oxide (SnO_2)[64] have also been used, the latter one exhibiting a conduction band around 0.5 eV lower in energy than titanium dioxide. Tin oxide can therefore be used in DSSCs incorporating dyes with low energy excited states, although such systems would be expected to exhibit a lower open circuit voltage (*V*oc).

The composition of the liquid electrolyte is also a key parameter for liquid electrolyte DSSCs. The I^-/I_3^- redox couple is mostly employed due to its slow rate of recombination with electrons from the titanium dioxide, its rapid rate of dye regeneration, and its fast kinetics of electron uptake at the cathode. However, in order to overcome the volatility problem of iodine and the electrolyte solvent, the cells must be sealed. In addition, the I^-/I_3^- redox couple can be corrosive towards the platinum electrode. Another drawback is the loss of the voltage during generation and the lack of long-term stability. For all these reasons, alternative redox couples are explored. The use of the other redox couple such as Br^-/Br_2, and $SeCN^-/(SeCN)_3^-$ has shown to give larger V_{OC} values than I^-/I_3^- due to their more positive redox potential. However devices incorporating them have been found to display rather low efficiencies.[65] Transition metal based systems such as cobalt complexes [Co (II/III)] have drawn attention due to higher oxidation potentials than that of I^-/I_3^-. Moreover the chemical stability, nonvolatility, tunability of physical chemical properties (i.e. redox potential, solubility and size) and noncorrosive nature of this redox couple make them favorable alternatives to the I^-/I_3^- system.[66] Very recently, Gratzel *et al*. achieved over 1 mV of Voc with cells by using a tridendate ligand cobalt complex as redox mediator in combination with a

---

63 a) G. Redmond, A. Okeeffe, C. Burgess, C. Machale, D. Fitzmaurice, *J. Phys. Chem*. **1993**, *97*, 11081. b) C. Bauer, G. Boschloo, E. Mukhtar, A. Hagfeldt, *Chem. Phys. Lett.* **2004**, *387*, 176. c) H. M. Nguyen, R. S. Mane, T. Ganesh, S. H. Han, N. Kim, *J. Phys. Chem. C.* **2009**, *113,* 9206.

64 a) K. Tennakone, G. R. R. Kumara, I. R. M. Kottegoda, V. S. P. Perera, *Chem. Commun.* **1999**, 15. b) A. Kay, M. Grätzel, *Chem. Mater.* **2002**, *14*, 2930. c) A. N. M. Green, E. Palomares, S. A. Haque, J. M. Kroon, J. R. Durrant, *J. Phys. Chem. B*, **2005**, *109*, 12525.

65 a) N. Vlachopoulos, P. Lisca, J. Augustynski, M. Grätzel, *J. Am. Soc*. **1988**, *110*, 1216. b) K. Hara, T. Horiguchi, T. Kinoshita, K. Sayama, H. Arakawa, *Sol. Energy Mater. Sol. Cells.* **2001**, *70*, 151. c) P. Wang, S. M. Zakeeruddin, J. E. Moser, R. Humphry-Baker, M. Grätzel, *J. Am. Chem. Soc*. **2004**, *126*, 7164. d) B. V. Bergeron, A. Marton, G. Oskam, G. J. Meyer, *J. Phys. Chem. B.* **2005**, *109*, 937. e) S. Yanagida, Y. Yu, K. Manseki, *Acc. Chem. Res.* **2009**, *42,* 1827.

66 a) H. Nusbaumer, J. E. Moser, S. M. Zakeeruddin, M. K. Nazeeruddin, M. Grätzel, *J. Phys. Chem. B.* **2001,** *105*, 10461. b) P. Wang, S. M. Zakeeruddin, P. Comte, R. Charvet, R. Humphry-Baker, M. Grätzel, *J. Phys. Chem. B.* **2003,** *107,* 14336. c) M. Zhang, J. Liu, Y. Wang, D. Zhou, P. Wang, *Chem. Sci*. **2011**, *2*, 1401.

cyclopentadithiophene-bridged donor-acceptor dye, adsorbed on TiO_2. A power conversion efficiency of over 10% was achieved.[67]

In DSSCs, the photovoltage (V_{OC}) is determined by the difference between the quasi Fermi level of TiO_2 and the redox potential of the electrolyte. The introduction of co-adsorbants, typically Li+, 4-tert-butylpyridine, 3α,7α-dihydroxy-5β-cholic acid (CHENO) changes the energy band of TiO_2, hence, altering the Voc and Jsc values. In particular, the concentration of lithium salts has been demonstrated to have a strong influence on the performance of DSSCs. Lithium ions affect the energy of the conduction band, shifting the potential towards more positive values by up to one volt (depending on the ion concentration) (Figure 22). The shifts in the conduction band potential of TiO_2 induced by lithium ions, makes electron injection from the sensitizer into the conduction band more thermodynamically favorable.[68] This characteristic is particularly useful for increasing the electron injection rate of sensitizers with excited state oxidation potentials close to the reduction potential of bare titanium dioxide. However it reduces the open circuit voltage, hence a balance of these factors must be considered when optimizing the efficiency of a device. On the other hand, 4-*tert*-butylpyridine (4TBP) or tetrabutylammonium (TBA) produces an increase the open circuit voltage by shifting the conduction band of the TiO_2 to higher energies (Figure 22).[69]

---

67 J. H. Yum, E. Baranoff, F. Kessler, T. Moehl, S. Ahmad, T. Bessho, A. Marchioro, E. Ghadiri, J. E. Moser, C. Yi, M. K. Nazeeruddin, M. Grätzel, *Nature Commun.* **2012**, *3*, 631.

68 a) Y. Tachibana, S. A. Haque, I. P. Mercer, J. E. Moser, D. R. Klug, J. R. Durrant, *J. Phys. Chem. B.* **2001**, *105*, 7424. b) D. F. Watson, G. J. Meyer, *Coord. Chem. Rev.* **2004**, *248*, 1391. c) R. Katoh, A. Furube, M. Kasuya, N. Fuke, N. Koide, L. Han, *J. Mater. Chem*. **2007**, *17*, 3190. d) S. E. Koops, B. C. O'Regan, J. R. Durrant, *J. Am. Chem. Soc*. **2009**, *131*, 4808.

69 a) G. Schlichthörl, S. Y. Huang, J. Sprague, A. J. Frank, *J. Phys. Chem. B.* **1997,** *101,* 8141. b) H. Kusama, H. Arakawa, S*ol. Energy Mater. Sol. Cells,* **2004**, *81*, 87. c) N. R. Neale, N. Kopidakis, J. Van de Lagematt, M. Grätzel, A. J. Frank, *J. Phys. Chem. B,* **2005**, *109*, 23183. d) A. N. M. Green, R. E. Chandler, S. A. Haque, J. Nelson, J. R. Durrant, *J. Phys. Chem. B.* **2005**, *109*, 142. e) G. Boschloo, L. Häggman, A. Hagfeldt, *J. Phys. Chem. B.* **2006**, *110*, 13144.

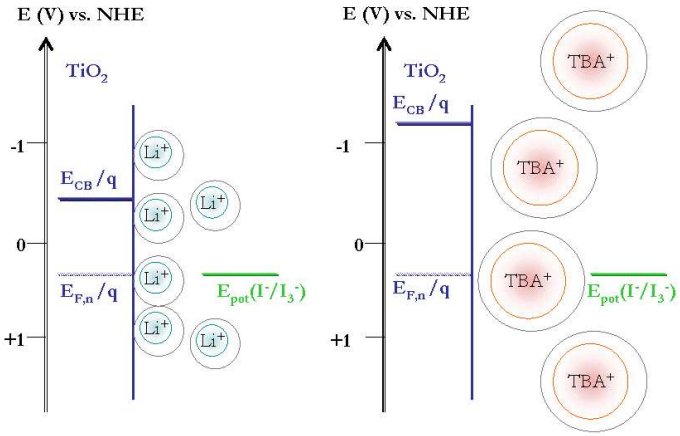

Figure 22. Schematic energy level diagram showing the positions of TiO_2 in the presence of lithium (Li^+) and tetrabutylammonium (TBA^+) additive.

The 3α,7α-dihydroxy-5β-cholic acid (CHENO) (Figure 23) has been successfully applied as co-adsorbent in DSSCs to prevent aggregation of the dye on the TiO_2 surface. CHENO bears a carboxylic acid functional group that allows its strong binding to the TiO_2 surface, in competition to the dye molecules. The addition of CHENO not only shifts the TiO_2 conduction band edge to negative potentials but also it breaks the dye aggregates, thus improving the electron injection into the semiconductor. It also decreases the recombination process at the TiO_2 surface. Therefore, it produces a remarkable increase in the photocurrent and in the photovoltage.[69a,70]

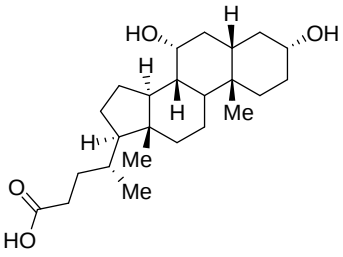

Figure 23. Molecular structure of CHENO coadsorbant.

[69] a) G. Schlichthörl, S. Y. Huang, J. Sprague, A. J. Frank, *J. Phys. Chem. B.* **1997,** *101,* 8141

[70] a) Z. S. Wang, Y. Cui, Y. Dan-oh, C. Kasada, A. Shinpo, K. Hara, *J. Phys. Chem.* C. **2007**, *111*, 7224. b) J. H. Yum, S. J. Moon, R. Humphry-Baker, P. Walter, T. Geiger, F. Nüesch, M. Grätzel, M. K. Nazeeruddin*, Nanotechnology* 2008, *19*, 424005.

2.4.2. DSSCs with Solid Electrolytes

Research on solid-state DSSCs has gained considerable attention. The advantage over liquid state devices is the avoidance of solvent evaporation, leakage, and electrode corrosion. The operating mechanism of is very similar to liquid based devices, that is, upon photoexcitation of the dye, electron injection from sensitizer into the TiO_2 is followed by regeneration of the dye by hole injection into the hole transporting material (HTM). Figure 24 shows the electronic process in ss-DSSCs.[71] However, HTM has several disadvantages. For example, since most HTMs are solids, one of the main problems is the pore filling within the TiO_2 layer which leads to incomplete dye regeneration, hence cause lower photocurrent and poor stability. Generally, the hole mobility is lower than that of liquid electrolyte. Furthermore, the difficulties in the infiltration of the organic HTM into the mesoporous layer limit the thickness of TiO_2 films in ss-DSSCs to only about 2 μm, which decreases the light harvesting capability and, therefore, the power conversion efficiencies.

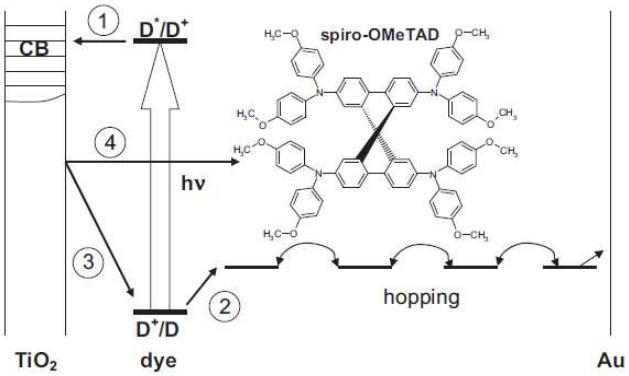

Figure 24. Schematic energy diagram for the electronic processes in the ss-DSSC

On the other hand, high Voc (1 V) values are obtained, due to the better match of the redox potential of the HTM with that of the sensitizer comparing to the I^-/I_3

[71] a) U. Batch, D. Lupo, P. Compte, J. E. Moser, F. Weissortel, J. Salbeck, H. Spreitzer, M. Grätzel, *Nature*, **1998**, *395*, 538. b) H. J. Snaith, L. Schmidt-Mende, *Adv. Mater.* **2007**,*19*, 3187. c) H. J. Snaith, C. Ducati, *Nano Lett.* **2010**, *10*, 1259.

couple.[72] A variety of organic hole transporting materials (HTM) such as, inorganic solids or conjugated polymers have been tested in ss-DSSCs.[73] The best overall efficiency of 5% has been achieved by using spiro-OMeTAD, with heteroleptic ruthenium sensitizer.[74] Hence, HTMs sytem are promising alternatives to liquid electrolyte if pore filling and recombination problems can be solved.

2.4.3. p- Type DSSCs

General construction of DSSCs, as already described previously, is based on wide band-gap n-type metal oxide semiconductors such as TiO_2 coated with a dye molecule. Alternatively, another type of DSSCs, based on a p-type semiconductor has emerged as a new generation of photochemical cells.[75] NiO has been widely used as p-type semiconductor due to its wide bandgap, good thermal and chemical stability.

The basic requirements of p-type DSSCs are: i) the HOMO level of the dye must be below the valence band of the p-semiconductor, ii) the LUMO level must be higher in energy than the redox potential of the electrolyte system to provide sufficient driving force for hole injection and dye regeneration. As shown in Figure 25, the working principle of p-DSSCs is the reverse mode of n-DSSCs. In that, upon excitation, the electrons flow from the excited dye to the electrolyte, and the ground state of the dye regenerated by electron transfer from valence band of a p-type semiconductor.[76]

---

[72] P. Chen, J. H. Yum, F. De Angelis, E. Mosconi, S. Fantacci, S. J. Moon, R. H. Baker, J. Ko, M. K. Nazeeruddin, M. Grätzel, *Nano Lett.* **2009***, 9,* 2487.

[73] a) B. O'Regan, D. T. Schwartz, S. M. Zakeeruddin, M. Grätzel, *Adv. Mater.* **2000**, *12*, 1263. b) Q. Meng, K. Takahashi, X. Zhang, I. Sutanto, T. Rao, O. Sato, A. Fujishima, H. Watanabe, T. Nakamori, M. Uragami, *Langmuir*, **2003**, *19*, 3572. c) K. J. Jiang, K. Manseki, Y. H. Yu, N. Masaki, J. B. Xia, L. M. Yang, Y. L. Song, S. Yanagida, *Adv. Funct. Mater*. **2009**, *19,* 2481. d) X. Liu, W. Zhang, S. Uchida, L. Cai, B. Liu, S. Ramakrisha, *Adv. Mater*. **2010,** *22*, E150.

[74] a) H. J. Snaith, A. J. Moule, C. Klein, K. Meerholz, R. H. Friend, M. Grätzel, *Nano Lett.* **2007**, *7,* 3372. b) M. Wang, C. Grätzel, S. Moon, R. Humphry-Baker, N. Rossier-Iten, S. M. Zakeeruddin, M. Grätzel, *Adv. Funct. Mater.* **2009**, *19,* 2163. c) M. Wang, S. J. Moon, D. Zhou, F. L. Formal, N. L. Cevey-Ha, R. Humphry-Baker, C. Grätzel, P. Wang, S. M. Zakeeruddin, M. Grätzel, *Adv. Funct. Mater.* **2010**, *20*, 1821.

[75] a) A. Nakasa, H. Usami, S. Sumikiro, S. Hasegawa, T. Koyama, E. Suzuki, *Chem. Lett.* **2005**, *34,* 500. b) P. Quin, J. Wiberg, E. A. Gibson, M. Linder, L. Li, T. Brinck, A. Hagfeldt, B. Albinsson, L. Sun, *J. Phys. Chem. C.* **2010**, *114*, 4738.

[76] a) A. Mishra, M. K. R. Fischer, P. Bauerle, *Angew. Chem. Int. Ed.* **2009**, *48*, 2474. b) F. Odobel, L. L. Pleux, Y. Pellegrin, E. Blart, *Acc. Chem. Res*. **2010**, *43*, 1063. c) Z. Huang, G. Natu, Z. Ji, P. Hasin, Y. Wu, *J. Phys. Chem. C***, 2011**, *115*, 25109.

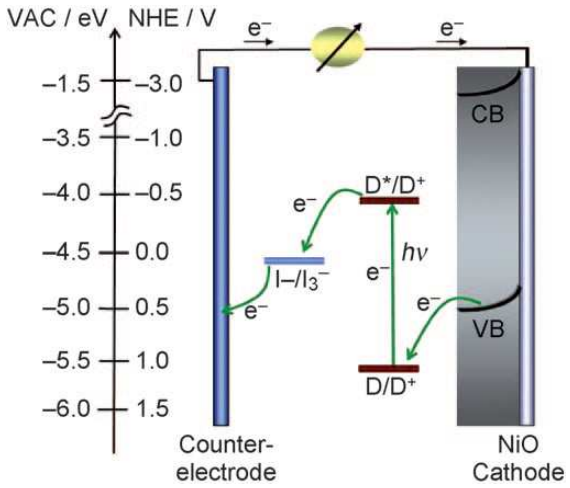

Figure 25. Energy-level diagram of a DSSc with a p-type NiO semiconductor electrode.

Although several different dyes such as triphenylamine based chromophores,[77] coumarins,[78] peryleneimides[79] and porphyrins[80] have been used as the sensitizers, the p-type DSSCs suffer from lower efficiency compared to conventional TiO_2 cells. The small difference in potential between the Fermi level in the semiconductor and redox potential of the electrolyte cause the low Voc (0.1V). Moreover, low currents due to the fast charge recombination and low light harvesting efficiency owing to the low dye loading on the NiO film limit the overall efficiencies.[77-80] Up to now, a maximum IPCE of 64% has been reported by Sun and coworkers.[81] This cell consisting of NiO films coated with a push-and-pull designed p-type organic dye (P1: triphenylamine donor and a malononitrile acceptor) (Figure 26) gave Jsc value of 5.48, Voc value of 84 mV and overall efficiency of 0.15%.

---

77 a) P. Qin, M. Linder, T. Brinck, G. Boschloo, A. Hagfeldt, L. Sun, *Adv. Mater.* **2009**, *21*, 2993. b) Y. S. Yen, W. T. Chen, C. Y. Hsu, H. H. Chou, J.T. Lin, M. C. P. Yeh, *Org. Lett*. **2011**, *13*, 4930.

78 a) A. Morandeira, G. Boschloo, A. Hagfeldt, L. Hammarström, *J. Phys Chem. B.* **2005**, *109,* 19403. b) S. Mori, S. Fukuda, S. Sumikura, Y. Takeda, Y. Tamaki, E. Suzuki, T. Abe, *J. Phys. Chem. C*. **2008**, *112*, 16134. c) A. Morandeira, G. Boschloo, A. Hagfeldt, L. Hammarstrom, *J. Phys. Chem. C.* **2008**, *112,* 9530.

79 a) A. Morandeira, J. Fortage, T. Edvinsson, L. L. Pleux, E. Blart, G. Boschloo, A. Hagfeldt, L. Hammarstrom, F. Odobel, *J. Phys. Chem. C.* **2008**, *112*, 1721. b) A. L. Smeigh, L. L. Pleux, J. Fortage, Y. Pellegrin, E. Blart, F. Odobel, L. Hammarstrom, *Chem. Commun*. **2012**, *48*, 678.

80 a) J. He, H. Lindstrom, A. Hagfeldt, S. E. Lindquist, *J. Phys. Chem. B.* **1999**, *103*, 8940. b) M. Borgstrom, E. Blart, G. Boschloo, E. Mukhtar, A. Hagfeldt, L. Hammarstrom, F. Odobel, *J. Phys. Chem. B.* **2005**, *109*, 22928.

81 a) P. Qin, H. Zhu, T. Edvinsson, G. Boschloo, A. Hagfeldt, L. Sun, *J. Am. Soc.* **2008**, *130*, 8570. b) L. Li, E. A. Gibson, P. Qin, G. Boschloo, A. Hagfeldt, L. Sun, *Adv. Mater.* **2010**, *22*, 1759.

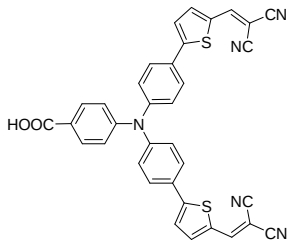

Figure 26. Molecular structure of P1 dye employed in p-type DSSCs.

Alternatively, the combination of a NiO based photoactive cathode with a TiO_2 based photoanode produces tandem dye sensitized solar cells which appears as a possible way to capture more light and improve the Voc.[82]

It has been reported that cobalt based redox couples can increase the photovoltage obtained from p-type DSSC due to the more negative potential compared to I^-/I_3^-.[83] Using the cobalt complex and the perylene based dyed on the NiO photoanode, the device exhibits threefold increase in Voc (0.35 V), while maintaining a Jsc of 1.7 $mAcm^{-2}$. Combining of this cell with a ruthenium complex on the TiO_2 photocathode in the concept of tandem cell, the Voc reached 910 mV.[84] However, the best photoconversion efficiency in tandem cells was recently obtained with the oligothiophene-perylenemonoimide dyad (Figure 27) and I^-/I_3^- electrolyte. The cell reached a 4.07 $mAcm^{-2}$ photocurrent, a 958 mV open circuit voltage and 2.42% efficiency.[85]

[82] a) J. He, H. Lindström, A. Hagfelt, S. E. Lindquist, *Sol. Energy. Mater. Sol. Cells*, **2000**, *62*, 265. b) A. Nattestad, M. Ferguson, R. Kerr, Y. B. Cheng, U. Bach, *Nanotechnology,* **2008**, *19*, 295304.

[83] E. A. Gibson, A. L. Smeigh, L. L. Pleux, L. Hammarsröm, F. Odobel, G. Boschloo, A. Hagfeldt, *J. Phys. Chem. C*. **2011**, *115*, 9772.

[84] E. A. Gibson, A. L. Smeigh, L. L. Pleux, J. Fortage, G. Boschloo, E. Blart, Y. Pellegrin, F. Odobel, A. Hagfeldt, L. Hammarstrom, *Angew. Chem. Int. Ed.* **2009**, *48*, 4402.

[85] A. Nattestad, A. J. Mozer, M. K. R. Fischer, Y. B. Cheng, A. Mishra, P. Bauerle, U. Bach, *Nat. Mat.* **2010**, *9*, 31.

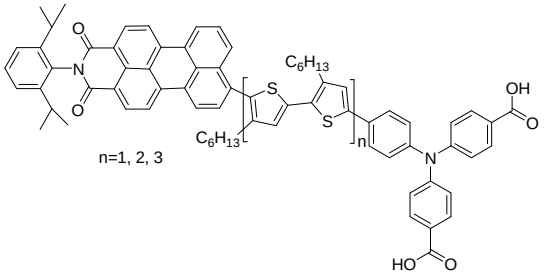

Figure 27. Molecular structure of the oligothiophene-perylenemonoimide dyad for p-type DSSCs.

2.4.4. Sensitizers for DSSCs

Obviously, a vital component of a DSSC is the dye sensitizer. Efficient photosensitizers are based on the following requirements [86]

- Its absorption spectrum should cover the whole visible region and even the part of near-infrared (NIR).
- It should have anchoring group such as –COOH, -PO_3H_2,- SO_3H to strongly bind the dye onto the semiconductor surface.
- Its excited state level of the photosenstizer should be higher in energy than the conduction band edge of semiconductor to take place efficient electron transfer process.
- For dye regeneration, the oxidized state level of the photosensitizer must be more positive than the redox potential of electrolyte.
- Unfavorable dye aggregation on the semiconductor surface should be avoided through optimization of the molecular structure of the dye or by addition of co-adsorbers that prevent aggregation.
- It should be photostable, and electrochemical and thermal stability are required.

Over the years, the most successful sensitizers employed in these cells have been ruthenium (II) polypyridyl-type complexes such as **N719** (Figure 28), achieving power conversion efficiencies around 12% in the presence of a volatile acetonitrile-based electrolyte. [87] Moreover, the introduction of hydrophobic alkyl chains on the bipyridyl ligand has been a key point not only for increasing the stability towards water-

[86] A. Hagfelt, G. Boschloo, L. Sun, L. Kloo, H. Pettersson, *Chem. Rev.* **2010**, *110*, 6595.
[87] M. K. Nazeeruddin, F. De Angelis, S. Fantacci, A. Selloni, G. Viscardi, P. Liska, S. Ito, B. Takeru, M. Grätzel, *J. Am. Chem. Soc.* **2005**, *127*, 16835.

induced dye desorption, but also repel iodide from the TiO_2-surface and thus reduce the recombination rate and give good efficiencies up to 8.2% under AM1.5 solar irradiation. Both features are, with no doubt, a major breakthrough in the potential outdoor applications of DSSCs.[88] The need of anchoring functions for attaching the dye to the semiconductor surface has been also demonstrated. In particular, carboxylate groups have shown very good electronic coupling between the π^* orbital of the electronically excited complex and the 3d orbitals of the TiO_2 film.

Despite the high efficiencies of these systems, there are several disadvantages, which arise from using ruthenium-based dyes. Ruthenium is a rare metal with limited resources indicating future problems with both supply and cost.[89] Second, ruthenium complexes are toxic a setback for production and disposal/recycling of the devices. In addition, ruthenium based dyes exhibit poor absorption in the near-IR that is a problem since around 50% of solar energy falls beyond 750 nm. Because of these drawbacks, efforts have been directed towards the synthesis of organic dyes which are either metal free, or which incorporate a cheap metal, to result in a non-toxic chromophore.

During the last decade, an impressive synthetic effort has been carried out on the development of various types of expensive ruthenium metal free organic dye sensitizers for DSSCs, achieving a remarkable progress in the comprehension about the relationship between the molecular structure and photovoltaic performance.[90] In particular, donor-acceptor organic molecules such as **JK2** (Figure 28) possessing both electron-donating and electron-withdrawing groups linked by π-conjugated linkers have

---

88 Y. Bai, Y. Lao, J. Zhang, M. Wang, R. Li, P. Wang, S. M. Zakeeruddin, M. Grätzel, *Nat Mater*, **2008**, *7,* 626.

89 a) N. Koumura, Z. S. Wang, S. Mori, M. Miyashita, E. Suzuki, K. Hara, *J. Am. Chem. Soc.* **2006**, *128*, 14256. b) H. Imahori, T. Umeyama, S. Ito, *Acc. Chem. Res.* **2009**, *42*, 1809. c) H. Tian, X. Yang, R. Chen, A. Hagfeldt, L. Sun, *Energy Environ. Sci.* **2009**, *2*, 674.

90 a) S. Kim, J. K. Lee, S. O. Kang, J. Ko, J. H. Yum, S. Fantacci, F. De Angelis, D. Di Censo, M. K. Nazeeruddin, M. Grätzel, *J. Am. Chem. Soc.* **2006**, *128*, 16701. b) S. Ito, S. M. Zakeeruddin, R. Humphry-Baker, P. Liska, R. Charvet, P. Comte, M. K. Nazeeruddin, P. Péchy, M.Takata, H. Miura, S. Uchida, M. Grätzel, *Adv. Mater.* **2006**, *18*, 1202. c) A. Burke, L. Schimidt-Mende, S. Ito, M. Grätzel, *Chem. Commun.* **2007**, 234. d) H. Choi, C. Baik, S. O. Kang, J. Ko, M. S. Kang, M. K. Nazeeruddin, M. Grätzel, *Angew. Chem. Int. Ed.* **2008**, *47*, 327. e) Y. Ooyama, Y. Harima, *Eur. J. Org. Chem*. **2009**, 2903. f) G. Zhang, H. Bala, Y. Cheng, D. Shi, X. Lv, Q. Yu, P. Wang, *Chem. Commun*. **2009**, 2198. g) M. K. R. Fischer, S. Wenger, M. Wang, A. Mishra, S. M. Zakeeruddin, M. Grätzel, P. Bäuerle, *Chem. Mater*. **2010**, *22*, 1836. h) S. Paek, H. Choi, C. Kim, N. Cho, S. So, K. Song, M. K. Nazeeruddin, J. Ko, *Chem. Commun*. **2011**, *47*, 2874.

shown power conversion efficiencies of up to 9.5% in liquid DSSCs. However, there is still a need to optimize these devices.

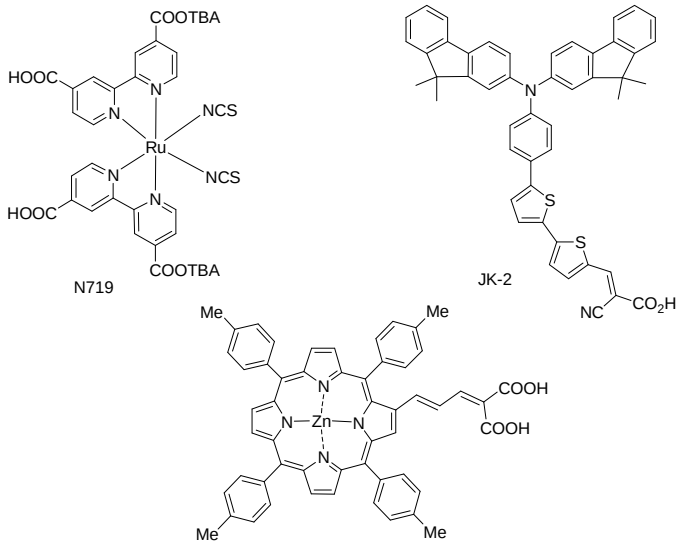

Figure 28. Molecular structure of some of the successful DSSC dyes.

Improvement of the devices performance has also been limited by the light-harvesting capability of the state-of-the-art dyes, which lack strong absorption in the red/near infrared region where the solar flux of photons is maximum. Dyes like porphyrinoids which have a high molar extinction coefficient in this spectral region would allow the preparation of thinner devices, minimizing charge recombination during the transport of charges to the electrode. Porphyrins are one of class of compounds, which has received much attention for application in the field of DSSCs. Their similarity to the structure of chlorophylls makes these chromophores an obvious choice for such devices. These natural occurring macrocycles are highly conjugated heteroaromatic compounds with a very intense absorption in the visible region (namely a strong Soret band centered between 400-500 nm and a moderate Q band in the spectral region 550-650 nm) and, therefore, are deeply colored. Many porphyrin models have been prepared in order to understand the natural system and, in many cases, as a means of

developing solar energy conversion systems.[91] Grätzel and Kay already reported in 1993 efficiencies of 2.6% for porphyrin-based DSSCs.[92] The improvement of efficiency up to 7.1% was achieved by using porphyrin bearing a conjugated bearing malonic acid binding group at the β-pyrrolic position (Figure 28).[93] The performance of these devices has been improved along the years up to 11% by rational push-pull design of the porphyrin structure at *meso* position, which facilitates charge transfer through the full conjugated system.[94]

2.4.5. Phthalocyanines as DSSCs sensitizers

Phthalocyanines have been widely used as sensitizers due to their improved light-harvesting properties in the far red- and near IR spectral region and their extraordinary robustness. However, efficiency values of Pc-based DSSCs are in general below those made of their porphyrin relatives although the reasons have not yet been rationalized.

The first examples of DSSCs based on Zn(II) phthalocyanines were performed by Grätzel, Wöhrle *et al* (Figure 29).[95a] The efficient injection of electrons from the excited state of $ZnPc(COOH)_4$ to the conduction band of the TiO_2 gave an acceptable efficiency in the near IR region (700 nm), reaching maximum photocurrent conversion of 45%. However, the tendency of Pcs to form aggregates, also on the metal oxide semiconductor surface, provoked problems associated with deactivation of the excited dye, therefore an overall conversion efficiency of 1% was achieved under full AM 1.5

---

91 a) W. M. Campbell, A. K. Burrell, D. L. Officer, K. W. Jolley, *Coord Chem Rev*. **2004**, *248*, 1363 b) M. K. Nazeeruddin, R. Humphry-Baker, D. L. Officer, W. M. Campbell, A. K. Burrell, M. Grätzel, *Langmuir*, **2004**, *20*, 6514. c) L. Schmidt-Mende, W. M. Campbell, Q. Wang, K. W. Jolley, D. L. Officer, M. K. Nazeeruddin, M. Grätzel, *ChemPhysChem,* **2005**, *6*, 1253. d) L. Giribabu, C. V. Kumar, M. Raghavender, K. Somaiah, P. Yella, P. V. Rao, *J. Chem. Sci*. **2008**, *120*, 455. e) S. Hayashi, Y. Matsubara, S. Eu, H. Hayashi, T. Umeyama, Y. Matano, H. Imahori, *Chem. Lett.* **2008**, *37*, 846. f) S. Hayashi, M. Tanaka, H. Hayashi, S. Eu, T. Umeyama, Y. Matano, Y. Araki, H. Imahori, *J. Phys. Chem. C.* **2008**, *112*, 15576. g) C. Y. Lin, C. F. Lo, L. Y. Luo, H. P. Lu, C. S. Hung, E. W. Diau, *J. Phys. Chem. C*. **2009**, *113*, 755. h) M. Ishida, S. W. Park, D. Hwang, Y. B. Yoo, J. L. Sessler, D. Y. Kim, D. Kim, D. *J. Phys. Chem. C.* **2011**, *115*, 19343.

92 A. Kay, M. Grätzel, *J. Phys. Chem*. **1993**, *97*, 6272.

93 W. M. Campbell, K. W. Jolley, P. Wagner, K. Wagner, P. J. Walsh, K. C. Gordon, L. Schmidt Mende, M. K. Nazeeruddin, Q. Wang, M. Grätzel, D. L. Officer, *J. Phys. Chem. C.* **2007***, 111*, 11760.

94 T. Bessho, S. M. Zakeeruddin, C. Y. Yeh, E. W. G. Diau, M. Grätzel, *Angew. Chem. Int Ed.* **2010**, *49*, 6646.

95 a) M. K. Nazeeruddin, R. Humphry-Baker, M. Grätzel, D. Wöhrle, G. Schnurpfeil, G . Schneider, A. Hirth, N. Trombach. *J. Porphyrins Phthalocyanines* **1999**, *3*, 230. b) J. He, G. Benkö, F. Korodi, T. Polivka, R. Lomoth, B. Åkermark, L. Sun, A. Hagfeldt, V. Sundstrom, *J. Am. Chem. Soc.* **2002**, *124*, 4922.

solar light. In this regard, in order to minimize the aggregation, phthalocyanine ZnPcTyr, peripherally substituted by four tyrosine groups was prepared by the group of Sundstrom (Figure 29).[95b] However, an overall conversion efficiency of only 0.54% was achieved for a cell based on a ZnPcTyr-sensitized TiO_2 electrode.

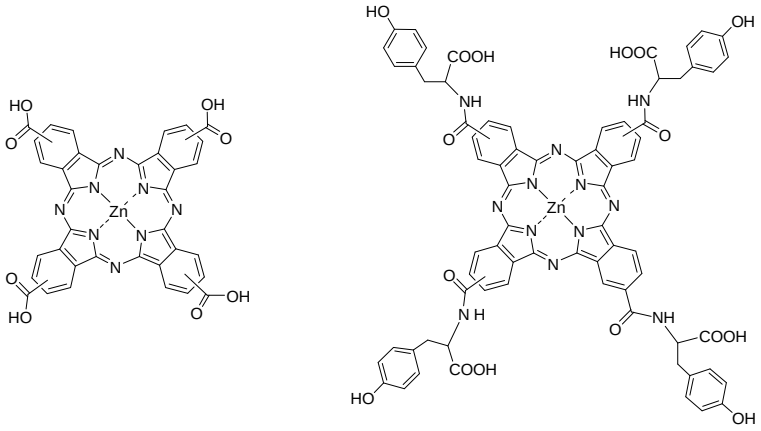

Figure 29. Molecular structures of some ZnPc(COOH)₄ and (ZnPcTyr) dyes.

Optimization of the dye component of the cell usually requires a systematic structural modification. In 2007, a major breakthrough was accomplished in the design and development of Zn(II)Pc-based sensitizers, based on the preparation of unsymmetrically functionalized A_3B type derivatives containing three bulky *tert*-butyl groups that would help to minimize macrocycle aggregation and carboxylic acid anchoring groups to graft the sensitizer onto metal oxide surface (Figure 30).[96] Liquid-electrolyte cells with power conversion efficiencies around 3.5% at 1 sun and IPCE values at the Q band maximum absorption (ca. 700 nm) of 80% were reported by the groups of Grätzel, Nazeeruddin and Torres employing derivatives **a** and **b** (that was called dye **TT1**) (Figure 30) with low tendency towards aggregation. In particular, the **TT-1** dye possesses a highly desirable "push-pull" structure with the carboxy group directly attached to the macrocycle, thus facilitating the charge transfer from the LUMO orbital of the dye to the Ti 3d orbital.

[96] a) Y. Reddy, L. Giribabu, C. Lyness, H. Snaith, C. Vijaykumar, M. Chandrasekharam, M. Lakshmikantam, J. H. Yum, K. Kalyanasundaram, M. Grätzel, M. K. Nazeeruddin, *Angew. Chem. Int. Ed.* **2007**, *46*, 373. b) J. J. Cid, J. H. Yum, S. R. Jang, M. K. Nazeeruddin, E. Martínez-Ferrero, E. Palomares, J. Ko, M. Grätzel, T. Torres, *Angew Chem Int Ed*. **2007**,*46*, 8358.

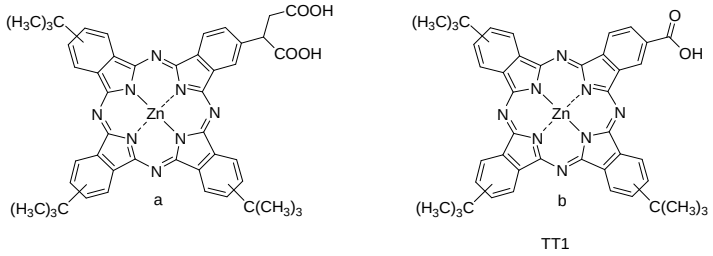

Figure 30. Molecular structures of unsymmetrically substituted tri-tert-butylcarboxyZn(II)Pcs.

Modification of the central metal at the macrocycles cavity, for instance by replacement of Zn(II) by Ti(IV)[97] or Si(IV)[98] metals, offers the possibility of axial coordination that avoids macrocycle aggregation. In particular, Ru(II)Pcs have been seriously considered as alternatives to Zn(II)Pcs due to both their appropriate HOMO-LUMO levels and the possibility of introducing axial ligand.[99] However, aggregation resulted not to be the only problem for achieving efficient Pc-based DSSCs, but also interfacial electron-transfer dynamics resulted relevant phenomena to be considered. In contrast to Zn(II)Pcs, Ru(II) derivatives **a** (Figure 31) exhibit slower electron injection rate constants (hundreds of ns), due to more efficient injection from the Ru(II)Pc's triplet state.[100] Thus, the relaxation of the singlet to the triplet-excited state by intersystem crossing is faster (100 ps) than electron injection from the RuPc singlet excited state (600 ps to 30 ns). The long lifetime of this T_1 state (200 ns) enables electron injection into TiO_2 to be slow, in competition with the T_1 decay to the ground state. Moreover, the photovoltaic performances of **TT1** (Figure 30b) and Ru(II)Pc derivative (**TT35**) were tested and compared in the same conditions, since these dyes have similar structures and energetics, but differ significantly in their photophysics.[101] Whereas, **TT1** exhibit a reasonably long lived singlet state, **TT35** exhibits rapid intersystem crossing to a long lived triplet state. Even though, Ru derivatives show higher injection efficiency than that

97 E. Palomares, M. V. Martínez-Díaz, S. A. Haque, T. Torres, J. R. Durrant, *Chem. Commun.* **2004**, 2112.

98 L. Macor, F. Fungo, T. Tempesti, E. N. Durantini, L. Otero, E. M. Barea, F. Fabregat-Santiago, J. Bisquert, *Energy Environ, Sci*. **2009**, *2*, 529.

99 a) B. C. O'Regan, I. Lopez-Duarte, M. V. Martinez-Diaz, A. Forneli, J. Albero, A. Morendeira, E. Palomares, T. Torres, J. R. Durrant, *J. Am. Chem. Soc*. **2008**, *130*, 2906. b) A. Morandeira, I. López-Duarte, B. O'Regan, M. V. Martínez-Díaz, A. Forneli, E. Palomares, T. Torres, J. R. Durrant, *J. Mater. Chem.* **2009**, *19*, 5016.

100 A. Morandeira, I. López-Duarte, M. V. Martínez-Díaz, B, O'Regan, C. Shuttle, N. A. Haji-Zainulabidin T. Torres, E. Palomares, J. R. Durrant, *J. Am. Chem. Soc.* **2007**, *129*, 9250.

101 A. Listorti, I. López-Duarte, M. V. Martínez-Díaz, T. Torres, T. DosSantos, P. R. F. Barnes, J. R. Durrant, *Energy Environ. Sci.* **2010**, *3*, 1573.

of Zn derivative, Zn Pc based cells showed higher performance, probably due to its improved harvesting efficiency.

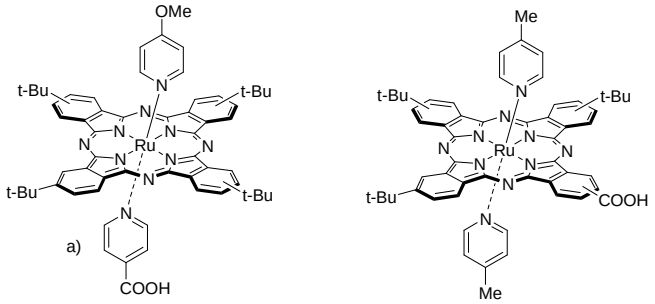

TT-35

Figure 31. Molecular structures of Ru(II)Pcs dyes.

Influence of Spacers between Anchoring Group and Phthalocyanine Sensitizer

In most sensitizers, the anchoring group is usually a carboxylic acid. Its electron withdrawing character is responsible for transferring the electron from the excited dye into the TiO_2 conduction band. Moreover, electron-donating groups, connected to the anchoring group through π-conjugated fragments, such as ethenyl, ethynylphenyl or bisthienyl, are quite recurrently employed in the organic dye skeleton to facilitate directional intramolecular charge transfer from the donor to the acceptor moiety of the dye, and subsequently to the semiconductor.[76a,91c] In this way, the cationic charge formed upon photoexcitation of the dye would be effectively delocalized and physically separated from the TiO_2 surface, restricting the recombination between the injected electrons and the oxidized dye. This donor-acceptor or "push-pull" concept has also led to successful designs of porphyrin sensitizers.

In the case of phthalocyanine sensitizers, Torres, Nazeeruddin and Palomares have reported a series of monocarboxylic acid Pc derivatives and systematically checked their performance in DSSCs compared with Pc sensitizer **TT1** in which the carboxy group is directly attached to the macrocycle (Figure 32).[102]

---

76 a) A. Mishra, M. K. R. Fischer, P. Bauerle, *Angew. Chem. Int. Ed*. **2009**, *48*, 2474.

91 c) W. M. Campbell, A. K. Burrell, D. L. Officer, K. W. Jolley, *Coord Chem Rev*. **2004**, *248*, 1363

102 a) J. J. Cid, M. García-Iglesias, J. H. Yum, A. Forneli, J. Albero, E. Martínez-Ferrero, P. Vázquez, M. Grätzel, M. K. Nazeeruddin, E. Palomares, T. Torres, *Chem Eur J.* **2009**, *15*, 5130. b) F. Silvestri, M.

As expected, the IPCE values dramatically drop to less than 1% overall efficiency when the carboxy anchoring group is separated from the Pc by insulating alkoxy or aryloxy spacers, *i.e.* using Pc **TT2** and **TT4**. On the contrary, rigid π-conjugated bridges do not interrupt the electronic coupling between the Pc and the semiconductor surface, rendering devices made of derivatives **TT3**, **TT14** and **TT20** average power conversion efficiencies of 2%. The conjugation of the carboxy anchoring group through an ethenyl spacer to the dye led to superior photovoltaic responses in DSSCs. Thus, Pc **TT5**, bearing a π-conjugated phenylenevinylene spacer, showed higher performance than phthalocyanines **TT20** that presents an opposite arrangement of the ethenyl and phenylene groups. In spite of this, the better results obtained with **TT1** suggest that the anchoring group should remain as close as possible to the chromophore to maximize the coupling between the Pc and the TiO_2.

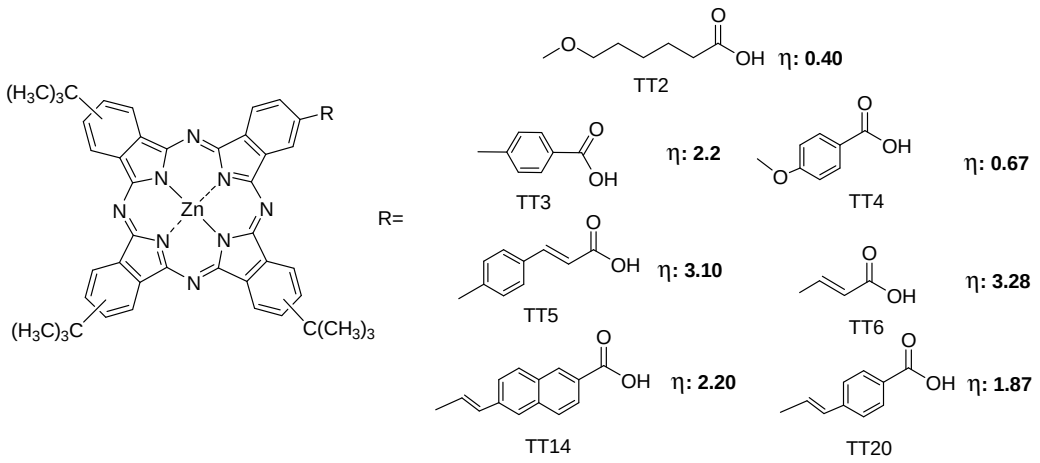

Figure 32. Molecular structures and efficiencies as DSSC-sensitizers of tri-tert-butyl carboxyZn (II) Pcs bearing different spacers between the macrocycle and the carboxylic anchoring group.

Influence of the Binding Group and the Light Harvesting Efficiency

The binding of monocarboxylic acid-functionalized dyes to the TiO_2 surface is frequently quite weak. Although more acidic sulphonic and phosphonic groups produce

Garcia-Iglesias, J.-H. Yum, P. Vazquez, M. V. Martinez-Diaz, M. Grätzel, M. K. Nazeeruddin, T. Torres, *J. Porphyrins Phthalocyanines,* **2009**, *13*, 369.

a stronger binding to the metal oxide, carboxylic acid derivatives typically show significant superior solar cell sensitization, therefore concluding about the good electronic coupling between the carboxylic acid function and the TiO_2 surface.

In the case of porphyrin sensitizers, the use of α-cyanoacrylic anchoring unit produces an enhancement of the light-harvesting properties and concomitant photovoltaic performance in comparison with the acrylic acid derivatives.[103] This structural modification has also been applied to Pc sensitizers **TT7** and **TT8** (Figure 33)[104] although with reduced success due to an increase in their aggregation tendency. However, the incorporation of two carboxylic acid functions in Pcs **TT15** and **TT16** has finally led to beat the record that **TT1** has held for three years within this family of good performance tri-*tert*-butylZnPc sensitizers (Figure 33) mainly due to an enhancement in the photocurrent response, consequence of its broader spectrum coverage. In conclusion, the optimization of this particular family of Pc sensitizers is a delicate matter, in which the most important parameter has revealed to be the choice of an appropriate π-conjugated binding segment, able to electronically connect the Pc dye and the TiO_2 surface and at the same time improve to the maximum the light harvesting efficiency without altering the aggregation properties of the macrocycle.

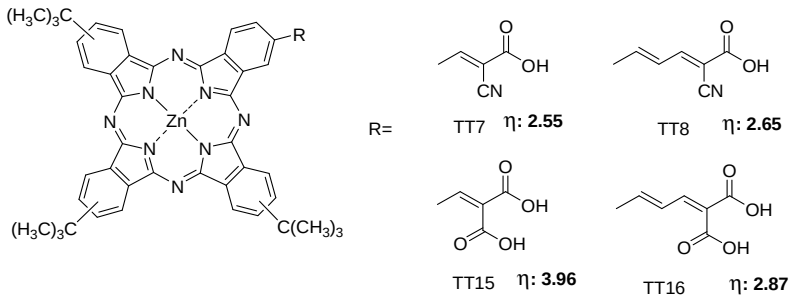

Figure 33. Molecular structures of tri-tert-butylcarboxyZn(II)Pcs bearing different carboxylic-based anchoring groups.

[103] a) Q. Wang, W. M. Campbell, E. E. Bonfantani, K. W. Jolley, D. L. Officer, P.J. Walsh, K. Gordon, R. Humphry-Baker, M. K. Nazeeruddin, M. Grätzel, *J. Phys Chem. B.* **2005***, 109*, 15397. b) H. Qin, S. Wenger, M. Xu, F. Gao, X. Jing, P. Wang, S. M. Zakkeruddin, M. Grätzel, *J. Am. Chem. Soc.* **2008**, *130*, 9202.

[104] M. García-Iglesias, J. J. Cid, J. H. Yum, A. Forneli, P. Vázquez, M. K. Nazeeruddin, E. Palomares, M. Grätzel, T. Torres, *Energy Environ. Sci*. **2011**, *4,* 189.

Recently, new Pc sensitizers were prepared, in which the structure of **TT-1** was modified either by incorporation of two carboxylic acid groups (**TT9**) or a phosphinic acid as anchoring group (**TT30, TT32**) (Figure 34).[105] Power conversion efficiencies were not significantly improved by using these new Pc sensitizers. However, both anchoring groups demonstrate stronger binding properties, subsequently increasing the stability of the DSSCs.

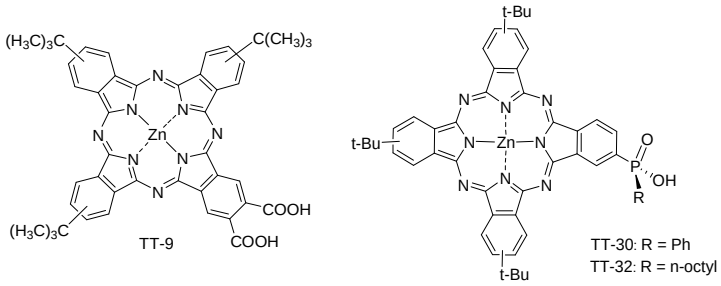

Figure 33. Molecular structures of Zn(II)Pcs TT9 and TT32.

Increasing the Light-Harvesting in DSSCs with Unattached Energy Relay Dyes

The combination of Pcs with other dyes having complementary absorption spectra is an interesting strategy to achieve panchromatic sensitization of TiO_2 films. Pcs dyes offer an optical window in the visible region that makes these molecules very appealing components of co-sensitizer blends. On the other hand, the use of long-range Forster resonance energy transfer (FRET) has been proposed as a new concept for increasing light harvesting in DSSCs using Pcs in combination with unattached energy relay dyes (ERDs).[106,107] In particular, a 26% increase in power conversion efficiency was achieved by incorporation an unattached highly luminescent PTCDI chromophore inside the liquid electrolyte in a TT1 sensitized solar cell (Figure 34).

[105] a) M. Garcia-Iglesias, J. H. Yum, R. Humphry-Baker, S. M. Zakeeruddin, P. Pechy, P. Vazquez, E. Palomares, M. Gratzel, M. Nazeeruddin, T. Torres, *Chem. Sci.* **2011**, *2*, 1145. b) I. López-Duarte, M. Wang, R. Humphry-Baker, M. Ince, M. V. Martínez-Díaz, M. Nazeeruddin, T. Torres, M. Grätzel, *Angew. Chem. Int. Ed.* **2012**, *51,* 1895.

[106] B. E. Hardin, E. T. Hoke, P. B. Armstrong, J. H. Yum, P. Compte, T. Torres, J. M. Frechet, M. K. Nazeeruddin, M. Grätzel, M. D. McGehee, *Nat. Photonics*. **2009**, *10*, 3077.

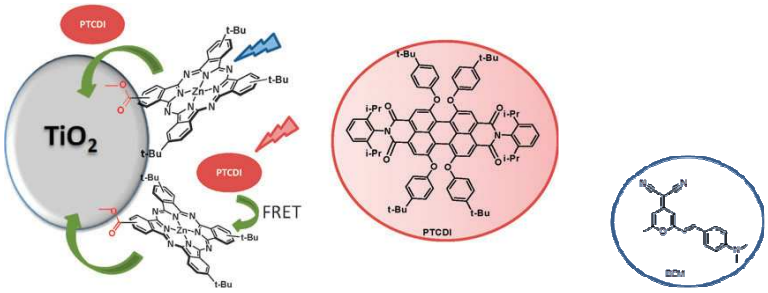

Figure 34. Schematic representation of a DSSC with energy relay dyes and molecular structure of PTCDI and DCM dyes.

Recently, another energy relay dye, 4-(dicyanomethylene)-2-methyl-6-(4-dimethylaminostyryl)-4H-pyran (DCM) (Fig. 34), has been used together with dye TT1 to increase the overall power conversion efficiency of a DSSC from 3.5% to 4.5%. In this case, the unattached DCM dyes exhibit an average excitation transfer efficiency of 96% inside TT1-covered, mesostructured TiO_2 films. This study shows that energy relay dyes can be efficiently implemented in optimized DSSCs, but also highlights the need to design highly soluble energy relay dyes with high molar extinction coefficients.[107a] Most recently, multiple energy relay dyes have been incorporated in Pc-based Liquid DSSCs.[107b]

[107] a) B. E. Hardin, J. H. Yum, E. T. Hoke, Y. C. Jun, P. Pechy, T. Torres, M. L. Brongersma, M. K. Nazeeruddin, M. Gratzel, M. D. McGehee, *Nano Lett*. **2010**, *10*, 3077. b) K. Driscoll, J. Fang, N. Humphry-Baker, T. Torres, W. T. S. Huck, H. J. Snaith, R. H. Friend, *Nano Lett*. **2010**, *10*, 4981. c) J. H. Yum, B. E. Hardin, E. T. Hoke, E. Baranoff, S. M. Zakeeruddin, M. K. Nazeeruddin, T. Torres, M. D. McGehee, M. Grätzel, *ChemPhysChem*. **2011**, *12*, 657.

Objectives

General Objectives and Chapters Distribution

The main goal of the present Doctoral Thesis is the **synthesis of novel phthalocyanine derivatives and analogues with different electronic properties as photo- and electroactive components for molecular photovoltaics**, namely for bulk heterojunctions (BHJ) and dye-sensitized solar cells (DSSCs). Based on the broad experience gained by our research group, which has been working in this field during the last 10 years, the molecular designs of phthalocyanines for photovoltaic applications is focussed on:

1) exploring the preparation of novel derivatives with absorption in the red and near-infrared domains in order to harvest light in the spectral regions where the flux of solar photons has its maximum of intensity,

2) to control their aggregation properties in the solid state in order to improve the morphology of the systems.

In relation to this, phthalocyanines bearing strong donor or strong electron withdrawing substituents will be prepared. On the other hand, new phthalocyanine analogues such as azulenocyanines, whose absorption extends from 400 to 1000 nm, and subphthalocyanines, strongly absorbing in the 550-600 nm region will be also synthetic targets of this Thesis.

Since C_{60} fullerene and SWNTs are the most frequent acceptor components of solar cells, some covalent and non-covalent donor-acceptor ensembles will be constructed, in a second stage, with the aim of reaching photoinduced electron transfer processes. The organization of the Pc/C_{60} ensembles into columnar liquid crystalline phases will be studied. When columnar mesophases are formed, charge carrier mobility is expected to increase along the column axis, a fact that can be of interest in the field of molecular photovoltaics since the control of the nanostructure of the active layer is a key point for the development of efficient devices.

Finally, some Pcs and Pc's analogues prepared in this Thesis have been tested as active components for solar cells.

The Thesis has been specifically structured in two chapters:

Chapter 1 is divided in three sections:

- The first one is devoted to donor-acceptor phthalocyanine-dendritic oligothiophene molecules with potential application in solution processed bulk heterojunction solar cells,
- the second one deals with azulenocyanine-C_{60} and azulenocyanine-SWNT ensembles, and
- the third one is focussed on the possibility of co-organizing phthalocyanines and C_{60} in liquid crystalline phases, through which the holes could be be delocalized after the electron transfer from the Pc to the C_{60} has taken place.

Chapter 2 deals with phthalocyanine and phthalocyanine analogues specifically decorated with anchoring groups to be incorporated in dye sensitized solar cells.

Chapter 1. Donor-Acceptor Systems Based on Phthalocyanines and Azulenocyanines

1.1. Phthalocyanine-Oligothiophene Derivatives for Bulk Heterojunctions

1.1.1. Background

Research into the design of organic molecules for solar cell applications has very much intensified in the last decade. As mentioned in the general introduction, research based on phthalocyanines has attracted great attention due to their fundamental scientific importance and utility in wide variety of photonic applications. Our group has been very interested in recent years in the preparation of phthalocyanine derivatives as electron donor materials for small molecule organic solar cells. For instance, very recently, a small molecule organic solar cell based on a soluble tetra-*tert*-butyl zinc phthalocyanine (ZnTBPc)/$PC_{61}BM$ blend has been reported.[60e] The device produces a short current density (Jsc) around 3.57 $mAcm^{-2}$, and open circuit voltage (Voc) around 0.53 V (Figure 35). This corresponds to power conversion efficiency of approximately 0.77%. However, this device suffers from low open circuit voltage because of the fast recombination dynamics.

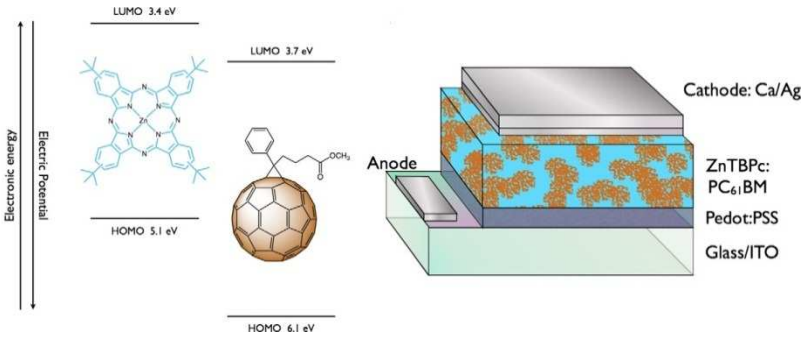

Figure 35. Bulk heterojunction solar cell based on ZnTBPc:PCBM.

In a previous work by our group,[60c] tetra-*tert*-butyl ruthenium(II) phthalocyanines, functionalized at their axial positions with dendritic oligothiophene ligands (DOTs) of different generations, have been used as an efficient electron donor for small molecule organic solar cells. Efficiencies of up to 1.6% in solution-processed bulk heterojunction solar cells have been reported. The cells consist of highly soluble RuPcs, which have pyridine functionalized dentritic oligothiophenes up to third generation (Figure 36), blended with fullerene derivatives (either $PC_{61}BM$ or $PC_{71}BM$).

[60] c) M. K. R. Fischer, I. Lopez-Duarte, M. M. Wienk, M. V. Martinez-Diaz, R. A. J. Janssen, P. Bauerle, T. Torres, *J. Am. Chem. Soc.* **2009**, *131*, 8669. e) A. Sánchez-Díaz, R. Pacios, U. Muñecas, T. Torres, E. Palomares, *Organic Electronics* **2011***, 12,* 329.

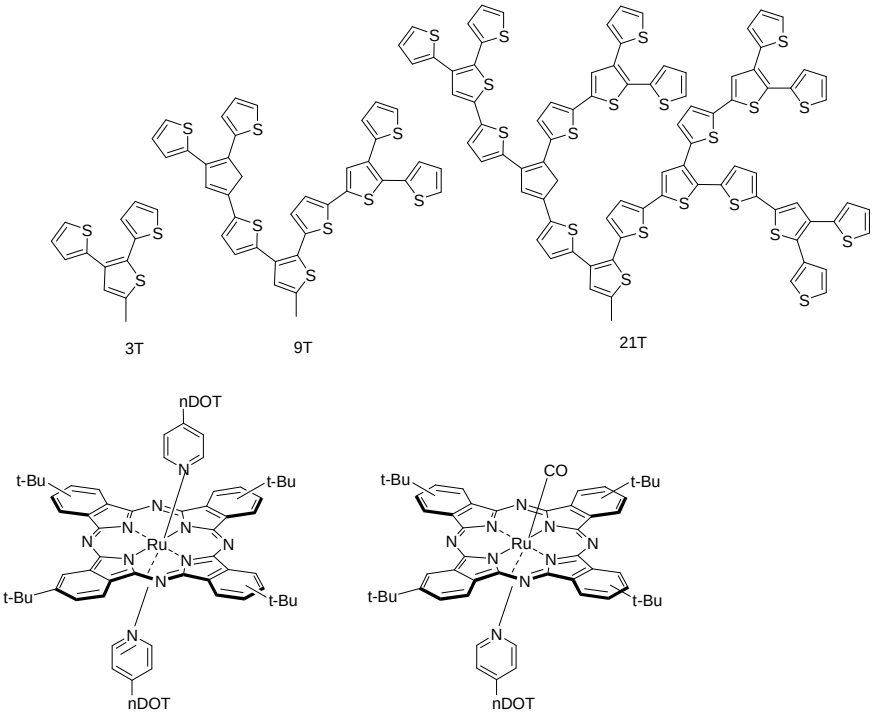

Figure 36. Molecular structures of RuPc-dendritic oligothiophene dyads.

A high short current density of 8.3 $mAcm^{-2}$ resulted from the introduction of dendritic oligothiophene ligands in the axial position of RuPc, which allowed the improvement of light harvesting ability between 380-550 nm, where the RuPc does not exhibit a strong absorption. Interestingly, the reference complexes RuPcCOPy and $RuPcPy_2$, (without any DOT substituent) showed very close efficiency (0.9%) to their DOT-functionalized derivatives (Table 1).

Table 1. Characteristic solar cell data of RuPc-DOTs dyads.

Compounds	**Jsc (mA/cm^2)[a]**	**Voc (V)**	**FF**	**η^b**
RuPcCOPy	4.6	0.63	0.31	0.9
RuPcCO(Py-3T)	4.5	0.60	0.37	1.0
RuPcCO(Py-9T)	3.9	0.34	0.27	0.4
RuPcCO(Py-21T)	4.1	0.48	0.35	0.7
$RuPc(Py)_2$	4.4	0.44	0.28	0.6
$RuPc(Py\text{-}3T)_2$	5.1	0.55	0.37	1.0
$RuPc(Py\text{-}9T)_2$	4.4	0.64	0.34	1.0
$RuPc(Py\text{-}21T)_2$	2.8	0.73	0.33	0.7
$RuPc(Py\text{-}3T)_2$[b]	7.1	0.55	0.38	1.5
RuPcCO(Py-3T)[b]	8.3	0.56	0.34	1.6

[a] *From convolution of the EQE spectra with the AM. 1.5G.* [b] *$PC_{71}BM$ was used as an acceptor.*

Despite these good results, the design of new Pc macrocycles for BHJ solar cells still needs some improvements.

1.1.2. Objectives

Modifications on the molecular structure of Pc by introducing different groups at different positions aimed at extending the absorption spectra, tuning the electronic configuration of the excited states, are expected to be efficient ways to improve the conversion efficiency of solution processed phthalocyanine-based BHJ solar cells.

One of the reasons for the low performance of Pcs is the low open circuit potential (Voc) values. Therefore, the main purpose of this section will consist on the preparation of soluble Zn(II) phthalocyanine derivatives, which match key requirements such as a relatively low-lying HOMO level and a narrow energy band gap, to be used as donor components of organic solar cells. In particular, new soluble ZnPc derivatives were designed based on the following criteria:

a) A broad absorption in the range of the solar emission spectrum and an effective harvesting of the solar photons were aimed. For this purpose oligothiophene-dendrons (DOTs) were planned to be linked to ZnPc derivatives.

b) Tailoring the electronic properties of the Pc for achieving ideal HOMO and LUMO levels. Considering this, a lower-lying HOMO level of the Pc donor would provide a larger Voc, and a suitable LUMO energy level of the Pc donor is required to have a good match with the PCBM acceptor.

Substitution of Pc macrocycle with electron withdrawing groups usually depressed the HOMO and LUMO levels and renders attractive n-type semiconductors for application in the field of organic electronic materials. In this regard, several Pc derivatives with strong electron withdrawing substituents such as, F, Cl, CN groups, at peripheral or non-peripheral positions, have been reported for the purpose of fabricating n-type organic semiconductors.[108] Among them, the alkylsulfonyl group plays an important role, not only promoting a considerable stabilization of the HOMO and the LUMO level of Pc, but also increasing the solubility due to the flexible alkyl chain.[109] Moreover, several alkylsulfonyl-containing unsymmetrically Pc derivatives have been synthesized by our group and studied as non-linear optical chromophores.[110] Therefore, the strong electron accepting octyl-sulfonyl group was chosen in our research project to decrease the HOMO level of Pc, aiming to increase the Voc values of the photovoltaic devices, in comparison with the *tert*-butyl substituted phthalocyanine-based solar cells, previously studied.

In particular, the new ZnPc derivatives planned to be studied as the donor component in BHJ solar cells are shown in Figure 37.

---

[108] a) Z. Bao, A. J. Lovinger, J. Brown, *J. Am. Chem. Soc.* **1998,** *120,* 207. b) Q. Tang, H. Li, Y. Liu, W. Hu, *J. Am. Chem. Soc.* **2006,** *128,* 14634*.* c*)* Y. Oh, S. Pyo, M. H. Yi, S. K. Kwon*, Org. Electron.* **2006***, 7,* 77*.*

[109] a) B. Tylleman, G. Gbabode, C. Amato, C. Buess-Herman, V. Lemaur, J. Cornil, R. Gomez Aspe, Y. H. Geerts, S. Sergeyev, *Chem. Mater*. **2009**, *21*, 2789. b) Y. Zhang, P. Zhu, X. Zhang, Y. Gao, D. Qi, Y. Bian, N. Kobayashi, J. J. Jiang, *J. Mater. Chem.* **2011**, *21*, 6515.

[110] a) E. M. Maya, P. Vázquez, T. Torres, *Chem. Eur. J.* **1999**, *5*, 2004. b) E. M. Maya, P. Vázquez, T. Torres, L. Gobbi, F. Diederich, S. Pyo, L. Enchegoyen, *J. Org. Chem*. **2000**, *65*, 823. c) E. M. Maya, C. García, E. M. García-Frutos, P. Vázquez, T. Torres, *J. Org. Chem*. **2000**, *65*, 2733. d) A. de la Escosura, M. V. Martínez-Díaz, P.Thordarson, A. E. Rowan, R. J. M. Nolte, T. Torres, *J. Am. Chem. Soc.* **2003**, *125*, 12300. e) A. de la Escosura, M. V. Martínez-Díaz, D. M. Guldi, T. Torres, *J. Am. Chem. Soc.* **2006**, *128*, 4112. f) A. de la Escosura, M. V. Martínez-Díaz, J. Barberá, T. Torres, *J. Org. Chem*. **2008**, *73*, 1475.

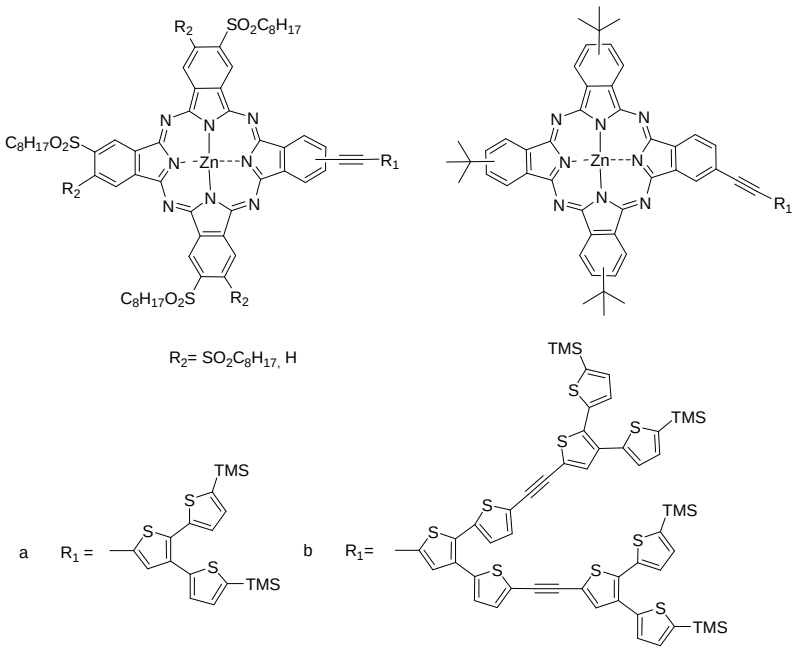

Figure 37. Structure of ZnPc-DOTs dyads.

This work have been developed in collaboration with Prof. Peter Bauerle at the University of Ulm, Germany

1.1.3. Results and Discussion

Three families of Zn(II)phthalocyanines covalently linked to oligothiophene dendrons (DOTs) were designed. One of them bearing three *tert*-butyl groups at the peripheral positions, and a second and third ones bearing three and six octylsulfonyl groups, respectively. In both cases, DOTs of first and second generation were attached through a terminal alkyne group.

1.1.3.1. Synthesis of Precursor Phthalonitriles

4-Iodophthalonitrile (**2**) was prepared according to literature procedures,[111] as shown in Scheme 1.

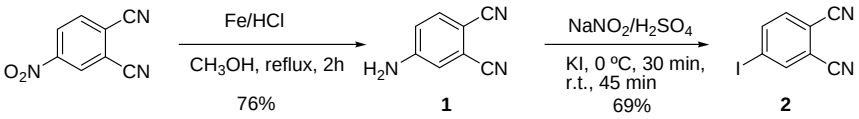

*Scheme 1. Synthesis of 4-iodophthalonitrile (**2**)*.

The 4-aminophthalonitrile (**1**) was synthesized by reduction of the 4-nitrophthalonitrile, with iron powder in hydrochloric acid.[111a] The 4-aminophthalonitrile was then transformed to 4-iodophthalonitrile (**2**) in 69% yield *via* diazotization and subsequent nucleophilic aromatic reaction in the presence of potassium iodide.[111b]

The synthetic pathway for the preparation of 4,5-bis(octylsulfonyl)phthalonitrile (**8**)[112] is displayed in Scheme 2.

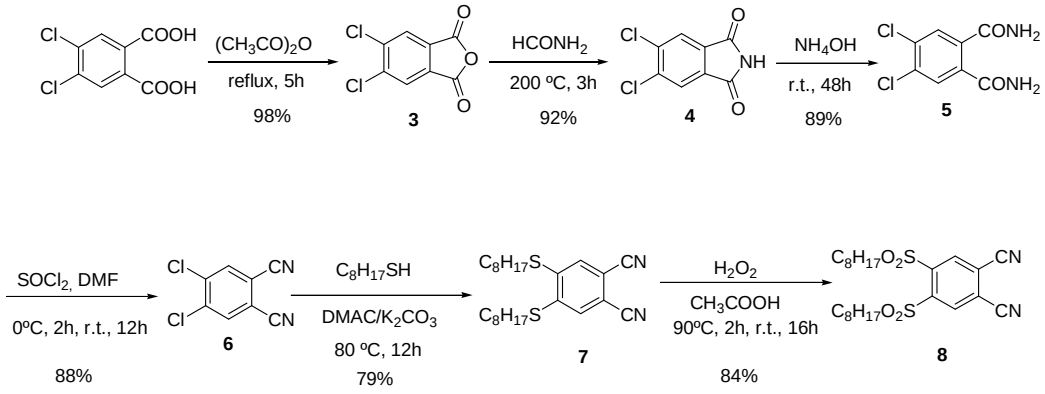

*Scheme 2. Synthesis of 4,5-bis(octylsulfonyl)phthalonitrile (**8**).*

[111] a) H. Lam, S. M. Marcuccio, P. I. Svirskaya. S. Greenberg, A. B. P. Lever, C. C. Leznoff, R. L. Cerny, *Can. J. Chem*. **1989**, *67*, 1087. b) J. G. Young, W. Onyebuagu, *J. Org. Chem.* **1990**, *55*, 2155.

[112] B. del Rey, U. Keller, T. Torres, G. Rojo, F. Agullo-Lopez, S. Nonell, C. Marti, S. Brasselet, I. Ledoux, J. Zyss, *J. Am. Soc.* **1998**, *120*, 12808.

4,5-Dichlorophthalonitrile (**6**)[113] was synthesized in four steps starting from 4,5-dichlorophthalic acid, which can be quantitatively dehydrated to yield the cyclic anhydride **3**. Reaction of this compound with formamide, followed by treatment with ammonium hydroxide led to phthalamide **5**, whose dehydration reaction with thionyl chloride afforded 4,5-dichlorophthalonitrile (**6**) in 88% yield. The phthalonitrile **7** was prepared from the 4,5-dichlorophthalonitrile (**6**) via the two fold nucleophilic substitution with 1-octanethiol.[112] The oxidation of phthalonitrile **7** with hydrogen peroxide led to 4,5-bis(octylsulfonyl)phthalonitrile (**8**) in 84% yield.

The synthesis of phthalonitrile **10** was carried out following a modification of the previously published procedures (Scheme 3).[112] Aromatic nucleophilic substitution of 4-nitrophthalonitrile with 1-octanethiol in the presence of K_2CO_3 in DMSO gave phthalonitrile **9** in 64% yield. The oxidation reaction of phthalonitrile **9** with hydrogen peroxide led to 4-octylsulfonylphthalonitrile (**10**) in 80% yield. The use of hydrogen peroxide instead of *m*-chloroperbenzoic acid decreased the reaction time from 12 h to 2 h.

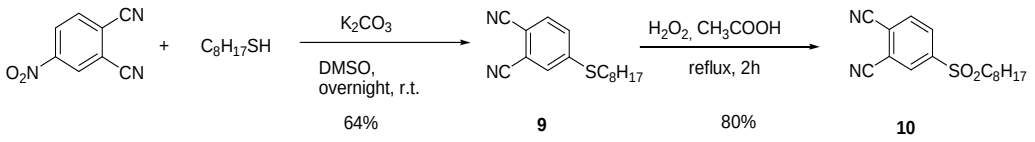

*Scheme 3. Synthesis of phthalonitrile **10***

The synthesis and electrochemical properties of the first and second-generation of trimethylsilylethynyl-functionalized oligothiophene dendrons **11** and **12** had been previously reported by Bauerle and co-workers.[114] They were prepared again for this project in Ulm according to literature procedures.[114] However, final deprotection of the TMS groups by K_2CO_3 in methanol was more conveniently carried out in Madrid, giving rise to derivates **11** and **12** in excellent yield, 85% and 86% respectively (Scheme 4).

[112] B. del Rey, U. Keller, T. Torres, G. Rojo, F. Agullo-Lopez, S. Nonell, C. Marti, S. Brasselet, I. Ledoux, J. Zyss, *J. Am. Soc.* **1998**, *120*, 12808.
[113] D. Wohrle, M. Eskes, K. Shigehara, A. Yamada, *Synthesis*, **1993**, 194.
[114] A. Mishra, C. Q. Ma, R. A. J. Janssen, P. Bauerle, *Chem. Eur. J.* **2009**, *15*, 13521.

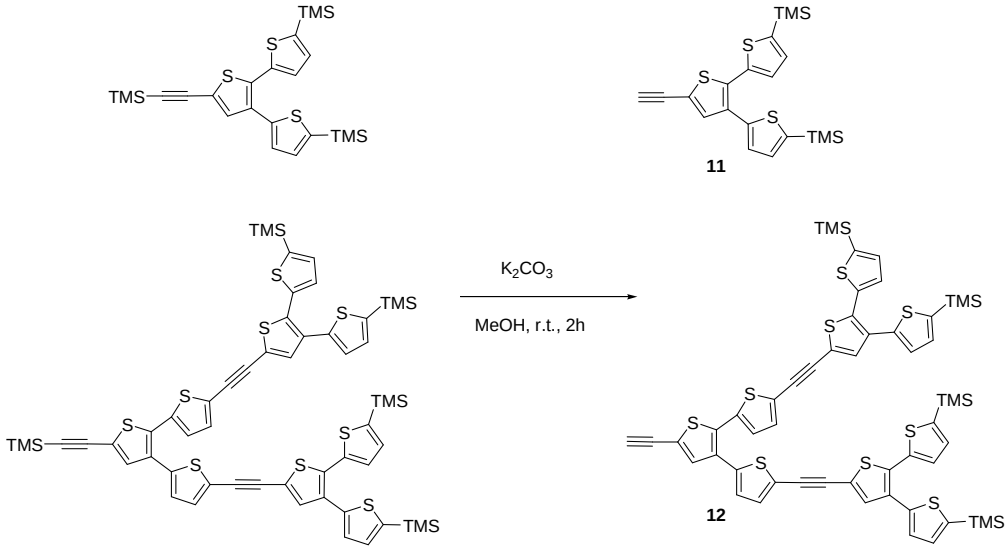

Scheme 4. Deprotection of TMS group of oligothiophene dendrons.

1.1.3.2. Synthesis of *tert*-butyl Substituted ZnPc-DOTs Dyads

The synthesis of phthalocyanines is usually based on the cyclotetramerization of either a phthalonitrile or a diiminoisoindoline precursor that assembles in the macrocyclic structure. The synthesis of symmetrically tetrasubstituted Pcs can be achieved from 3- or 4-substituted phthalonitriles which result in a mixture of four possible structural isomers with different symmetries.[115]

On the other hand, the synthesis of unsymmetrically substituted Pcs consisting of three identical isoindole subunits and a fourth different one (A_3B), is a more complex process. The approach relying on the statistical reaction of two different phthalonitrile precursors A and B in ratios of 3:1 appears to be the most commonly applied. However, this method produces a mixture of all the possible macrocycles (A_4, A_3B, A_2B2, AB_3, etc.), and the isolation of desired Pcs from the mixture usually requires extensive chromotographic purification. Consequently, the steric effect, reactivity, and ratio of the precursors have to be taken into account to facilate the separation and to increase the

[115] a) M. Sommerauer, C. Rager, M. Hanack, *J. Am. Chem. Soc.* **1996**, *118*, 1085. b) S. Rodríguez-Morgade, M. Hanack, *Chem. Eur. J.* **1997**, *3*, 7.

yield of the desired compound.[116] This approach has been successfully employed in the synthesis of tri(*tert*-butyl)iodophthalocyanine, which was previously reported by our group (Scheme 5).[110a]

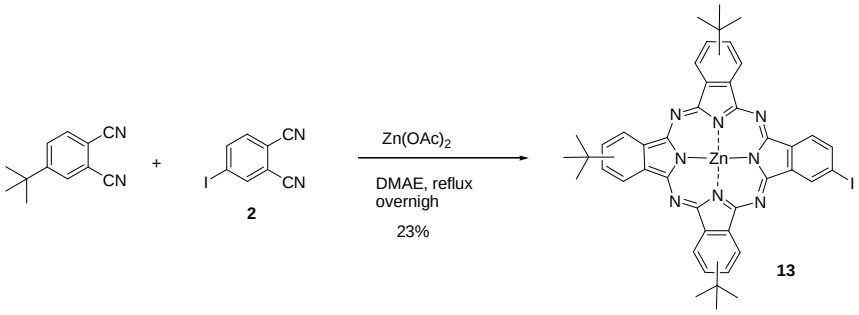

*Scheme 5. Synthesis of tri(tert-butyl)iodoZn(II) phthalocyanine (**13**).*

Thus, the condensation reaction of 4-iodophthalonitrile (**2**) with 4-*tert*-butylphthalonitrile in the presence of zinc(II) acetate generates a statistical mixture of compounds in which the major components are tetra-*tert*-butylphthalocyanine followed by tri(*tert*-butyl)iodophtalocyanine (**13**). Purification by silica gel column chromatography gave phtalocyanine **13** in 23% yield. Compound **13** consists of a mixture of up to eight regioisomers.

Dyads **14a**-**b** were prepared by Sonagashira coupling between tri(t*ert*-butyl)iodoPc (**13**) and terminal alkyne DOTs **11** or **12** in 67% and 51% yield, respectively. Both reactions were carried out in dry THF in the presence of $[PdCl_2(PPh)_3]$ as a catalyst, triethylamine as the base, and a catalytic amount of copper iodide. The preparation of dyads **14a**-**b** is depicted in Scheme 6.

[110] a) E. M. Maya, P. Vázquez, T. Torres, *Chem. Eur. J*. **1999**, *5*, 2004.
[116] a) G. de la Torre, C. G. Claessens, T. Torres, Eur. *J. Org. Chem*. **2000**, 2821. b) T. Torres, *J. Porphyrins Phthalocyanines* **2000**, *4*, 325. c) G. de la Torre, T. Torres, *J. Porphyrins Phthalocyanines* **2002**, *6*, 274.

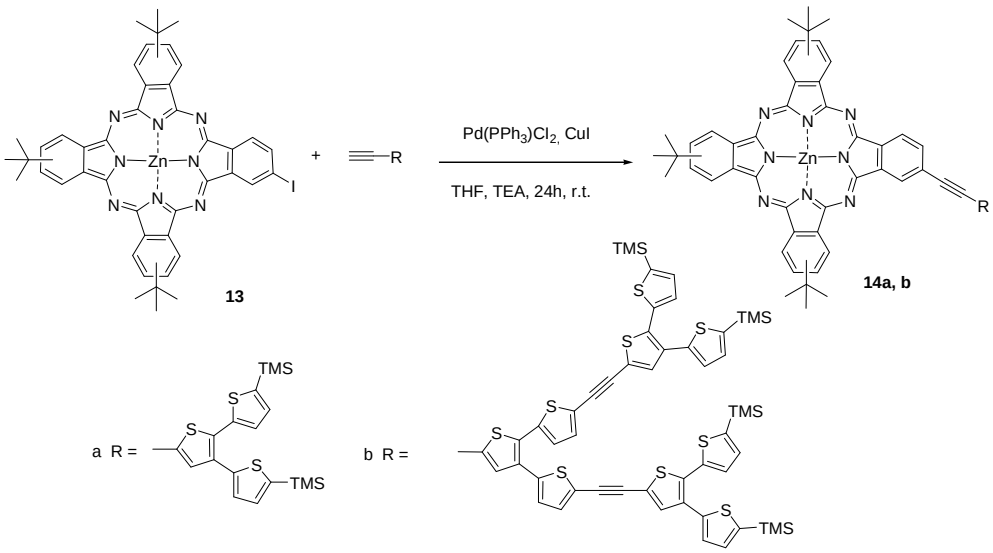

*Scheme 6. Synthesis of tri(tert-butyl)ZnPc-DOTs dyads **14a-b**.*

1.1.3.3. Synthesis of Octylsulfonyl Substituted ZnPc-DOTs Dyads

Synthesis of Hexakis(octylsulfonyl) ZnPc-DOTs dyads

The synthesis of propylsulfonyl-containing, symmetrically or unsymmetrically, Ni (II) or Pd (II) Pc derivatives, by cyclic tetramerization of the corresponding phthalonitrile or preferably diiminoisoindoline precursor, was previously reported by our group.[110] Therefore, the synthesis of hexakis(octylsulfonyl)iodo Pc (**15**) was initially attempted by the statistical cyclotetramerization of 4-iodophthalonitrile (**2**) and 4,5-bis(octylsulfonyl)phthalonitrile (**8**) (in a 1:3 molar ratio). The reaction, carried out in the presence of $Zn(OAc)_2$ in the mixture of DMF and o-dichlorobenzene, led to the corresponding mixture of compounds in a statistical distribution.

[110] a) E. M. Maya, P. Vázquez, T. Torres, *Chem. Eur. J*. **1999**, *5*, 2004. b) E. M. Maya, P. Vázquez, T. Torres, L. Gobbi, F. Diederich, S. Pyo, L. Enchegoyen, *J. Org. Chem.* **2000**, *65*, 823. c) E. M. Maya, C. García, E. M. García-Frutos, P. Vázquez, T. Torres, *J. Org. Chem*. **2000**, *65*, 2733. d) A. de la Escosura, M. V. Martínez-Díaz, P. Thordarson, A. E. Rowan, R. J. M. Nolte, T. Torres, *J. Am. Chem. Soc.* **2003**, *125*, 12300. e) A. de la Escosura, M. V. Martínez-Díaz, D. M. Guldi, T. Torres, *J. Am. Chem. Soc.* **2006**, *128*, 4112. f) A. de la Escosura, M. V. Martínez-Díaz, J. Barberá, T. Torres, *J. Org. Chem*. **2008**, *73*, 1475

The choice of solvent (DMF/o-DCB instead of DMAE which is typically used) was made in order to avoid nucleophilic displacement of the sulfonyl group.[110] Unfortunately, all attempts for the separation of unsymmetrically substituted Pc **15** from the reaction mixture failed due to the very similar polarities of the different Pcs produced in the reaction.

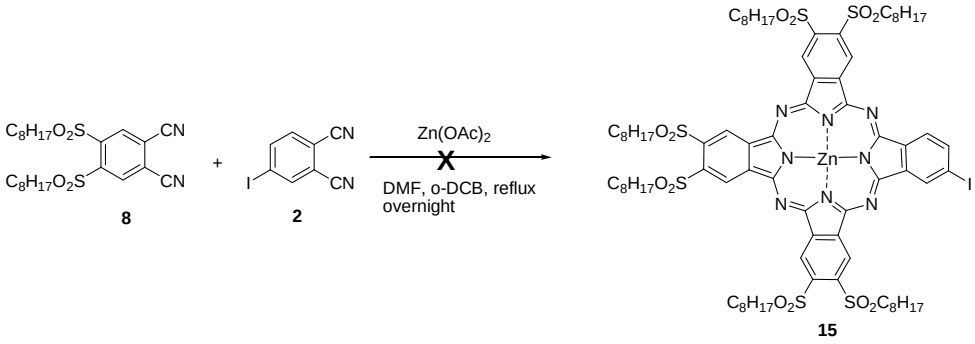

*Scheme 7. An unsuccessful attempt at the synthesis of Pc **15**.*

We therefore developed an alternative route to synthesize Pc **15**, which relies on a six-fold oxidation of the corresponding hexakis(octylthio)phthalocyanine (**16**). Thus, Pc **16** was synthesized by cyclotetramerization reaction of 4-iodophthalonitrile (**2**) and 4,5-bis(octylthio)phthalonitrile (**7**) in the presence of $Zn(OAc)_2$ in DMAE. Separation of the reaction mixture by column chromatography gave Pc **16** in 22% yield. However, the oxidation reaction of Pc **16** with *m*-chloroperbenzoic acid under exclusion of light, gave a mixture of partially oxidized compounds, which could not be separated.

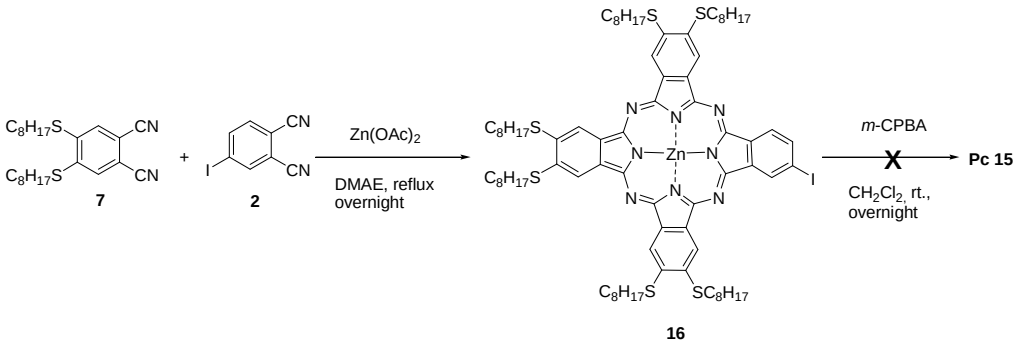

*Scheme 8. An unsuccessful attempt at the synthesis of Pc **15**.*

Synthesis of Tris(octylsulfonyl) ZnPc-DOTs Dyads

The synthesis of tris(octylsulfonyl)iodophthalocyanine (**17**) is featured in Scheme 9. The statistical crossover condensation of 4-iodophthalonitrile (**2**) with 4-octylsulfonylphthalonitrile (**10**) in the presence of $Zn(OAc)_2$ in the mixture of DMF and o-dichlorobenzene yielded the electron-deficient Pc **17** in 16% yield as a mixture of regioisomers.

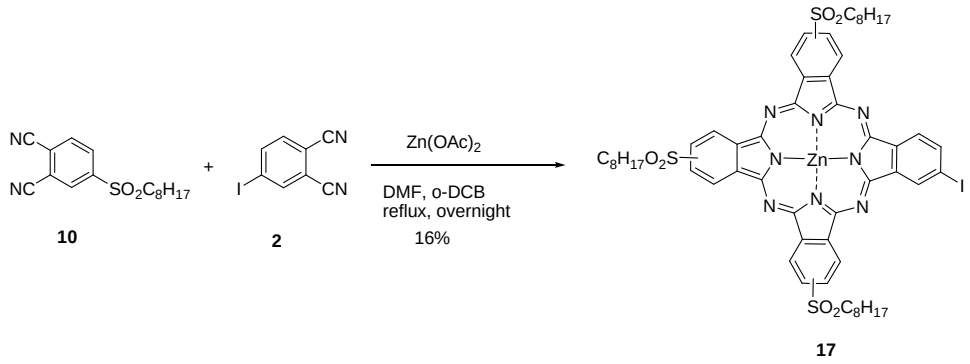

*Scheme 9. Synthesis of tri(octylsulfonyl)phthalocyanine (**17**).*

The preparation of compounds **18a** and **18b** was achieved by a modified Sonagashira procedure (Scheme 10). Following literature procedures for similar cases (Sonagashira coupling reaction with tri-(propylsulfonyl)phthalocyanine) a copper-free palladium catalyzed reaction was employed to avoid the homocoupling side reaction.[110a] The synthesis of compounds **18a** and **18b** was carried out in 25% and 21% yield, respectively, by using $[Pd_2(dba)_3]$ and triphenylarsine in a freshly distilled and deareated piperidine.

[110] a) E. M. Maya, P. Vázquez, T. Torres, *Chem. Eur. J*. **1999**, *5*, 2004.

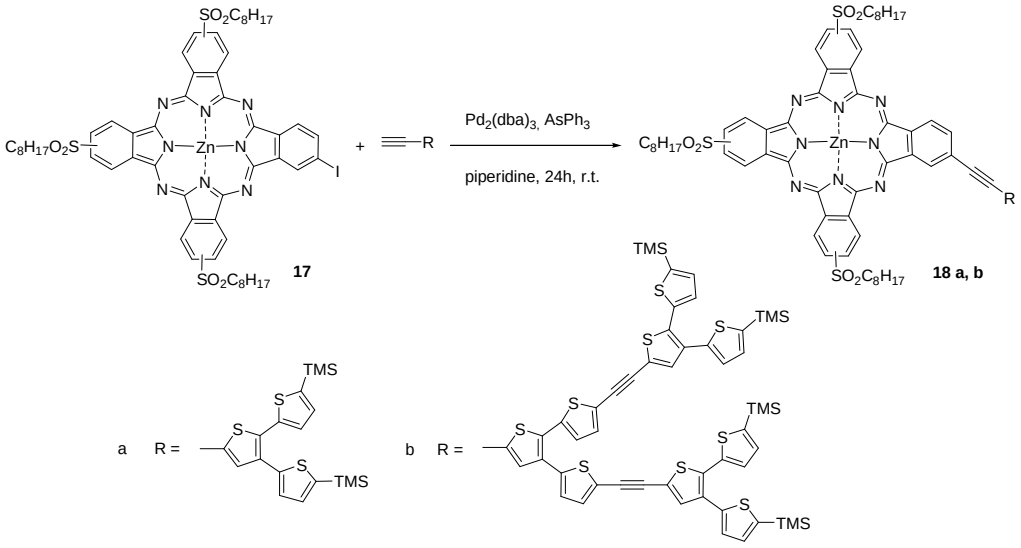

*Scheme 10. Synthesis of tris(octylsulfonyl)ZnPc-DOTs dyads (**18a,b**).*

All new compounds were fully characterized by ^{1}H-NMR, UV-Vis, FT-IR and MALDI-TOF spectroscopies. The ^{1}H-NMR spectra of tris(*tert*-butyl)ZnPc-DOTs (**14a**,**b**) in d_8-THF show similar and several multiplets corresponding to the phthalocyanine protons in the aromatic region, between 9.5 and 8.0 ppm. The oligothiophene-dendron protons can be easily distinguishable in the region between 7.7 and 7.2 (Figure 38).

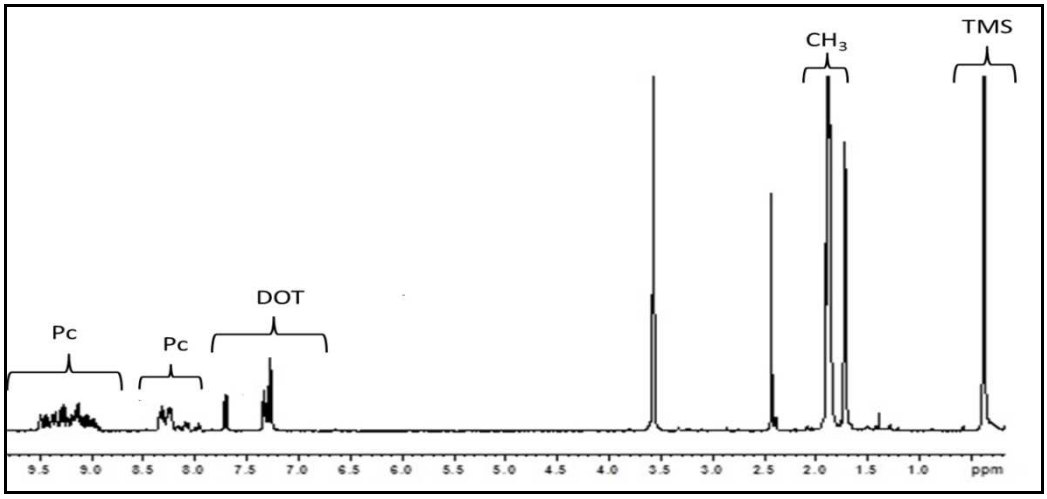

*Figure 38. ^{1}H NMR (d_8-THF) spectrum of dyad **14a**.*

On the other hand, the ^{1}H-NMR spectra of the sulfonylPc-dendrons **18a** and **18b** in d_8-THF gave broad signals for the aromatic Pc protons owing to aggregation (Figure 39).

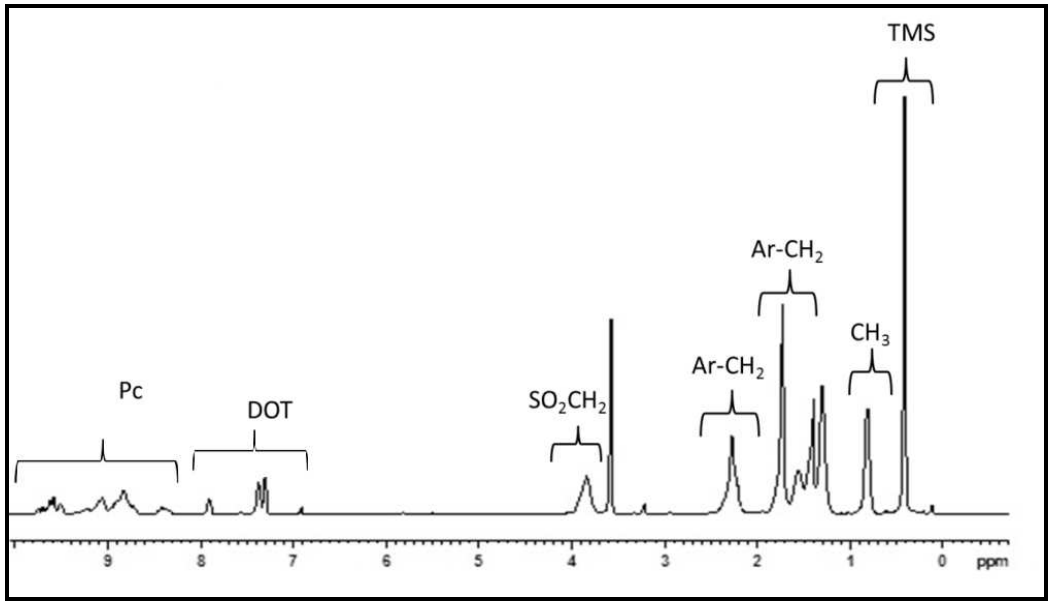

*Figure 39: ^{1}H NMR (d_8-THF) spectrum of dyad **18a**.*

The absorption spectra of dyads **14a**,**b** (Figure 40) are dominated by an intense Q band at 695 nm and Sored-bands at 350 nm. In comparison with their precursor Pc **13**, the Q-bands of dyads **14a** and **14b** undergo a red shifting, *i.e*. 20 nm, which has been attributed to the enlargement of the π-conjugated system, with concomitant splitting of the Q band. Furthermore, an additional strong absorption in the UV/blue region, between 300-500 nm, is mainly due to the DOTs unit.

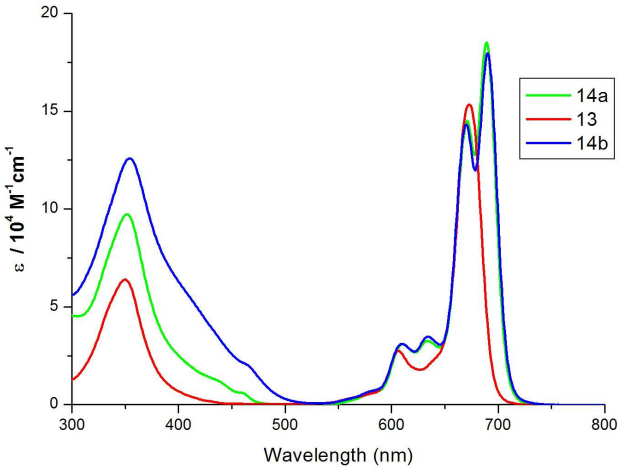

*Figure 40. Absorption spectra of dyad **14a**,**b** and Pc **13** in THF~1x10^{-5} M.*

The absorption spectra of dyad **18a**,**b** in comparison to that of the iodo derivative Pc **17** are depicted in Figure 41. Concerning the spectra of dyads **18a**,**b**, the extended conjugation gives rise to small red shift of the Q band relative to Pc **17**. As for the analogous sulfonyl substituted dyads, a remarkable change in the intensity of Soret-band is the consequence of the presence of the dendron.

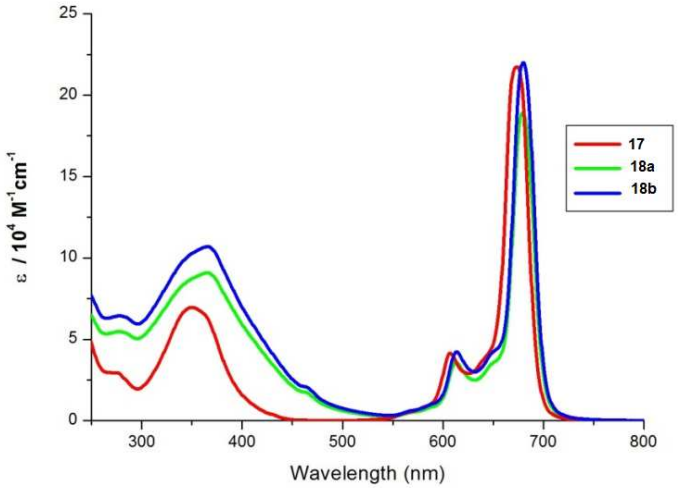

*Figure 41. Absorption spectra of dyad **18a**,**b** and Pc **17** in THF in THF~1x10^{-5} M.*

1.1.3.4. Photovoltaic Performance in Bulk Heterojunction Solar Cells

The HOMO and LUMO energy levels of ZnPc-DOTs hybrid compounds **14a**,**b** and **18a**,**b** were determined in the group of Prof. Bauerle at Ulm University (Germany) by cyclic voltammetry (CV) in combination with differential pulse voltammetry (DPV) in CH_2Cl_2 solution. The electrochemical data are summarized in Table 2.

Table. 2. Cyclic voltammetry results of **14a**,**b** and **18a**,**b** dyads[a]

Compounds	E^1ox (V)	E^1ox (V)	E^1red (V)	HOMO (V)	LUMO (V)
14a	0.01	0.35	-1.43	-5.15	-3.88
14b	0.01	0.21	-1.4	-5.1	-3.89
18a	0.60	0.85	-1.28	-5.3	-3.97
18b		0.93	-1.32	-5.31	-3.93[b]

[a] Measured in dichloromethane/tetrabutylammonium hexafluorophosphate (TBAHFP) (0.1M), c=1x10-3 mol·l^{-1}, 295 K, scan rate=100 mVs^{-1}, vs. Fc/Fc+. E_{HOMO}= -(5.1+E^{onset}_{ox}) eV; Fc/Fc+ E_{HOMO}= -5.1 eV. E_{LUMO}=E_g+E_{HOMO}. b: calculated using optical absorption spectrum.

As expected, the oxidation of *tert*-butylPc-DOTs dyads is easier than the sulfonylPc-DOTs dyads. The reduction of dyads **18a**,**b** is facilitated by the presence of strong acceptor sulfonyl groups. The LUMO levels of all dyads were measured to be approximately 3.9 eV and do not change significantly for the different substituents and generations. On the other hand, the electron donating ability of dendrons decreased the LUMO level of dyads **14a**,**b** in comparison with the levels of *t*Bu-ZnPc or RuPc derivatives**,** but the HOMO levels of all *tert*-butyl derivatives have the same HOMO values. The formal replacement of the *tert*-butyl group on the Pc unit in dyads **14a**,**b** with the stronger electron withdrawing sulfonyl group in dyads **18a**,**b**, resulted in the HOMO levels of **18a**,**b** dropping by 0.14 eV.

Figure 42 shows the energy level diagram for the new donor ZnPc-DOTs dyads and the PCBM acceptor. In addition, the HOMO-LUMO level of tetra-*tert*-butylZnPc and tetra-*tert*-butylRuPc previously incorporated in solar cells are including for comparison. The energy level information suggests that the LUMO energy levels for all ZnPc-DOTs dyads are higher than that of PCBM. This means that they should be suitable

candidates as electron donor materials in BHJ solar cells together with PCBM as the acceptor.

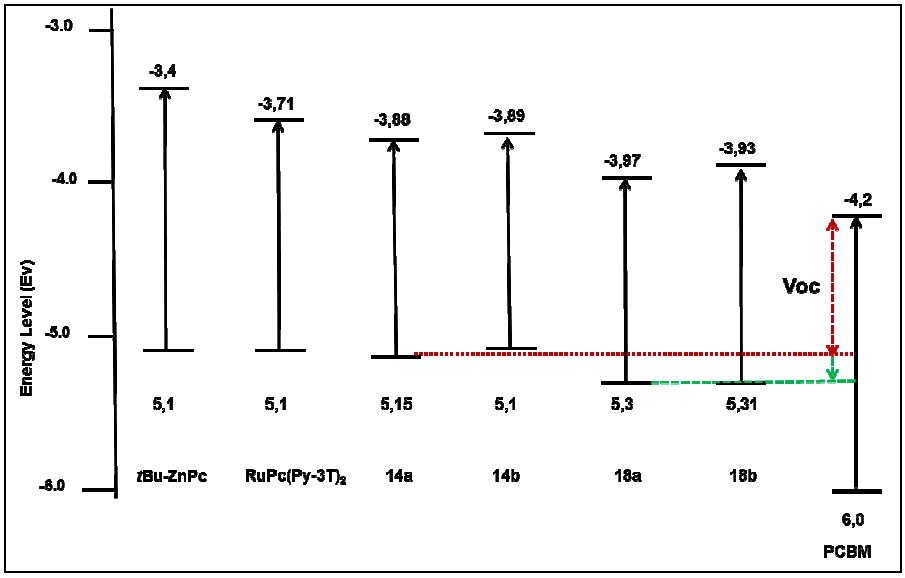

Figure 42. Energy level diagram of Pc-DOTs dyads. The values for PCBM, tetra-tert-butyl-ZnPc[60e] and (RuPc(Py-3T)$_2$[60c] are given for comparison and were taken from the literature.

Bulk-heterojunction solar cells based on ZnPc-DOT dyads were made in collaboration with Prof. R. A. J. Janssen (Eindhoven University of Technology, The Netherlands).

BHJ solar cells using dyads **14a**,**b** and **18a**,**b** as electron donor and fullerene derivative PCBM as an electron acceptor in the active layer were fabricated and characterized. The device structure was ITO/PEDOD:PS/Pc-DOT:PCBM (1:2 w/w)/LiF/Al. A device with compound **14a**, and $PC_{71}BM$ as an acceptor was also prepared and tested for comparison purposes. The ratio of donor to acceptor materials was optimized at 1:2 and the thickness of the active layer was optimized for each donor/acceptor blend, and was typically 60-70 nm. Unfortunately, films formed from dyad **14b** have an inhomogeneous morphology (Figure 43) due to the poor wetting behaviour, which could not be solved by heating either the solution or the substrates. Table 3 summarizes the device performance of various solar cells.

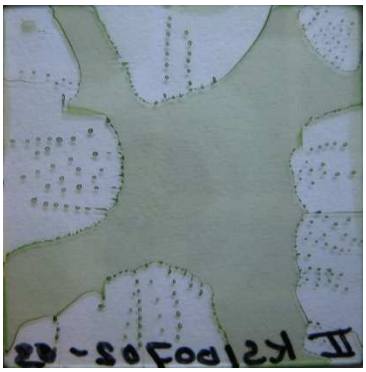

*Figure 43. Device fabricated using films of dyad **14b** spin-coating at 1500 rpm at room-temperature in chlorobenzene.*

Table 3. Device performance of BHJ solar cells.

Compounds	**Jsc (mA/cm^2)[a]**	**Voc (V)**	**FF**	**η[b]**
14a	3.05	0.624	0.296	0.563
14b	0.81	0.635	0.263	0.135
18a	0.16	0.42	0.32	0.022
18b	0.16	0.17	0.29	0.008
14a[c]	4.28	0.55	0.30	0.71
***t*-BuZnPc[60e]**	3.57	0.53	0.39	0.77
RuPc(Py-3T)$_2$[60c]	5.1	0.55	0.37	1.6

[a] Determined by convoluting the EQE spectra with the AM. 1.5G spectrum (100 mWcm^{-2}). [b] $\eta = V_{OC} x J_{SC} x FF$ (FF= fill factor), [c] $PC_{71}BM$ was used as an acceptor instead of $PC_{60}BM$.

Dyads **14a** and **14b** led to comparatively higher Voc values (0.62 V) than its comparative compounds, tetra-*tert*-butylZnPc and RuPc(Py-3T)$_2$ which exhibit a Voc of around 0.53 V[60e] and 0.55 V[60c], respectively. This higher Voc value can be explained by the reduction of the difference between the LUMO of the donor and the acceptor. It has

[60] c) M. K. R. Fischer, I. Lopez-Duarte, M. M. Wienk, M. V. Martinez-Diaz, R. A. J. Janssen, P. Bauerle, T. Torres, *J. Am. Chem. Soc.* **2009**, *131*, 8669. e) A. Sánchez-Díaz, R. Pacios, U. Muñecas, T. Torres, E. Palomares, *Organic Electronics* **2011**, *12,* 329.

been reported that a minimum offset of approximately 0.3-0.4 eV between LUMO of the donor and LUMO of the acceptor is necessary to ensure efficient exciton dissociation at the D/A interface.[43b,e] However, the lower Jsc and FF values limited the performance of the device.

SulfonylPc **18a**,**b** based devices gave low efficiency due to both low Voc and Jsc values. Unfortunately, a diode behavior was not found in the current-density-voltage curves due to a poor mixture of donor and acceptor. Current density–voltage (J–V) characteristics were recorded under dark as well as under illumination of AM1.5G (1sun). Figure 44 and 45 shows J-V curves and external quantum efficiency spectra (EQE) of devices based on dyads **14a**,**b** and **18a**,**b**.

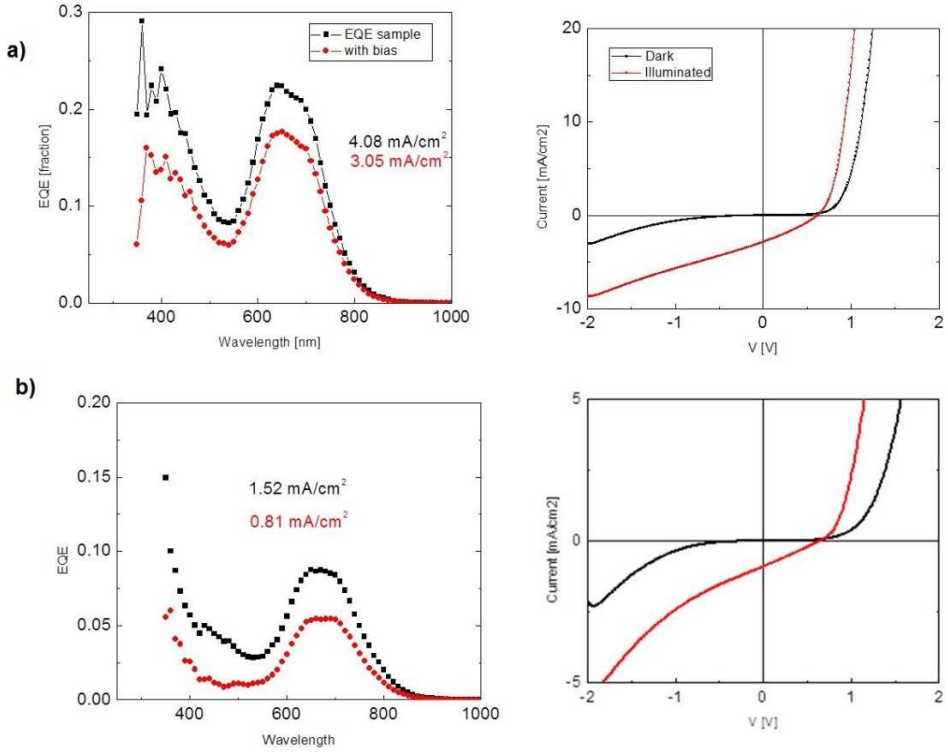

Figure 44. EQE spectrum and J-V curves of devices a) ***14a*** *and b)* ***14b***.

[43] b) B. C. Thompson, J. M. Fréchet, *Angew. Chem. Int. Ed. Engl*. **2008**, *47*, 58. e) A. Mishra, P. Bäuerle, *Angew. Chem. Int, Ed*. **2012**, *51*, 2020.

EQE spectra reveal the photocurrent response of each device. EQE maxima of devices based on dyads **14a**,**b** were observed at around 680 nm, where the maximum of the Q band the Pc macrocycle is located. Consequently, for these devices, the main contribution to the current comes from the Pc component. On the other hand, as can be seen in Figure 45, both sulfonylPc-DOTs based devices exhibit a maximum value at wavelengths in the range of 400-450 nm with tailings extending up to 800 nm. This result indicates that photocurrents mainly come from the absorption of the thiophene dendron group. In particular, the intensity of EQE in the range of 600-800 nm where the Q-band of Pc dominate, decreased when increasing the size of thiophene dendron for all devices. As a result, the thiophene dendron might be hindering the contribution of the Pc macrocycle to the solar cell performance, which could be responsible for the low Jsc.

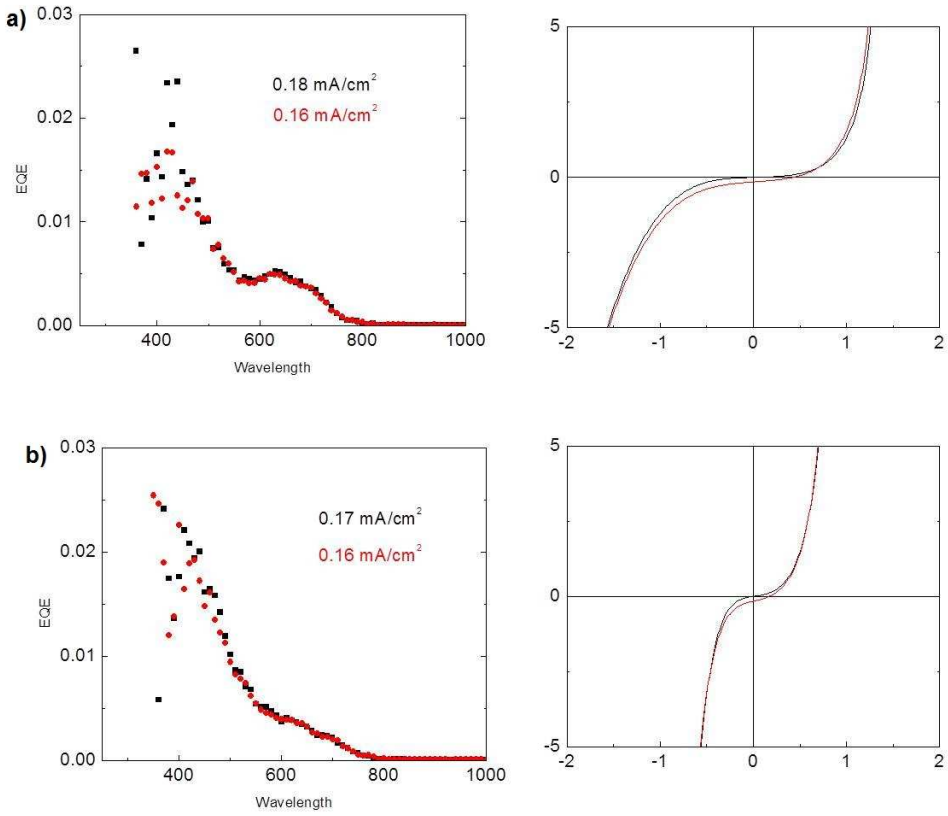

*Figure 45. EQE spectrum and J-V curves of devices a) **18a** and b) **18b**.*

In order to improve the performance of the most promising cell based on dyad **14a**, an additional device was fabricated with dyad **14a**-$PC_{71}BM$ in a 1:2 ratio. The device allowed for increased performances of J_{SC}= 4.28 mA/cm^2 leading to a PCE of 0.71%. Compared to the $PC_{61}BM$ device, the improved performance for $PC_{71}BM$ device is mainly due to the large increment of the short circuit current, which could be attributed to the better absorption properties of $PC_{71}BM$ in the range of 450-700 nm, as evident from the EQE spectrum (Figure 46).

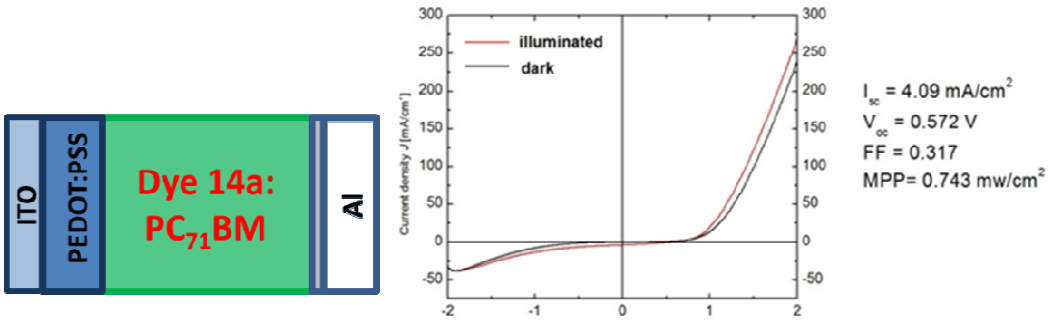

Figure 46. J-V curves of devices 14a:$PC_{71}BM$ device.

1.1.4. Summary and Conclusion

In summary

- A series of new zinc phthalocyanine-DOTs dyads were designed and synthesized to serve as new electron donor components for BHJ solar cells.

- As demonstrated by electrochemical measurements, peripheral substitution of zinc phthalocyanines by electron-deficient sulfonyl group gives rise to lower HOMO energy levels that should lead to higher Vocs. However, this hypothesis could not be tested, since a poor mixture of tris(octylsulfonyl)ZnPc-DOT dyads with the PCBM acceptor prevented the fabrication of meaningful photovoltaic devices.

- The best photovoltaic results (0.56% efficiency, an open-circuit voltage (Voc) of 0.62 V, a short-circuit current (Jsc) of 3.05 mAcm^{-2}, and a fill factor of 0.29) was achieved for dyad **14a** consisting of three-*tert*-butyl-substituted ZnPc bearing a first

generation of oligothiophene dendron. When $PC_{71}BM$ used as an acceptor instead of PCBM, the device demonstrated a short-circuit current density of 4.28 mA/cm^2, a Voc of 0.55 V, a fill factor (FF) of 0.3, and a PCE of ~0.71%.

General conclusion

Preliminary BHJ solar-cell measurements showed that tri-*tert*-butylZnPc-DOTs dyads did not produce any improvement in the photovoltaic performance in comparison to previously studied, symmetrical tetra-*tert*-butylZnPc and tetra-*tert*-butylRuPc.

Even though, substitution of Pc by the electron-deficient sulfonyl group decreases the HOMO level that should have led to a positive effect in the Voc photovoltaic performance, this influence could not be properly studied. Further work should be carried out to obtain better understanding of the effect of the sulfonyl group on the Pc in the photovoltaic performance.

Chapter 1.1. Experimental Section

1.1.5. Experimental Section

In this *Experimental Section*, the preparation and characterization of the compounds has been organized following the order as they appear in the text.

Chemical reagents were purchased from Aldrich Chemical Co., Acros Organics, or Fluka Chemie and were used without further purification. The monitoring of the reactions has been carried out by thin layer chromatography (TLC), employing aluminium sheets coated with silica gel type 60 F254 (0.2 mm thick, Merck). Purification and separation of the synthesized products was performed by column chromatography, using silica gel Merck-60 (230-400 mesh). The Size Exclusion Chromatography (SEC) was performed using Bio-Beads S-X1 (200-400 mesh).

Melting points (Mp) were determined in a Buchi 504392-S equipment and are uncorrected.

Nuclear magnetic resonance spectra (NMR) (^{1}HNMR) were recorded with Bruker AC-300 spectrometer. In this case, the deuterated solvents employed (commonly $CDCl_3$ and d_8-THF) are indicated in parentheses.

Matrix-assisted laser desorption/ionization time of flight (MALDI-TOF) MS and high resoltion mass spectrometry (HRMS) spectra were recorded with a Bruker Reflex III spectrometer and were carried out in the Sevicio Interdepartamental de investigacion (Sidl) of the Universidad Autonoma de Madrid. The most common matrix employed were dithranol (1,8,9-antracenetriol) and DCTB (trans-2-[3-(4-t-butyl-phenyl)-2-methyl-2-propenylidene]malononitrile).

UV/Vis spectra were recorded with a Hewlett-Packard 8453 instrument. In brackets is expressed the logarithm of the molar absorption coefficient (ε).

Infrared spectra (IR) were recorded on a Bruker Vector 22 spectrophotometer, using solid samples (KBr pellets) or as thin films (film), in the Departamento de Quimica Organica (UAM).

Cyclic voltammetry experiments were performed with a computer-controlled PGSTAT 30 potentiostat in a three-electrode single-compartment cell with a platinum working electrode, a platinum wire counter electrode, and a Ag/AgCl reference electrode with a scan rate of 100 mVs^{-1}. The sample concentration was maintained at $1x10^{-3}$M and TBAHFP (0.1m) as supporting electrolyte in $CHCl_2$ solution. All potentials were internally referenced to the Fc/Fc^+ couple.

Bulk Heterojunction solar cells were fabricated using ZnPc-DOTs dyads as the electron donor and PCBM as the electron acceptor. The ITO-coated glass substrates were cleaned with detergent, distilled water, acetone, and isopropyl alcohol in an ultrasonic bath and then dried. The ITO substrates were then treated in UV ozone cleaner for 30 min followed by spin coating of PEDOT:PSS (3000 rpm, 60s). The active layer was deposited by spin coating from a chlorobenzene solution of Pc-DOTs:PC_{60}BM (1:2) mixture with a total concentration of 25 mg/ml on the ITO/ PEDOT:PSS. The counter electrodes of LiF and Al were deposited by vacuum evaporation on the BHJ layer. All data were obtained under white light AM 1.5 G illuminations from a calibrated solar simulator with irradiation intensity of 100 mW cm^{-2}**.**

1.1.5.1. Synthesis of Precursor Phthalonitriles

1.1.5.1.1. Synthesis of 4-iodophthalonitrile (2)[111]

4-Aminophthalonitrile(**1**)[111a]

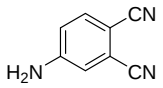

To a mixture of MeOH (450 ml) and concentrated HCl (96 ml), 4-nitrophthalonitrile (20 g, 115 mmol) was added. Upon heating to reflux, total dissolution of the solid was observed and iron powder (22 g, 392 mmol) was added in small portions over 1 h. The brown solution was stirred at reflux for another 1 h and allowed to warm up to room temperature. Cold water (600 ml) was then poured into the mixture resulting in the precipitation of a yellow-green solid, which was filtered, washed with water and vacuum-dried. Recrystallization from toluene led to compound **1** (12.6 g, 88 mmol) as white crystalline needles. Yield: 76%.

Mp: 171-173 ºC (reported: [111a] 172-174 ºC).

^{1}H NMR (DMSO-d_6, 300 MHz): δ (ppm) = 7.6 (d, *J*= 8.7 Hz, 1H, H-6), 7.0 (d, *J*= 2.5 Hz, 1H; H-3), 6.8 (dd, *J* = 8.7, 2.5 Hz, 1H; H-5), 6.7 (br. s, 2H; NH_2).

4-Iodophthalonitrile (**2**)[111b]

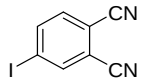

A suspension of 4-aminophthalonitrile (**1**) (5.0 g, 35 mmol) in H_2SO_4 2.5 M (70 ml) was cooled to -10 ºC and a solution of $NaNO_2$ (2.8 g, 39 mmol) in water (10 ml) was added dropwise under stirring. After total addition, the mixture was further stirred at 0 ºC for 30 min and then poured over a solution of KI (6.5 g, 39 mmol) in cold water (40

[111] a) H. Lam, S. M. Marcuccio, P. I. Svirskaya. S. Greenberg, A. B. P. Lever, C. C. Leznoff, R. L. Cerny, *Can. J. Chem.* **1989**, *67*, 1087. b) J. G. Young, W. Onyebuagu, *J. Org. Chem.* **1990**, *55*, 2155.

ml). The resulting mixture was stirred at room temperature for 45 min and the brown solid was filtered, washed with water and dissolved in $CHCl_3$ (200 ml). This solution was then washed with a saturated solution of $Na_2S_2O_3$ (30 ml) and water (30 ml), and dried over Na_2SO_4. After filtration of the drying agent, the solvent was evaporated and the yellow solid obtained was subjected to column chromatography on silica gel using CH_2Cl_2 as eluent. Compound **2** was obtained (6.1 g, 24 mmol) as a white solid. Yield: 69%.

Mp: 141-143 ºC (reported: [111b] 142-143 ºC).

^{1}H NMR ($CDCl_3$, 300 MHz): δ (ppm) = 8.2 (d, *J*= 1.6 Hz 1H; H-3), 8.1 (dd, *J*= 8.2 Hz, 1H; H-5), 7.5 (d, *J* = 8.6, 1H; H-6).

1.1.5.1.2. Synthesis of 4, 5-dichlorophthalonitrile (6)[113]

4, 5-Dichlorophthalic anhydride (**3**)

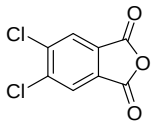

A solution of 4,5-dichlorophthalic acid (15g, 64 mmol) in acetic anhydride (25 ml) was heated to reflux while distilling the acetic acid being formed in the reaction. After 5h, the remaining acetic acid was removed by vacuum distillation. The solid obtained was stirred in petroleum ether over 12 h, obtaining a solid that was filtered and thoroughly washed with the same solvent (3x20 ml). Compound **3** was obtained (13.5 g, 62.5 mmol), in 98% yield.

Mp: 182-184 ºC (reported: [113] 184-186 ºC).

^{1}H NMR ($CDCl_3$, 300 MHz): δ (ppm) = 8.1 (s, 2H, H-3, H-6).

[113] D. Wohrle, M. Eskes, K. Shigehara, A. Yamada, *Synthesis*, **1993**, 194.

4, 5-Dichlorophthalimide (**4**)

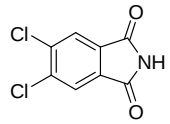

A mixture of 4,5-dichlorophhtalic anhydride (**3**) (13.5 g, 62.5 mmol), and formamide (20 ml) was heated to 200 ºC over 3 h. after cooling to room temperature, the solid obtained was filtered, washed with water (1x20 ml) and vacuum-dried. 4,5-dichlorophthalimide (**4**) was obtained (12, 4 g, 57.7 mmol) as a white solid. Yield: 92%.

Mp: 192-194 ºC (reported:[113] 193-195 ºC).

^{1}H NMR ($CDCl_3$, 300 MHz): δ (ppm)= 8.1 (s, 2H, H-3, H-6).

4, 5-Dichlorophthalamide (**5**)

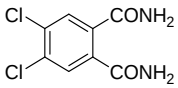

A suspension of 4,5-dichlorophthalimide (**4**) (12.4g, 57.7 mmol) in 25% aqueous ammonia (173 ml) was stirred at room temperature for 24 h. Then, a 33% ammonium hydroxide solution (58 ml) was added and the mixture was further stirred for 24 h. The white solid was filtered, washed with water (3x15ml) and vacuum-dried. Compound **5** was obtained (12 g, 51.3 mmol) as a white solid. Yield: 89%.

Mp: 241-244 ºC (reported:[113] 245-247 ºC).

^{1}H NMR ($CDCl_3$, 300 MHz): δ (ppm) = 7.9 (s, br, 2H, NH_2), 7.7 (s, 2H, H-3, H-6), 7.4 (s, br, 2H, NH_2).

4,5-Dichlorophthalonitrile (**6**)

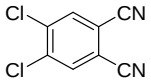

Freshly distilled thionyl chloride (42 ml) was cautiously poured over dry DMF (60 ml) at 0 ºC and under argon atmosphere. The mixture was vigorously stirred for 2h at that temperature and then 4, 5-dichlorophthalamide (**5**) (11.9, 51.3 mmol) was added. After stirring for 12 h at room temperature the reaction mixture was poured onto ice (100 ml), resulting in the precipitation of a slightly gray solid, which was filtered and washed with water (1x20 ml). Compound **6** was obtained (8.8 g, 45 mmol), after recrystallization from methanol, as a white solid. Yield: 88%.

Mp: 180-183 ºC (reported:[113] 182-184 ºC).

^{1}H NMR ($CDCl_3$, 300 MHz): δ (ppm) = 7.9 (s, 2H, H-3, H-6).

1.1.5.1.3. Synthesis of 4,5-bis(octylsulfonyl)phthalonitrile (8)[112]

4,5-Bis(octylthio)phthalonitrile (**7**)

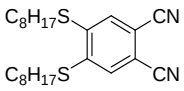

A mixture of 4,5-dichlorophthalonitrile (**6**) (2.4 g, 12.2 mmol) and K_2CO_3 (5 g, 36.2 mmol) was stirred in dimethylacetamide (DMAC) (30 ml) at room temperature and under argon atmosphere for 10 min. Then, 1- octanethiol (4.65 ml, 26.8 mmol was added, and the mixture was stirred at 80 ℃ for 12 h. The crude reaction was diluted with CH_2Cl_2, and the organic phase was washed with H_2O. The solvent was removed at reduced pressure. 4,5-bis(octylthio)phthalonitrile (**7**) (4 g, 9.6 mmol) was obtained, after recrystallization from ethanol, as white needles. Yield: 79%.

---

[112] B. del Rey, U. Keller, T. Torres, G. Rojo, F. Agullo-Lopez, S. Nonell, C. Marti, S. Brasselet, I. Ledoux, J. Zyss, *J. Am. Soc.* **1998**, *120*, 12808.

Mp: 61 ºC (reported:[112] 62 ºC).

^{1}H NMR ($CDCl_3$, 300 MHz): δ (ppm)= 7.4 (s, 2H, H-3, H-6), 3 (m, 4H, SCH_2), 1.8-1.6 (m, 4H, CH_2), 1.5-1.3 (M, 4H, CH_2), 1.3-1.1 (m, 16H, CH_2), 0.88 (m, 6H, CH_3).

4,5-Bis(octylsulfonyl)phthalonitrile (**8**)

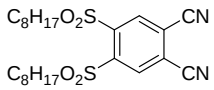

To solution of 4,5-bis(octylthio)phthalonitrile (**7**) (1.2 g, 2.91 mmol) in acetic acid (35 mL) at 90 ºC, a 33% H_2O_2 (15 ml) solution was added slowly, in the course of 4 h. The mixture was then stirred at room temperature for 16 h. The white precipitate formed was collected by filtration, washed several times with water, and recrycystallized from ethanol to yield 4,5-bis(octylsulfonyl)phthalonitrile (**8**) (1.17g, 2.4 mmol) as a white solid. Yield: 84%.

Mp: 74 ºC (reported:[112] 75 ºC).

^{1}H NMR ($CDCl_3$, 300 MHz): δ (ppm) = 8.6 (s, 2H, H-3, H-6), 3.6 (m, 4H, SCH_2), 1.8-1.6 (m, 4H, CH_2), 1.5-1.3 (m, 4H, CH_2), 1.3-1.1 (m, 16H, CH_2), 0.9 (m, 6H, CH_3).

1.1.5.1.4. Synthesis of 4-octylsulfonylphthalonitrile (10)[112]

4-Thiooctylphthalonitrile (**9**)

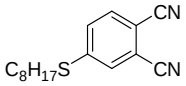

A mixture of 4-nitrophthalonitrile (3 g, 17.3 mmol) and 1-octanethiol (3.6 ml, 20.8 mmol) was stirred for 10 min in DMSO (10 ml). Then K_2CO_3 (2.8 g, 20.8 mmol)

[112] B. del Rey, U. Keller, T. Torres, G. Rojo, F. Agullo-Lopez, S. Nonell, C. Marti, S. Brasselet, I. Ledoux, J. Zyss, *J. Am. Soc.* **1998**, *120*, 12808.

was added slowly over a period of 3h, and the reaction was stirred overnight at room temperature. The mixture was extracted with CH_2Cl_2, washed with a 5% solution of K_2CO_3 and dried over sodium sulfate. The solvent was removed under reduced pressure. The yellow oil was purified by column chromatography on silica gel (CH_2Cl_2/hexanes, 2:1) to yield **9** (3.02 g) as a yellow-white solid. Yield: 64%.

Mp: 31-33 ºC (reported:[112] 32-35 ºC).

^{1}HNMR ($CDCl_3$, 300 MHz): δ (ppm)= 7.6 (d, *J* =9 Hz, 1H), 7.5 (br, s, 1H), 7.4 (dd, *J*= 3, 9 Hz 1H), 2.9 (t, *J*= 6 Hz, 2H), 1.7-1.6 (m, 2H), 1.5-1.4 (m, 2H), 1.38-1.18 (m, 8H), 0.8 (t, *J*=6, 3H, CH_3).

4-Octylsulfonylphthalonitrile (**10**)

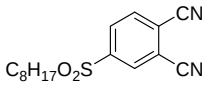

4-thiooctylphthalonitrile (**9)** (3g, 11mmol) was stirred with acetic acid (20 ml) at reflux. H_2O_2 (60ml) was added slowly, and the mixture was refluxed for 2 h. The solution was poured into water and the white solid obtained was then filtered, washed several times with water and dried. Compound **10** (2.7 g, 8.8 mmol) was obtained as a white solid. Yield:80%.

Mp: 68-71 ºC (reported:[112] 70-72 ºC).

^{1}HNMR ($CDCl_3$, 300 MHz): δ (ppm) = 8.3 (br,s, 1H), 8.2 (dd, *J*= 1.5, 8.1 Hz 1H), 8.0 (d, *J* =8.1 Hz, 1H), 3.1 (t, *J*= 8.1 Hz, 2H), 1.7-1.6 (m, 2H), 1.5-1.1 (m, 10H), 0.8 (t, *J*=6.1, 3H).

1.1.5.1.5. Deprotection of the TMS groups for DOTs[114]

General procedure: To a solution of TMS-protected dendron in THF-MeOH (2.5:2.5 ml) K_2CO_3 was added. The reaction mixture was stirred for 2 h at room temperature. Then the solvent was evaporated under reduced pressure and the crude product was purified by column chromatography on silica gel.

5'-Ethynyl-5,5"-bis(trimethylsilyl)-2,2':3',2"-terthiophene (**11**) and 5'- Ethynyl-5,5''-bis[5,5''-bis(trimethylsilyl)-2,2':3',2''-terthien-5'-yl-ethynyl]-2,2':3',2''-terthiophene (**12**):

Compound **11** was prepared according to the general procedure using corresponding TMS-protected dendron (100 mg, 0.2 mmol) and K_2CO_3 (56 mg, 0.41 mmol). Purification by column chromatography (Hexanes/CH_2Cl_2, 1:1) yielded compound **11** (70 mg, 0.17 mmol) as a yellow viscous oil. Yield: 85%

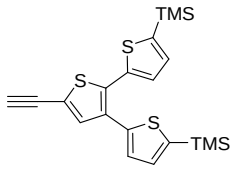

^{1}HNMR ($CDCl_3$, 300 MHz): δ (ppm) = 7.3 (s, 1H), 7.1 (d, *J* = 5.3 Hz, 1H), 7.2 (dd, *J* = 3.3, 3.5 Hz, 2H), 7.0 (d, *J* = 3.5 Hz 1H), 3.4 (s, 1H), 0.3, (s, 18H, TMS).

Compound **12** was prepared according to the general procedure using corresponding TMS-protected dendron (90 mg, 0.07 mmol) and K_2CO_3 (21 mg, 0.15 mmol). Purification by column chromatography (Hexanes/CH_2Cl_2, 1:1) yielded compound **12** (72 mg, 0.06 mmol) as a yellow viscous oil. Yield: 86 %

^{1}HNMR ($CDCl_3$, 300 MHz): δ (ppm) = 7.4 ppm (s, 2H), 7.3, (s, 1 H), 7.1–7.2 (m, br,10H), 7.0 (d, *J*=3.8 Hz, 1H), 6.9 (d, *J*=3.8 Hz, 1H), 0.3 (s, 36H, TMS).

[114] A. Mishra, C. Q. Ma, R. A. J. Janssen, P. Bauerle, *Chem. Eur. J.* **2009**, *15*, 13521.

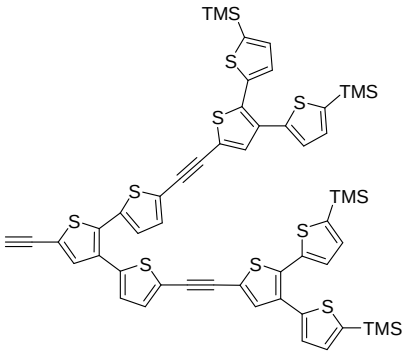

1.1.5.2. Synthesis of Zinc Phthalocyanine-DOTs Dyads

1.1.5.2.1. Synthesis of tri(tert-butyl)phthalocyanine-DOTs dyads 14a,b.

Zinc (II) 9(10),16(17),23(24)-tri-*tert*-butyl-2-iodophthalocyaninato(2-)-N^{29}, N^{30}, N^{31}, N^{32} (**13**)[110a]

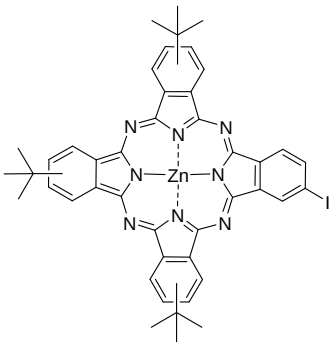

A mixture of 4-*tert*-butylphthalonitrile (1g, 5.42 mmol) and 4-iodophthalonitrile (**2**) (0.27 g, 1.08 mmol) was refluxed in DMAE (5ml) under argon for 20 h in the presence of $Zn(OAc)_2$ (0.36 g, 2.7 mmol). The solvent was removed under reduced pressure and the blue solid was washed with a MeOH-H_2O (5:1) mixture. The tri-t*ert*-butyliodo phthalocyanine was purified by column chromatography on silica gel (Hexanes/dioxane, 3:1), to yield **13** (0.22 mg) as a blue solid. Yield: 23%.

[110] a) E. M. Maya, P. Vázquez, T. Torres, *Chem. Eur. J.* **1999**, *5*, 2004.

Mp >250 ºC.

^{1}HNMR ($CDCl_3$, 300 MHz): δ (ppm) = 8.7-7.3 (m, 12H), 1.9-1.7 (m, 27H, $C(CH_3)_3$).

UV/Vis (THF): λ_{max} (log ε) = 673 (5.1), 612 (4.3), 351 (4.8).

Synthesis of tris(tert-butyl)ZnPc-DOTs dyads (**14a,b)**

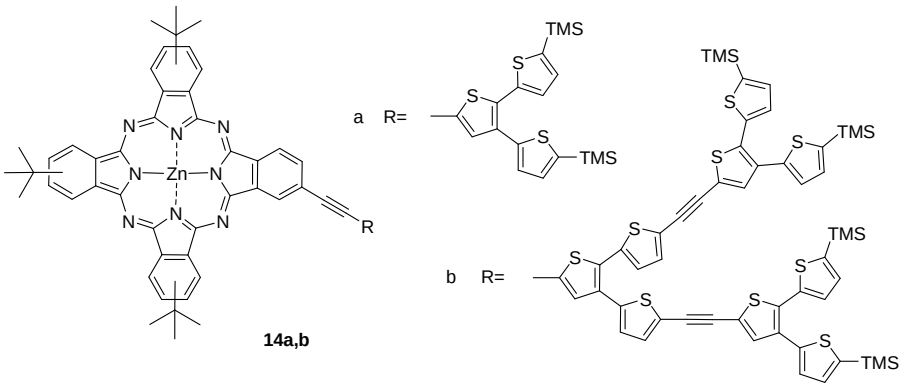

14a,b

General procedure: To a freshly distilled and deaerated THF/ TEA (8:1) solution containing Pc **13** (64 mg, 0.07 mmol), [$Pd(PPh_3)Cl_2$] (5 mg, 0,007mmol) and CuI (1.5 mg, 0.007 mmol), the corresponding DOT derivative **11** or **12** (0.22 mmol) was added and the mixture was stirred for 24 h at room temperature. The solvent was then removed under reduced pressure, and the green solid was extracted with $CHCl_3$, washed with water and dried over Na_2SO_4. The crude product was purified by column chromatography on silica gel (Hexanes/dioxane, 3:1). Compound **14a** was obtained (55 mg, 0.047 mmol) as a green solid. Yield: 67%.

Mp >250 ºC.

^{1}HNMR (d_8-THF, 300 MHz): δ (ppm) = 9.5-8.8 (m, 9H, Ar-H), 8.3-8.1 (m, 3H, Ar-H), 7.7 (d, *J*=9 Hz, 1H, Ar-H), 7.3-7.2 (m, 4H, Ar-H), 1.8 (s, 27H, $C(CH_3)_3$), 0.3 (s, 18H, TMS).

IR (film): v (cm^{-1}) = 2955, 2928, 1620, 1491, 1400, 1325, 1094, 997, 839, 762, 748.

UV/Vis ($CHCl_3$): λ_{max} (log ε) = 695 (5.2), 678 (5.1), 642 (4.4), 617 (4.4), 352 (4.9).

HRMS (MALDI-TOF, DCTB): calc. for $C_{64}H_{62}N_8S_3Si_2Zn$: [M^+]: m/z: 1158.3084, found 1158.3051.

Compound **14b** (65 mg, 0.035 mmol) was obtained as a green solid. Yield: 51%.

Mp >250 ºC.

^{1}HNMR (d_8-THF, 300 MHz): δ (ppm)= 9.5-8.9 (m, 9H, Ar-H), 8.4-8.1 (m, 3H, Ar-H), 7.7 (d, *J*=12 Hz, 1H, Ar-H), 7.5 (s, 2H, Ar-H), 7.4 (t, *J*=3 Hz 2H, Ar-H), 7.3-7.2 (m, 2H, Ar-H), 7.2-7.1 (m, 8H, Ar-H), 1.8 (s, 27H, $C(CH_3)_3$), 0.3 (s, 36H, TMS).

IR (film): v (cm^{-1}) = 2957, 2920, 1728, 1624, 1497, 1254, 1101, 993, 839, 758.

UV/Vis ($CHCl_3$): λ_{max} (log ε) = 696 (5.2), 678 (5.1), 640 (4.5), 617 (4.4), 345 (5.0).

HRMS (MALDI-TOF, dithranol): calc. for $C_{98}H_{90}N_8S_9Si_4Zn$: [M^+]: m/z: 1842.3138, found 1842.3148.

1.1.5.2.2. Synthesis of tris(octylsulfonyl)phthalocyanine-DOTs dyads (18a,b)

Zinc (II) 9(10),16(17),23(24)-tris(octylsulfonyl)-2-iodophthalocyaninato(2-)-N^{29}, N^{30}, N^{31}, N^{32} (**17**)

A mixture of 4-octylsulfonylphthalonitrile (**10**) (1g, 3.28 mmol) and 4-iodophthalonitrile (**2**) (0.27 g, 1.08 mmol) was refluxed in a mixture of o-DCB/DMF (2:2) overnight under argon in the presence of $Zn(OAc)_2$ (0.20 g, 1.09 mmol). The solvent was evaporated and the blue solid obtained was dissolved in CH_2Cl_2 and washed with water. The crude product was purified by column chromatography on silica gel (CH_2Cl_2/THF, 100:3), to yield **17** (0.2 g, 0.16 mmol) as a blue solid. Yield: 16%.

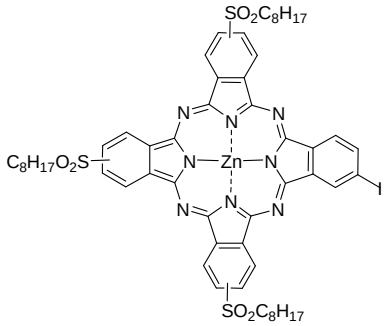

Mp >250 ºC.

^{1}HNMR (d_8-THF, 300 MHz): δ (ppm)= 9.7-9.5 (m, 3H; Ar-H), 9.4-8.7 (m, 9H; Ar-H), 4.0-3.6 (m, 6H, Alkyl-H), 2.3-2.2 (m, 6H, Alkyl H), 1.8-1.3 (m, 30H, Alkyl-H), 0.9-0.8 (m, 9H, CH_3).

IR (film): ν (cm^{-1}) = 2934, 2853, 2650, 1705, 1597, 1489, 1313, 1138, 908, 841.

UV/Vis (THF): λ_{max} (log ε) = 673 (5.3), 607 (4.6), 350 (4.8).

MS (MALDI, dithranol): m/z: 1230.3 [M^+].

Synthesis of tris(octylsulfonyl)ZnPc-DOTs dyads (**18a,b**).

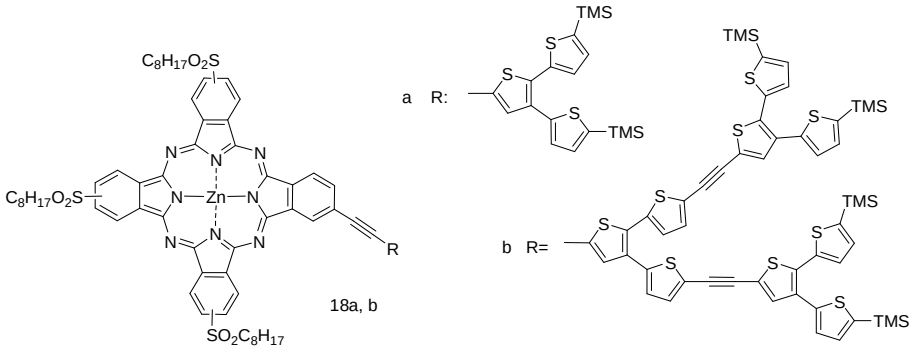

General Procedure: A mixture of tri-(octylsulfonyl)iodophthalocyanine (**17)** (100mg, 0.08 mmol), [$Pd_2(dba)_3$] (14mg, 0.016mmol) and $AsPh_3$ (10 mg, 0.03 mmol) was stirred in freshly distiiled and deaerated piperidine. The corresponding DOT derivatives (**11** or **12**) (0.08 mmol) were then added and the reaction was stirred under

argon at 35 ºC for 20 h. The solvent was removed under reduced pressure, and the green solid was extracted with CH_2Cl_2, washed with water, and dried over Na_2SO_4. The crude product was purified by column chromatography on silica gel (CH_2Cl_2/THF, 100:3).

Compound **18a** (33 mg, 0.021 mmol) was obtained as a green solid. Yield: 25%.

Mp >250 ºC.

^{1}HNMR (d_8-THF, 300 MHz): δ (ppm)= 9.9-9.4 (m, 3H, PcH), 9.4-8.6 (m, 8H, PcH), 8.5-8.2 (m, 1H, PcH), 7.9-7.8 (m, 1H, Ar-H), 7.4-7.2 (m, 4H, Ar-H), 3.8-3.7 (m, 6H, Alkyl-H), 2.2-2.1 (m, 6H, Alkyl-H), 1.6-1.1 (m, 30H, Alkyl-H), 0.8-0.7 (m, 9H, CH_3), 0.4 (s, 18H, TMS).

IR (film): ν (cm^{-1}) = 2959, 2932, 2864, 1605, 1485, 1404, 1210, 1148, 1094, 986, 841,746.

UV/Vis ($CHCl_3$): λmax (log ε) = 680 (5.3), 614 (4.5), 353 (4.8).

HRMS (MALDI-TOF, dithranol): calc. for $C_{76}H_{86}N_8O_6S_6Si_2Zn$: [$M^+$]: m/z: 1518.3819, found 1518.3808.

Compound **18b** (38 mg, 0.017 mmol) was obtained as a green solid after purification. Yield: 21**%.**

Mp >250 ºC.

^{1}HNMR (d_8-THF, 300 MHz): δ (ppm)= 9.7-9.5 (m, 3H, Pc-H), 9.2-8.7 (m, 8H, Pc-H), 8.4-8.3 (m, 1H, Pc-H), 7.94-7.89 (m, 1H, Ar-H), 7.5-7.4 (m, 6H, Ar-H), 7.2-7.1 (m, 8H, Ar-H) 3.8-3.7 (m, 6H, Alkyl-H), 2.3-2.2 (m, 6H, Alkyl-H), 1.5-1.2 (m, 30H, Alkyl-H), 0.8 (s, 9H, CH_3), 0.32 (s, 36H, TMS).

IR (film): ν (cm^{-1}) = 2959, 2932, 2851, 1603, 1481, 1400, 1306, 1252, 1144, 1090, 995, 849, 806, 752.

UV/Vis ($CHCl_3$): λmax (log ε) = 680 (5.3), 614 (4.6), 366 (5.0).

HRMS (MALDI-TOF, dithranol): calc. for $C_{110}H_{114}N_8O_6S_{12}Si_4Zn$: [$M^+$]: m/z: 2202.3873, found 2202.3953.

Zinc (II) 9,10,16,17,23,24- hexakis(octylthio)-2-iodophthalocyaninato(2-)-N^{29}, N^{30}, N^{31}, N^{32} (**16**)

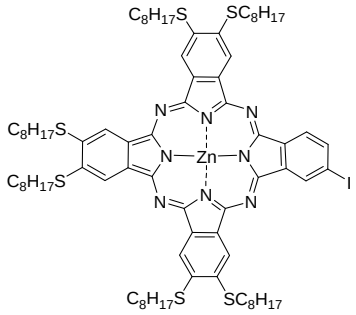

A mixture of 4,5-bis(octylthio)phthalonitrile (**6**) (1g, 3.67 mmol) and 4 iodophthalonitrile (**2**) (310 mg, 1.22 mmol) was refluxed in DMAE (5ml) under argon for 20 h in the presence of $Zn(OAc)_2$ (227 mg, 1.2 mmol). The solvent was removed under reduced pressure and the blue solid was washed with a MeOH-H_2O (5:1) mixture. Compound **16** was purified by column chromatography on silica gel (Hexanes/dioxane, 4:1), to yield **16** (300 mg, 0.26 mmol) as a green solid. Yield: 22%.

Mp >250 ºC.

^{1}HNMR (d_8-THF, 300 MHz): δ (ppm) = 8.9-7.8 (m, 9H, Ar-H), 4.2-3.5 (m, 12H, CH_2SO_2), 2.4-1.9 (m, 12H, CH_2), 1.8-1.3 (m, 60H, CH_2), 1.1-0.8 (m, 18H, CH_3).

IR (film): v (cm^{-1}) = 2958, 2902, 1565, 1460, 1350, 1100, 930.

UV/Vis (THF): λ_{max} (log ε) = 670 (5.1), 615 (4.3), 341 (4.5).

MS (MALDI, dithranol): m/z: [M^+]. 1166.5

Chapter 1.2. Azulenocyanine-SWNTs and Azulenocyanine-C_{60} dyads

1.2.1. Introduction

Chromophores which absorb light in the near–infrared (NIR) region (750 to 2500 nm) have become of increasing interest in recent years in many applications such as photovoltaic and photodynamic therapy (PDT).[117] PDT is a medical treatment, in which light energy absorbed by chromophores is transferred to oxygen molecules in the cell to produce toxic singlet oxygen, which causes cell death. Near-IR light can penetrate deeper into tissues and causes less damage than shorter wavelength light, hence dyes that absorb in the near-IR region are attractive candidates for PDT.

Concerning photovoltaic applications, although significant achievements have been made in all-organic bulk heterojunction and dye-sensitized solar cells, organic photovoltaic devices have not yet reached practical power conversion efficiencies to compete with commercial silicon-based solar cells.[43b-e,86] There is still need for the design of new organic materials for improving the device efficiencies. Some evidence suggests that the present limit of device efficiency is related to the light harvesting ability of the molecular components of the active layer. Ideal organic dyes should efficiently absorb light throughout a large portion of the solar emision spectrum, especially in the red and the near-infrared regions. Nearly 50% of the solar energy lies in the near-IR, indicating that the development of photovoltaic devices capable of absorbing in this region could lead to great advances in the solar energy technology. Not many organic molecules fulfil, however, this requirement and the preparation of stable NIR dyes remains a great challenge.[118]

---

[43] b) B. C. Thompson, J. M. Fréchet, *Angew. Chem. Int. Ed. Engl.* **2008**, *47*, 58. c) T. M. Clarke, J. R. Durrant, *Chem. Rev.* **2010**, *110*, 6736. d) C. W. Schlenker, M. E. Thompson, *Chem. Commun.* **2011**, *47*, 3702. e) A. Mishra, P. Bäuerle, *Angew. Chem. Int, Ed.* **2012**, *51*, 2020.

[86] A. Hagfelt, G. Boschloo, L. Sun, L. Kloo, H. Pettersson, *Chem. Rev.* **2010**, *110*, 6595.

[117] a) R. Bonnett, *Chem. Soc. Rev.* **1995**, *24*, 19. b) M. C DeRosa, R. J. Crutchley, *Coord. Chem. Rev*. **2002**, *233*, 351. c) S. Luo, E. Zhang, Y. Su, T. Cheng, C. Shi, *Biomaterials,* **2011**, *32*, 7127.

[118] a) A. Samanta, M. Vendrell, R. Das, Y. T. Chang, *Chem. Commun*. **2010**, 7406. b) G. Qian, Z. Wang, *Chem. Asian J.* **2010**, *5*, 1006. c) C. Jiao, K. W. Huang, J. Wu, *Org. Lett.* **2011**, *13*, 632. d) G. Ulrich, S. Goeb, A. De Nicola, P. Retailleau, R. Ziessel, *J. Org. Chem.* **2011**, *76*, 4489. e) M. Luo, Q. Wang, Z. Y. Wang, *Org. Lett.* **2011**, *13*, *4092*.

NIR Absorbing Phthalocyanines

Pcs are among the molecules that reveal an intense NIR absorption. Currently many efforts are directed towards modifying the optical and electronic properties of phthalocyanine since most them have their main absorption band at 650-700 nm, whereas 50% of solar energy occurs beyond 750 nm.[16c-f] There are many possible modifications of the molecular structure of Pcs that can provide control of the physical, electronic and optical properties of the materials; namely, 1) incorporation of different metals inside the macrocycle, 2) extension of the π-system, 3) substitution with electron-donating or electron-withdrawing moieties at the peripheral or axial positions. In particular, functionalization at the α positions of the Pc by electron donating groups[119] (Figure 47a) or enlargement of the ring system by using naphthalene (naphthalocyanine)[120] (Figure 47b) or anthracene (anthracocyanine)[120b] (Figure 47c) instead of benzene allows to decrease the HOMO-LUMO gap shifting the absorption into the near–IR region. However, the main drawback of these methods is that they cause an destabilization of the HOMO level which results in an easier oxidation and therefore reduced stability.

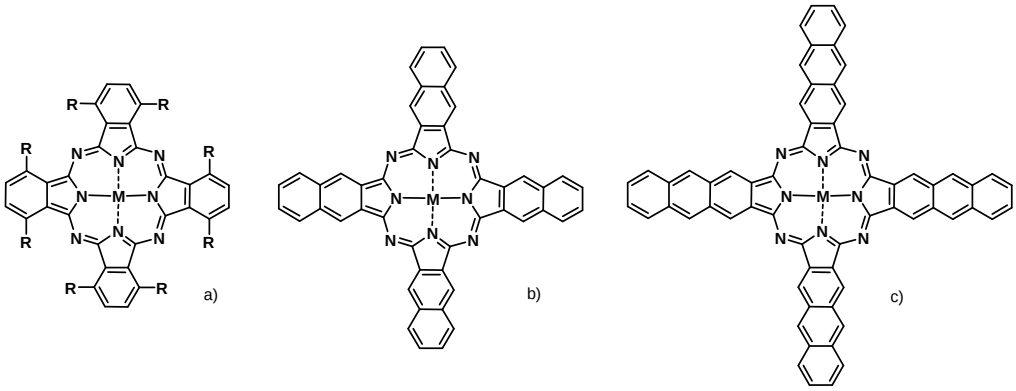

Figure 47. Molecular structure of a) α-substituted Pc, b) napthalocyanine and c) anthracocyanine.

16 c) G. de la Torre, C. G. Claessens, T. Torres, *Chem. Comm*. **2007**, 2000. d) C. G. Claessens, U. Hahn, T. Torres, *Chem. Record*. **2008**, *8*, 75. e) Y. Rio, M. S. Rodríguez-Morgade, T. Torres, *Org. Biomol. Chem.* **2008**, *6*, 1877. f) J. Mack, N. Kobayashi, *Chem. Rev.* **2011**, *111*, 281.

119 a) M. Cook, *J. Chem. Rec.* **2002**, *2*, 225. b) N. Kobayashi, H. Ogata, N. Nonaka, E. A. Lukyanets, *Chem. Eur. J*. **2003**, *9*, 5123. c) T. Fukuda, S. Homma, N. Kobayashi, *Chem. Eur. J.* **2005**, *11*, 5205.

120 a) Y. G. Yang, M. Hanack, Y. W. Lee, Y. Chen, M. Y. K. Lee, D. Dini, *Chem. Eur. J.* **2003**, *9*, 2758. b) N. Kobayashi, S. I. Nakajima, H. Ogata, T. Kukuda, *Chem. Eur. J.* **2004**, *10*, 6294. c) S. Shimizu, H. Zhu, N. Kobayashi, *Chem. Eur. J.* **2010**, *16*, 1151.

Recently, Kobayashi and co-workers reported on stable Pcs having Q bands beyond 1000 nm by using several synergistic effects; namely, destabilization of the HOMO via introduction of electron donating groups at the α positions and stabilization of the LUMO by the introduction of the strongly electron withdrawing phosphorus atom in the centre and deformation of the planarity of the Pc plane (Figure 48).[121] The same authors also reported, recently, novel expanded Pc congeners containing two Mo=O or W=O central cores which are further coordinated by two pyrrole nitrogen atoms and two amino nitrogen atoms of the macrocycle (Figure 48).[122] The HOMO-LUMO energy difference of these compounds is smaller than that of tetra-*tert*-butyl-H_2Pc and relatively stable, since the stabilization of the LUMO is rather larger than the destabilization of the HOMO. These new Pcs have a 22-π-electron system and strong electronic absorption beyond 900nm.

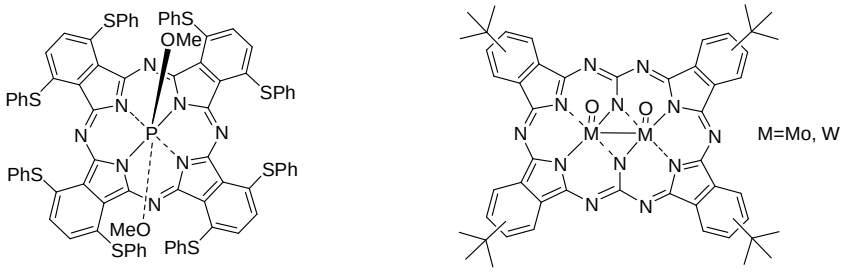

Figure 48. Molecular structure of Near-IR phthalocyanines.

Azulene

Bicyclo[5.3.0]decapentaene, also known as *azulene*, (Figure 49) is a 10-π-electron nonbenzenoid, aromatic compound with unique properties such as a remarkable polarizability, which can be explained by polar resonance structures, in which a fused tropylium cation and a cyclopentadienyl anion are formed. Therefore, in contrast to structurally isomeric and isoelectronic nonpolar naphthalene, azulenes give rise to strong dipole moments (1.08 D) due to the charge drift from the seven- to the

[121] N. Kobayashi, T. Furuyama, K. Satoh, *J. Am. Chem. Soc.* **2011***, 133*, 19642.
[122] O. Matsushita, V. M. Derkacheva, A. Muranaka, S. Shimizu, M. Uchiyama, E. A. Lukyanets, N. Kobayashi, *J. Am.Chem.Soc*. **2012**, *134*, 3411.

five-membered ring, and absorb light in the visible range, which gives rise to a remarkable blue colour of its solutions.[123]

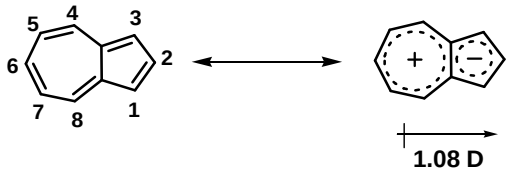

Figure 49. Azulene and its stable resonance forms, its dipole moment, and carbon atom numbering.

Azulenes exhibit weak absorption in the visible spectral range (450-750 nm) due to a S_0-S_1 transition and a strong absorption in the UV range, which relates to the S_0-S_2 transition (Figure 50). Another unusual characteristic of azulene is the violation of Kasha`s rules: fluorescence generally occurs from the lowest excited state of the molecule.[124] Owing to this feature, azulene displays long-lived (~3 ns) and strong fluorescence from the second excited state (S_2) and an ultra-fast internal conversion within 1ps from the S_1 state to the S_0 state.[125] This is because of the low-lying excited state, S_1 and large S_2-S_1 energy gap. These properties make azulene extremely suitable component for developing advanced materials including nonlinear chromophors,[126] conducting polymer[127] and charge transfer complexes.[128] Furthermore,

---

[123] a) G. Anderson, J. A. Nelson, J. J. Tazuma, *J. Am. Chem. Soc*. **1953**, *75*, 4980. b) K. Hafner, C. Bernhard, *Angew. Chem. Int. Ed.* **1957**, *69*, 533. c) A. G. Anderson, J. B. M. Steckler, *J. Am. Chem. Soc*. **1959**, *81*, 4961. d) K. Hafner, *Pure. Apply. Chem.* **1971**, *28*, 153. e) A. Hinchliffe, H. J Soscun, *Chem. Phys. Lett.* **2005**, *412*, 365. f) M. Kedziorek, P. Mayer, H. Mayr, *Eur. J. Org. Chem*. **2009**,1202.

[124] M. Kasha, *Discuss. Farady Soc.* **1950**, *9*, 14

[125] a) B. D. Wagner, D. Tittelbach-Helmrich, R. P. Steer, *J. Phys. Chem.* **1992**, *96*, 7904. b) D.Tittelback-Helmrich, B. D. Wagner, R. P. Steer, *Chem. Phys. Lett.* **1993**, *209*, 464. c) D. Tittelback-Helmrich, B. D. Wagner, R. P. Steer, *Can. J. Chem.* **1995**, *73*, 3003. d) M. J. Bearpark, F. Bernardi, S. Clifford, M. Olivucci, M. A. Robb, B. R. Smith, T. Vreven, *J. Am. Soc.* **1996**, *118*, 169. e) L. Ciano, P. Foggi, P. R. Salvi, *J. Photochem. Photobiol. A.* **1997**, *105*, 129. f) B. R. Bearpark, T. Vreven, *J. Am. Chem. Soc*. **1996**, *118*, 169. g) N. Tetreault, R. S. Muthyala, R. S. H. Liu, R. P. Steer, *J. Phys. Chem. A.* **1999,** *103,* 2524. h) Y. Zhang, K. Aslan, M. J. R. Previte, C. D. Geddes, *Chem. Phys. Lett.* **2006**, *432*, 528. i) Y. Numata, S. Toyoshima, K. Okuyama, M. Yasunami, I. Suzuka, *J. Phys. Chem. A*. **2009**, *113*, 9603.

[126] a) A. E. Asato, R. S. H. Liu, V. P. Rao, Y. M. Cal, *Tetrahedron Lett.* **1996**, *37*, 419. b) P. G. Lacroix, I. Malfant, G. Iftime, A. Razus, K. Nakatani, J. A. Delaire, *Chem. Eur. J.* **2000**, *6*, 2599. c) C. Lambert, G. Nöll, M. Zabel, F. Hampel, E. Schmalzlin, C. Brauchle, K. Meerholz, *Chem. Eur. J*. **2003**, *9*, 4232. d) Z. Essaidi, J. Niziol, B. Sahraoui, *Optical Materials* **2011**, 1387.

[127] a) F. Wang, Y. Lai, Y. H. Han, *Org. Lett.* **2003**, *5*, 4791. b) F. Wang, Y. H. Lai, M. Y. Han, *Macromolecules* **2004**, *37*, 3222. c) X. Wang, J. K. P. Ng, P. Jia, T. Lin, C. M. Cho, J. Xu, X. Lu, C. He,

azulene and its derivatives find applications in medicine and the production of various cosmetics because of their anti-inflammatory and antimicrobial properties.[129]

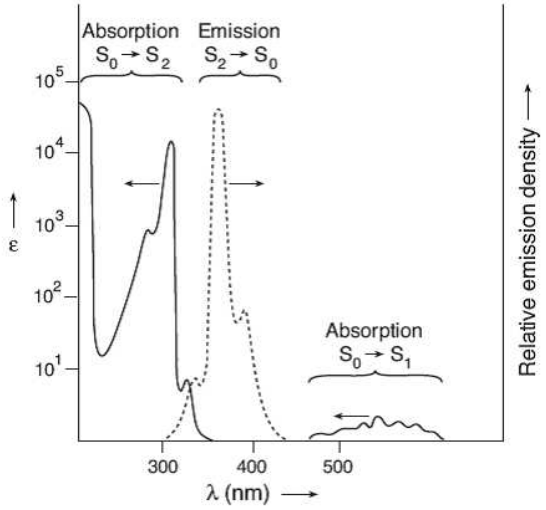

Figure 50. Absorption and emission spectra for azulene.

Comparing to naphthalene, azulene has a smaller HOMO-LUMO gap, in the order of 1.8 eV. The origin of this difference is that naphthalene is alternant (all alternating starred and unstarred carbons) whereas azulene is a non-alternant hydrocarbon (two adjacent unstarred carbons at the ring junction). The HOMO, LUMO orbitals of naphthalene and azulene are shown in Figure 51.[130] The electrons occupy the same region in the naphthalene molecule with considerable overlap and electron-electron repulsion. Thus, the large electron–electron correlation energy significantly raises the S_1 level of naphthalene, making it absorb only in the UV region. On the other hand, the HOMO and LUMO electron pair occupy different regions at the azulene molecule with a little overlap between the two orbitals. Consequently, electron-electron repulsive interactions are substantially reduced, giving rise to a low lying S_1 state. As a

Macromolecules **2009**, *42*, 5534. d) G. Nöll, J. Daub, M. Lutz, K. Rurack, *J. Org.Chem*. **2011**, *76*, 4859. e) E. Amir, R. J. Amir, L. M. Campos, C. J. Hawker, *J. Am. Chem. Soc.* **2011**, *133*, 10046.

128 a) S. Schmitt, M. Baumgarten, J. Simon, K. Hafner, *Angew. Chem. Int. Ed*. **1998**, *37*, 1077. b) A. F. M. M. Rahman, S. Bhattacharya, X. Peng, T. Kimura, N. Komatsu, *Chem. Commun.* **2008**, 1196.

129 a) F. A. Andersen, D. R. Teufel, *Int. J. Toxicol.* **1999**, *18*, 27. b) M. Guarrera, L. Turbino, A. Rebora, J. Eur. Acad. *Dermatol. Venerol.* **2001**, *15*, 486.

130 a) D. M. Lemal, G. D Goldman, *J. Chem. Ed.* **1988**, *65*, 923. b) R. S. H. Liu, A. E. Asato, *Photochem. Photobiol. C*. **2003**, *4*, 179.

result, the energy of the HOMO-LUMO orbitals is reduced causing absorption in the visible region with typical blue color. Conversely, the electron distribution of azulene is similar between HOMO and LUMO+1 orbitals which causes an increase in the energy of the S_2 state. As a result the exclusive emission from S_2 state result to an unusually large S_1-S_2 energy gap.[125]

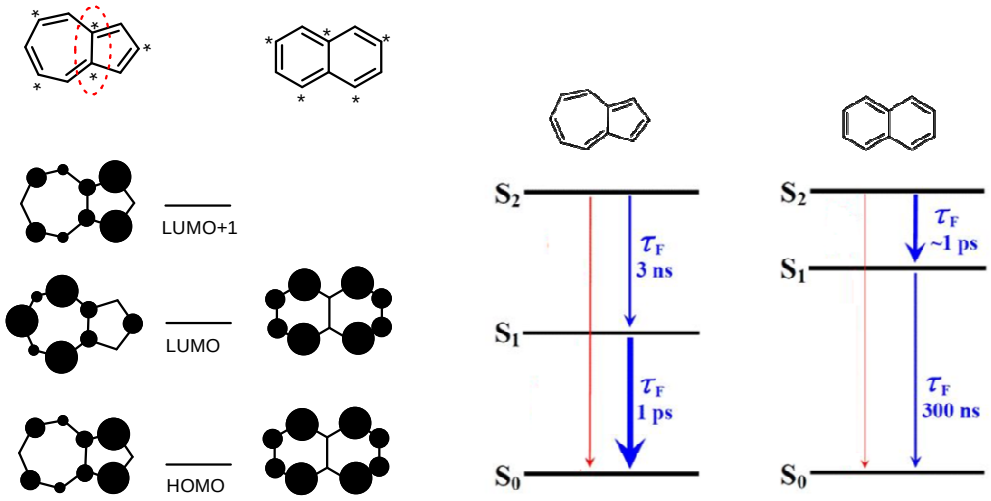

Figure 51. The energy levels of azulene and naphthalene. The S_0, S_1 and S_2 levels correspond to HOMO, LUMO, and LUMO+1 orbitals of azulene.

The azulene ring system can be considered as a combination of the aromatic cyclopentadienyl anion and cycloheptatrienyl (tropylium) cation, therefore it exhibits a high chemical reactivity for both nucleophiles, mostly at the 4, 6, 8 positions, and electrophiles, particularly at the 1 and 3 positions.[131] However, the 2, 5 and 7 positions are much less reactive to either nucleophilic or electrophilic attack. Nevertheless, when the more reactive sites are already substituted, substitution can occur at these less

[131] a) R. N McDonald, R. R. Reitz, J. M. Richmond, *J. Org. Chem.* **1976**, *41*, 1822. b) M. Makosza, R Podraza, *Eur. J. Org. Chem*. **2000**, 193. c) R. Yokoyama, S. Ito, M. Watanabe, N. Harada, C. Kabuto, N. Morita, *J. Chem. Soc. Perkin. Trans*, **2001**, 2257. d) Y. Lou, J. Chang, J. Jorgensen, D. M. Lemal, *J. Am.Soc,* **2002**, *124*, 15302. e) R. Yokoyama, S. Ito, T. Okujima, T. Kubo, M. Yasunami, A. Tajiri, N. Morita, *Tetrahedron Lett.* **2003**, 8191. f) M. A. Petersen, S. l. Broman, A. Kadziola, K. Kilsa, M. B. Nielsen, *Eur. J. Org. Chem.* **2009**, 2733. g) M. A. Petersen, K. Kilsa, A. Kadziola, M. B. Nielse*, Eur. J. Org. Chem*. **2007**, 1415. h) M. S. M. Timmer, B. L. Stocker, P. T. Northcote, B. A. Burkett, *Tetrahedron Lett.* **2009**, *50*, 7199.

reactive positions under harsher conditions.[132] The reactivity of the positions of azulene can be explained by resonance structures. For example, as can be seen in Figure 52, addition of an electrophile at the 3-position, allows the formation of tropylium resonance structure whereas addition at the 2 position prohibits its formation.

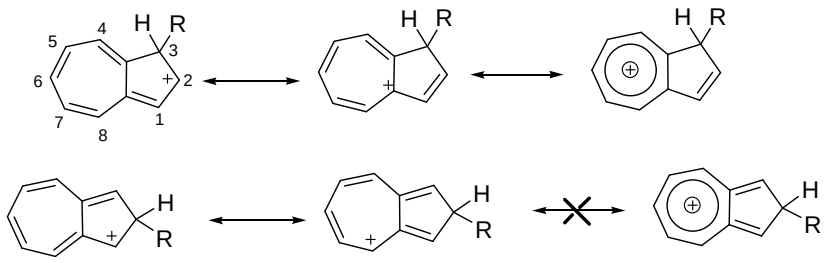

Figure 52. Resonance structures resulting of the electrophilic addition to position 2 and 3 of azulene.

The optical and electronical properties of azulene depend on the substituted positions and the electronic nature of the substituents. These two factors alter the optical behaviour of azulene resulting in different colours for different derivatives. For example, while azulene is blue, 1-methylazulene is dark-blue, 1,3-diformlylazulene is red and 1,3-difluorazulene is green.[133] Incorporation of electron donating groups at 1 or 3 positions, has the effect of destabilising the HOMO orbitals by donating electron density, but does not cause any change in the LUMO energy due to the very little electron density at the 1 and 3 positions (Figure 53). The decrease of the HOMO-LUMO bad gap, therefore, causes the red shift of the azulene. On the other hand, blue shift occurs when electron-withdrawing units are attached at the same positions of the azulene due to stabilization of the HOMO energy. In the case of substitution at the 2, 4, 6 or 8 positions with electron withdrawing units red shift occurs due to the stabilization

[132] a) K. H. H. Fabian, A. H. M. Elwahy, K. Hafner, *Tetrahedron Lett.* **2000**, 2855. b) T. Shoji, S. Ito, M. Watanabe, K. Toyota, M. Yasunami, N. Morita, *Tetrahedron Lett.* **2007**, 3009.

[133] a) R. S. Muthyala, R. S. H. Liu, *J. Fluorine Chem*. **1998**, *89*, 173. b) R. S. H. Liu, R. S. Muthyala, X. Wang, A. E. Asato, *Org. Lett*. **2000**, *2*, 269. c) R. S. H. Liu, *J. Chem. Ed.* **2002**, 183.

of the LUMO whereas blue shift occurring with electron donating substitution, owing to the destabilization of the LUMO, respectively (Figure 53). [134]

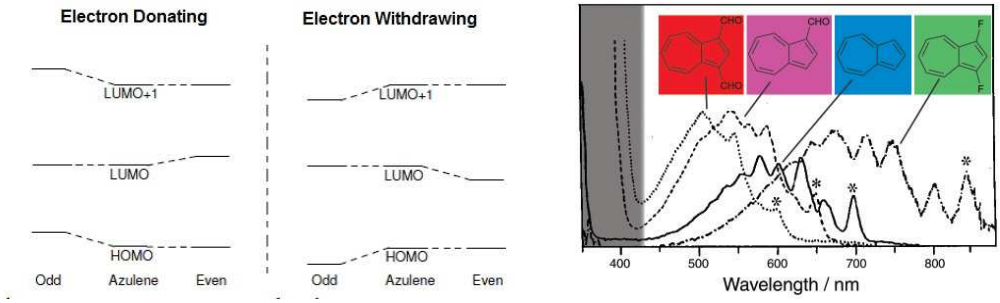

Figure 53. Substituent effects on azulene's HOMO, LUMO and LUMO+1 and UV–vis absorption spectra and colours of some azulene derivatives

Azulene-Fused Macrocycles

Osuka and co-workers have explored the synthesis of a family of azulene-fused porphyrins, which involves either directly linked or direct fusion of azulene units to a porphyrin. [135] The unfused porphyrins linked to azulene units at the *meso*-positions show absorption typical of tetraaryl porphyrins. However, fusion of the azulene units at the β-positions of the porphyrin periphery, results in a dramatic red shift in the absorption spectra. Bisazulene-fused porphyrin shows a red-shifted absorption spectrum compared to monoazulene-fused porphyrin. On the other hand, fusion of four azulene units to the porphyrin shows a further red shift with a long wavelength up to 1200 nm. Increasing the number of azulene groups fused to the porphyrin ring periphery increases the degree of conjugation in the system, as seen from the absorption spectra in Figure 54. Moreover, the same authors prepared a series of directly linked *meso*-azulenylporphyrins and found that azulene derivatives served as electron donating or electron accepting substituents, toward a Zn porphyrin, but the

134 S. V. Shevyakov, H. Li, R. Muthyala, A. E. Asato, J. C. Croney, D. M. Jameson, R. S. H. Liu, *J. Phys. Chem. A*. **2003**, *107*, 3295.
135 K. Kurotobi, K. S. Kim, S. B. Noh, D. Kim, A. Osuka, *Angew. Chem. Int. Ed*. **2006**, *45*, 3944.

influence of such singly linked azulene groups upon the electronic system of the porphyrin is only small.[136]

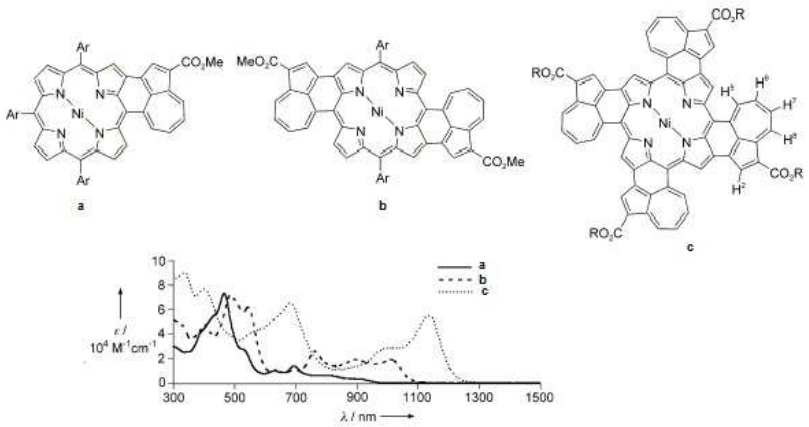

Figure 54. Azulene-fused porphyrins. The absorption spectra show an increase in red-shift upon increasing the number of fused azulene units from one (a), to two (b) to four (c).

Very recently, a new type of tetrapyrrole derivative, namely *azulenocyanine*, was synthesized by Muranaka and Uchiyama in 2010. [137] This compound consist of four di-*tert*-butylazulene units fused at the 5- and 6-positions to a tetraazaporphyrin. The metal free tetra-*tert*-butylazulenocyanine, which is prepared as a mixture of four structural isomers, shows good solubility in organic solvents and very intense/broad absorptions. In contrast to the isoelectronic compound naphthalocyanine with the same 18 π-electron conjugated planar molecular structure, azulenocyanines exhibit significantly different electronic properties (Figure 55).

[136] a) K. Kurotobi, A. Osuka, *Org. Lett*. **2005,** *7*, 6. b) K. S. Kim, S. B. Noh, T. Katsuda, S. Ito, A. Osuka, D. Kim, *Chem. Commun*. **2007**, 2479.

[137] A. Muranaka, M. Yonehara, M. Uchiyama, *J. Am. Chem. Soc.* **2010**, *132*, 7844.

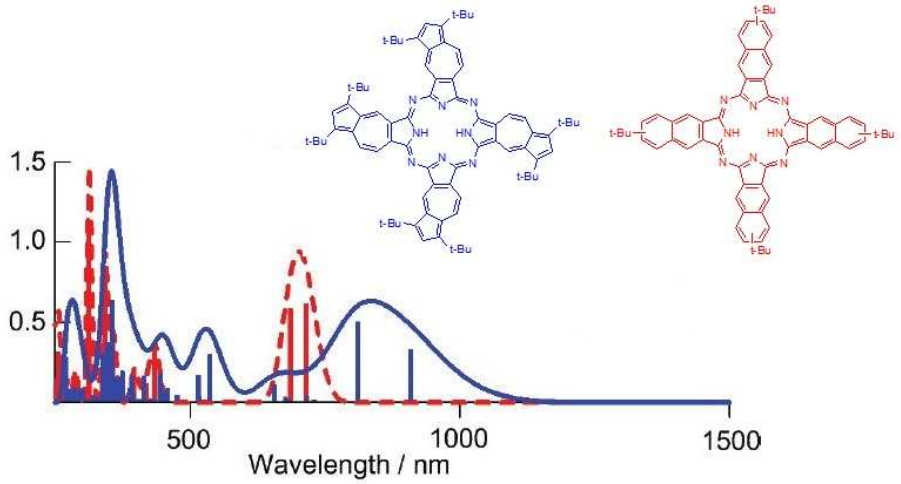

Figure 55. Electronic absorption spectra of Cs isomer of azulenocyanine and naphthalocyanine.

In fact, azulenocyanines absorb in the UV, visible, and NIR regions, from 300 to 1300 nm, and, as such, bear great potential for efficient light harvesting in photovoltaic applications. The origin of these spectral features correlates well with frontier molecular orbital analyses. These indicate a small HOMO-LUMO gap (i.e. 1.5 eV), which is much lower in comparison to other tetrapyroles such as naphthalocyanine (1.92 eV) and phthalocyanine (2.19 eV). The intense NIR absorption of azulenocyanine, evolves from a stabilization of the LUMO orbital rather than a HOMO destabilization, compared to Pc HOMO-LUMO transitions energies. Thus, the observation of absorption bands between Q and Soret bands from 720 to 1050 nm is considered to result from a charge transfer between the fused azulene rings and the 18 electron-π-conjugated aromatic porphyrazine core.[138]

Notably, an azulene fused phthalocyanine bearing one azulene and three phthalonitrile building blocks has also recently been reported. [139] The Ni(II) azulenotribenzotetraazaporphyrinato was prepared to investigate the effect of the azulene unit in the tetraazaporphyrin skeleton. The monoazulene-fused macrocycle

[138] D. Qi, L. Zhang, Y. Zhang, Y. Bian, J. Jiang, *J. Phys. Chem. A*. **2010**, *114*, 13411.
[139] A. Muranaka, M. Yonehara, M. Hirayama, A. Saito, N. Kobayashi, M. Uchiyama, *Chem. Lett.* **2011**, *40*, 714.

exhibited a broad absorption band 600 to 900 nm owing to lowering of the LUMO level compared to that of the Pc derivative (Figure 56).

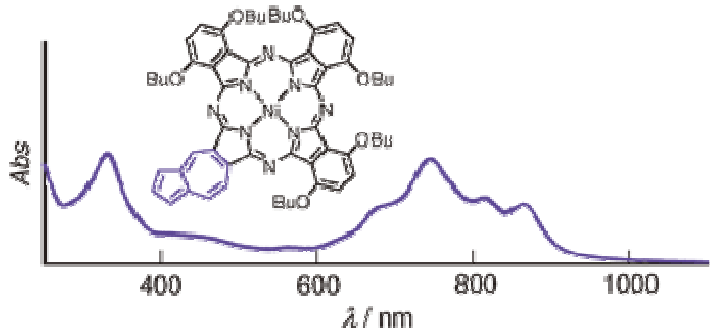

Figure 56. Absorption spectra of azulene-fused tribenzotetraazaporphyrin.

1.2.2. Objectives

Broad optical absorption of organic molecules is a highly desirable feature for enhancing the efficiency of photovoltaic and artificial photosynthetic devices. In order to avoid loss of photons, light-harvesting systems, covering large portions of the solar spectrum, including the NIR region, are desirable. Hence, the main purpose of the work to be developed within the present section will be the synthesis of new stable NIR absorbing unsymmetrical azulenocyanine-phthalocyanine hybrid molecules (the model structure is shown below), which eventually can also incorporate reactive functional groups that pave the way for the preparation of more elaborated derivatives.

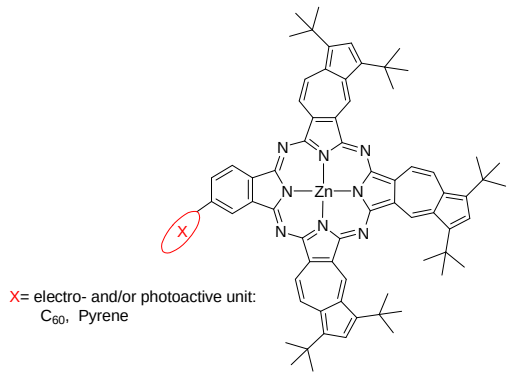

As previously discussed, up to now, phthalocyanines have been successfully utilized as electron donor in the construction of donor-acceptor systems, which contain fullerene or SWNT as acceptor units, owing to efficient photoinduced electron transfer processes. The utilization of either symmetrical Zn(II) octa-*tert*-butylazulenocyanine or unsymmetrical analogues in which one azulene unit is formally replaced by a benzene ring (Zn(II) azulenocyanine-phthalocyanine) for the construction of both covalent or non-covalent D-A hybrids is still an unexplored field, that could offer several advantages. For that reason, supramolecular and covalent donor-acceptor assemblies based on NIR absorbing azulenocyanines and either C_{60} or SWNT will be studied in this section. In addition, photoinduced electron transfer process and scope of introducing these NIR dyes in solar cells will be studied.

1.2.2.1. Covalent and Supramolecular Azulenocyanine/C_{60} Systems

Background

As already discussed in the general introduction, the design of donor-acceptor systems, which can generate long-lived charge-separated states on photoexcitation, is one of the main objectives of the present investigation. The much-desired long-lived charge-separated states have been achieved by a number of covalently linked Pc-C_{60} dyads or triads. However, the covalently-bonded donor-acceptor system substantially differs from natural system; therefore, exploration of non-covalently associated donor-acceptor models to mimic natural system appears to be more promising in the field of artificial photosynthesis.

Among the supramolecular interactions, metal-directed self-assembly has become an important tool to prepare large and elaborate complex ensembles from structurally simpler components. Moreover, these self-assembled supramolecular architectures often present large K_a, approaching, in some cases, the stabilities observed for the covalent systems. In this context, several examples of self-assembled, supramolecular D-A systems based on C_{60} fullerene functionalized with pyridine (Py) or Imidazole (Im) moieties complexing a central metal (zinc, magnesium, or ruthenium) of macrocyclic compounds, such as Pors, Pcs or Ncs, have been synthesized and

studied.[23,140] For instance, a system based on tetra-*tert*-butylZn(II)Pc and a pyridine-appended fulleropyrrolidine was prepared and the photophysical properties of the resulting ensemble studied (Figure 57).[24b]

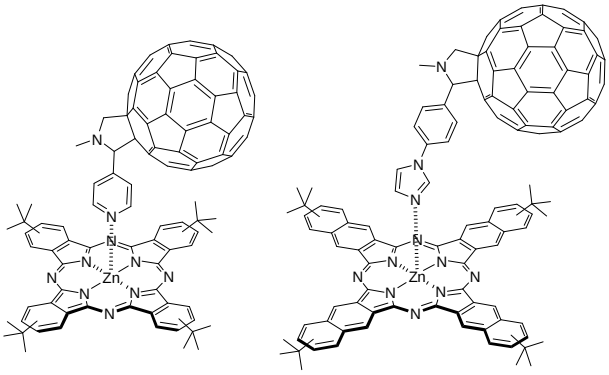

Figure 57. Molecular structures of Zn(II)Pc/pyridine-substituted C_{60} and Zn(II)Nc/Im-substituted C_{60} .

The coordination constant for this complex was 4.8 x 10^3 M^{-1}. It was demonstrated that the weak K_a of the complex facilitates, after photoexcitation of the dyad and rapid intramolecular electron transfer, the crucial break-up of the radical pair Zn(II)$Pc^{\bullet+}$/pyridine-substituted $C_{60}^{\bullet-}$ species into the free radical ions, Zn(II)$Pc^{\bullet+}$ and pyridine-substituted $C_{60}^{\bullet-}$. The lifetime of this radical pair species is governed by a nearly diffusion controlled, intermolecular back electron transfer. In contrast, the much

[23] a) M. E. El-Khouly, L. M. Rogers, M. E. Zandler, G. Suresh, M. Fujitsuka, O. Ito, F. D'Souza, *ChemPhysChem*. **2003**, *4*, 474. b) M. E. El-Khouly, Y. Araki, O. Ito, S. Gadde, M. E. Zandler, F. D'Souza, *J. Porphyrins Phthalocyanines* **2006**, *10*, 1156. c) F. D'Souza, E. Maligaspe, K. Ohkubo, M. E. Zandler, N. K. Subbaiyan, S. Fukuzumi, *J. Am. Chem. Soc.* **2009**, *131*, 8787. d) M. S. Rodriguez-Morgade, M. E. Plonska-Brzezinska, A. J. Athans, E. Carbonell, G. de Miguel, D. M. Guldi, L. Echegoyen, T. Torres, *J. Am. Chem. Soc.* **2009**, *131*, 10484.

[24] b) D. M. Guldi, J. Ramey, M. V. Martínez-Díaz, A. de la Escosura, T. Torres, T. Da Ros, M. Prato, *Chem. Commun.* **2002***,* 2774.

[140] a) F. D'Souza, G. R. Deviprasad, M. S. Rahman, J. P. Choi, *Inorg. Chem*. **1999**, *38*, 2157. b) N. Armaroli, F. Diederich, L. Echegoyen, T. Habicher, L. Flamigni, G. Marconi, J. F. Nierengarten, *New J. Chem.* **1999**, 77. c) T. Da Ros, M. Prato, D. M. Guldi, M. Ruzzi, L. Pasimeni, *Chem. Eur. J*. **2001**, *7*, 816. d) F. D`Souza, G. R. Deviprasad, M. E. Zandler, V. T. Hoang, A. Klykov, M. VanStipdonk, A. Perera, M. E. El-Khouly, M. Fujitsuka, O. Ito, *J. Phys. Chem. A.* **2002**, *106*, 3243. e) S. R. Wilson, S. MacMahon, F. T. Tat, P. D. Jarowski, D. I. Schuster, *Chem. Commun.* **2003**, 226. f) F. T. Tat, Z. Zhou, S. MacMahon, F. Song, A. L. Rheingold, L. Echegoyen, D. I. Schuster, S. R. Wilson, *J. Org. Chem*. **2004**, *69*, 4602. g) A. M. V. M. Pereira, A. R. M. Soares, A. Hausmann, M. G. P. M. S. Neves, A. C. Tomé, A. M. S. Silva, J. A .S. Cavaleiro, D. M. Guldi, T. Torres, *Phys. Chem. Chem. Phys*. **2011**, *13*, 11858. h) A. M. V. M. Pereira, A. Hausmann, J. P. C. Tomé, O. Trukhina, M. Urbani, M. G. P. M. S. Neves, J. A. S. Cavaleiro, D. M. Guldi, T. Torres, *Chem. Eur. J*. **2012**, *18*, 3210.

stronger binding typical of Pc-C_{60} covalent systems prevents this splitting and, hereby, shortens the radical pair lifetime to the nanoseconds time regime.

A stronger binding was observed for a Zn(II)Nc/C_{60} system consisting in an Im-substituted fulleropyrrolidine axially coordinated to a Zn(II)Nc (Figure 57).[23a] Zn(II)Nc was chosen as a sensitizer to extend the absorption properties of the resulting dyad, whereas Im-appended fullerene, which present a higher basicity than its pyridine-functionalized analogue, provided stronger binding between the two entities. The K_a of the dyad was 6.2 x 10^4 M^{-1} in toluene that is an order of magnitude higher than the values for Zn(II)Pc/C_{60}. Picosecond transient absorption measurements on Zn(II)Nc/C_{60} revealed the formation of the radical pair Zn(II)$Nc^{\bullet+}$/$C_{60}^{\bullet-}$, which presented rates of CS and quantum yields of 1.4 x 10^{10} s^{-1} and 0.97 in toluene and 8.9 x 10^9 s^{-1} and 0.96 in *o*-DCB.

In this context, construction of novel donor-acceptor systems by using an azulenocyanine unit as an electron donor and fullerene as an electron acceptor *via* covalent and non-covalent interactions would be beneficial not only to extend the absorption of the resulting dyads but would also allow the comparison of the two different assemblies. Using metal-ligand interaction between Zn(II) azulenocyanine and pyridine functionalized C_{60} would be an easy and effective way to construct stable self-assembled donor-acceptor conjugates. To this end, the supramolecular and covalent donor-acceptor systems depicted in Figure 58 were designed.

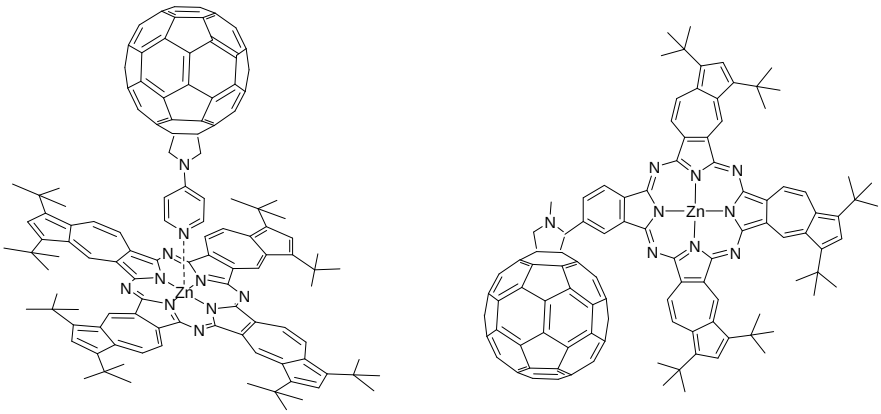

Figure 58. Molecular structures of the supramolecular and covalent azulenocyanine-C_{60} systems designed for PET.

Synthesis, Photochemistry, and Electrochemistry of Supramolecular and Covalent Azulenocyanine-C_{60} Dyads

Synthesis of Precursor Phthalonitriles

4-(Hydroxymethyl)phthalonitrile **20** was synthesized according to a procedure previously described by our group Scheme 11.[141]

First, bromination of 4-methylphthalonitrile using NBS and AIBN gave a mixture of mono- di- and tribrominated compounds at the benzylic position in a 1:2:1 ratio, respectively (determined by ^{1}H-NMR analysis). Treatment of the mixture with an excess of diethyl phosphite and DIPEA yielded 4-(bromomethyl)phthalonitrile **19** (65% yield). Reaction of **19** with calcium carbonate in a refluxing aqueous solution of dioxane led to 4-(hydroxymethyl)phthalonitrile **20** with an overall yield of 39%.

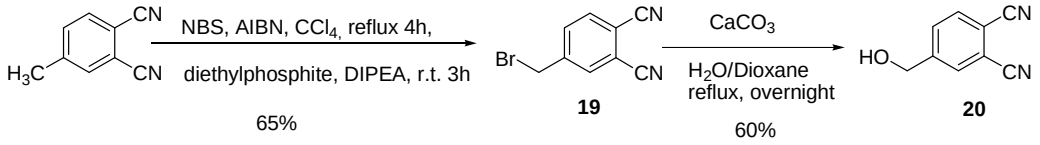

*Scheme 11. Synthesis of 4-(hydroxymethyl)phthalonitrile (**20**).*

1,3-Di-*tert*-butyl-5,6-dicyanoazulene (**24**) was successfully synthesized via a multistep procedure (Scheme 12). The synthesis of azulene is a [6+4] cycloaddition reaction between aminofulvene, which is used as the six-electron component, and thiophene dioxide, which serves as the four-electron component. Thus, 5,6-dibromoazulene (**22**), synthesized according to a literature procedure.[142] The oxidation of 3,4-dibromothiophene with peroxytrifluoroacetic acid to give 3,4-dibromothiophene-1,1-dioxide (**21**) in 60% yield. The [6+4] cycloaddition of the 6-(dimethylamino)fulvene to 3,4-dibromothiophene-1,1-dioxide (**21**) followed by elimination of SO_2 and dimethyl amine led to a blue solid of 5,6-dibromoazulene (**22**) in 24% yield.

141 R. F. Enes, J. J. Cid, A. Hausmann, O.Trukhina, A. Gouloumis, P. Vazquez, J. A. S. Cavaleiro, A. C. Tomé, D. M. Guldi, T. Torres, *Chem. Eur. J.* **2012**, *18*, 1727.
137 A. Muranaka, M. Yonehara, M. Uchiyama, *J. Am. Chem. Soc.* **2010**, *132*, 7844.
142 Y. Lu, D. M. Lemal, J. P. Jasinski, *J. Am. Chem. Soc.* **2000,** *122,* 2440.

5,6-Dicyanoazulene (**23**), was prepared following a modification of the described Rosemund–von Braun reaction on 5,6-dibromoazulene (**22**),[137] which, in our hands, gave much lower yield that the one reported. Considering that the low yield could be associated with the low stability of the azulene in the reaction conditions, therefore, the 5,6-dicyanoazulene (**23**) was prepared under much milder conditions by microwave-assisted cyanation of 5,6-dibromoazulene (**22**) using $Zn(CN)_2$ as the cyanide source and $[Pd(PPh_3)_4]$ as a catalyst in DMF.[143] This procedure allows decreasing the reaction time from 17 h to 10 min with a good impurity profile when compared to the classical thermal conditions. Cyanation of 5,6-dibromoazulene (**22**) gave a green colour 5,6-dicyanoazulene (**23**). This colour change, from blue to green, can be explained by the effect of the electron-withdrawing substituents at even-numbered carbons caused a red-shift of the S_1 band, as mentioned above. Finally, 1,3-di-*tert*-butyl-5,6-dicyanoazulene (**24**) was synthesized in 55% yield by means of Friedel-Crafts alkylation.[137]

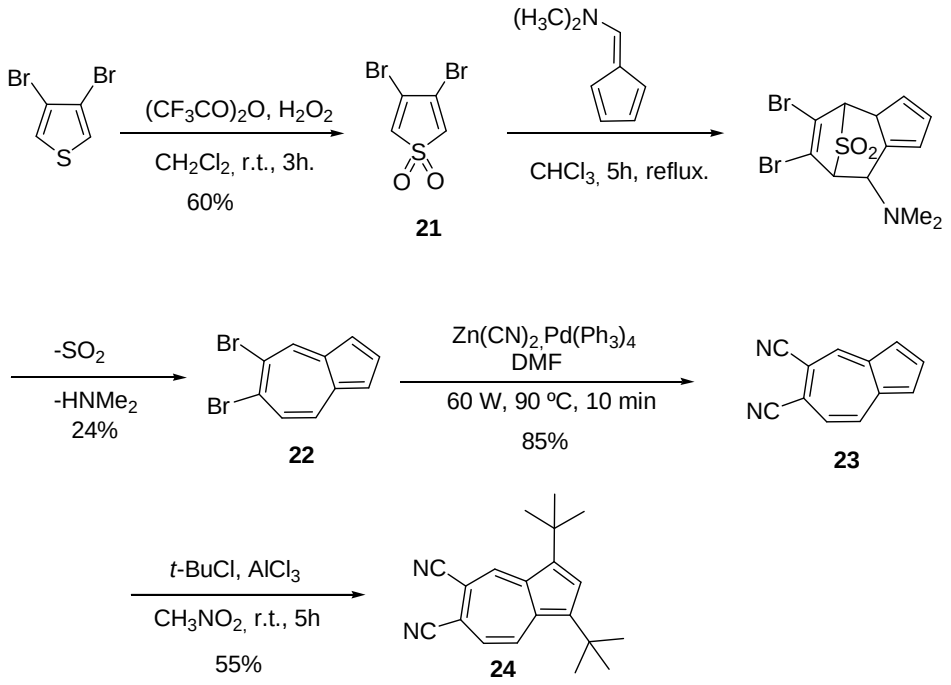

*Scheme 12. Synthesis of 1,3-di-tert-butyl-5,6-dicyanoazulene (**24**).*

[143] M. Alterman, A. Hallberg, *J. Org. Chem.* **2000**, *65*, 7984

Synthesis of Azulenocyanines

Scheme 13 shows the synthetic approach *en-route* towards symmetrical Zn(II) azulenocyanine (**25**) and unsymmetrically substituted Zn(II) azulenocyanine-phthalocyanine (**26**).

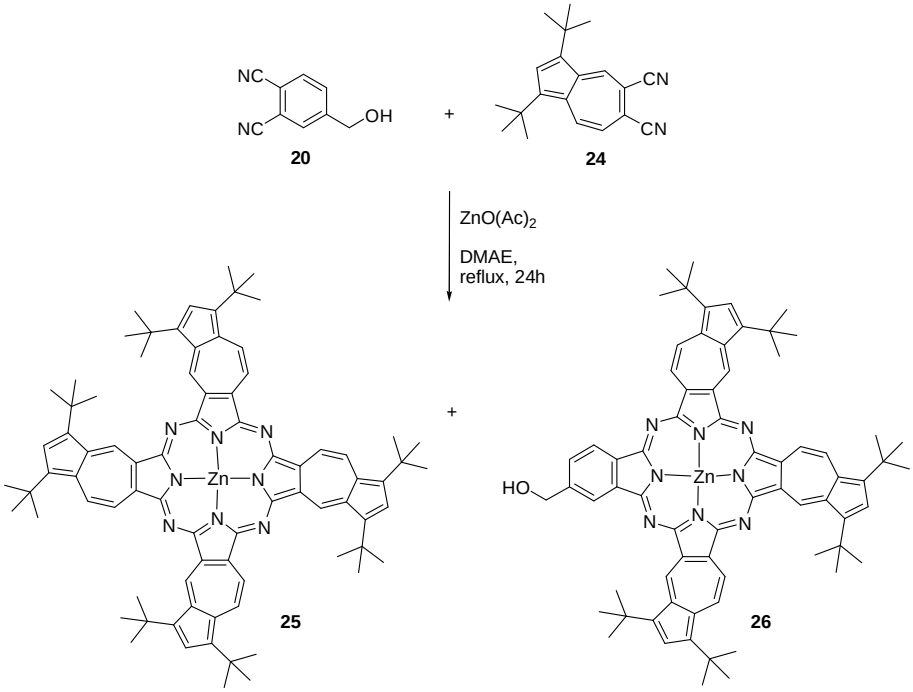

*Scheme 13. Synthesis of Zn(II) azulenocyanine (**25**) and azulenocyanine-phthalocyanine (**26**).*

According to the classical methodology for the preparation of unsymmetrical Pcs, a 4:1 molar mixture of 1,3-di-*tert*-butyl-5,6-dicyanoazulene (**24**) and 4-hydroxymethylphthalonitrile (**20**) were reacted under reflux of DMAE in the presence of $Zn(OAc)_2$. A dark solid, constituted by a mixture of compounds, was obtained from which the symmetrical Zn(II)azulenocyanine (**25**) was isolated by column chromatography on silica gel in 34% yield as a first eluting black-colored fraction. The unsymmetrically substituted hydroxymethyl derivative **26** was isolated in 22% yield after evaporating the second black-colored fraction. Azulenocyanines **25**, and **26** were obtained as mixtures of structural isomers (4, and 8 possible regioisomers,

respectively), which could not be separated by conventional column chromatography. Molecular structures of the eight-constitutional isomers of compound **26** are shown in Figure 59.

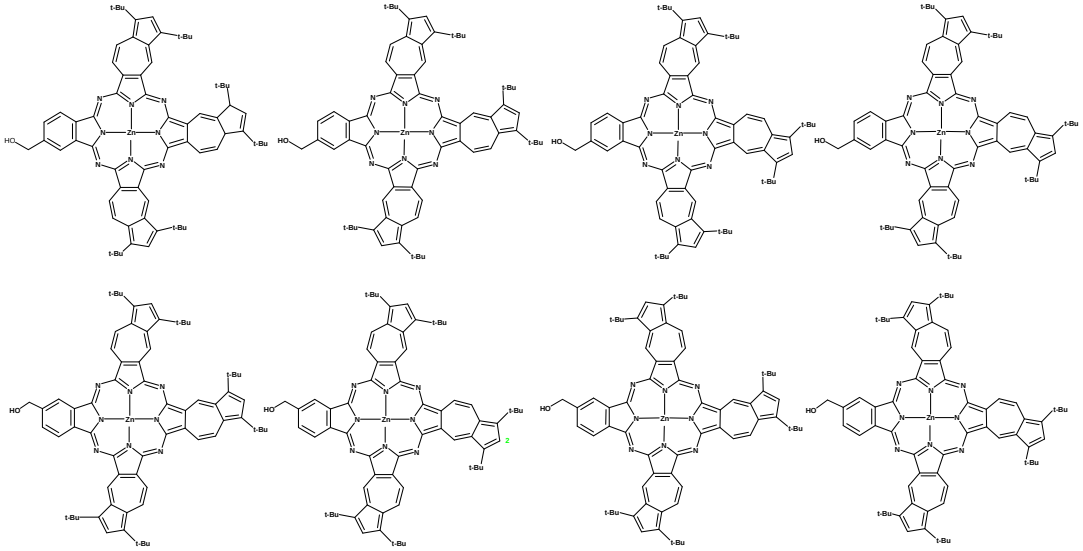

*Figure 59. Structures of the eight-constituonal isomers of compound **26**.*

The synthetic route to azulenocyanine-C_{60} (**28**) is depicted in Scheme 14. Firstly, the hydroxymethyl-functionalized azulenocyanine (**26**) was subjected to oxidation in the presence of IBX to yield the formyl-derivative **27**. Subsequently, a Prato reaction between **27** and C_{60} in the presence of N-methylglycine was carried out, affording **28** in 42% yield.

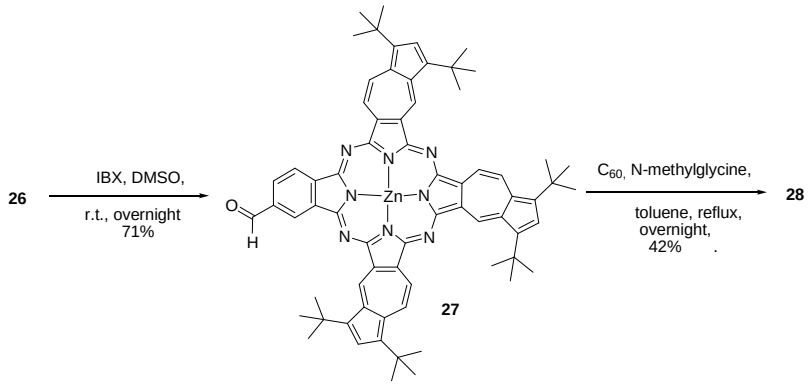

*Scheme 14. Synthetic route to azulenocyanine-C_{60} (**28**) dyad.*

All compounds were reasonably soluble in organic solvents and fully characterized by MALDI-MS, ^{1}H-NMR, UV-Vis, and FT-IR spectroscopy. The ^{1}H NMR spectra of azulenocyanine derivatives are poorly resolved due to aggregation even in coordinating solvents such as d_8-THF or 1,4-dioxane-d_8 or upon increasing the temperature to 353 K. Figure 60 shows the ^{1}H-NMR spectrum of compound **25** in d_8-THF as an example. The chemical shifts of azulene protons near the tetraazaporphyrin skeleton (a and b) exhibited down-field shifts, which can be interpreted in terms of the strong ring current of the macrocycle and strongly electron-withdrawing nature of the azulene group.

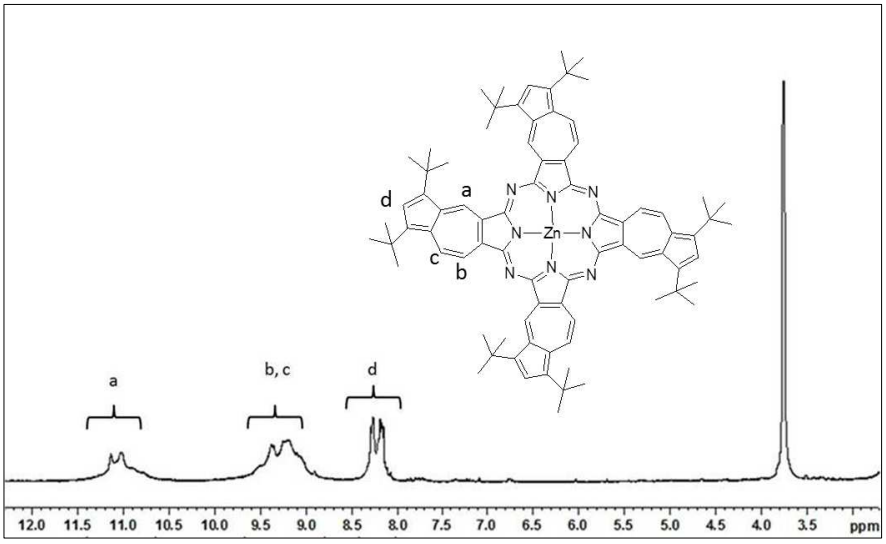

*Figure 60. Aromatic part of the ^{1}H-NMR spectrum of compound **25** in d_8-THF.*

^{1}H NMR spectra of **26, 27** and **28** gave multiplets in ratios of 3:8:4 between 11.5 and 8 ppm for three sets of azulenocyanine ring protons, integrating for a total of 15 protons. In addition, compound **28** showed signals between 5.3 and 5.6 ppm corresponding to the pyrolidine and the N-CH_3 resonance at 3.3 ppm (Figure 61).

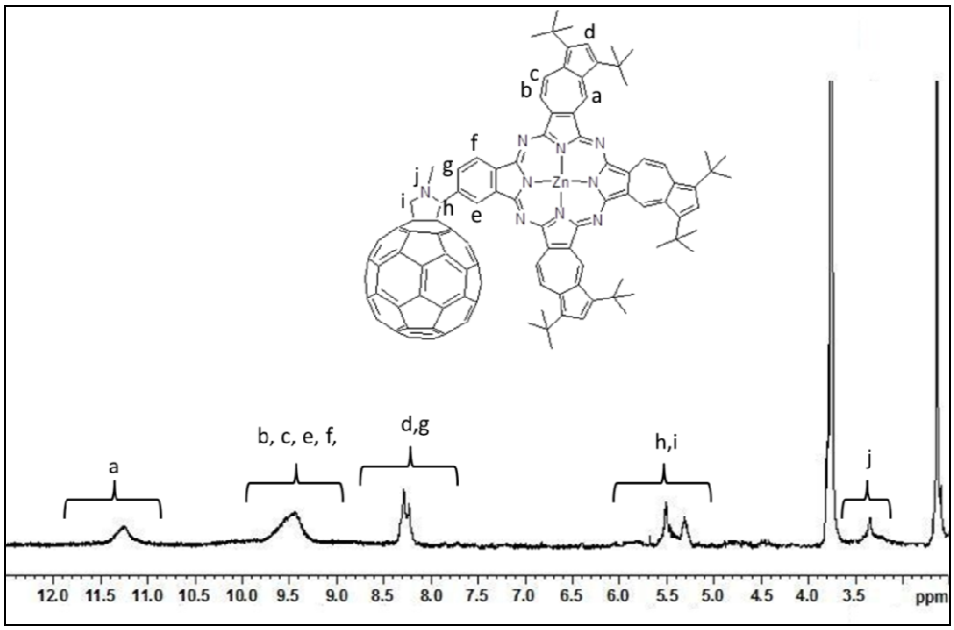

*Figure 61. ^{1}H-NMR spectrum of compound **28** in d_8-THF.*

Photochemistry and Electrochemistry of Azulenocyanine-C_{60} Hybrids

Photophysical and electrochemical characterization of the azulenocyanine-C_{60} hybrids was made in collaboration with the group of Prof. Dirk M. Guldi (University of Erlangen, Germany).

Treatment of Zn(II)azulenocyanine **25** with N-pyridylfulleropyrrolidine,[144] an electron-acceptor system containing a nitrogen ligand, gave rise to a novel electron donor–acceptor hybrid Zn(II)azulenocyanine•C_{60} through ligation to the central metal of the Zn(II)azulenocyanine.

Figure 62 shows the UV-Vis spectra of **28** in chlorobenzene solution compared with those of **25**, Zn(II)azulenocyanine•**C_{60}** **(25•C_{60})**, and N-pyridylfulleropyrrolidine. Hybrid **25•C_{60}** and dyad **28** have absorption spectra, which are essentially the sum of its molecular constituents, and effectively span the entire 300-1200 nm region. Regarding

[144] S. R. Wilson, S. MacMahon, F. T. Tat, P. D. Jarowski, D. I. Schuster, *Chem. Commun.* **2003**, 226.

hybrid **25•C_{60}**, upon titrating a constant concentration of **25** with variable concentrations of N-pyridylfulleropyrrolidine or vice versa, the absorption and fluorescence spectra of either N-pyridylfulleropyrrolidine or **25** gave rise to some appreciable changes. In terms of absorption, a marked blue-shift of the **25** centered transition goes hand in hand with coordinating N-pyridylfulleropyrrolidine and, in turn, forming **25•C_{60}**. For example, the 1060 nm maximum for just **25** shifted to 1040 nm for **25•C_{60}**. The low fluorescence quantum yields of **25**, with values of << 10-5, prevented a meaningful analysis.

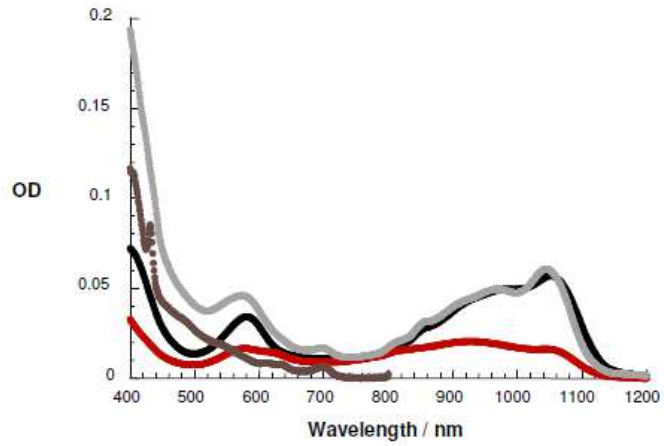

*Figure 62. UV/Vis absorption spectra of **25** (black spectrum), **28** (red spectrum),* **25•C_{60}** *(grey spectrum), and* N-pyridylfulleropyrrolidine *(brown spectrum) - all in argon-saturated chlorobenzene ~ 1x10^{-6} M .*

On the contrary, following the fluorescence of N-pyridylfulleropyrrolidine in the presence of variable concentrations of **25** was a more successful approach (Figure 63). Here, a non-linear fluorescence quenching of N-pyridylfulleropyrrolidine was established in either toluene or chlorobenzene. From the corresponding dependence, that is, fluorescence intensity versus concentration of **25**, binding constants of around 10^5 M^{-1} were derived. The absorption of **25** proved, however, to be insufficiently strong to be used in these titrations as a marker for the formation of **25•C_{60}**.

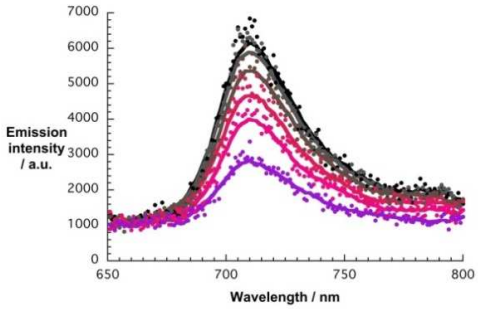

*Figure 63. Room temperature fluorescence spectra of N-pyridylfulleropyrrolidine (1.0 x 10^{-6} M) in chlorobenzene titrated with variable concentrations of **25** (0 – 7.6 x 10^{-6} M) at 500 nm excitation wavelength*.

When turning to transient absorption measurements conducted with **25**, two very short-lived transients with lifetimes of 0.6 and 10 ps were noted (Figure 64). In terms of transient absorption, near-infrared features of the 0.6 ps lived excited state included a set of minima at 930 and 1024 nm and a set of maxima at 800 and 1105 nm. On the other hand, the 10 ps lived excited state exhibited maxima at 970 and 1080 nm, while minima evolved at 880, 925, and 1020 nm. We assign these transients to a higher singlet excited state / higher vibrationally singlet excited state and a lowest vibrationally singlet excited state, respectively. In going beyond a time window of 50 ps no residual transient remained detectable, a finding that suggests the inefficient intersystem crossing in photoexcited **25**. In the visible, the singlet excited state revealed maxima at 450 and 665 nm that flanks a 570 nm minimum.

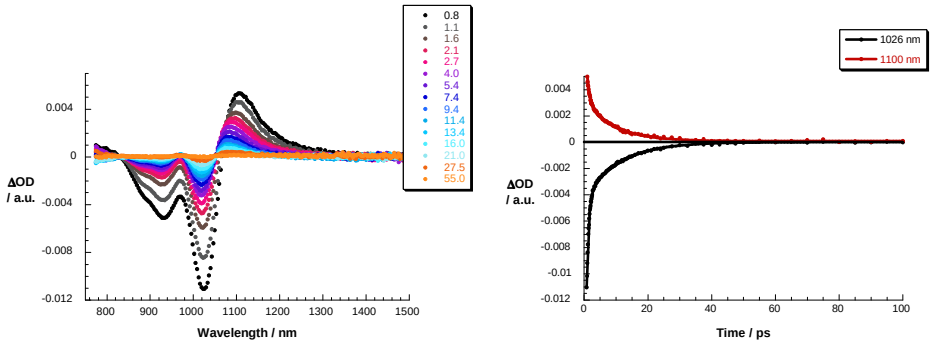

*Figure 64. Differential absorption spectra (near-infrared) obtained upon femtosecond flash photolysis (387 nm) of **25** in argon-saturated chlorobenzene at different time delays between 0.8 amd 55.0 ps at room temperature (right). Time absorption profiles of the spectra shown above at 1026 (black spectrum) and 1100 nm (red spectrum) (left).*

Coordination of N-pyridylfulleropyrrolidine to **25** has a profound impact on the aforementioned photophysics (Figure 65). In terms of transient absorption measurements, lifetimes of 5 and 790 ps seemed to transform the initial excited state of **25** into a radical ion pair state and into the ground state, respectively, in toluene. Again, maxima at 840 and 1095 nm as well as minima at 885, 935, and 1020 nm attested the formation of the singlet excited state of **25** despite the presence of C_{60}.

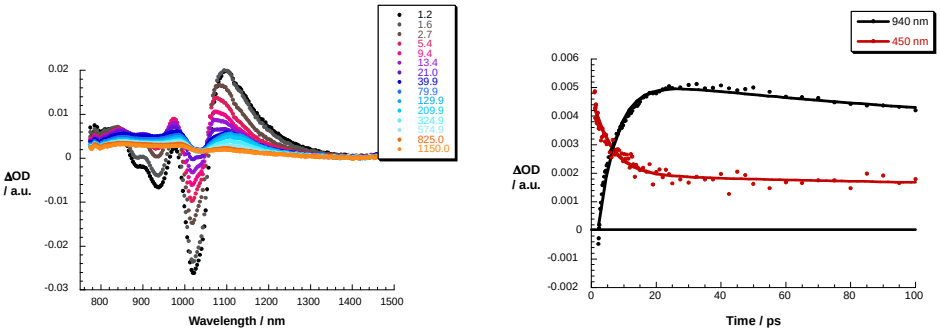

Figure 65. Differential absorption spectra (near-infrared) obtained upon femtosecond flash photolysis (387 nm) of ***25•C$_{60}$*** *in argon-saturated toluene at different time delays between* ***C$_{60}$•25*** *and 1150.0 ps at room temperature (right). Time absorption profiles of the spectra shown above at 450 (red spectrum) and 940 nm (black spectrum) (left).*

At the conclusion of the singlet excited state, decay features developed that bear no particular resemblance to those known for any excited state of either **25** or N-pyridylfulleropyrrolidine. To this end, a series of maxima (i.e., 430, 650, 855, 985, and 1120 nm) and minima (i.e., 580 and 1035 nm) were noted. Important is the fact that these features were a superimposition of those seen upon spectroelectrochemical oxidation of **25** (Figure 66) and pulse radiolytic reduction of N-pyridylfulleropyrrolidine.

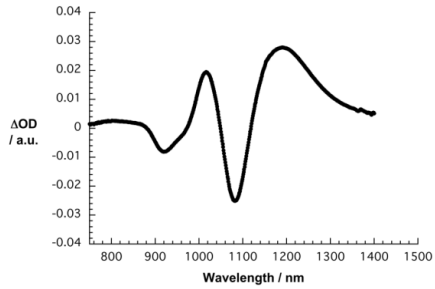

*Figure 66. Spectroelectrochemical oxidation of **25** in dichloromethane at an applied potential of +0.25 V.*

In other words, a radical ion pair state, that is, the one-electron oxidized form of **25** (430, 645, 1015, and 1190 nm) and the one-electron reduced form of N-pyridylfulleropyrrolidine (i.e., 1000 nm), was formed (5.9 ps) as it evolved from the singlet excited state of **25**.

Finally, compound **28** was probed in solvents of different polarity (i.e., toluene, anisole, THF). However, the only appreciable transient that was noted in these experiments was that of the azulenocyanine moiety centered excited state (Figure 67).

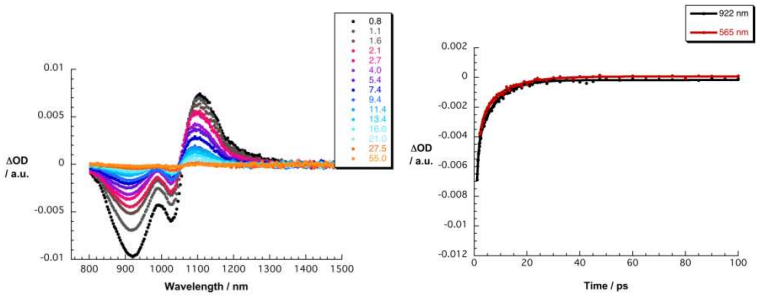

Figure 67. Right: Differential absorption spectra (near-infrared) obtained upon femtosecond flash photolysis (387 nm) of an argon saturated THF solution of 3 at different time delays (between 0.8 and 55.0 ps) at room temperature. Left: Time profiles of the spectra shown above at 565 (red line) and 922 nm (black line).

In addition, the decay dynamics were virtually identical with those noted for **25.** The aforementioned leads to the conclusion that **28** in its excited state fails to show any electron transfer activity.

1.2.2.2. Azulenocyanine/SWNT Supramolecular Systems Assembled through π-π Interactions

Background

The covalent functionalization of SWNT was discussed in the general introduction. Here, we will give a brief discussion the non-covalent immobilization of phthalocyanines onto SWNTs.

The noncovalent functionalization of pristine carbon nanotubes with appropriately derivatized, electron-donor chromophores represents an interesting strategy for the preparation of D-A, carbon nanotube-based ensembles, since it fully preserves the excellent electronic properties of these tubular nanoobjects. Such a supramolecular approach, leads to the immobilization of the dyes onto the carbon nanotubes sidewalls is highly desirable, especially for application of these carbon nanotube-based materials in the field of optoelectronics and photovoltaics. Up to date, a variety of supramolecular assemblies based on phthalocyanines and SWNTs have been explored to achieve higher solubility of the nanotubes and alter the electronic properties, with the aim of integrating these systems in a variety of electronic applications[28f,g]. However, the interactions between Pc and SWNT are intrinsically weak, it is therefore, necessary to utilize linking units such as pyrene to adhere the SWNT sidewalls. In one example, pyrene-substituted, free base and ZnPcs have been prepared and their interactions with SWNTs probed (Figure 68).[145] The formation of stable, H_2Pc-pyrene/SWNT and Zn(II)Pc-pyrene /SWNT supramolecular complexes has been demonstrated by means of various spectroscopic and microscopic techniques.

[28] f) J. Bartelmess, A. R. M. Soares, M. V. Martinez-Diaz, M. G. P. M. S. Neves, A. C. Tomé, J. A. S. Cavaleiro, T. Torres, D. M. Guldi, *Chem. Commun*. **2011**, *47*, 3490. g) J. Bartelmess, C. Ehli, J. J. Cid, M. Garcia-Iglesias, P. Vazquez, T. Torres, D. M. Guldi, *Chem. Sci.* **2011**, *2*, 652.

[145] J. Bartelmess, B. Ballesteros, G. de la Torre, D. Kiessling, S. Campidelli, M. Prato, T. Torres, D. M. Guldi, *J. Am. Chem. Soc.* **2010**, *132*, 16202.

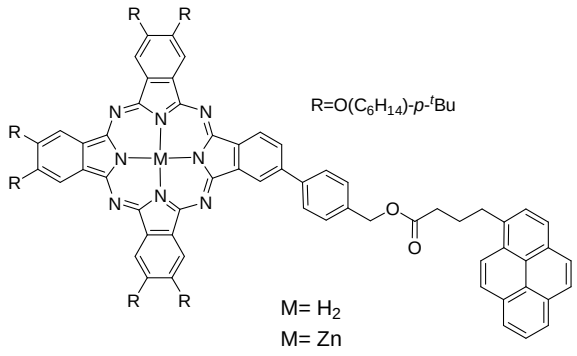

Figure 68. Molecular structures of pyrene-substituted Pcs.

UV/vis and steady-state fluorescence titration studies carried out on a suspension of SWNTs in THF with Zn(II)Pc-pyrene solutions revealed a significant broadening and red-shift of the Pcs Q-band absorption, as well as an important quenching of the Pcs fluorescence. The formation of such Pc-pyrene/SWNT complexes was also inferred by the red-shift of the SWNTs NIR absorption and the quenching and red-shift of the SWNTs fluorescence, a phenomenon due to the occurrence of a CT dynamics between the Pc donor and the SWNT acceptor moieties as demonstrated by transient absorption measurements. The solar energy conversion potential of such Pc/SWNT ensembles has also been tested. These studies revealed the formation of stable and reproducible photocurrents with monochromatic internal photoconversion efficiency values, for the H_2Pc-Py/SWNT hybrid material, as large as 23 and 15%, with and without an applied bias of +0.1 V, respectively.

Even though the formation of stable Pc/SWNT supramolecular complexes has been achieved by using pyrene-based Pc derivatives, the synthetic procedure is a difficult task and time consuming. Hence, ideally, Pcs should be able to π-interact with the sidewalls of SWNTs independently. In this connection, Pc/SWNT supramolecular hybrids based on a series of dendritic (i.e., first to third generations), electron-donor H_2Pcs have been reported. [146] In such systems, the dendritic nature of the oligoethylene-functionalized Pcs as well as their π-extended aromatic surface allow

[146] U. Hahn, S. Engmann, C. Oelsner, C. Ehli, D. M. Guldi, T. Torres, *J. Am. Chem. Soc.* **2010**, *132* , 6392.

effective interaction of the Pc core to the surface of the SWNTs without the requirement for any pyrene anchoring group (Figure 69). In the case of the third generation-dendrimer, Pc/SWNT ensemble, a particularly stable complex was obtained as demonstrated by a series of optical and microscopy techniques. Once again, transient absorption studies were carried out in order to shed light on the fate of the photogenerated products, suggesting the occurrence of a CT process between the Pc and SWNT with the formation of the $Pc^{\bullet+}$ and $SWNT^{\bullet-}$ species, with lifetime of about 250 ps. It is interesting to notice that the presence of dendritic oligoethylene glycol end groups allowed dispersing SWNTs both in common organic solvents and in aqueous media.

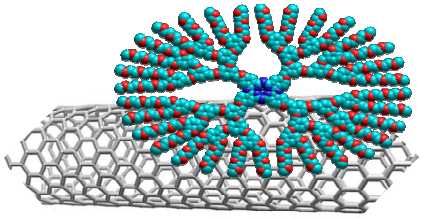

Figure 69. Schematic representation of the noncovalent assembly of a third-generation, dendritic Zn(II) Pc onto a SWCNT.

By virtue of all these results, we planned to immobilize either symmetric azulenocyanine or pyrene functionalized azulenocyanine hybrid on SWNT with the aim of building stable supramolecular donor-acceptor nanohybrid systems. These systems could also be integrated in prototype photoelectrochemical cells to test their solar energy conversion potential. Molecular structures of target molecules are shown in Figure 70.

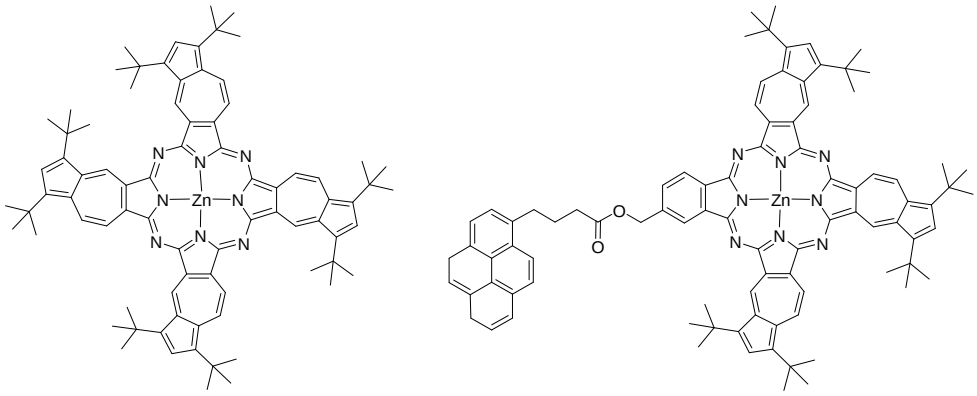

Figure 70. Molecular structures of Zn(II)azulenocyanine, and Zn(II)azulenocyanine-phthalocyanine derivatives proposed for the formation of stable supramolecular assemblies with SWNTs.

Synthesis, Photochemistry, and Electrochemistry of Azulenocyanine Derivatives

Synthesis of Azulenocyanines-Pyrene Derivative

The synthetic strategy employed for the preparation of azulenocyanine-pyrene **29** is depicted in Scheme 15. Azulenocyanine-pyrene **29** was obtained by an esterification reaction of compound **26** with 1-pyrenebutyric acid in the presence of dicyclohexylcarbodiimide (DCC) and N,N-dimethylaminopyridine (DMAP) in 58% yield after purification by column chromatography.

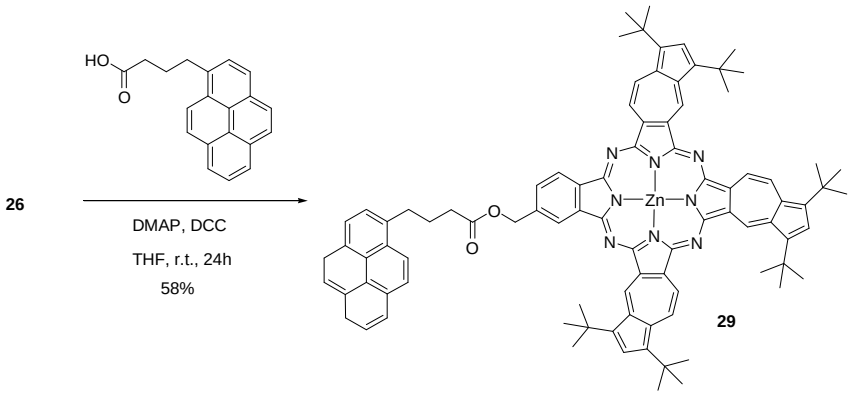

*Scheme 15. Synthesis of Zn(II) azulenocyanine-pyrene (**29**).*

Azulenocyanine-pyrene **29** was fully characterized by MALDI-MS, ^{1}H-NMR, UV-Vis, and FT-IR spectroscopy. Compound **29** shows the typical ^{1}H NMR spectrum of azulenocyanine derivatives, with broad signal in the aromatic region between 11.5 and 7.5 ppm owing to aggregation. Furthermore, a broad signal at 5.5 ppm corresponding to CH_2O protons is present in the spectra of compound **29** (Figure 71).

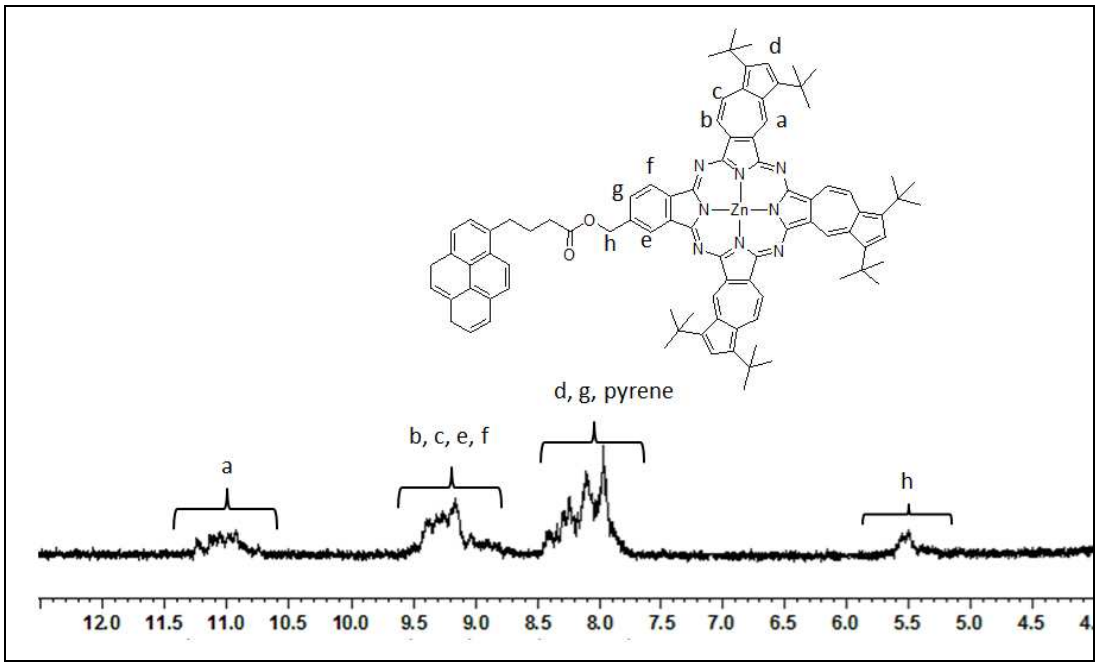

*Figure 71. Aromatic part of the ^{1}H-NMR spectrum of compound **29** in d_8-THF.*

Photochemistry and Electrochemistry of Azulenocyanine Derivatives

Photophysical, electrochemical characterization of complexes were made in collaboration with Prof. Dirk M. Guldi at University of Erlangen (Germany).

The spectroscopic characterization of **25** and **29** were carried out in solvent mixtures of 25% THF and 75% DMF. The absorption spectrum of **25** in the solvent mixture shows panchromatic absorptions from 270 to 1150 nm with maxima at 303, 403, 575, and 1020 nm as well as a shoulder at 940 nm (Figure 72). The absorption spectrum of **29** is slightly different. On one hand, the absorption features of pyrene are

discernable in the form of maxima at 277, 327, and 344 nm. On the other hand, the absorption bands of the aromatic macrocycle shift and change in relative ratio when compared to that of **25**, due to the formal replacement of one of the fused azulene units by a benzene ring. Nevertheless, the absorption of **29** is also panchromatic and reaches from 270 to 1130 nm with maxima at 302, 389, 569, 890, and 1005 nm and a shoulder at 610 nm. Interesting is the shoulder at 610 nm, which is not seen in **25**, and the band at 890 nm, which resembles the shoulder seen in the spectrum of **25** at 940 nm, that dominants the NIR. **25** shows maximum molar extinction coefficients of up to 96.000 L mol^{-1} cm^{-1} (i.e., 303 nm) and 58.000 L mol^{-1} cm^{-1} (i.e., 1019 nm), while **29** features values as high as 86.000 L mol^{-1} cm^{-1} (i.e., 302 nm) and 45.000 L mol^{-1} cm^{-1} (i.e., 890 nm).

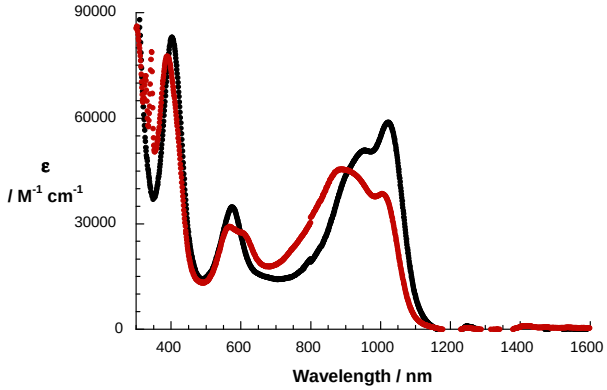

*Figure 72: Room temperature absorption spectra of **25** (black spectrum) and **29** (red spectrum) in 25% THF / 75% DMF.*

In the fluorescence spectrum of **25**, for example upon excitation at 910 nm, a 1050 nm fluorescence band is seen that is followed by a weaker fluorescing band at 1250 nm (Figure 73). For **25** and **29**, the fluorescence quantum yields are rather low (i.e., << 10^{-4}). Reasonably resolved spectra required an integration time of 120 s, which rendered it, however, impossible to determine the exact fluorescence quantum yields as well as the exact fluorescence lifetimes. The latter is, however, significantly shorter than the instrumental limits of the TCSPC set up. The fluorescence spectrum of **29** is very similar to that of **25** with emission maxima at 1030 and 1245 nm, when excited, for instance, at 910 nm excitation.

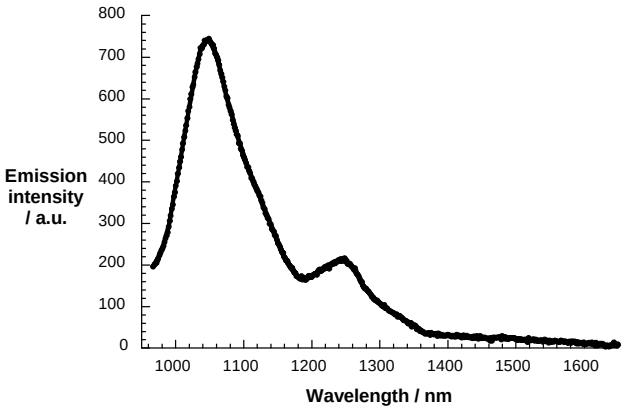

*Figure 73: Room temperature fluorescence spectrum of **25** in 25% THF / 75% DMF upon photoexcitation at 910 nm – 120 s integration time.*

The redox behaviour of **25** and **29** was studied with particular focus on their oxidations. Firstly, square wave voltammetric measurements were performed that led to oxidation potentials of +0.20, +0.50, and +1.01 V for **25**, while the oxidation potentials of **29** are registered at +0.24, +0.57, and +1.11 V. Cyclic voltammetric measurements corroborate these values and show that the first and second oxidations of **25** and **29** are reversible, while the third oxidation is irreversible for **25** and **29**. These finding allowed performing spectroelectrochemistry and a Pt gauze was used as working electrode. For **25**, the spectra were recorded under oxidative conditions, that is, 15 min of an applied potential of +0.2 V, while for **29** a potential of +0.3 V was applied. **25** and **29** showed distinct changes of their absorption features during the oxidations. The differential absorption changes were determined by subtracting the initial spectra (i.e., without an applied potential) from the final spectra (i.e., with 15 min of an applied potential) (Figure 74). In this regard, the differential absorption spectrum of **25** reveals minima, which are imprints of the ground state bleaching, at 305, 402, 581, 941, and 1031 nm. New absorption bands, representing the absorption of the one electron oxidized form of **25** develop at 345, 461, 520 (shoulder), 647, and 1140 nm. Very similar is the differential absorption spectrum monitored for **29** with minima at 384, 556, 621, 873, and a shoulder at 1020 nm. Here, the newly developed maxima are located at 336, 460, 592, 660, and 1118 nm. These features serve as important fingerprints for the identification of radical ion pair states when combining **25** and **29** with SWNT as electron acceptors.

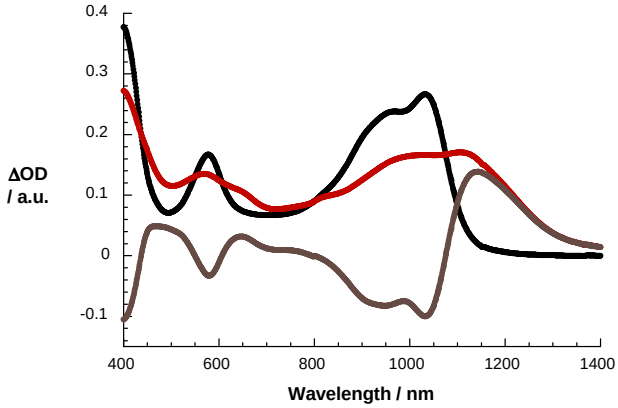

*Figure 74: Absorption spectra of **25** without (black spectrum) and with (red spectrum) an applied potential of +0.2 V for 15 min in deoxygenated dichloromethane containing 0.2 M tetrabutylammonium hexafluorophoshate. The differential absorption spectrum (grey spectrum) illustrates the changes in absorption – calculated by subtracting the initial spectra from the spectra recorded after applying the aforementioned potential.*

Preparation and Characterization of Self-assembled SWNT-Azulenocyanines

To investigate the interactions of **25** and **29** with SWNTs, titration experiments were carried out. Towards this end, SWNTs suspended in mixtures of 25% THF and 75% DMF, in which SWNTs are readily dispersed affording stable suspensions, were used.[28f-g,145,146] The preparation procedure to obtain these SWNT suspensions include the following steps, 0.2 mg of SWNT were added to about 8 ml of the solvent mixture, sonicated for 15 minutes, and centrifuged at 10 kRPM for 15 minutes for purification. The resulting greyish SWNT suspensions were titrated with increasing amounts (i.e., up to ~ 10^{-6} mol/l in the last step) of **25** and **29** in 25% THF and 75% DMF (Figure 75).

---

[28] f) J. Bartelmess, A. R. M. Soares, M. V. Martinez-Diaz, M. G. P. M. S. Neves, A. C. Tomé, J. A. S. Cavaleiro, T. Torres, D. M. Guldi, *Chem. Commun*. **2011**, *47*, 3490. g) J. Bartelmess, C. Ehli, J. J. Cid, M. Garcia-Iglesias, P. Vazquez, T. Torres, D. M. Guldi, *Chem. Sci*. **2011**, *2*, 652.

[145] J. Bartelmess, B. Ballesteros, G. de la Torre, D. Kiessling, S. Campidelli, M. Prato, T. Torres, D. M. Guldi, *J. Am. Chem. Soc.* **2010**, *132*, 16202.

[146] U. Hahn, S. Engmann, C. Oelsner, C. Ehli, D. M. Guldi, T. Torres, *J. Am. Chem. Soc*. **2010**, *132* , 6392.

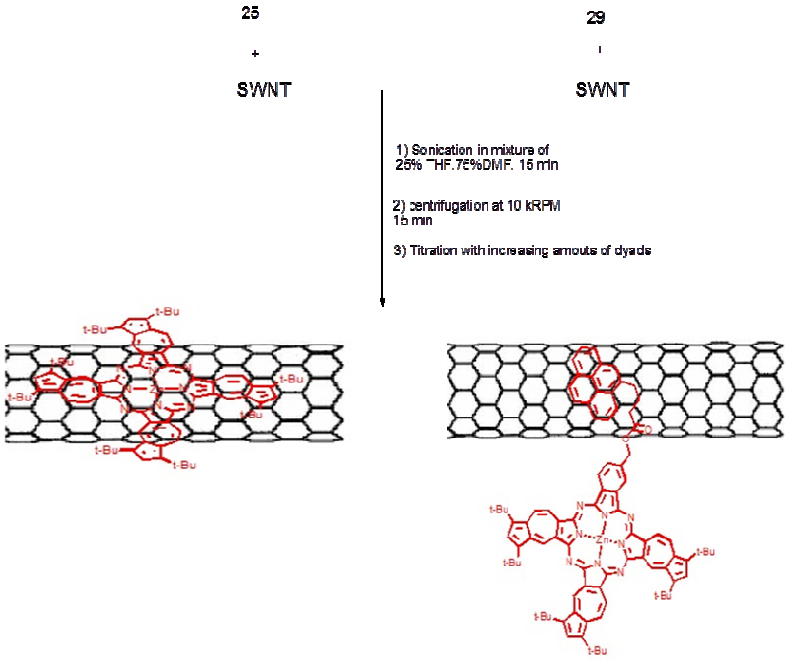

*Figure 75. Preparation of suspensions of SWNT/**25** and SWNT/**29**.*

In Figure 76 the absorption spectra are surveyed and compared with the spectrum of just **25** in the absence of SWNTs. Differential absorption spectra was also calculated the to visualize the absorption shifts (Figure 77).

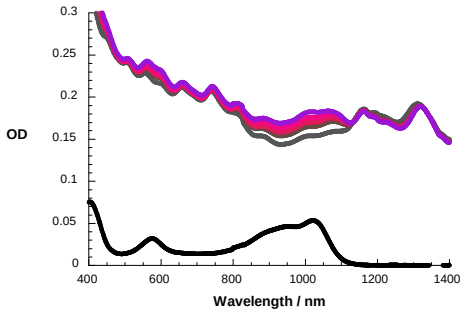

*Figure 76: Titration of SWNTs suspended in 25% THF / 75% DMF with increasing amounts of **25**. Black: absorption spectrum of **25** (10^{-6} M). Gray: absorption spectrum of suspended SWNT. From brown to purple: absorption spectra reflecting the titrations of SWNTs with **25** (up to 10^{-6} M of **325**).*

Clearly visible is an overall broadening of the absorption features of **25**. In addition, a red shift is seen. For example, next to the band at 403 nm a shoulder forms at around 420 nm and next to the band at 575 nm a shoulder forms at 610 nm. The largest changes evolve, however, around the band at 1020 nm. The latter shows a bathochromic shift of around 45 nm. The SWNT absorption bands also undergo successive red shift, from 1312 to 1320 nm. When comparing these results with those seen for phthalocyanines a strong resemblance is concluded. Also for SWNT / Pc hybrids a broadening and a red shift of the Pc's absorption bands were noted.[28f, g,145,146] Another similarity is the red shift that is associated with the SWNT absorption bands in the NIR region of the spectrum.

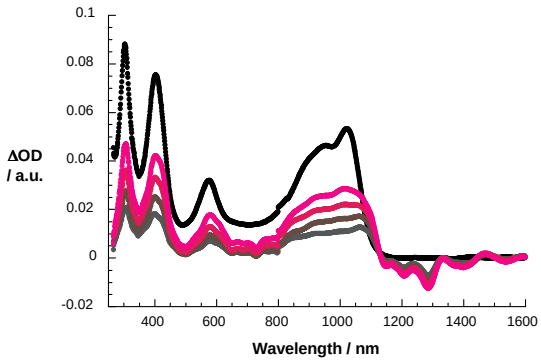

*Figure 77: Room temperature absorption spectrum of **25** (black spectrum) (10^{-6} M) in 25% THF / 75% DMF and differential absorption spectra (from gray to magenta) of suspended SWNTs titrated with increasing amounts of **25** illustrating the shift of absorption bands upon addition of **25**. The differential absorption spectra were calculated by subtracting the initial SWNT spectrum from the spectra recorded after addition of **25**.*

In summary, the red shifted absorption bands of **25** as well as those of SWNTs indicate the successful immobilization of **25** onto SWNTs and their mutual interactions. The results for SWNT/**29** are quite similar. In particular, the absorption bands of **29** are

---

[28] f) J. Bartelmess, A. R. M. Soares, M. V. Martinez-Diaz, M. G. P. M. S. Neves, A. C. Tomé, J. A. S. Cavaleiro, T. Torres, D. M. Guldi, *Chem. Commun*. **2011**, *47*, 3490. g) J. Bartelmess, C. Ehli, J.J. Cid, M. Garcia-Iglesias, P. Vazquez, T. Torres, D.M. Guldi, *Chem. Sci*. **2011**, *2*, 652.

[145] J. Bartelmess, B. Ballesteros, G. de la Torre, D. Kiessling, S. Campidelli, M. Prato, T. Torres, D. M. Guldi, *J. Am. Chem. Soc.* **2010**, *132*, 16202.

[146] U. Hahn, S. Engmann, C. Oelsner, C. Ehli, D. M. Guldi, T. Torres, *J. Am. Chem. Soc*. **2010**, *132* , 6392.

broadened and red shifted. Likewise, the SWNT absorptions in the infrared region undergo a red shift. This result shows that **29** was also immobilized onto the surface of SWNTs. To gain deeper insights into the interactions, fluorescence experiments were performed, where solutions of **25** or **29** were titrated with SWNTs. After taking the initial fluorescence spectra of **25** and **29**, 200 µL of a suspension of 0.2 mg SWNT in 2 mL solvent were added, followed by 15 minutes of ultrasonication. Important is the fact that **25** and **29** are stable under ultrasonication. The results of these titration experiments are shown in Figures 78. Again, the samples were excited at 910 nm to monitor the fluorescence of **25** and **29**. The fluorescence bands of **25** at 1050 nm are quenched after the second addition step of SWNT. The results for **29** are similar and include a quenched fluorescence band at 1030 nm upon addition of SWNTs. This quenching serves as further evidence for the successful immobilization of **25** and **29** onto the surface of SWNTs.

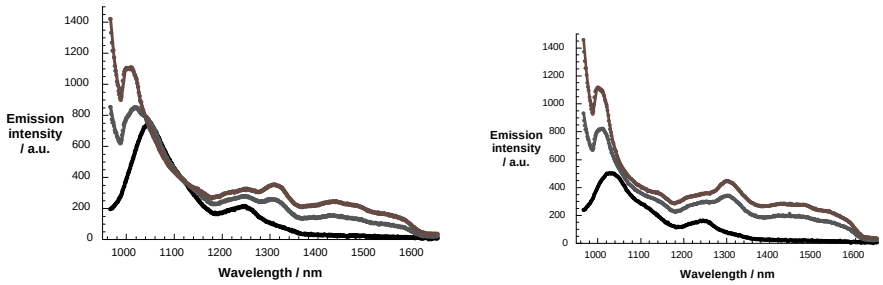

*Figure 78: Room temperature fluorescence spectra of **25** (black spectrum)(right part) and **29** (black spectrum) (left part) in 25% THF / 75% DMF titrated with increasing amounts of SWNTs (gray and brown spectra). Fluorescence spectra recorded upon photoexcitation at 910 nm and 120 s integration time.*

In terms of SWNT fluorescence, the fluorescence spectra of SWNT/**25** and SWNT/**29** were compared with that of SWNT/sodium dodecylbenzenesulfonate (SDBS) in D_2O. The preparation of the SWNT/SDBS reference suspensions was similar to the aforementioned procedure with the exception that we employed D_2O containing 2 wt % of SDBS. It is well known that in SWNT/SDBS, SWNT are well debundled and, in turn, exhibit strong fluorescence.[147] All investigated samples exhibit SWNT ground state

[147] a) M. J. O'Connell, S. M. Bachilo, C. B. Huffman, V. C. Moore, M. S. Strano, E. H. Haroz, K. L. Rialon, P. J. Boul, W. H. Noon, C. Kitt rell, J. Ma, R. H. Hauge, R. B. Weisman, R. E. Smalley, *Science*, **2002**, *297*, 593. b) M. F. Islam, E. Rojas, D. M. Bergey, A. T. Johnson, A. G. Yodh, *Nano Lett*., **2003**, *3*, 269.

absorptions that are similar throughout the excitation area, that is, between 550 and 800 nm. 3-D fluorescence landscapes (Figure 79) were generated for SWNT/SDBS, SWNT/**25**, and SWNT/**29**. SWNT/SDBS, for example, exhibits the strongest fluorescence maxima from SWNT that are ascribed to (9,4), (7,6), (8,6), (11,3), (9,5), (10,5), (8,7), and (9,7). At first glance, the fluorescence of SWNT/**25** and SWNT/**29** is strongly quenched when compared to SWNT/SDBS. Importantly, we consider this as sound proof for mutually interacting SWNT, on one hand, and **25** or **29**, on the other hand. A closer look reveals, however, subtle differences in the fluorescent features of SWNT/**25** and SWNT/**29** (Figure 80). In particular, the fluorescence bands of SWNT/**25** and SWNT/**29** are red shifted compared to SWNT/SDBS. In addition, the fluorescence intensities of SWNT/**25** (i.e., 1130, 1220, and 1310 nm) are notably weaker than those of SWNT/**29**. The only exception is the fluorescence maximum at 1440 nm, which turns out to be stronger in the case of SWNT/**25**. This behavior prompts unambiguously to stronger interactions in SWNT/**25**.

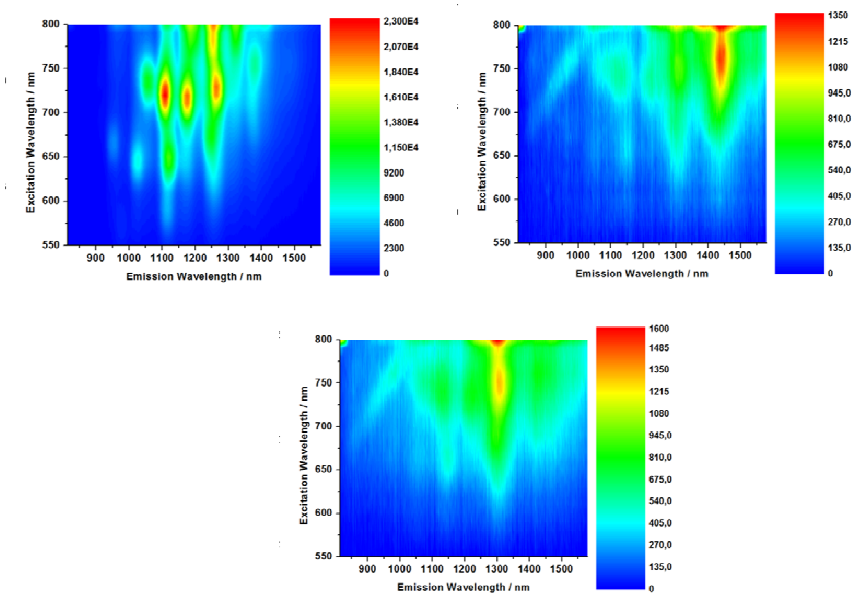

*Figure 79: 3D steady-state fluorescence spectra – with increasing intensity from blue to green to yellow and to red – of SWNT/SDBS in D_2O (right). 3D steady-state fluorescence spectra – with increasing intensity from blue to green to yellow and to red – of SWNT/**25** in 25% THF/75% DMF (left) 3D steady-state fluorescence spectra – with increasing intensity from blue to green to yellow and to red – of SWNT / **29** in 25% THF/75% DMF (below).*

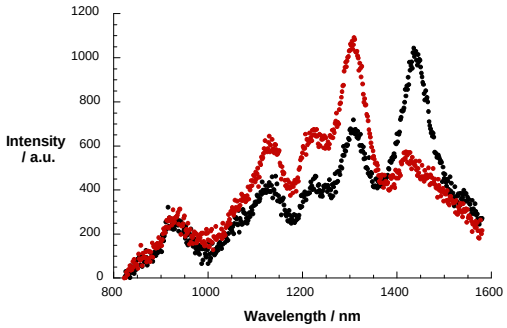

*Figure 80. Room temperature fluorescence spectra of SWNT/**25** (black spectrum) and SWNT/**29** (red spectrum) upon photoexcitation at 730 nm.*

Next, femtosecond transient absorption measurements were performed with **25** and **29** in the mixture of 25% THF and 75% DMF using 387 nm excitation pulses (Figure 81).

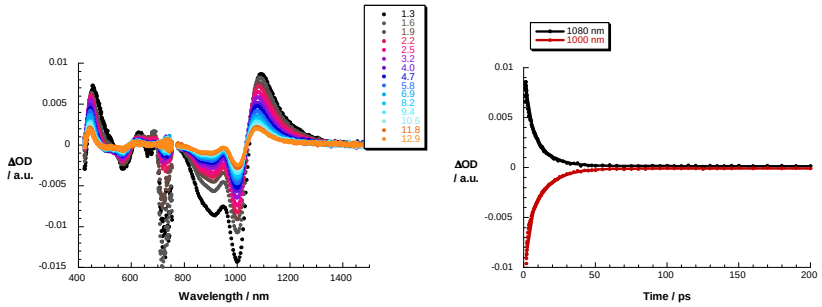

*Figure 81: Differential absorption spectra (visible and near-infrared) obtained upon femtosecond flash photolysis (387 nm) of **25** in 25% TH /75% DMF with different time delays between 1.3 and 12.9 ps at room temperature(right). Time absorption profiles at 1000 and 1080 nm monitoring the excited state decay(left).*

Ground-state bleach is observed across the 475 to 600 nm and 980 to 1025 nm ranges with local minima at 565 and 1000 nm. In addition, we note transient maxima at 445 and 1085 nm, which are attributed to the singlet excited state features of **25**. For **29**, the singlet excited state features are shifted to the blue – a finding that is consistent with the shifted ground state features. These singlet excited features convert *via* a very rapid intersystem crossing (i.e., 4.1 ± 0.2 ps) to the energetically lower lying triplet excited features. The corresponding triplet excited state characteristics resemble those

of the singlet excited state with the exception of an overall band narrowing and a blue shift (i.e., from 1085 to 1075 nm). The latter reinstate with 12.0 ± 0.2 ps the singlet ground state.

We started our SWNT investigations with SWNT/SDBS upon 387 nm photoexcitation. The baseline is in the case of SWNT/SDBS replaced with strong bleaching that dominates the differential absorption spectra throughout the visible and near-infrared regions, where absorptive transitions of metallic and semiconducting SWNTs appear, respectively. The major minima are seen at 975, 1020, 1135, and 1260 nm. Multiwavelength analyses of the bleaching characteristics in the near-infrared resulted in two lifetimes, 1.2 and 520 ps. Throughout these biexponential decays the original absorption / baseline is quantitatively reinstated.

Finally, transient absorption spectroscopy with SWNT/**25** and SWNT/**29** in the solvent mixture was employed to substantiate the ultrafast singlet excited state deactivations and, in addition, to characterize the nature of the photoproducts. The singlet excited characteristics of **25** and **29** , despite the presence of SWNT, were registered upon 387 nm photoexcitation of SWNT/**25** and SWNT/**29** (Figures 82 and 83). This confirms the successful excitation of **25** or **29**. Simultaneously with the singlet excited state decay of either **25** or **29** (i.e., 20 ps), the formation of a new transient species evolves with distinct minima at 550, 950, and 1050 nm as well as maxima at 630 and 1140 nm. Of key importance is the resemblance of these attributes with those of the one-electron oxidized radical cations of either **25** or **29**, as they were determined in the aforementioned spectroelectrochemistry measurements.

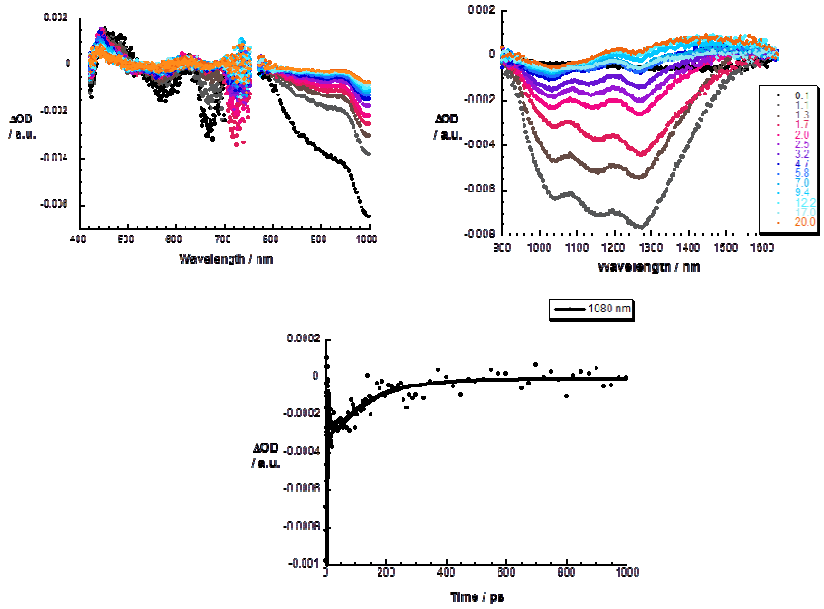

*Figure 82: Differential absorption spectra (visible and near-infrared) obtained upon femtosecond flash photolysis (387 nm) of SWNT/**25** in 25% THF / 75% DMF with different time delays between 0.1 and 20 ps at room temperature (right). Differential absorption spectra (extended near-infrared) obtained upon femtosecond flash photolysis (387 nm) of SWNT/**29** in 25% THF / 75% DMF with different time delays between 0.1 and 20 ps at room temperature (left). Time absorption profile at 1080 monitoring the charge separation and charge recombination (below).*

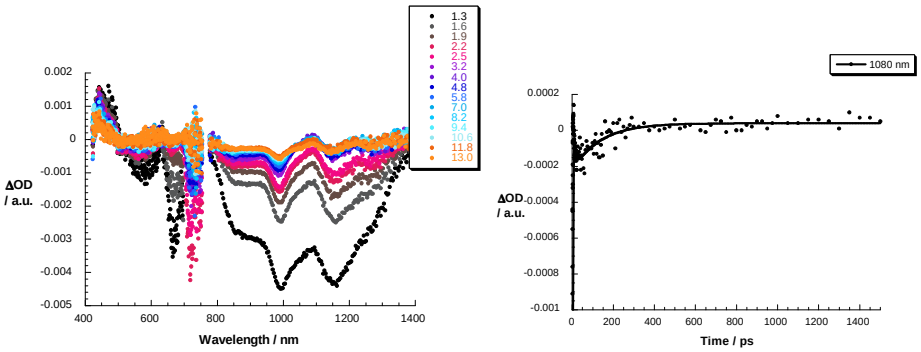

*Figure 83. Differential absorption spectra (visible and near-infrared) obtained upon femtosecond flash photolysis (387 nm) of SWNT/**29** in 25% THF / 75% DMF with different time delays between 1.3 and 13.0 ps at room temperature (right). Time absorption profile at 1080 monitoring the charge separation and charge recombination (left).*

Similarly, the range beyond 1000 nm (i.e., 1000-1600 nm) is important, which immediately after the photoexcitation is dominated by a negative imprint of the SWNT centered van Hove singularities (i.e., 1040, 1155, and 1270 nm). Here, appreciable blue shifts were noted during the transient decay with minima that shift from 1040, 1155, and 1270 nm to 1030, 1120, and 1260 nm, respectively. Implicit are new conduction band electrons, injected from photoexcited **25** or **29**, shifting the transitions to higher energies. Thus, we reach the conclusion that photoexcitation of SWNT / **25** and SWNT / **29** is followed by a rapid charge transfer. A multi-wavelength analysis of the newly developed charge transfer state reveals its metastable character with decays of 124 and 137 ps for SWNT / **25** and SWNT / **29**, respectively. We would like to point out that a transduction of excited state energy from photoexcited **25** or **29** to SWNT cannot be ruled out.

Photovoltaic Performance of SWNT-Azulenocyanines

Photoelectrochemical devices based on the azulenocyanine-SWNT hybrids were made in the group of Prof. Dirk M. Guldi at University of Erlangen (Germany).

To test the applicability of SWNT/**25** and SWNT/**29** in solar cells, electrochemical test cells were constructed. To fabricate photoactive SWNT/azulenocyanine layers on top of the conductive glass, different amounts of SWNT/**25** or SWNT/**29** containing suspensions (in a solvent mixture of 25% THF/75% DMF) were filtrated onto a 200 µm pore sized PTFE filter. PTFE filter, retaining all the functionalized tubes, at the same time removing all excess amounts of **25** and **29**. Consecutively, the filtrate residue was hot stamped on top of the pretreated ITO at 130 ℃ under pressure. The resulting slides were covere d with a homogenous smooth black film, with average thickness of 300-500 nm depending on amount and concentration of the suspensions. All attempts of spin-coating the material onto ITO were futile, due to the restriction in choice of solvents. After optical inspection for irregularities they were characterized in terms of absorption (i.e., 560 nm, Figure 84) to ensure comparable thickness. In a next step, an active layer was defined by removing the SWNT/**25** or SWNT/**29** films leaving an effective circle of 6 mm diameter.

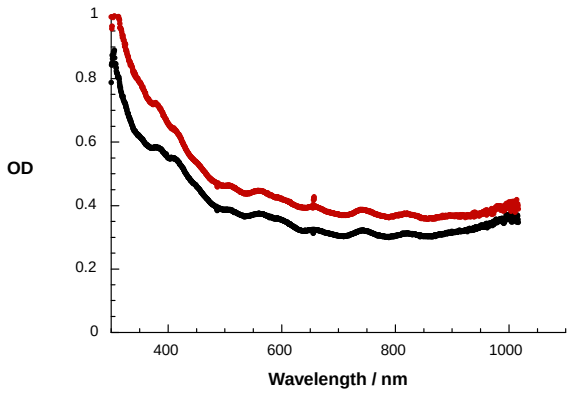

*Figure 84. Room temperature absorption spectra of SWNT/**25** (black spectrum) and SWNT/**29** (red spectrum) films.*

The devices were investigated measuring the white light response under AM 1.5 conditions as well as the wavelength dependent IPCE. Using optimal absorption the photoresponse is 25.7 and 19.7 μA/cm^2 for SWNT/**25** and SWNT/**29**, respectively (Figure 85). The IPCE spectra resemble the broad and featureless absorption spectra of SWNT/**25** and SWNT/**29**, that is, a gradual increase in efficiency from the NIR to the visible region with a maximum IPCE of nearly 2.5 percent around 400 nm (Figure 86) without revealing distinct features. As expected, overall higher values were registered for SWNT/**25** than for SWNT/**29**. A possible rationale for the better performance is a better interface between SWNT and **25** when compared with that between SWNT and **29**.

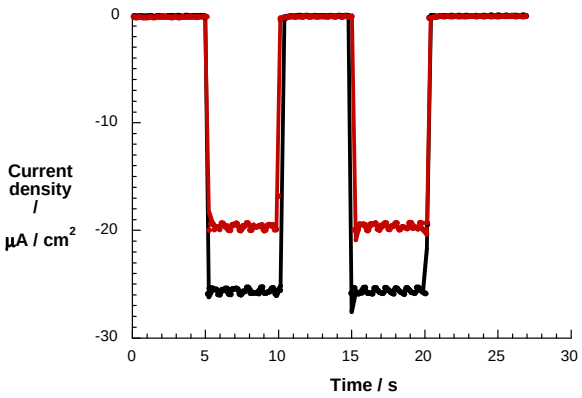

*Figure 85. Photovoltage responses upon ON-OFF light cycles under AM 1.5 illumination of SWNT / **25** (black spectrum) and SWNT / **29** (red spectrum) photoelectrochemical cells.*

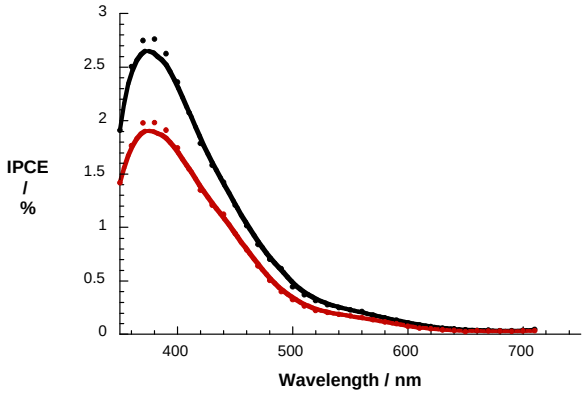

*Figure 86: IPCE spectra of SWNT / **25** (black spectrum) and SWNT / **29** (red spectrum) thin films in I^-/I_2 sandwich cells.*

1.2.3. Summary and Conclusion

In summary

- New symmetric Zn(II)octa-*tert*-butylazulenocyanine and unsymmetrical azulenocyanine-phthalocyanine hybrids were synthesized. These dyads exhibit a broad absorption band, which covers the range between 300-1200 nm due to the low HOMO-LUMO band-gap.

- A supramolecular and a covalent approach have been applied for the preparation of azulenocyanine-C_{60} dyads for a comparison purpose. Covalently linked azulenocyanine-C_{60} dyad did not show any electron transfer activity in its excited state. This can be explained by the fact that the excited state is spread over the azulenoids, while the electron accepting fullerene is linked to the benzoids. In other words, a rather poor electronic coupling shuts down the electron transfer. On the other hand, axial coordination of N-pyridylfulleropyrrolidine to Zn(II)octa-*tert*-butylazulenocyanine **25** leads not only to the successful formation of **25•C_{60}**, but also to a nearly nanosecond lived radical ion pair state (0.78 ns) despite the extremely short lived nature of the azulenocyanine moiety centered excited state (10 ps). In this context, the benefit is the rather strong axial coordination, which is based on a complement of strong sigma bonds and moderate π-back bonding.

- The noncovalent functionalization of SWNT with Zn(II) octa-*tert*-butylazulenocyanine **25** and Zn(II)azulenocyanine-pyrene **29** by virtue of π-π interactions resulted in suspendable, room temperature stable, and photoactive donor acceptor hybrids. Zn(II)octa-tert-butylazulenocyanine (**25)** allowed to strong π-π interaction between the macrocycle core and the surface of the SWNTs without requirement of any conjugate unit.

- SWNT/**25** and SWNT/**29** exhibited strong interactions in the ground state, and a rapid charge separation in the excited state. The accordingly formed radical ion pair states decay with lifetimes of 124 and 137 ps for SWNT/**25** and SWNT/ **29**, respectively.

- Prototype solar cells were constructed using the SWNT/**25** and SWNT/**29** hybrids. The IPCE spectra resemble the broad and featureless absorption spectra of SWNT/**25** and SWNT/**29**, that is, a gradual increase in efficiency from the NIR to the visible region with a maximum IPCE of nearly 2.5 percent around 400 nm due to ultrafast charge separation and hundreds of femtosecond lasting charge recombination.

General conclusion

The design of novel donor-acceptor systems, which can generate charge-separated states upon photoexcitation is one of the main objectives of the present investigation. Even though low energy band gap is one of the most important parameters for efficient solar photon harvesting, photovoltaic and efficient charge transfer performance is governed by the interplay of several factors.

As light harvesting materials, azulenocyanine derivatives are promising candidates for many applications due to low energy bad gap, which allows strong absorption in the NIR. However, donor-acceptor systems based on these azulenocyanine derivatives exhibit relatively short charge transfer lifetimes and low fluorescence quantum yields. These results could arise from the low band gap of azulenocyanines, which makes more favourable a non-radiative decay mechanism. Therefore, suitable HOMO-LUMO energy levels of donor is required not only to absorb efficient light but also to get efficient charge transfer from donor to acceptor.

Chapter 1.2. Experimental Section

1.2.4. Experimental Section

SWNTs (HiPCO Batch Nr.: R0510C) were purchased from CNI.

Photophysical and electrochemical measurements were performed at room temperature and ambient conditions. Steady-state absorption spectra were measured by a Cary5000 (Varian) two beam spectrometer. NIR emission spectra were measured by a Fluorolog spectrometer (HORIBA Jobin Yvon).

The optical detection was performed by a Symphony InGaAs array in combination with an iHR320 imaging spectrometer. The samples were excited by a 450 W Xenon lamp or the SHG (532 nm) of a Nd/YAG laser. Femtosecond transient absorption studies were performed using 387 nm laser pulses with a 150 fs pulse width (1 kHz, 200 nJ), from an amplified Ti:sapphire laser system (SHG, CPA 2001, Clark-MXR Inc.) additional excitation experiments was carried by using 660 nm pulses created by a NOPA (Clark-MXR Inc.). For the detection, a Helios TAPPS from Ultrafast Inc was used.

Electrochemical measurements were carried out by using a HEKA elektronik HEKA 510 potentiostat/galvanostat with a glassy carbon working electrode, a Pt wire counter electrode and Ag wire reference electrode. Potentials were measured vs. Fc/Fc^+ in deoxygenated samples in dichloromethane containing 0.2 M tetrabutylammonium hexafluorophosphate electrolyte. Spectroelectrochemical measurements were performed on a Varian Cary5000 absorption spectrometer with a custom made cell including a Pt mesh working electrode, a Pt counter electrode and a Ag wire reference electrode. The filter for the transfer process was a PTFE membrane filter, Millipore, 200 nm pore size.

The ITO covered glass slides were pretreated by subsequent ultrasonication in water/detergent mixture following acetone and finally isopropanol. A surlyn ionomer with 50 µm thickness connects the covered ITO with a $Pt(Cl)_6$ treated FTO counter electrode and simultaneously seals the device. To finalize the test cells, the gaps between the electrodes were filled with an I_2 based electrolyte through a hole in the counter electrode (i.e., 0.6 M 1-butyl-*3*-methylimidazolium iodide; 0.03 M I_2; 0.1 M guanidinium thiocyanate; 0.5 M 4-tert-butylpyridine in a mixture of

acetonitrile:valeronitrile 85:15). The light source for the solar simulator was a LOT-Oriel Xenon lamp (350-1000 Watt). AM 1,5 conditions are achieved using the appropriate filter and a Newport 1919-C optical power meter. Monochromatic light was obtained via a B&M Spectronic monochromator (600 grooves/nm grating, 10 nm bandwidth). All currents were measured and applied by a Keithley 2400 sourcemeter.

1.2.4.1. Synthesis of Precursors

1.2.4.1.1. 4-(Hydroxymethyl)phthalonitrile (20)[141]

4-(Bromomethyl)phthalonitrile (**19**)

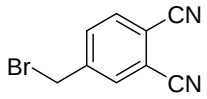

A mixture of 4-methylphthalonitrile (6.20 g, 43.60 mmol), NBS (23.30 g, 0.13 mol), and AIBN (300 mg, 1.84 mmol) in degassed CCl4 (350 ml) was heated at reflux under argon for 4 h under irradiation by a high-pressure 125 W mercury lamp (>300 nm). The reaction was monitored by ^{1}H-NMR until the disappearance of the starting material. After cooling down, succinimide as a by-product was filtered off and washed with CCl_4. Afterwards, the solvent was evaporated affording a red oil residue consisting of mono-, di-, and tribromination products (in an approximate 1:2:1 ratio by ^{1}H-NMR) at the benzylic position. The crude mixture was dissolved in dry THF (50 ml) and cooled at 0ºC with an ice bath. Then, diethyl phosphite (2.30 g, 17.9 mmol) and DIPEA (2.20 g, 17.02 mmol) were added dropwise. The solution was allowed to reach room temperature and left stirring for 3 h. The reaction was monitored by TLC and by ^{1}H-NMR until the disappearance of the di and tri bromination products. Then, the solvent was evaporated and the residue was dissolved in $CHCl_3$ (100 ml). The solution was washed with an 0.1M solution of HCl (3x50 ml), then with a saturated solution of $NaHCO_3$ (2x50 ml), and finally with brine (2x50 ml). After drying over Na_2SO_4 and filtration, the solvent was removed under vacuum affording red oil that solidified upon standing. The crude was chromatographed on silica gel column chromography (CH_2Cl_2) to yield 4-(bromomethyl)phthalonitrile (**19**) (6.19 g, 0.03mol) as a beige solid. Yield: 65%.

Mp: 64-66 ºC (reported:[141] 65-67 ºC).

[141] R. F. Enes, J. J. Cid, A. Hausmann, O. Trukhina, A. Gouloumis, P. Vazquez, J. A. S. Cavaleiro, A. C. Tomé, D. M. Guldi, T. Torres, *Chem. Eur. J.* **2012**, *18*, 1727.

^{1}H NMR ($CDCl_3$, 300 MHz): δ (ppm) = 7.9 (d, *J*=1.7 Hz), 7.80 (d, *J*=8.1 Hz), 7.7 (dd, *J*=8.1, 1.7 Hz), 4.5 (s, 2H).

4-(Hydroxymethyl)phthalonitrile (**20**)

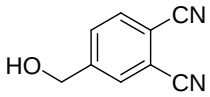

4-(Bromomethyl)phthalonitrile (**19**) (2.17 g, 9.82 mmol) was added to a suspension of calcium carbonate (3.92 g) in dioxane - water (1:1.5, 80 ml) and the mixture was stirred at reflux temperature for 24 h. The reaction mixture was allowed to cool, and then filtered from $CaCO_3$. The compound was extracted with Et_2O (3X150 ml). The combined organic layers were dried over Na_2SO_4 and concentrated under reduced pressure giving pale yellow oil that solidifies upon standing. Recrystallization from toluene (15 ml) afforded of **20** (0.93 g, 5.8 mmol) as a white solid. Yield: 60%.

Mp: 48-50 ºC (reported:[141] 49-51 ºC).

^{1}H NMR ($CDCl_3$, 300 MHz): δ (ppm) = 7.9 (s, 1H), 7.8–7.7 (m, 2H), 4.8 (s ,2H), 2.0 ppm (m, 1H, OH).

1.2.4.1.2. 1,3-Di-tert-butyl-5,6-dicyanoazulene (24)

3,4-Dibromothiophene-1,1-dioxide (**21**)[142]

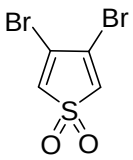

H_2O_2 33% (3.3 ml, 33 mmol) was stirred in a $CaCl_2$-ice bath (-15 ºC). Trifluoroacetic anhydride (8.3 ml, 59 mmol) was added dropwise at 0ºC. The solution was stirred for another 10 min, and 3,4-dibromothiophene (1g, 4.1 mmol) in CH_2Cl_2 (5

[142] Y. Lu, D. M. Lemal, J. P. Jasinski, *J. Am. Chem. Soc.* **2000,** *122,* 2440.

ml) was then added. The mixture was stirred for 3h at room temperature. Then the solution was transferred to an ice bath, and saturated Na_2CO_3 (50 ml) was slowly added to bring the pH up to around 5. The organic layer was separated and the aqueous layer was extracted with CH_2Cl_2 (20 ml) four times.

The organic solutions were combined and washed with saturated solution of Na_2CO_3 (10 ml) and water (10 ml), then dried over $MgSO_4$. The solvent was evaporated. Recrystallization from ethanol led to **21** (0.68 g, 2.4 mmol) as yellow crystals. Yield: 60%.

Mp: 102-104 ºC (reported:[142] 104-106 ºC).

^{1}H NMR ($CDCl_3$, 300 MHz): δ (ppm) = 6.82 (s, 2H).

5,6-Dibromoazulene (**22**)[142]

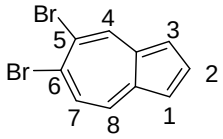

To a solution of 3,4-dibromothiophene 1,1-dioxide (21) (4.82 g, 17.6 mmol) in $CHCl_3$ (10 ml),, 6-dimethylaminofulvene (2.2 g, 17.6 mmol) was slowly added and the reaction mixture was refluxed under argon for 5h. After cooling to room temperature the solvent was evaporated and the remaining solid was stirred in 10 ml hexane at 50 ºC until all the tar turned to fine powder. The reaction was allowed to reach room temperature and the mixture was directly poured onto a silica gel column (hexane) to give **22** (1.2 g, 4.2 mmol) as a blue solid. Yield: 24%.

Mp: 183 ºC (reported:[142] 185 ºC dec.).

[142] Y. Lu, D. M. Lemal, J. P. Jasinski, *J. Am. Chem. Soc.* **2000,** *122,* 2440.

^{1}H NMR ($CDCl_3$, 300 MHz): δ (ppm) = 8.78 (s, 1H, H-4), 7.98-7.927 (m, 2H, H-8, H-2), 7.71 (d, J = 10.2 Hz, 1H, H-7), 7.40 (d, J = 3.1Hz, 1-H, H-3), 7.37 (d, J = 3.2 Hz, 1H, H-1).

5,6-Dicyanoazulene (**23**)[143]

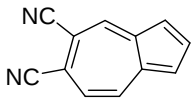

In a 10 ml CEM Voyager microwave tube a solution of 5,6-dibromoazulene (**22**) (100 mg, 0.35 mmol) in DMF (3 ml), $ZnCN_2$ (82 mg, 0.70 mmol), and $[Pd(PPh_3)_4]$ (25 mg, 0.02 mmol) were added. The reaction tube was sealed and heated to 90 ºC under microwave irradiation with a 10 min hold time, and 60 W maximum power input. The suspension was then poured onto a 2M ammonia solution (100 ml). The mixture was extracted with ethyl acetate (2×100 ml). The combined organic extracts were washed with brine (20 ml), dried over $MgSO_4$ and evaporated *in vacuo*. The solid residue was purified by column chromatography on silica gel (Hexanes/ EtOAc, 5:1) to yield 5,6-dicyanoazulene **23** (0,53 mg, 0.3 mmol) as a green solid. Yield: 85%.

Mp: 201-203 ºC (reported:[137] 203-204 ºC).

^{1}H NMR ($CDCl_3$, 300 MHz): 8.62 (s, 1H, H-4), 8.42 (d, *J* = 9.6 Hz 1H, H-8), 8.24 (t, *J* = 3.8 Hz, 1H, H-2), 7.82 (d, *J* = 3.1, 1H, H-3), 7.77 (d, *J* = 3.2, 1H, H-1), 7.56 (d, *J* = 9, 1H, H-7).

[143] M. Alterman, A. Hallberg, *J. Org. Chem.* **2000**, *65*, 7984

1,3-Di-tert-butyl-5,6-dicyanoazulene (24)[137]

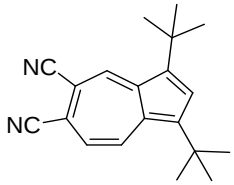

A mixture of 5,6-dicyanoazulene (**23**) (100 mg, 0.56 mmol) and *t*-BuCl (0.37 ml, 3.36 mmol) were dissolved in CH_3NO_2 (15 ml). Then $AlCl_3$ (224 mg, 1.68 mmol) was added and the reaction mixture was stirred for 4h at room temperature under argon atmosphere. The reaction mixture was quenched by addition of water.The mixture was extracted with EtOAc (2x300 ml) and the combine organic extracts washed with water and brine, dried over $MgSO_4$ and evaporated *in vacuo*. The crude product was purified by column chromotography on silica gel, (Hexanes/EtOAc (10:1)), to yield **24** (89 mg, 0.31 mmol) as a green solid. Yield: 55%.

Mp: 159-161 ºC (reported:[137] 161-162 ºC).

^{1}H NMR ($CDCl_3$, 300 MHz): 8.8 (s, 1H, H-4), 8.5 (d, *J* = 9 Hz 1H, H-8), 8.0 (s, 1H, H-2), 7.3 (d, *J* = 9,9 1H, H-7), 1.6 (s, 9H, $C(CH)_3$), 1.5 (s, 9H, $C(CH)_3$).

[137] A. Muranaka, M. Yonehara, M. Uchiyama, *J. Am. Chem. Soc.* **2010**, *132*, 7844.

1.2.4.2. Synthesis of Azulenocyanine Derivatives

1.2.4.2.1. Synthesis of Azulenocyanines-Fullerene Dyad (**28**)

1,3,10(11),12(13),19(20),21(22),28(29),30(31) –octakis(*tert*-butyl)tetraazuleno [6,5(5,6)-a:5',6' (6',5')f:5'',6''(6'',5'')k] -porphyrazinato Zn(II) (**25**) (mixture of regioisomers)

A mixture of 1,3-di-tert-butyl-5,6-dicyanoazulene (**24**) (100 mg, 0.34 mmol), 4-hydroxymethylphthalonitrile (**20**) (13.6 mg, 0.086 mmol) and $(ZnOAc)_2$ (25.3 mg, 0.13 mmol) in DMAE (6 ml) was heated at reflux for 24 h with stirring under argon atmosphere. After cooling to room temperature, the solvent was removed. The crude product was purified by column chromatography on silica gel (Hexanes/dioxane, 4:1). The symmetric Zn(II)azulenocyanine **25** was eluted first, obtained as a black solid (35 mg, 0,028mmol), 34% yield, followed by Zn(II)azulenocyanine-phthalocyanine **26** (20 mg, 0.018 mmol) as a dark-greyish solid, 22% yield.

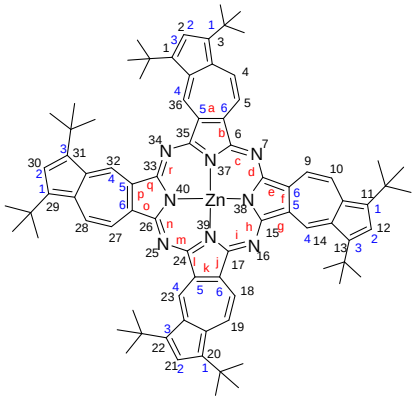

Mp> 250ºC.

^{1}H-NMR (300 MHz, THF-d_8): δ (ppm) = 11.4-10.6 (m, 4H, ArH), 9.6-8.8 (m, 8H, ArH), 8.4- 8.0 (m, 4H, ArH), 2.2-1.8 (m, 72H, alkylH).

UV/Vis (THF/DMF (25:75%): λmax (log ε)= 1020 (4.76), 940 (4.69), 575 (4.53),403 (4.91), 303 (4.98).

FT-IR (film):ν(cm^{-1}) = 2955, 2944, 2855, 1567, 1530, 1462, 1408, 1383, 1330, 1243,1142, 1046, 998, 893, 715, 669.

HRMS (MALDI-TOF, DCTB): calc. for $C_{80}H_{88}ZnN_8$: [M^+]: m/z: 1224.6418 found 1224.6417.

1, 3, 9(10,11),11(12,13),18(19,20),20(21,22)-hexa-tert-butyl-27(28,29)-hydroxymetyl -triazuleno-[6,5(5,6)-a:5',6' (6',5')f:5'',6''(6'',5'')k] benzo[2''',3'''p]-porphyrazinato Zn(II) (**26**) (mixture of regioisomers)

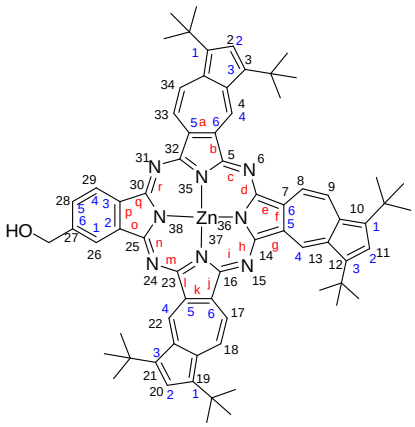

Mp> 250ºC.

^{1}H-NMR (300 MHz, THF-d_8): δ (ppm) = 11.4-10.8 (m, 3H, ArH), 9.7-8.8 (m, 8H, ArH), 8.5- 8.0 (m, 4H, ArH), 5.6-5.0 (m, 2H), 2.1-1.8 (m, 54H, alkylH).

UV/vis (THF/DMF (25:75%): λmax (log ε)= 1010 (4.60), 889 (4.66), 610 (4.41), 565 (4.42), 403 (4.84), 303 (4.78).

FT-IR (film): ν (cm^{-1}) = 3418, 2955, 2946, 2852, 1569, 1458, 1407, 1364, 1328, 1208, 1168, 1045, 996, 955, 893, 714, 684.

HRMS (MALDI-TOF, DCTB): calc. for $C_{69}H_{72}ZnN_8O$: $[M]^+$: m/z: 1092.5115 found 1092.5095.

1, 3, 9 (10,11), 11 (12,13),18(19,20),20 (21,22)-hexa-tert-butyl-27 (28,29)-formyltriazuleno [6,5(5,6)a:5',6' (6',5')f:5'',6''(6'',5'')k] benzo[2''',3'''p]-porphyrazinato Zn(II)) (**27**) (mixture of regioisomers)

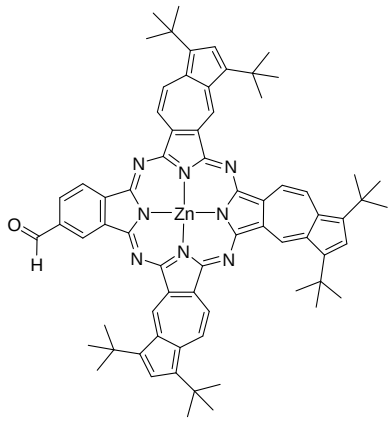

Hydroxymethyl-azulenocyanine (**26**) (50 mg, 0.045 mmol) was added to a solution of IBX (38 mg, 0.137 mmol) in DMSO (5 ml). The mixture was stirred at room temperature overnight. The reaction was monitored by TLC (Hexanes/dioxane, 3:1) until all the starting azulenocyanine was consumed. Brine was then added and the mixture was extracted with THF. The combined organic layers were dried over $MgSO_4$ and concentrated *in vacuo*. The solid residue was purified by column chromatography on silica gel (Hexanes/dioxane, 3:1) to give **27** (35 mg, 0.03 mmol) a black-greyish solid. Yield: 71 %.

Mp> 250ºC.

^{1}H-NMR (d_8-THF, 300 MHz) δ (ppm): 11.1-10.7 (m, 3H, ArH), 10.4-10.2 (m, 1H, ArH), 9.4-9.1 (m, 8H, ArH), 8.5- 8.2 (m, 4H, ArH), 2.1-1.5 (m, 54H, alkylH).

UV/vis (THF/DMF (25:75%): λmax (log ε)= 1009 (4.61), 888 (4.67), 612 (4.39), 566 (4.42), 402 (4.84), 303 (4.78).

FT-IR (film): ν (cm^{-1}): 2954, 2924, 2870, 2218, 1690, 1589, 1570, 1408, 1364, 1208, 1046, 995, 893, 716, 689.

HRMS (MALDI-TOF, DCTB): calc. for $C_{69}H_{70}ZnN_8O$: $[M]^+$: m/z: 1090.4962 found 1090.4968.

1, 3, 9 (10,11), 11 (12,13),18(19,20),20 (21,22)-hexa-tert-butyl-27 (28,29)-fulleropyrrolidinetriazuleno [6,5(5,6)a:5',6' (6',5')f:5'',6''(6'',5'')k] benzo[2''',3'''p]-porphyrazinato Zn(II) (**28**) (mixture of regioisomers)

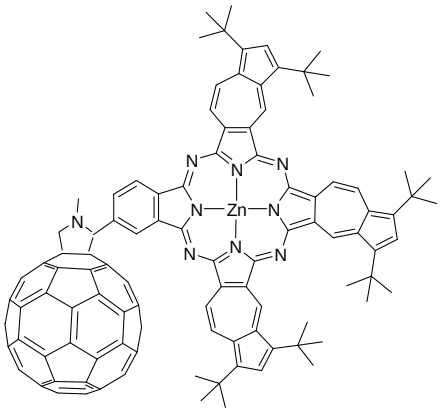

A mixture of C_{60} (54.5 mg, 0.075 mmol), N-methylglycine (5mg, 0.054 mmol) and azulenocyanine **27** (30 mg, 0.027 mmol) was heated under reflux overnight in dry toluene (60 ml) under argon atmosphere. After cooling to room temperature, the solvent was evaporated to dryness. Purification of the solid residue by column chromotography on silica gel (toluene followed by toluene/THF, 10:1), and then size-exclusion column chromotograpy (Bio-Beads SX1, THF) gave pure azulenocyanine-C_{60} **28** (21 mg, 0.011 mmol) as a black greyish solid. Yield: 42%.

Mp> 250ºC.

^{1}H-NMR (d_8-THF, 300 MHz) δ (ppm): 11.5-11.0 (m, 3H, ArH), 9.8-9.2 (m, 8H, ArH), 8.3-8.2 (m, 4H, ArH), 5.5- 5.3 (m, 3H, pyrrolidine H), 3.34 (s, 3H, NCH_3), 2.0-1.4 (m, 54H, alkylH).

UV/Vis (THF): λ_{max} (nm) = 301 (4.7), 380 (4.5), 576 (3.2), 924 (3.3) 1042 (4.2).

FT-IR (film) ν (cm^{-1}): 2920, 2866, 1740, 1564, 1524, 1416, 1362, 1335, 1240, 1213, 1051, 957, 889, 768, 675.

HRMS (MALDI-TOF, DCTB): calc. for $C_{131}H_{75}ZnN_9$: $[M]^+$: m/z: 1837.5431 found 1837.5394.

1.2.4.2.1. Synthesis of Azulenocyanines-Pyrene Dyad (**29**)

1, 3, 9 (10,11), 11 (12,13),18(19,20),20 (21,22)-hexa-tert-butyl-27 (28,29)-p-(4`-pyrene-methylbutanoate)phenyltriazuleno [6,5(5,6)a:5',6' (6',5')f:5'',6''(6'',5'')k] benzo[2''',3'''p]-porphyrazinato Zn(II) (**29**) (mixture of regioisomers)

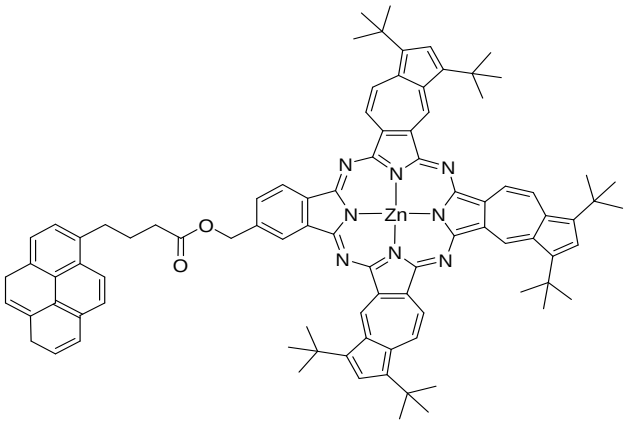

A mixture of 1-pyrenebutyric acid (26.3 mg, 0.091 mmol), DMAP (11.1 mg, 0.091 mmol) and DCC (18.7 mg, 0.091 mmol) in THF (3 ml) was cooled to 0ºC under argon atmosphere. A solution of Zn(II)azulenocyanine **39** (100 mg, 0.091 mmol) in THF (2 ml) was then added dropwise. The mixture was stirred at 0 ºC for 1h and then warmed up to room temperature. Stirring was continued for 24h. The solvent was removed, and the residue was washed with MeOH. The crude product was purified by column chromatography on silica gel (Hexanes/dioxane (4:1). Zn(II)azulenocyanine **29** (0,72 mg, 0.052 mmol) was obtained as a dark-greyish solid. Yield: 58%.

Mp> 250ºC.

^{1}H-NMR (300 MHz, THF-d_8): δ(ppm) = 11.3-10.7 (m, 3H, ArH), 9.5-8.9 (m, 8H, ArH), 8.4-7.7 (m, 13H, ArH), 5.6-5.2 (m, 2H), 3.7-3.5 (m, 2H) , 2.9-2.6 (m, 4H), 2.1-1.7 (m, 54H, alkylH).

UV/Vis (THF/DMF (25:75%): λmax (log ε) = 1005 (4.58), 890 (4.67), 610 (4.43), 569 (4.46),389 (4.88), 302 (4.93).

FT-IR (KBr): ν (cm^{-1}) = 2959, 2918, 2864, 1734, 1572, 1531, 1454, 1248, 1207, 1167, 1047, 993, 953, 887, 847, 744.

HRMS (MALDI-TOF, dithranol): calc. for $C_{89}H_{86}N_8O_2Zn$: [M^+]: m/z: 1362.6160 found 1362.6121.

Chapter 1.3. Co-Organization of Phthalocyanines and Fullerene in Liquid Crystalline Phases

1.3.1. Introduction

Liquid crystals (LCs) were discovered in 1888 by the austrian botanist Friedrich Reinitzer when he was studying the melting behaviour of cholesteryl benzoate.[148] He observed a "double melting" point of this material, which melted at 145.5 ºC into a cloudy fluid, and upon further heating to 178.5 ºC, became clear. Later on, and based on these initial observations, Lehmann concluded that a new state of matter had been discovered that was intermediate in ordering between the crystalline solid and isotropic liquid phases. Accordingly, this intermediate phase became known as the *liquid crystal phase* or *mesophase*. Supramolecular interactions such as van der Waals forces, charge transfer interactions, dipolar or quadrupolar interactions and hydrogen bonds are driving forces to organize molecules into liquid crystalline systems.

Liquid crystals combine the properties of solid-crystals and liquids, that is, whereas they flow like liquids, additionally have the ordering properties of solids. When a solid melts into a liquid, orientational and positional order are lost completely; the molecules move randomly. When a solid melts into a liquid crystal, however, the positional order may be lost, but some of the orientational order remains. Compounds, which form liquid crystalline phases, are referred to as *mesogens* and called to exhibit *mesomorphism*.[149]

Although, there are many types of liquid crystal states (mesomorphic states), they can be classified into two main categories based on their self-organization in the material. *Thermotropic liquid crystals* show one or more phase transitions by the influence of temperature. *Lyotropic liquid crystals* are formed in a solvent and show phase transitions depending on the concentration (and the temperature as well).[150]

---

148 F. Reinitzer, *Monatsh. Chem*. **1888**, *9*, 421.

149 a) M. J. Stephen, J. P Straley, *Rev. Mod. Phys.* **1974**, *46*, 617. b) O. Z. Lehmann, *Phys. Chem.* **1889**, *4*, 462. c) B. Wunderlich, J. Grebowich, *Adv. Polym. Sci.* **1984**, *2*, 60. d) J. L. Serrano, Ed. *Metallomesogens, Synthesis, Properties, and Applications*, VCH, Weinheim, **1996**. e) Handbook of Liquid Crystals, Ed. D. Demus, J. W. Goodbye, G. W. Gray, H. W. Spiess, V. Vill, Wiley-VCH, Weinheim, vols. 1-3, **1998**. f) P. J. Collings, *Liquid Crystals: Nature's Delicate Phase of Matter*, 2nd ed. Princeton University, **2002**.

150 a) H. Ringsdorf, B. Schlarb, J. Venzmer, *Angew. Chem. Int. Ed. Engl*. **1988**, 27, 113. b) P. Espinet, M. A. Esteruelas, L. A. Ore, J. L. Serrano, E. Sola, *Coord. Chem. Rev.* **1992**, *2*, 15. c) P. J. Collings, M. Hird, *Introduction to Liquid crystals*, *Chemistry and Physics, Taylor & Francis Ltd*, *London,* **1997.**

Discotic Liquid Crystals

In the field of thermotropic liquid crystals, a significant number of *discotic mesogenic* compounds have been prepared and identified by many research groups, since the first discotic liquid crystal (DLC) discovered by Chandrasekhar in 1977.[151] In general, DLCs consist of molecules containing a central aromatic core, which stack on top of each other in a columnar fashion. The aromatic core is surrounded by different numbers of flexible chains, which are crucial for the formation of discotic liquid crystals. In their absence, the mesophase is generally not formed. The most important aromatic cores of DLCs, such as triphenylene,[152] perylenediimide,[153] hexa-*peri*-hexabenzocoronene,[154] phthalocyanine[155] or porphyrin,[156] are shown in Figure 87.

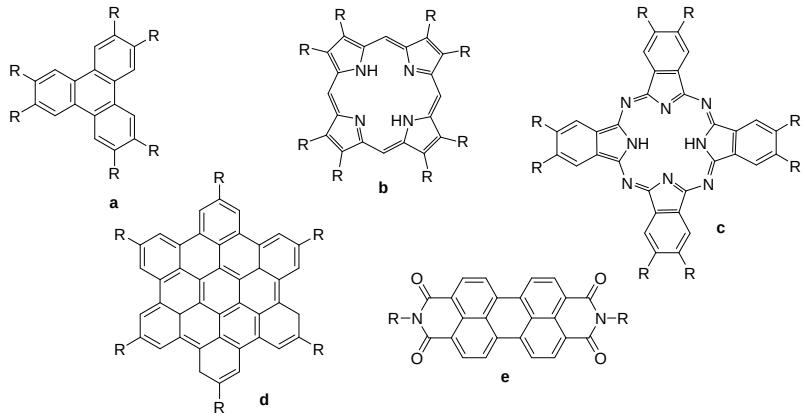

Figure 87. Examples of discotic mesogens, a) triphenylenes, b) porphyrins c) phthalocyanines, d) hexabenzocoronenes, e) perylenediimide; R= flexible substituents.

151 a) S. Chandrasekhar, B. K. Sadashiva, K. A. Uresh, *Pramana*. **1977**, *9,* 471. b) S. Kumar, *Liquid crystals*, Cambridge University Press, Cambridge, **2001**. c) A. Ciferri, *Liq. Cryst.* **2004**, *31*, 1487. d) E. M. García-Frutos, A. Omenat, J. Barberá, J. L. Serrano, B. Gómez-Lor, *J. Mater. Chem.* **2011**, *21*, 6831.

152 a) D. Markovitsi, I. Lecuyer, P. Lianos, J. Malthete, *J. Chem. Soc. Faraday Trans*. **1991**, *87*, 1785. b) R. J. Bushby, K. J. Donavan, T. Kreouzis, O. R. Lozman, *Opto. Electron. Rev*. **2005**, *13*, 269.

153 a) B. A. Gregg, R. A. Cormier, *J. Phys. Chem. B*. **1998**, *102*, 9952. b) A. Wicklein, A. Lang, M. Much, M. Thelakkat, *J. Am. Chem. Soc*. **2009**, *131*, 14442. c) X. Kong, Z. He, Y. Zhang, L. Mu, C. Liang, B. Chen, A. N. Cammidge. *Org. Lett.* **2011**, *13*, 764.

154 a) S. P. Brown, I. Schnell, J. D. Brand, K. Müllen, H. W. Spiess, *J. Am. Chem. Soc.* **1999**, *121*, 6712. b) C. D. Simpson, J. S. Wu, M. D. Watson, K. Müllen, *J. Mater. Chem.* **2004**, *14*, 494. c) A. C. Grimsdale, J. Wu, K. Müllen, *Chem. Commun.* **2005**, 2197.

155 a) D. Masurel, C. Sirlin, J. Simon, *New J. Chem*. **1987**, *11*, 455. b) M. J. Cook*, J. Mater. Chem.* **1996**, *6*, 677. c) K. Msayib, S. Makhseed, N. B. McKeown, *J. Mater. Chem*. **2001**, *11*, 2784.

156 a) B. R. Patel, K. S. Suslick, *J. Am. Chem. Soc.* **1998**, *120*, 11802. b) A. Segade, M. Castella, F. Lopez-Calahorra, D. Velasco, *Chem. Mater.* **2005**, *17*, 5366.

Thermotropic discotic liquid crystals organize into various mesophases, such as columnar hexagonal (Coh), columnar rectangular (CoIr), columnar oblique, columnar plastic, and columnar helical, depending on the arrangement of molecules within the columns and the two-dimensional lattice symmetry of the column packing (Figure 88). Columnar hexagonal phase is characterized by the hexagonal packing of the molecular columns and the columns possess two-dimensional long-range positional order. The columnar rectangular mesophase consist of stacking of the aromatic cores of the molecules in columns surrounded by the disordered aliphatic chains and packed in a rectangular way.[151]

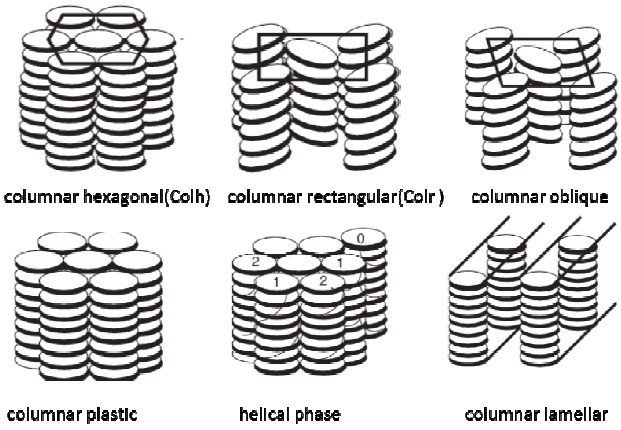

Figure 88. Schematic drawing of columnar phases.

Liquid-Crystalline Phthalocyanines

Phthalocyanine derivatives are among the most widely investigated DLCs due to the combined properties of wide temperature range of the mesophase, high thermal stability and quasi-1D charge carrier mobility, which make them promising candidates for electronic devices. They consist of a planar, rigid aromatic core, which is substituted by flexible substituents in the periphery, ensuring solubility and phase formation. The partial orbital overlap of adjacent molecules leads to the formation of charge carrier pathways.

The first Pc mesogen was reported by Piechocki et al. in 1982, and it involved the substitution of copper(II) phthalocyanine with eight peripheral alkoxymethyl groups.[157] Since then, many different Pc mesogens, octa- or tetra-substituted derivatives, have been described with the aim to explore the influence of parameters such as the number and length of the side chains. Most common substituents are alkyl, alkoxy and alkoxymethyl groups.[158]

The transition from the solid state to the liquid crystalline phase (melting point) corresponds to the melting of the flexible side chains. At that point, the aromatic cores keep their positional and orientational order. The transition from the mesophase to the isotropic liquid (clearing point) corresponds to the breakdown of the columns.

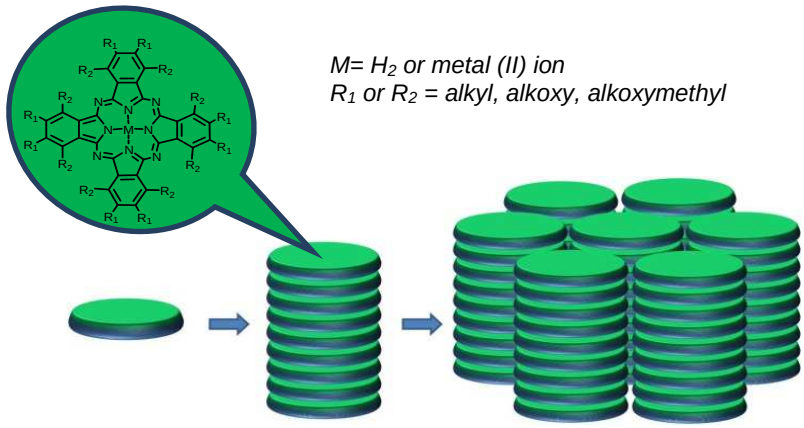

Figure 89. Peripheral and nonperipheral substitution leading to liquid crystalline phthalocyanines.

Phthalocyanines show columnar mesophases within a temperature range over 39-190℃. [158] The liquid crystalline properties of Pcs are strongly related to their

[157] C. Piechocki, J. Simon, A. Skoulios, D. Guillon, P. Weber, *J. Am. Soc.* **1982**, *104*, 5245.

[158] a) J. J. Andre, M. Bernard, C. Piechocki, J. Simon, *J. Phys. Chem.* **1986**, *90*, 1327. b) P. Weber, D. Guillon, A. Skoulios, *J. Phys. Chem.* **1987**, *91*, 2242. c) K. Ohta, L. Jacquemin, C. Sirlin, J. Simon, *New J. Chem.* **1988**, *12*, 751. d) J. Vacus, P. Doppelt, J. Simon, G. Memetzidis, *J. Mater. Chem.* **1992**, *2*, 1065. e) K. M. Engel, P. Bassoul, L. Bosio, H. Lehmann, M. Hanack, J. Simon, *Liq. Cryst.* **1993**, *15*, 709. f) T. Komatsu, K. Ohta, T. Fujimoto, I. Yamamoto, *J. Mater. Chem.* **1994**, *4*, 533. g) M. J. Cook, *Adv. Mater*, **1995**, *7*, 877. h) J. A. Duro, G. de la Torre, J. Barberá, J. L. Serrano, T. Torres, *Chem. Mater*. **1996**, *8*, 1061. i) J. C. Swarts, E. H. G. Langner, N. Krokeide-Hove, M. J. Cook, *J. Mater. Chem*. **2001**, *11*, 434. j) M. J. Cook, *Chem. Rec.* **2002**, *2*, 225. k) A. N. Cammidge, H. Gopee, *Chem. Commun.* **2002**, 966. l) M. Ichihara, A. Suzuki, K. Hatsusaka, K. Ohta, *Liq. Crys*. **2007**, *34*, 5.

chemical structure. By changing, the central atom or the number, length and position of the aliphatic substituents as well as introducing bulky or branched alkyl chains substituents, a wide range of mesomorphic properties can be obtained. Generally, the introduction of long alkyl chains or bulky branched substituent provide a decrease in the melting and clearing point due to a reduction the stacking between the flat aromatic cores of discotic molecules.[158,159] Recently, Sergeyev and co-workers reported a metal-free Pc bearing eight electron-acceptor bulky branched alkylsulfonyl chains which forms a columnar rectangular LC mesophase above 89 ºC.[109a]

An interesting and unique example of unsymmetrically substituted LC Pc was studied in our group. The ethynyl-substituted Ni(II)Pc depicted in Figure 90 formed hexagonal columnar mesophases, wherein each disk was composed by two Pc units, due to additional non-covalent interactions between the ethynyl moieties.[160]

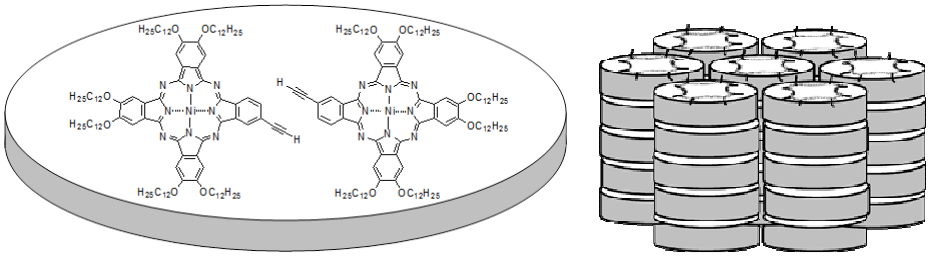

Figure 90. Proposed model for the stacking of ethynyl-substituted hexadodecyloxyNi(II)Pc in a Colh mesophase.

[109] a) B. Tylleman, G. Gbabode, C. Amato, C. Buess-Herman, V. Lemaur, J. Cornil, R. Gomez Aspe, Y.H. Geerts, S. Sergeyev, *Chem. Mater*. **2009**, *21*, 2789.

[159] a) D. M. Collard, C. P. Lillya, *J. Am. Chem. Soc*, **1991**, *113*, 8577. b) J. Sleven, T. Cardinaels, K. Binnemans, D. Nelis, J. Mullens, D. Hinx-Hubner, G. Meyer, *Liq. Cryst.* **2003**, *30*, 143. c) M. Ichihara, A. Suzuki, K. Hatsusaka, K. Ohta, *Liq. Cryst.* **2007**, *34*, 555. d) J. Sleven, C. Görller-Walrand, K. Binnemans, *Mater. Sci. Eng. C*, **2001**, *18*, 229.

[160] E. M. García-Frutos, G. Bottari, P. Vázquez, J. Barberá, T. Torres, *Chem. Commun.* **2006**, 3107.

Liquid Crystals for Photovoltaic Applications

Liquid crystals, particularly discotic liquid crystals, are promising candidates in the field of functional materials, especially in photovoltaic solar cells,[161] light emitting diodes[162] and field effect transistors[163] because of their advantages over amorphous and crystalline materials. DLCs have proved to have relatively high charge carrier mobilities due to their high degree of order, which is the most important parameter in determining the performance of organic semiconductors. The practical applications of single crystals, on the other hand, even though they have high charge carrier mobilities, are limited by high-cost production and difficulty to produce under laboratory conditions.

In discotic mesophases, the molecules form efficient columnar stacks that produce high-charge carrier mobility, due to intense π-π interactions between the polyaromatic cores. The core-core distance in a columnar mesophase is about 3.5 Å, as there is a significant overlap of π-orbitals. The intercolumnar distance is usually in the order of 20-40 Å, depending on the size of the mesogens. The long flexible aliphatic chains surrounding the cores insulate the column from the neighbour one. The interaction between adjacent molecules within the same column is, thus, much stronger than the interaction between neighbouring columns. The charge migration is, therefore, expected to be significantly higher along the column axis than in perpendicular direction (Figure 91).[164] Consequently, DLC columns can provide one-dimensional charge transport, and thus, can be described as molecular wires.

---

[161] a) K. Petritsch, R. H. Friend, A. Lux, G. Rozenberg, S. C. Moratti, A. B. Holmes, *Synthetic Metals*, **1999**, *102*, 1776. b) O. Sun, L. Dai, X. Zhou, L. Li, O. Li, *Appl. Phys. Lett*. **2007**, *91*, 253505. c) L. Li, S. W. Kang, J. Hardena, Q. Sun, X. Zhou, L. Dai, A. Jakli, S. Kumarb, Q. Li. *Liq. Cryst.* **2008**, *35*, 233. d) W. W. H. Wong, C. Q. Ma, W. Pisula, C. Yan, X. Feng, D. J. Jones, K. Müllen, R. A. J. Janssen, P. Bäuerle, A. B. Holmes, *Chem. Mater.* **2010**, *22*, 457.

[162] a) S. Benning, H. S. Kitzerow, H. Bock, M. F. Achard, *Liq. Cryst*. **2000**, *27*, 901. b) I. Seguy, P. Destruel, H. Bock, *Synth. Met.* **2000**, *111*, 15.

[163] a) A. M. van de Craats, N. Stutzmann, O. Bunk, M. M. Nielsen, M. Watson, K. Müllen, H. D. Chanzy, H. Sirringhaus, R. Friend, *Adv. Mater.* **2003**, *15*, 495. b) W. Pisula, A. Menon, M. Stepputat, I. Lieberwirth, U. Kolb, A. Tracz, H. Sirringhaus, T. Pakula, K. Müllen, *Adv. Mater.* **2005**, *17*, 684. c) W. W. H. Wong, T. B. Sing, D. Vak, W. Pisula, C. Yan, X. Feng, E. L. Williams, K. L. Chan, Q. Mao, D. J. Jones, C. Q. Ma, K. Müllen, P. Bäuerle, A. L. Holmes, *Adv. Funct. Mater*, **2010**, *20*, 927.

[164] a) S. Kumar, *Liq. Cryst.* **2004**, *31*, 1037. b) S. Kumar, *Chem Soc. Rev.* **2006**, *35*, 83. c) X. Feng, W. Pisula, K. Müllen, *Pure. Appl. Chem*. **2009**, *81*, 2203. d) A. E. Murschell, T. C. Sutherland, *Langmuir*, **2010**, *26*, 12856. e) B. R. Kaafarani, *Chem. Mater.* **2011**, *23*, 378.

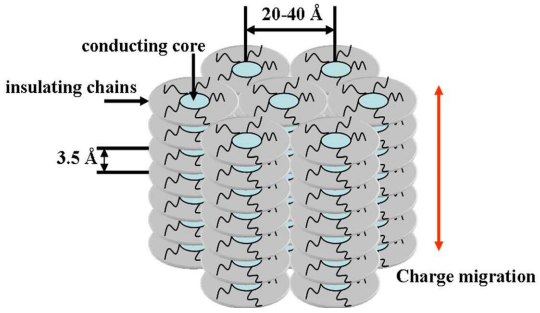

Figure 91. Schematic view of charge migration in columnar phases.

From the device performance point of view, the alignment of columnar liquid crystalline phases plays a critical role. If the columns are aligned parallel to each other and perpendicular to the electrodes, the so-called face on or homeotropic alignment (Figure 92A), the charge carriers would travel the shortest distance through the materials to the electrodes, thus, providing the best possible performance for OPV or OLED applications.[164e,165] On the other hand, the planar alignment (Figure 92B), that is achieved when the column axes are parallel to the plane of the substrate, is ideal for OFEDs applications.[164e,165]

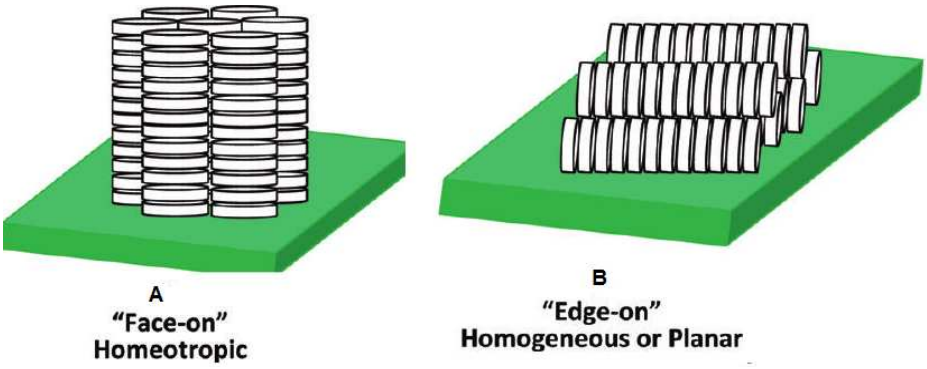

Figure 92. Different possibilities for aligning discotic liquid crystals at a surface.

[165] a) W. Pisula, Z. Tomovic, B. El Hamaoui, M. D. Watson, T. Pakula, K. Müllen, *Adv. Funct. Mater.* **2005**, *15*, 893. b) R. I. Gearba, D. V. Anokhin, A. I. Bondar, W. Bras, M. Jahr, M. Lehmann, D. A. Ivanov, *Adv. Mater*. **2007**, *19*, 815. c) G. Schweicher, G. Gbabode, F. Quist, O. Debever, N. Dumont, S. Sergeyev, Y. H. Geerts, *Chem. Mater.* **2009**, *21*, 5867. d) M. O'Neil, S. M. Kelly, *Adv. Mater.* **2011**, *23*, 566.

As a result, discotic liquid crystals are recognized as a new class of organic semiconductors characterized by high charge carrier mobility.[166]. In particular, hexa-peri-hexabenzocoronenes have established record charge carrier mobilites of 1 $cm^2 V^{-1}s^{-1}$.[167] Relatively high values, over 0.7 $cm^2V^{-1}s^{-1}$, have also been obtained for phthalocyanines,[166a,168] and for triphenylenes (0.1 $cm^2V^{-1}s^{-1}$).[169] This revealed a dependence of the intrinsic charge carrier mobility on the size of the aromatic core in the hexagonal liquid crystalline. These mobility values are already in the range of amorphous silicon.

In this respect, several mesogens including phthalocyanines have found application in photovoltaic devices as the active component. More specifically, focusing on bulk heterojunction organic solar cells, the control of the nanostructure of the active layer is a key point for the development of efficient devices.[43] One of the most popular concept in the design of organic photovoltaic devices is the active layer being formed by blends of donor and acceptor materials, with the drawback of this design, however, being the phase separation within the active layer, which limits the total conversion efficiency. Morphological disorder within the photoactive layer always causes structural defects that can act as trapping and/or recombination centers for charge carriers, resulting in low performance of the devices. The use of a liquid crystalline component

[43] a) C. J. Brabec, A. Cravino, D. Meissner, N. S. Sariciftci, T. Fromherz, M. T. Rispens, L. Sanchez, J. C. Hummelen, *Adv. Funct. Mater*. **2001**, *11*, 374. b) B. C. Thompson, J. M. Fréchet, *Angew. Chem. Int. Ed.* **2008**, *47*,58. c) T. M. Clarke, J. R. Durrant, *Chem. Rev.* **2010**, *110*, 6736. d) C. W. Schlenker, M. E. Thompson, *Chem. Commun*. **2011**, *47*, 3702. e) A. Mishra, P. Bäuerle, *Angew. Chem. Int. Ed*. **2012**, *51*, 2020.

[166] a) A. M. van de Craats, M. P. de Haas, J. M. Warman, *Synth. Met.* **1997**, 2125. b) J. M. Warman, M. P. deHaas, G. Dicker, F. C. Grozema, J. Piris, M. G. Debije, *Chem. Mater.* **2004,** *16,* 4600. c) T. Kato, N. Mizoshita, K. Kihimimoto, *Angew. Chem. Int. Ed*. **2006**, *45*, 38. d) W. Pisula, M. Zorn, J. Y. Chang, K. Müllen, R. Zentel, *Macromol. Rapid Commun.* **2009**, *30*, 1179.

[167] a) A. M. van de Craats, J. M. Warman, K. Müllen, Y. Geerts, J. Brand, *Adv. Mater.* **1998**, *10*, 36. b) M. G. Debije, J. Piris, M. P. De Haas, J. M. Warman, Z. Tomovic, C. D. Simpson, M. D. Watson, K. Müllen, *J. Am. Chem. Soc.* **2004**, *126*, 4641. c) F. J. M. Hoeben, P. Jonkheijm, E. W. Meijer, A. P. H. J. Schenning, *Chem. Rev*. **2005**, *105*, 1491.

[168] a) K. Ban, K. Nishizawa, K. Ohta, A. M. van de Craats, J. M. Warman, I. Yamamoto, H. Shirai, *J. Mater. Chem.* **2001**, *11*, 321. b) J. M. Warman, J. E. Kroeze, P. G. Schouten, A. M. van de Craats, *J. Porphyrins Phthalocyanines* **2003**, *7*, 342.

[169] a) D. Adam, P. Schuhmacher, J. Simmerer, L. Häussling, K. Siemensmeyer, K. H. Etzbach, H. Ringsdorf, D. Haarer, *Nature* **1994**, *371*, 141. b) A. M. van de Craats, L. D. A. Siebbeles, I. Bleyl, D. Haarer, Y. A. Berlin, A. A. Zharikov, J. M. Warman, *J. Phys. Chem. B.* **1998**, *102*, 9625 c) H. Iino, Y. Takayashiki, J. Hanna, R. J. Bushby, D. Haarer, *Appl. Phys. Lett.* **2005**, *87*, 192105.

exhibiting long-range order in the bulk and at the interfaces[170] is a promising approach to overcome this problem.

Mullen and co-workers reported in 2001 organic photovoltaic devices incorporating discotic liquid crystals, namely hexa-peri-hexabenzocoronene HBC-PhC_{12} as a hole conductor, and a perylene dye electron-accepting component (Figure 93). [171] A device with an external quantum efficiency of 34% and power efficiency up to 2% was achieved. In this device, self-organization of discotic LC donor materials encouraged high interfacial surface and perpendicularly ordered composition. The external quantum efficiency result from large artificial area within bilayer structure and high exciton diffusion ranges in the separated donor-acceptor regions. Also high charge carrier mobility 0.22 $cm^2V^{-1}s^{-1}$ was reported for intracolumnar charge carrier motion in HBC-PhC_{12}. An efficient photoinduced charge transfer between donor-acceptor and effective charge transport responses are necessary for obtaining high efficiencies.

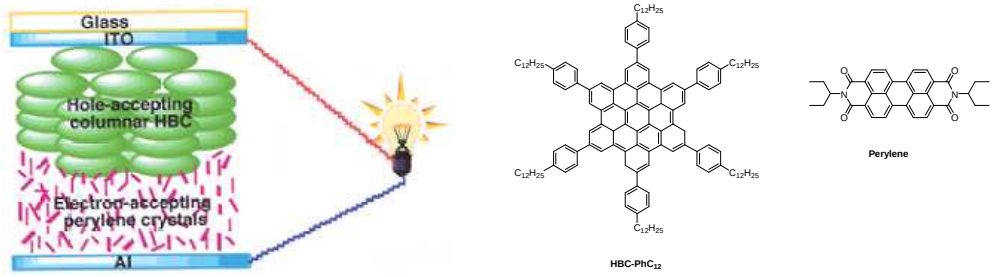

Figure 93. Molecular structures of HBC-PhC_{12} and perylene dye used in discotic LC- based solar cells, represented schematically in the left side of the figure.

Very recently, Heeger and coworkers reported a liquid crystalline porphyrin-fullerene dyad and its incorporation into BHJ solar cell.[172] The dyad self-organized into a supramolecular double-cable structure with the porphyrin forming a column via π–π

[170] a) M. D. Watson, A. Fechtenkötter, K. Müllen, *Chem. Rev.* **2001,** *101,* 1267. b) A. Pecchia, O. R. Lozman, B. Movaghar, N. Boden, R. J. Bushby, K. J. Donovan, T. Kreouzis, *Phys. Rev. B*. **2002**, *65*, 104204. c) J. Hanna, *Opto. Electron. Rew*. **2005**, *13*, 259. d) J. Wu, W. Pisula, K. Müllen, *Chem. Rev.* **2007**, *107*, 718. e) S. Sergeyev, W. Pisula, Y. H. Geerts, *Chem. Soc. Rev.* **2007**, *36*, 1902.

[171] L. Schmidt-Mende, A. Fechtenkötter, K. Müllen, E. Moons, R. H. Friend, J. D. MacKenzie, *Science*, **2001**, *293*, 1119.

[172] C. L. Wang, W. B. Zhang, R. M. Van Horn, Y. F. Tu, X. Gong, S. Z. D. Cheng, Y. M. Sun, M. H. Tong, J. Seo, B. B. Y. Hsu, A. J. Heeger, *Adv. Mater.* **2011**, *23*, 2951.

interactions and the C_{60} moieties interacting intercolumnarly to form continuous C_{60} channels. The BHJ solar cell was fabricated using the porphyrin-fullerene dyad as a acceptor and SiPCPDTBT as a donor (Figure 94). The cells gave higher Jsc and larger Voc but modest efficiency of 3.35 %, as compared with that of PCBM. The larger photocurrent suggested that a controlled ambipolar transporting property within the electron acceptor domain could lead to improved photovoltaic performance.

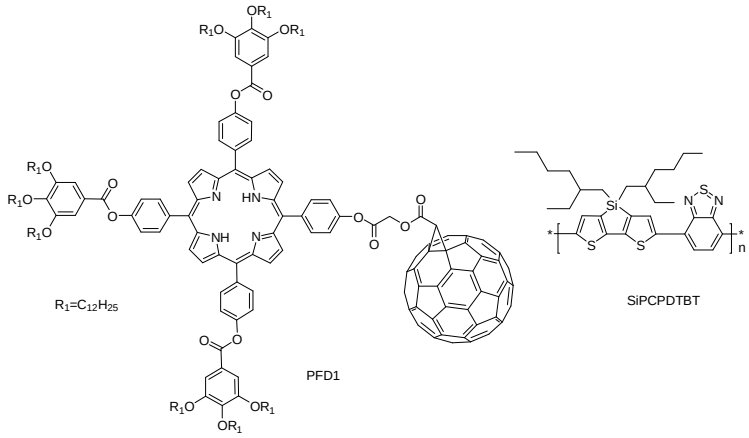

Figure 94. Molecular structures of acceptor PFD1 and donor SiPCPDTBT components employed in BHJ.

Liquid Crystalline Phthalocyanine-Fullerene Dyads

The molecular heterojunction formed by covalently linked donor-acceptors is one of the possible ways to control the morphology within the photoactive layer to prevent the occurrence of phase separation, since the material is basically one molecule with two different pathways for opposite charges.[173] Therefore, combination of the molecular heterojunction donor-acceptor system with the self-organizing properties of liquid crystals could prove to be useful in solar cell technology.

[173] a) A. Caravino, N. S. Sariciftci, *J. Mater. Chem.* **2002**, *12*, 1931. b) A. Caravino, N. S. Sariciftci, *Nature Mater*. **2003**, *2*, 360.

Few liquid-crystalline fullerene–donor dyads with potential photovoltaic applications have been described,[174] therefore the incorporation of fullerene into liquid crystalline columnar phases is a challenging task, since its bulky three-dimensional structure tends to disturb the arrangement of molecules in columnar structures. Fullerene-containing liquid crystals based on the functionalization of the C_{60} core with different mesogenic subunits have been intensively investigated by Deschenaux and coworkers.[174] More interestingly, supramolecular interactions between mesogenic compounds such as porphyrins or cyclotriveratrylenes and C_{60} have been exploited for the preparation of liquid crystalline supramolecular complexes[175] in which the attractive physicochemical properties of C_{60} are fully preserved. The organization at supramolecular level of Pc-C_{60} multicomponent systems have been recently reviewed by our group.[17]

By using an indirect strategy, the first example of a mesogenic Pc-C_{60} blend was reported by our group in 2002.[176] This strategy consists of blending an equimolar mixture (1:1) of non-mesogenic Pc–C_{60} dyad with a symmetric mesogenic octakis(hexadecylthio)-Zn(II)Pc (Figure 95). Differential scanning calorimetry (DSC) / and X-ray results revealed that the Pc-C_{60} dyad had been successfully incorporated into the mesophase structure of the symmetric Pc. The blends show the formation of hexagonal columnar mesophases with lower transition temperatures (60-70 ºC) than pure mesogenic Pc compound (89 ºC).

---

17 a) G. Bottari, G. de la Torre, D. M. Guldi, T. Torres, *Chem. Rev.* **2010**, *110*, 6768. b) G. de la Torre, G. Bottari, U. Hahn, T. Torres, *Struct. Bonding*, **2010**, *135*, 1. c) G. Bottari, J. A. Suanzes, O. Trukhina, T. Torres, *J. Phys. Chem Lett*. **2011**, *2*, 905.

174 a) T. Chuard, R. Deschenaux, *Helv. Chim. Acta*, **1996**, *79*, 736. b) M. Even, B. Heinrich, D. Guillon, D. M. Guldi, M. Prato, R. Deschenaux, *Chem. Eur. J*. **2001**, *7*, 2595. c) S. Campidelli, R. Deschenaux, J. F. Eckert, D. Guillon, J. F. Nierengarten, *Chem. Commun*. **2002**, 656. d) S. Campidelli, T. Brandmuller, A. Hirsch, I. M. Saez, J. W. Goodby, R. Deschenaux, *Chem. Commun.* **2006**, 4282. e) R. Deschenaux, B. Donnio, D. Guillon, *New J. Chem*., **2007**, *31*, 1064. f) N. Maringa, J. Lenoble, B. Donnio, D. Gullion, R. Deschenaux, *J. Mater. Chem.* **2008**, *18*, 1524.

175 a) D. Felder, F. Heinrich, D. Guillon, J. F. Nicoud, J. F. Nierengarten, *Chem. Eur. J.* **2000**, 6*,* 3501. b) M. Kimura, Y. Saito, K. Ohta, K. Hanabusa, H. Shirai, N. Kobayashi, *J. Am. Chem. Soc.* **2002***, 124,* 5274.

176 A. de la Escosura, M. V. Martínez-Díaz, J. Barbera, T. Torres, *J. Org. Chem.* **2008**, *73*, 1475.

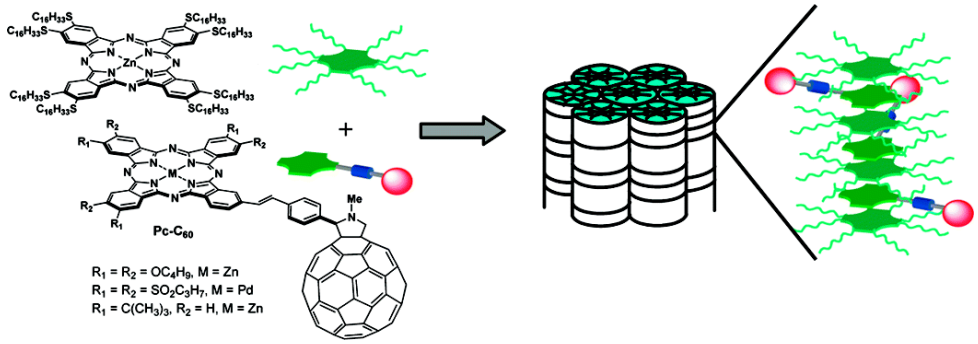

Figure 95. Schematic representation of the probable structure of the mesophases formed by the Pc/Pc-C_{60} blends.

On the other hand, during the development of this PhD, the first example of a intrinsically LC phthalocyanine–C_{60} dyad was reported.[177] Pc-C_{60} dyads with different flexible spacer lengths (n = 3-6) between the Pc and C_{60} were prepared (Figure 96). POM and DSC studies showed that Pc-C_{60} dyads, which had relatively short linker, that is, three and four methylene units, were not mesogens at room temperature. However, the dyads with aliphatic linkers comprising 5 and 6 methylene units display mesogenic properties at room temperature with transitions to isotropic liquid at 120 and 90 ºC, respectively. These results suggested that the length of the spacer between Pc and C_{60} significantly affects the thermotropic properties of Pc-C_{60} dyad.

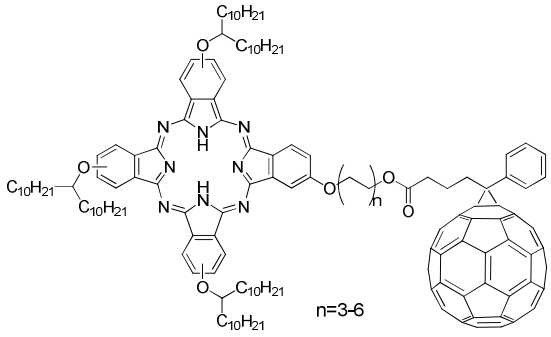

Figure 96. Chemical structure of the first intrinsically mesogenic Pc-C_{60} dyad reported by Geerts et. al.

[177] Y. H. Geerts, O. Debever, C. Amato, S. Sergeyev, *Beilstein J. Org. Chem*. **2009**, *5*, 49.

A more recent example of liquid crystalline Pc-C_{60} dyad consisting of a hexadodecyloxyphenyl-substituted Zn(II)Pc covalently linked through a phenoxy spacer to fullerene (Figure 97) was reported by Hayashi et al.[178] The XRD pattern of Pc-C_{60} dyad at 160 ºC exhibits formation of rectangular columnar phase with an ordered organization of the C_{60} unit along the ZnPc 1D column, leading to D-A bicontinus structure in the LC. Additionally, the electron and hole mobility of the mesogenic Pc-C_{60} was determined by the time-of-flight (TOF) method, which shows ambipolar charge transfer character with 0.26 $cm^2V^{-1}s^{-1}$ hole mobility and 0.11 $cm^2V^{-1}s^{-1}$ electron mobility between ZnPc-C_{60} intercolumns. This values increase by 26 and 7 times, respectively, after the heating and cooling treatment. This result reveal that organization of ZnPc-C_{60} molecules into the LC phase allows to more regular intercolumn and intracolumnar arrangement, leading to improvement of the ambipolar charge transport properties.

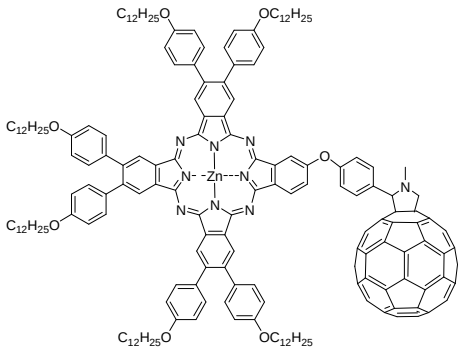

Figure 97. Molecular structure of mesogenic Pc-C_{60} dyad reported by Imahori et al. exhibiting an ambipolar charge transport.

[178] H. Hayashi, W. Nihashi, T. Umeyama, Y. Matano, S. Seki, Y. Shimizu, H. Imahori, *J. Am. Chem. Soc.* **2011**, *133*, 10736.

1.3.2. Objectives

Two concepts were followed to attempt the general goal of obtaining liquid crystals containing both phthalocyanines and C_{60}, namely, the covalent and the non-covalent (blend) approach to achieve efficient charge-transport properties in a liquid crystalline phase.

- In the covalent approach, Pc-C_{60} derivatives that could on their own form discotic mesophases, thus integrating donor (Pcs) and acceptor (C_{60}) in a controlled morphology were targeted. A hexadodecyl-substituted Pc core was selected as liquid crystalline subunit, which could induce mesogenic properties into the Pc-C_{60} dyads. Different Pc-C_{60} dyads were designed in order to get a deeper understanding of the structure-supramolecular organization relationship of covalent Pc-C_{60} systems. Compounds were classified within two series:

a) Pc–C_{60} dyads, containing either rigid or flexible spacers between the Pc and fullerene subunits, respectively (Figure 98).

b) Potentially mesogenic bisphthalocyanine-C_{60} and Pc-C_{60}-dendrimer molecules, which consist of two discotic units, either two hexadodecylPcs or one hexadodecylPc and a poly(benzyl ether) dendrimer, connected through a flexible chain chain to C_{60}.

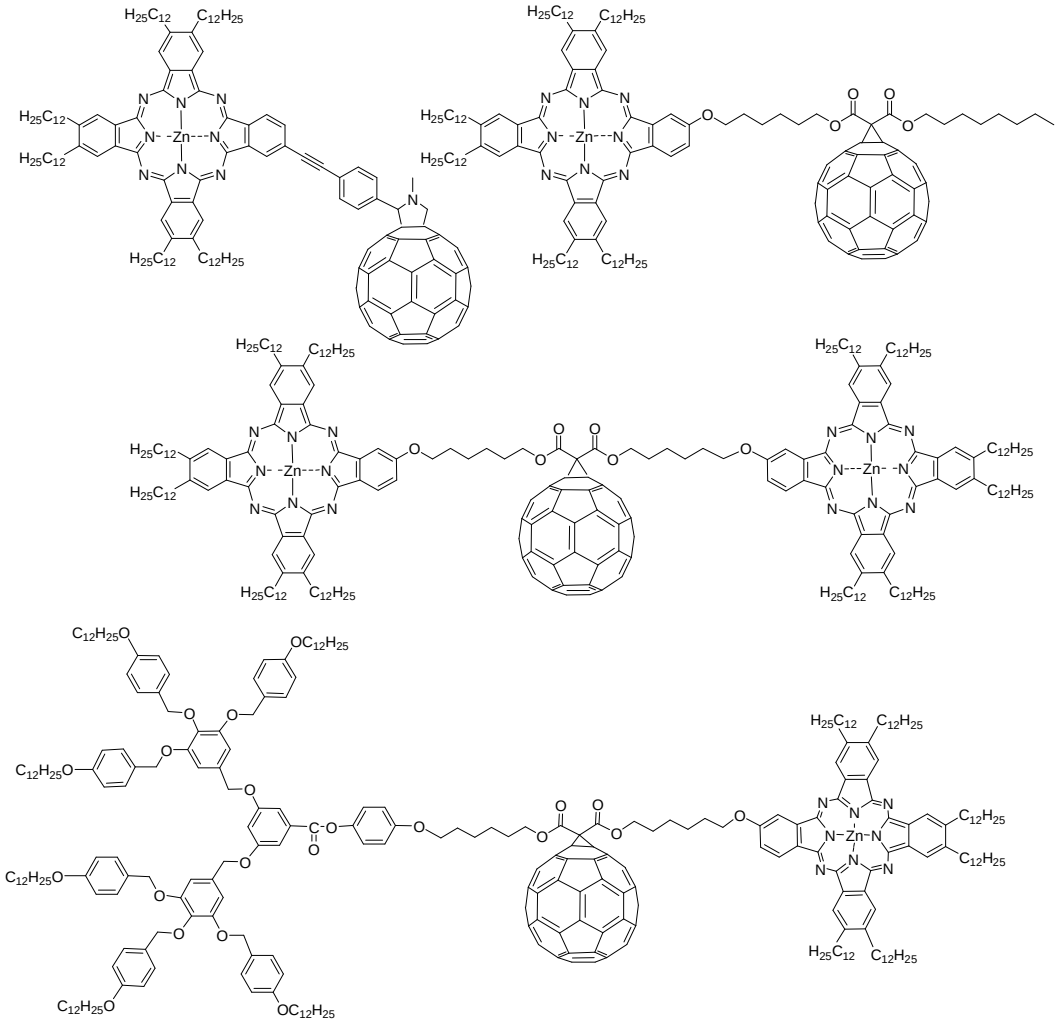

Figure 98. Structure of potentially mesogenic ZnPc compounds functionalized with C_{60}.

- In the <u>non-covalent (blend) approach</u>, mesogenic Pc/C_{60} derivatives blends could be formed by mixing liquid crystalline Pc derivatives**,** with non-mesogenic Pc-C_{60} dyads or even pristine C_{60} (Figure 99).

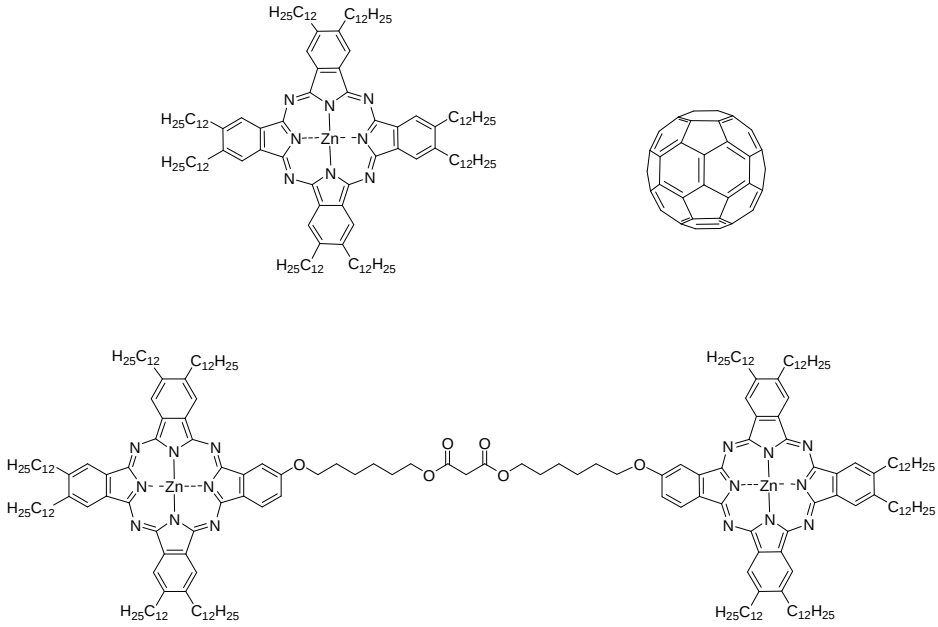

Figure 99. Molecular structure of mesogenic and potentially -mesogenic compounds selected to form mesogenic blends with C_{60}.

1.3.3. Results and Discussion

The synthesis of the targeted Pc–C_{60} dyads required the preparation of unsymmetrical substituted Pcs bearing long aliphatic chains, that is usually a difficult task due to the strong tendency of these macrocycles to form aggregates. However, the separation process of the final statistical mixture of Pcs obtained may be facilitated by using phthalonitriles bearing substituents with rather different polarity, such as hydrocarbon chains versus hydroxyl groups. For this reason, hydroxy-substituted phthalonitriles were chosen as precursors of our unsymmetrically substituted liquid crystalline Pcs.

1.3.3.1. Synthesis of Precursor Phthalonitriles

The synthetic route for the preparation phthalonitriles **30** and **31** is shown in Scheme 16.

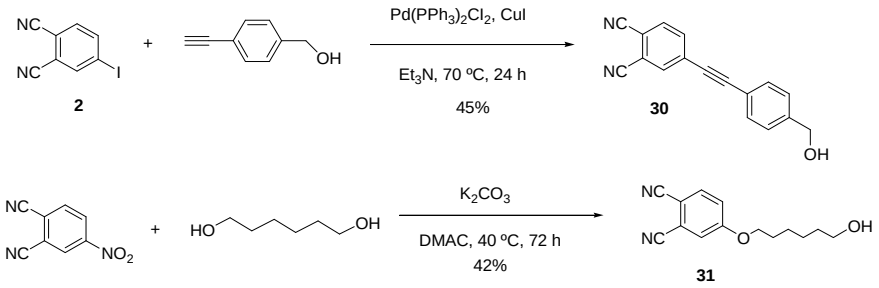

*Scheme 16. Synthesis of precursor phthalonitriles **30** and **31**.*

Phthalonitrile **30** was prepared by Sonogashira reaction of 4-(ethynyl)benzyl alcohol with 4-iodophthalonitrile (**2**) in the presence of $[Pd(PPh)_3Cl_2]$ and catalytic amounts of copper(I) iodide in 45% yield. 4-(6-Hydroxyhexyloxy)phthalonitrile (**31**) was synthesized according to a procedure previously described by our group.[179] The aromatic nucleophilic substitution of 4-nitrophthalonitrile with hexan-1,6-diol in the presence of K_2CO_3 in DMAC gave phthalonitrile **31** in 42% yield.

4,5-Diiodophthalonitrile (**34**)[180] and 4,5-didodecylphthalonitrile (**36**)[181] were prepared according to literature procedures, as shown in Scheme 17.

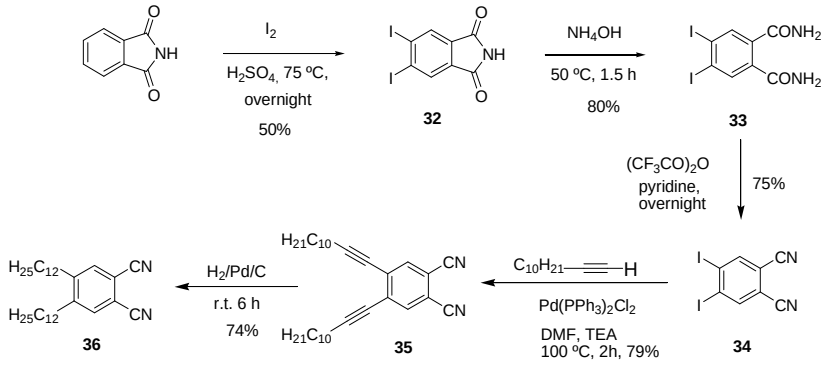

*Scheme 17. Synthesis of 4,5-diiodophthalonitrile (**34**) and 4,5-didodecylphthalonitrile (**36**).*

[179] J. J. Cid, *PhD thesis*, Universidad Autonoma de Madrid, Madrid, **2008**.
[180] D. S. Terekhov, K. J. M. Nolan, C. R. McArthur, C. C. Leznoff, *J. Org. Chem.* **1996**, *61*, 3034.
[181] W. M. Sharman, J. E. van Lier, *Bioconjugate Chem.* **2005,** *16*, 1166.

Phthalimide was directly iodinated with iodine in 30% fuming sulfuric acid at 75 ℃ to give 4,5-diiodophthalimide (**32**)**,** which was isolated in 50% yield. Treatment with concentrated ammonia, gave pure 4,5-diiodophthalamide (**33**), which was successfully converted to 4,5-diiodophthalonitrile (**34**) in 75% yield by using trifluoroacetic anhydride in pyridine. Coupling of an excess of the terminal alkyne, 1-dodecyne, with 4,5-diiodophthalonitrile (**34**) in triethylamine (TEA) at 110 ℃ using $[Pd(PPh_3)_2Cl_2]$ and CuI as catalysts gave the 4,5-didodecynylphthalonitrile (**35**) in 79% yield. The Pd/C catalyzed reduction of phthalonitrile **35** gave 4,5-didodecylphthalonitrile (**36**) in 74 % yield.

1.3.3.2. Synthesis of Phthalocyanine Precursors

The desired hydroxy-functionalized unsymmetrical substituted Pcs **38** and **39** were prepared, as outlined in Scheme 18 and 19, in 39 and 27% yields, respectively, by refluxing 5 equivalents of 4,5-didodecylphthalonitrile (**36**) and one equivalent of the appropriate hydroxy-functionalized phthalonitrile **30** or **31** DMAE in the presence of $Zn(OAc)_2$. The final reaction crudes consisted of mixtures of two main Pc products, namely, the desired unsymmetrically substituted (**38** or **39**) Pc and the symmetrically substituted Zn(II)octadodecylphthalocyanine (**37**). Purification by column chromatography on silica gel using a mixture of toluene/THF (10:1) allowed the adequate separation of these two Pc components.

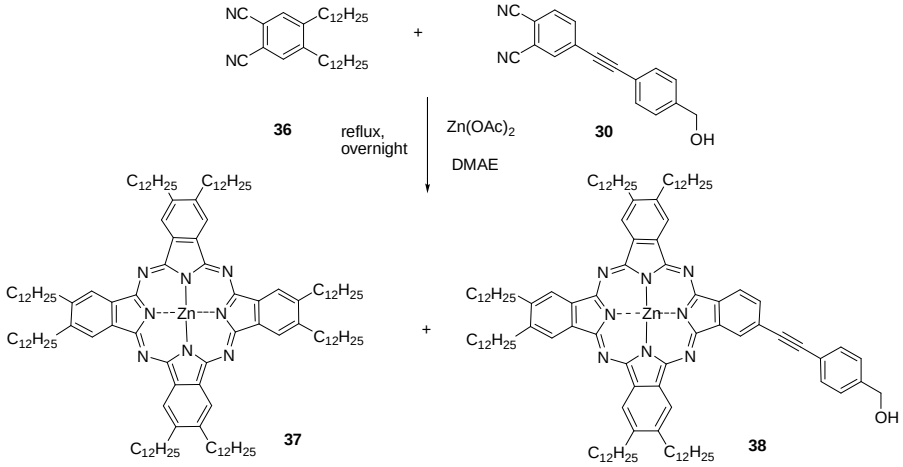

*Scheme 18. Synthesis of Pcs **37** and **38**.*

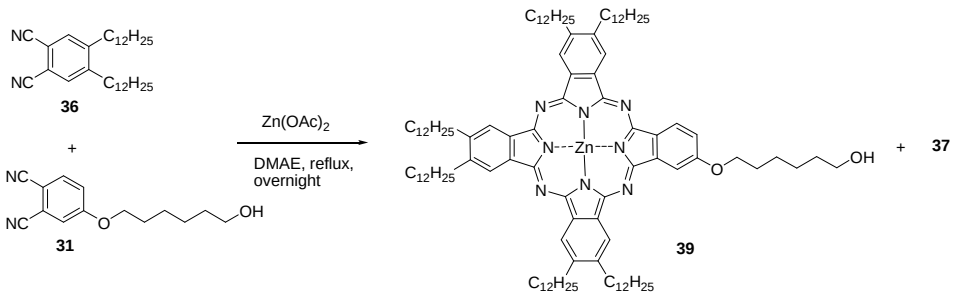

*Scheme 19. Synthesis of phthalocyanine **39.***

Pcs **37**, **38** and **39** were fully characterized by mass spectrometry, ^{1}H-NMR, UV-Vis and FT-IR spectroscopy. Unlike typical broadened resonances of phthalocyanines due to the tendency of their π-system to form aggregates, Pcs **37**, **38** and **39** yield very informative and well resolved ^{1}H-NMR spectra in d_8-THF, where signals between 7.5 and 9.6 ppm were easily assigned to each proton of the Pc macrocycle. Figure 100 shows the ^{1}H-NMR spectrum of compound **39** as an example.

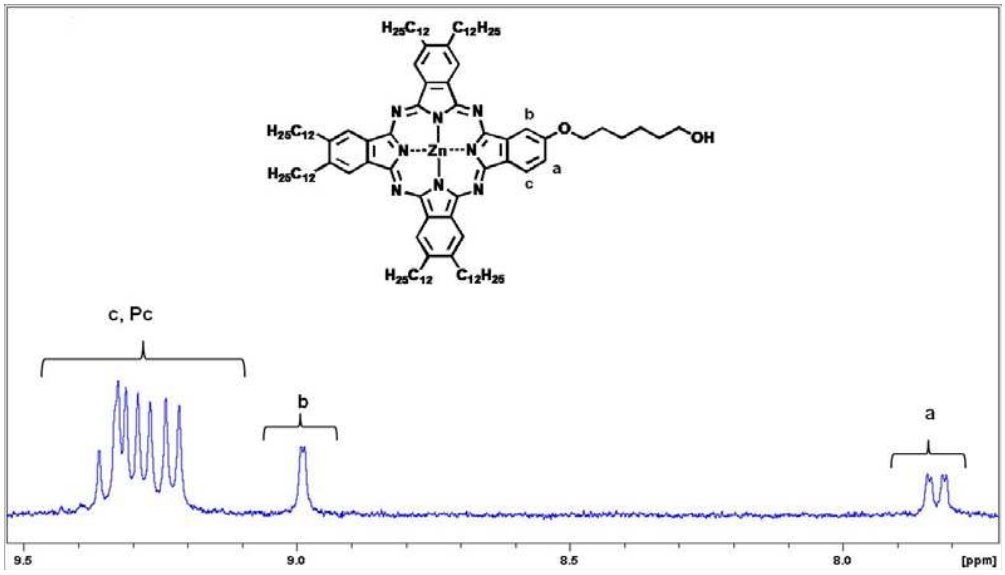

*Figure 100. Aromatic part of the ^{1}H-NMR spectrum of compound **39** in d_8-THF.*

1.3.3.3. Synthesis of Pc-C_{60} Dyads

Two routes were employed to prepare the potentially liquid crystalline Pc–C_{60} dyads **41, 44, 46** and **49.** The first one consisted on the derivatization of C_{60} by a 1,3-dipolar cyloaddition reaction (also known as Prato reaction) with a Pc aldehyde giving rise to fulleropyrrolidines. The second strategy pursuits the functionalization of C_{60} with Pc derivatives *via* Bingel reaction, leading to methanofullerenes.

The synthesis of Pc–C_{60} **41** bearing a rigid spacer between the photoactive Pc and C_{60} units is depicted in Scheme 20. First, the hydroxy-substituted Pc **38** was subjected to oxidation in the presence of IBX to yield formyl-derivative **40** in good yield. Subsequently, a 1,3-dipolar cycloaddition between Pc **40** and fullerene C_{60} in the presence of N-methylglycine was carried out, affording dyad **41** in a low, 15%, yield. Additional purification by gel permeation chromatography (Bio Beads SX-1) was necessary for all Pc-C_{60} dyads in order to eliminate traces of bis(adduct) by-products.

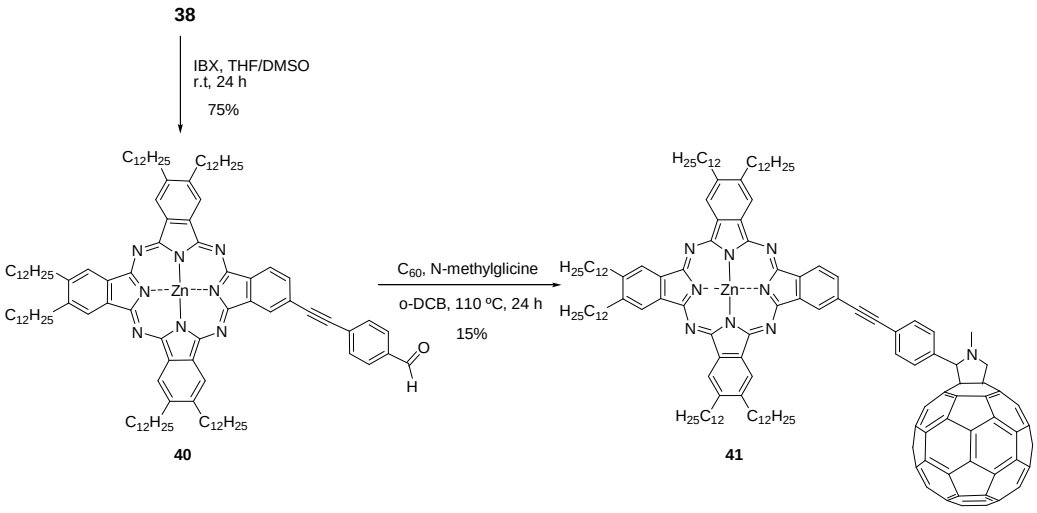

*Scheme 20. Synthesis of dyad Pc-C_{60} **41**.*

In the case of Pc–C_{60} **44** containing a flexible hexyloxy spacer, condensation reaction of Pc **39** with Meldrum acid gave the carboxy derivative **42** (Scheme 21). A esterification reaction of **42** with 1-octanol in the presence of DCC and DMAP formed

he malonate derivative **43**, which was used in the final addition reaction with C_{60} under Bingel–Hirch conditions to obtain **44** in 40% yield.

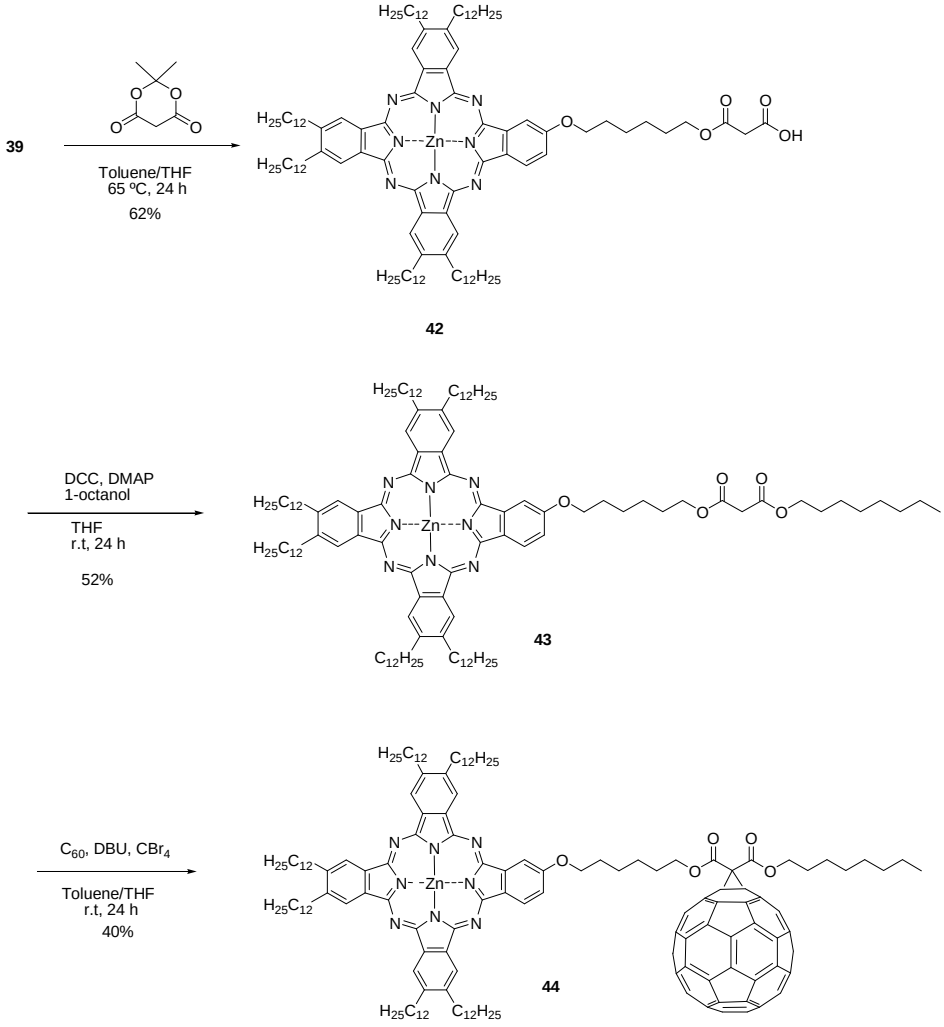

Scheme 21. Synthesis of dyad Pc-C_{60} ***44.***

Symmetrical bisPc-C_{60} dyad **46** was prepared following the route depicted in Scheme 22. First, condensation reaction between the unsymmetrical hydroxy-Pc **39** and malonyl chloride gave bisPc malonate compound **45** in 49% yield. Then, the compound **45** was added onto C_{60} using the Bingel conditions, leading to the methanofullero-bisphthalocyanine **46** in a low, 12% yield. The low yields obtained in the

final addition to C_{60} were rationalized as a consequence of the steric hindrance of the bulky Pc.

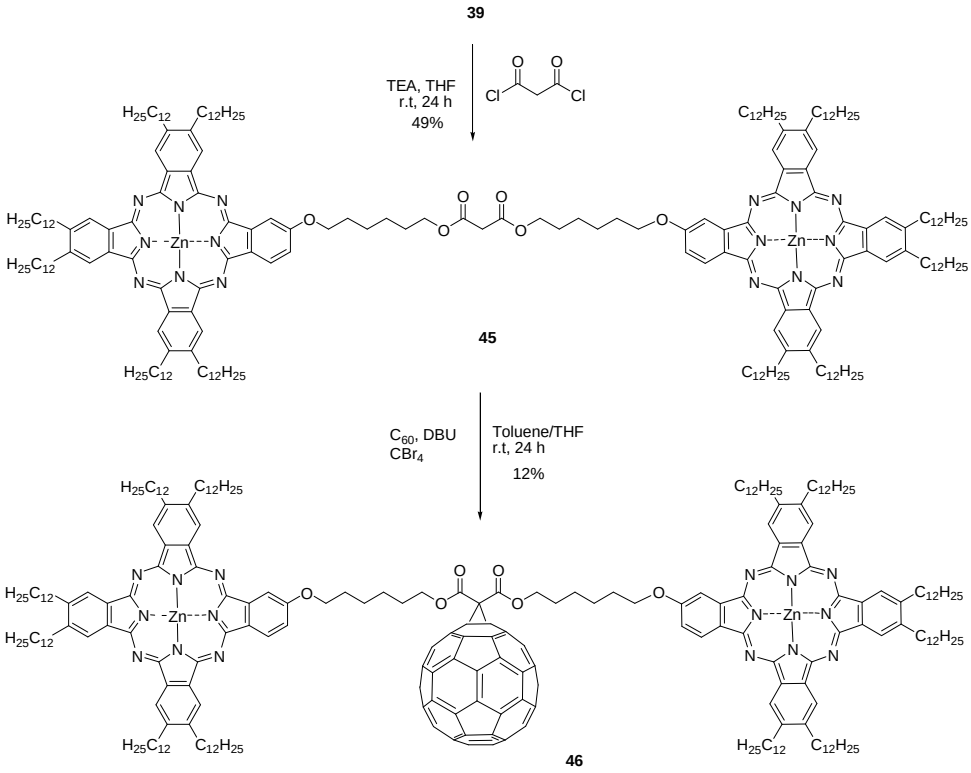

*Scheme 22. Synthesis of methanofullero-bisphthalocyanine **46.***

The stepwise synthesis of the unsymmetrical phthalocyanine-methanofullero-dendrimer **49** was based on the methodology previously developed by Deschenaux and coworkers (Scheme 23). Poly(benzyl ether)dendrimer precursor of derivative **47** was synthesized in the group of Prof. Deshenaux according to literature procedures.[174f] Its transformation into **47** by reaction with Meldrum acid was carried out by us due to the lack of stability of the carboxy–derivatized dendrimer.

[174] f) N. Maringa, J. Lenoble, B. Donnio, D. Gullion, R. Deschenaux, *J. Mater. Chem.* **2008**, *18*, 1524.

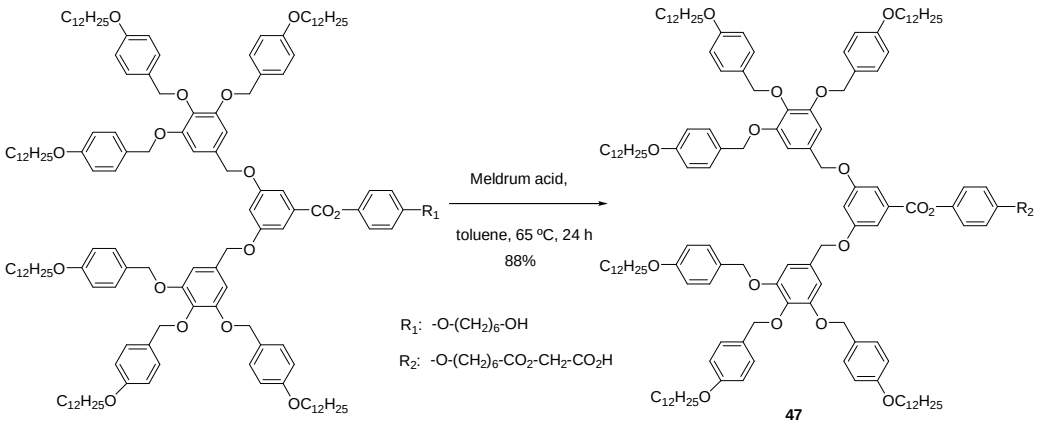

*Scheme 23. Synthesis of dendrimer **47**.*

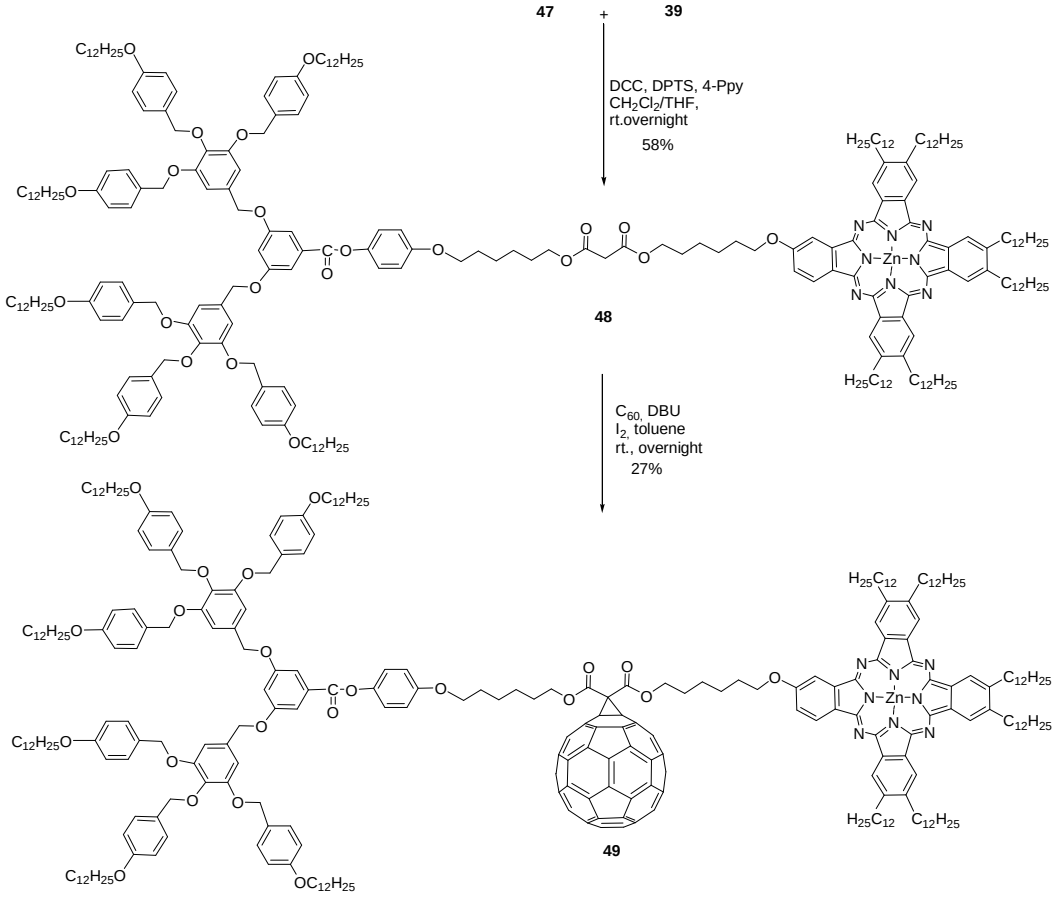

*Scheme 24. Synthesis of phthalocyanine-methanofullero-dendrimer **49**.*

Finally, esterification of the carboxylic acid **47** with hydroxyl-Pc **39** in the presence of *N,N*-dicyclohexylcarbodiimide (DCC), 4-(dimethylamino)pyridinium *p*-toluenesulfonate (DPTS) and 4-pyrrolidinopyridine (4-Ppy) led to unsymmetrical malonate **48**, which was then used in the Bingel reaction with C_{60} to furnish derivative **49** in 27% yield (Scheme 24).

All new compounds were characterized by ^{1}H-NMR, IR spectroscopy, UV-Vis and mass spectrometry. ^{1}H-NMR spectra in d_8-THF gave well resolved signals between 7.6 and 9.6 ppm for the Pc aromatic macrocycle. Additionally, characteristic resonances for the protons close to the different functional groups were assigned. Figure 101 shows the ^{1}H-NMR spectrum of Pc-C_{60} **44** as an example.

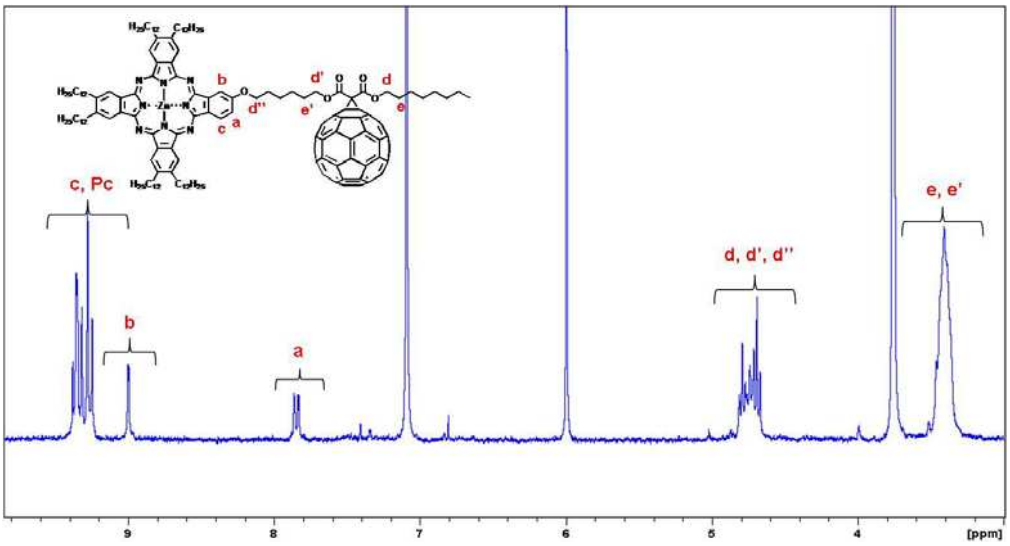

*Figure 101. ^{1}H-NMR spectrum of Pc-C_{60} **44** in d_8-THF.*

UV-Vis spectra of compounds **41** and **44** in THF are depicted in Figure 102. Pc–C_{60} dyad **41** gives a split Q band with maxima at 693 and 675 nm, the spectrum of the flexible derivative **44** shows a narrow Q band centered at 678 nm.

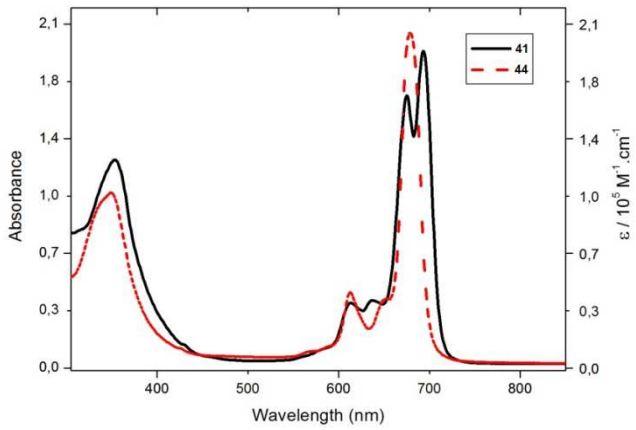

*Figure 102. UV-Vis spectra of Pc–C_{60} **41** and **44** in THF~1x10^{-5}M.*

The UV-Vis spectra of bisPc–C_{60} **46** and its precursors, bisPc malonate **45** and Pc **39** in THF is shown in Figure 103. The absorption spectra of **45** and **45** exhibited broadened Q bands with an absorption maximum located at 679 nm (Figure 103a). Even though the single Pc **39** shows sharp Q-bands in the same region, this is not the case for **46** and **45**. It is known that not only intermolecular but also intramolecular aggregation is possible in binuclear phthalocyanines.[110a,b] The broad absorption spectra of **46** and **45** can be, therefore, attributed to intramolecular or intermolecular interactions between Pc molecules. The UV-vis spectra of **45** and **46** in THF and pyridine are compared in Figure 103b. It is well established that the electronic absorption spectra of phthalocyanines strongly depends on the solvent nature. For example, in non-coordinating solvents such as toluene or $CHCl_3$ a broad absorption is observed in the range of 600-900 nm. Interestingly, the absorption spectra of **46**, and **45** are broad even in polar and coordinating solvents such as THF. When the solvent changes from THF to pyridine, similar molecular aggregation features are observed. As shown Figure 103 b, the characteristic signal of methanofullerene at 435 nm appears in the spectra of **46** in pyridine. These results suggested that the main driving force for the self-aggregation of Pcs **46** and **45** is the intramolecular π-π interaction between the two Pc macrocycles within a molecule and additionally the intermolecular π-π interaction.

[110] a) E. M. Maya, P. Vázquez, T. Torres, *Chem. Eur. J*. **1999**, *5*, 2004. b) E. M. Maya, P. Vázquez, T. Torres, L. Gobbi, F. Diederich, S. Pyo, L. Enchegoyen, *J. Org. Chem*. **2000**, *65*, 823.

With THF the intermolecular interaction can be broken up, however the intramolecular interaction persists even when pyridine is used.

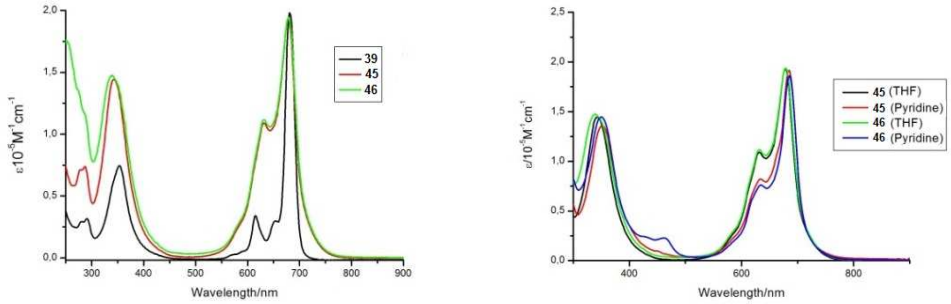

*Figure 103. a) UV/Vis spectra of **39**, **45** and **46** in THF (1 x 10^{-5} M), b) **45** and **46** in pyridine (1 x 10^{-5} M).*

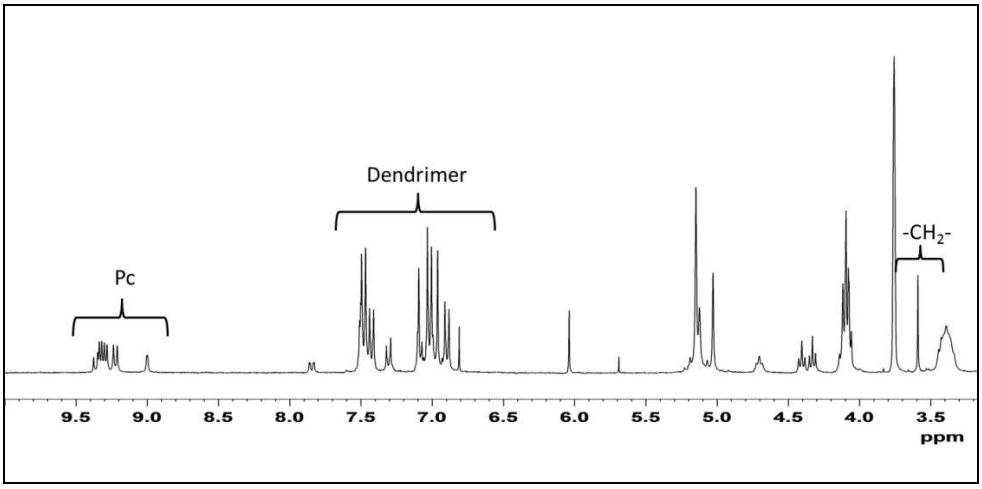

*Figure 104: ^{1}H NMR (d_8-THF) of Pc-Dendrimer **48**.*

As for Pc **39**, the ^{1}H NMR spectrum of compound **48** revealed well resolved signals, with each proton of the Pc unit assigned between 9.4 and 7.7 ppm, and the aromatic protons of the dendrimer fragment appearing in the range of 7.5-6.8 ppm. In addition, the characteristic methylene of the malonate at 3.6 ppm is also apparent in the spectra (Figure 104).

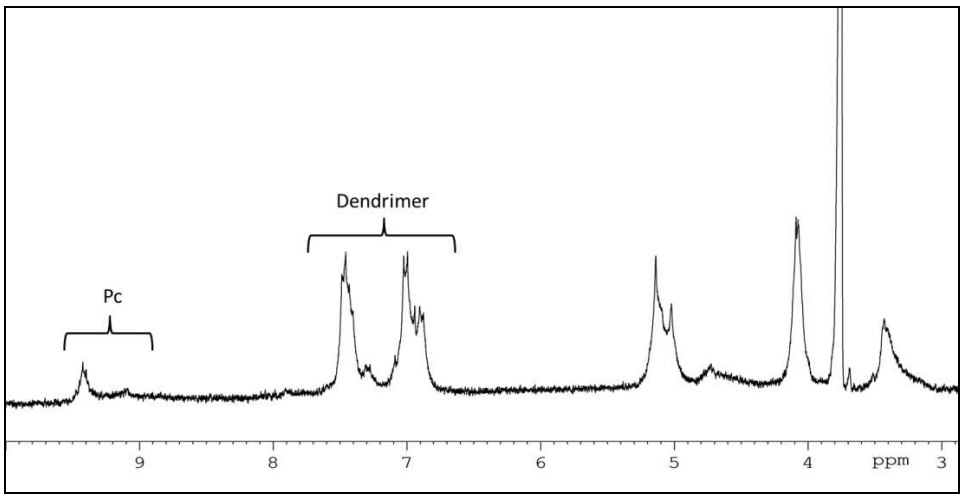

*Figure 105: ^{1}H NMR (d_8-THF) spectrum of Pc-C_{60}-Dendrimer **49**.*

On the other hand, although Pc protons and dendrimer protons can be easily distinguished, the ^{1}H NMR spectrum of compound **49** is more complex due to the presence of the C_{60} unit, which produces higher aggregation at the experimental concentration (Figure 105).

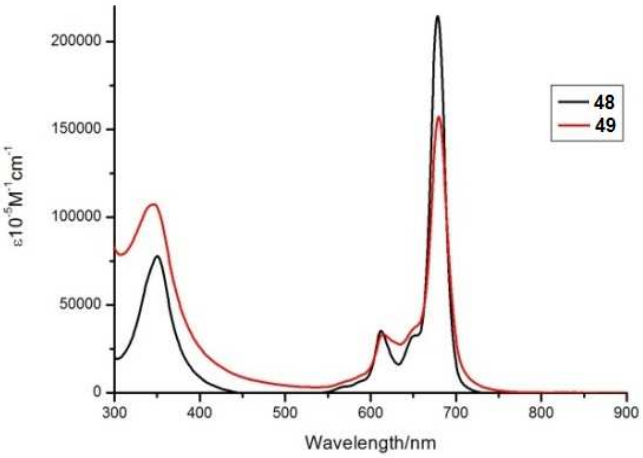

*Figure 106. UV/Vis spectra of **48** and **49** in THF~ 1x10^{-5} M.*

Figure 106 displays the UV-vis absorption spectra of the Pc-Dend-C_{60} **49** and its precursor Pc-dendrimer malonate **48.** The optical features of **49** closely resemble

those of compound **48,** with the only difference being a higher extinction coefficient for compound **49** in the UV region due to the fullerene absorption. The Q band for **49** is at 680 whereas for **48** is 679 nm, vibrational bands at 612 and 615 and B-bond at 346 nm and 350 nm, respectively. On the other hand, the aggregation of **49** is demonstrated by a decrease of the maximum extinction coefficient of the Q-band.

1.3.3.4. Liquid Crystalline Properties of Phthalocyanine Derivatives

The liquid crystalline properties of fullero-phthalocyanines **41, 44, 46, 49** and phthalocyanine derivatives, **37, 38, 39, 45**, and **48** were studied in collaboration with Dr. P.H.J. Kauwer at Institute for Molecules and Materials, Radboud University Nijmegen, Netherlands and Prof. Joaquín Barberá at Universidad de Zaragoza during predoctoral stays of the canditate in both centers.

In order to identify mesophases, three important experimental techniques; Polarized optical microscopy, Differential scanning calorimetry and X-ray diffraction were performed.

Polarized Optical Microscopy (POM) is the most common method used to look at optical texture, which is typical for various mesophases. It allows distinction between isotropic and anisotropic materials. Isotropic materials show the same optical properties in all directions due to have only one refractive index and therefore cannot cause an image to occur, while anisotropic materials demonstrate a range of refractive indices, which can cause an image to appear.

Differential scanning calorimetry (DSC) is a thermoanalytical technique in which can measure the enthalpy change associated with a phase transition. The information is obtained as a graph with a peak for each melting, mesophase-to-mesophase and clearing transitions.

X-ray diffraction (XRD) is a very useful tool in the structural classification of a liquid crystal phase type and the determination of how the molecules pack together.

Mesogenic Properties of Symmetric Pc 37

As expected, symmetrical Pc **37** displays columnar mesomorphism. A characteristic texture, shown in Figure 107, was observed by cooling the sample from the isotropic liquid. The clearing point was detected at 300 ºC by POM. By DSC, two main transitions were observed upon heating and cooling. On heating, crystal-to-crystal modification was observed at 85 ºC (ΔH=30.4 kJ/mol) and crystal to mesophase transition was detected at 126 ºC (ΔH=29.8 kJ/mol. Up on second heating, the two peaks became sharper and the crystal to mesophase transition shifted slightly (to 129 ºC).

On cooling, two exothermic peaks were detected at 96 ºC and 83 ºC corresponding to the mesophase-to-crystal and crystal-to-crystal transitions, respectively. The mesophase-to-isotropic liquid transition (clearing) was not detected by DSC. According to the DSC results, compound **37** is in its liquid crystal state above the endothermic transition detected at 126 ºC.

The thermal stability of Pc **37** was confirmed by thermogravimetric analysis (TGA), which indicates that no decomposition occurred upon heating to 350 ºC (a 5% weight loss was measured at 397 ºC).

X-Ray diffraction was carried out at 131 ºC (Table 5). The recorded pattern was unambiguously characteristic of a hexagonal columnar (Colh) mesophase. The hexagonal lattice constant was 31.4 Å and the stacking distance was about 3.6 Å.

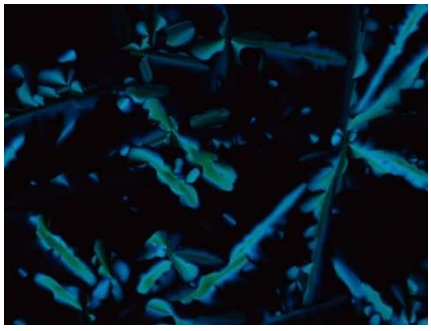

*Figure 107. Texture of symmetric Pc **37** between crossed polarizers in hexagonal columnar mesophase at 280 ºC.*

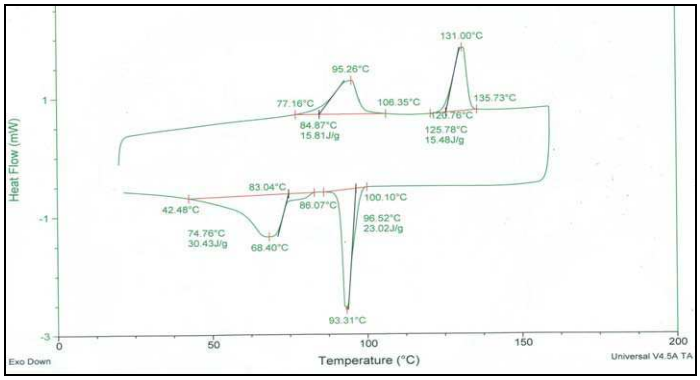

*Figure 108. The DSC curves and texture of Pc **37.***

Mesogenic Properties of hydroxy-substituted Pcs 38 and 39

In the case of unsymmetrically hydroxy-substituted Pc **38**, the clearing point was observed at 302 ºC by POM and a characteristic texture was obtained on cooling (Figure109). By DSC two endothermic peaks were detected on heating: a broad peak centered around 99 ºC (ΔH= 23.7 kJ mol^{-1}) and a sharp peak at 174 ºC (ΔH=11.8 kJ mol^{-1}). Two exothermic peaks were recorded at 168 ºC and 116 ºC on cooling. The compound was also studied at variable temperatures by XRD. At 120 ºC and 150 ºC the structure was crystalline, whereas at 190 ºC the pattern was consistent with a columnar mesophase with rectangular symmetry (Colr). The rectangular lattice constants were a= 42 Å and b= 30 Å (Table 5). No scattering maximum related to the stacking distance was detected. From these dimensions, it can be deduced that in this mesophase there are probably two columns per unit cell: one column is located at the centre of the two-dimensional rectangular lattice and another is located at the corner. It is concluded that the higher-temperature peak detected by DSC corresponds to the crystal-to-mesophase transition and the lower temperature peak corresponds to a crystal modification.

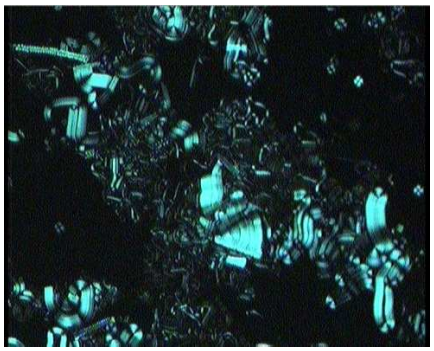

*Figure 109. Texture of Pc **38** between crossed polarizers in rectangular columnar mesophase at 150 ºC.*

On the contrary, Pc **39** is not mesogenic. On first heating an endothermic peak recorded by DSC at 61 ºC corresponds to a crystal-to-crystal transition, whereas an endothermic peak recorded at 104 ºC corresponds to the crystal-to-isotropic liquid transition, as indicated by the disappearance of birefringence. This fact was confirmed by X-ray diffraction. The pattern recorded at 80 ºC in the cooling process (after heating to the isotropic liquid) is characteristic of a three-dimensional crystalline structure.

Inter- or intramolecular Zn/OH interactions between the central metal of Pc **39** and the terminal oxygen of one of its substituents should be responsible for hindering the formation of columnar mesophases, making difficult the needed stacking among Pc cores. The flexible hydroxy-terminated chain in compound **39** may be better adapted for this type of interactions in comparison with the rigid hydroxymethyl fragment in Pc **38**, which additionally has an extended aromatic region that seems to favor the stacking of the compound and therefore mesomorphic properties.

Mesogenic Properties of BisPc 45 and Pc-Dendrimer 48

Compound **45** shows birefringent textures when observed in the polarising optical microscope at 110 ºC (Figure 110). Clearing point of **45** was detected at 298 ºC by POM. In DSC, one single reproducible transition is detected upon heating, corresponding to the solid-to-mesophase transition. On the second heating scan this transition takes place at 70 ºC and the molar enthalpy involved is 64.2 kjmol^{-1}. No DSC peak corresponding to the mesophase-to-isotropic liquid transition is detected.

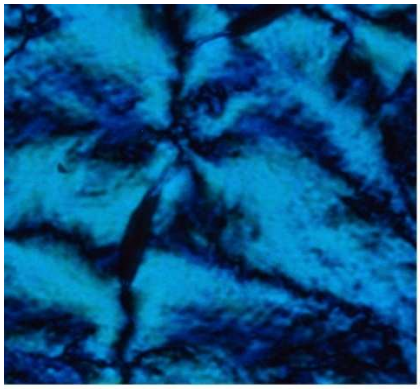

*Figure 110. Texture of bisPc **45** between crossed polarizers in hexagonal columnar mesophase at 110 ºC.*

The thermal behaviour of **48** is comparable to that of **45**. Birefringent textures are observed at 120 ºC (Figure 111), and clearing point was detected 250 ºC by POM In DSC, one single reproducible peak is observed corresponding to the solid-to-mesophase transition at a temperature of 74 ºC with a molar enthalpy of 34.7 kjmol-1. No other transitions are detected. Consequently, the malonate precursors **45** and **48** formed hexagonal columnar mesophases, characteristic of discotic molecules, at temperatures around 70 ºC. This lower transition temperature in comparison with that of symmetric octadodecylZnPc reference (126 ºC) is reflecting a more difficult molecular packing, considering they are mesogenic compounds composed of two discotic units separated by a flexible common chain.

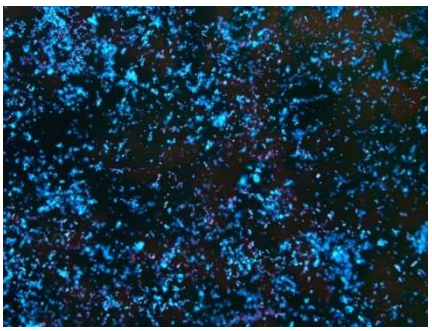

*Figure 111. Texture of Pc **48** between crossed polarizers at 120 ºC.*

The XRD experiments were performed at 95ºC on bisPc **45** were clearly characteristic of a hexagonal columnar organization. The set of sharp maxima found at small angles are the reflections from a 2D-hexagonal structure with a lattice constant *a*= 29.7 Å. Simple calculations assuming a mesophase density of 1 g.cm^{-3} allows to estimate that on average 0.5 molecules (*Z*= 0.5) are contained in a column *slice* of thickness *h* = 3.8 Å (Table 5). This estimation admits two possible organizations (Figure 112) : (a) one in which each phthalocyanine ring acts as a separate disc entity, so that the dimeric molecule locates its two phthalocyanine rings in different columns. (b) an alternative organization would consist on bisphthalocyanine molecules folded forming cofacial dimers, and therefore one molecule is contained in a column *slice* 3.8 Å x 2 = 7.6 Å thick.

The XRD patterns of **48** are simpler than **45** and the presence of only one reflection in the small-angle region precludes the unambiguous assignation of the mesophase type. However, the pattern is compatible with a hexagonal columnar structure if we consider that the small-angle peak is the fundamental reflection (Miller indices *1 0*) from a 2D-hexagonal lattice. Assuming a mesophase density of 1 g.cm^{-3}, it can be estimated that on average 0.5 molecules are contained in a column slice 3.3 Å thick. Therefore, for this compound mesophase packing models can be proposed similar to those described for **45**, although with a shorter stacking distance.

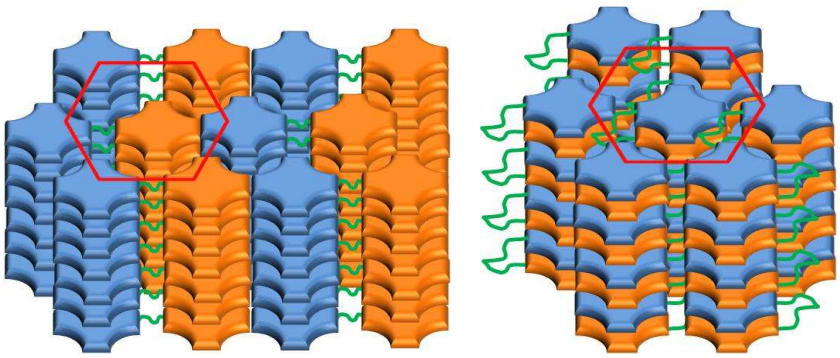

(a) (b)

*Figure 112. Postulated supramolecular organization of **45** within the hexagonal columnar phase, In (a) each Pc ring locates in different columns. In (b) the malonate-based* spacer is bent and two phthalocyanines locate on top of each other in the same column.

Mesogenic Properties of Phthalocyanine-Fullerene Systems

The thermal study of Pc–C_{60} dyads **41, 46** and **49** indicated that these molecules were non-mesogenic, that is, they did not show any texture under a polarized optical microscope and only a diffuse scattering, characteristic of an amorphous phase, was observed by XRD.

In the case of Pc–C_{60} **44** no typical textures were observed on heating from room temperature to the clearing or cooling from the isotropic liquid. However, the DSC diagrams of Pc–C_{60} **44** show two endotherms at 80 ºC (ΔH= 58.5 kJmol^{-1}) and 185ºC (ΔH= 4.8 kJ mol^{-1}) during the first heating and one exotherm at 180 ºC on cooling (ΔH= 4.5 kJ mol^{-1}) (Figure 113). The endotherm at 80 ºC corresponds to the crystal-to-mesophase transition (melting) and the endotherm at 185 ºC corresponds to the mesophase-to-isotropic liquid transition (clearing). The presence of only one exotherm in the cooling process, corresponding to the isotopic liquid-to-mesophase transition, means that this compound does not crystallize in the DSC conditions. The X-ray patterns recorded at 108 ºC are consistent with a Colr mesophase with a= 60 Å and b= 28 Å (Figure 114).

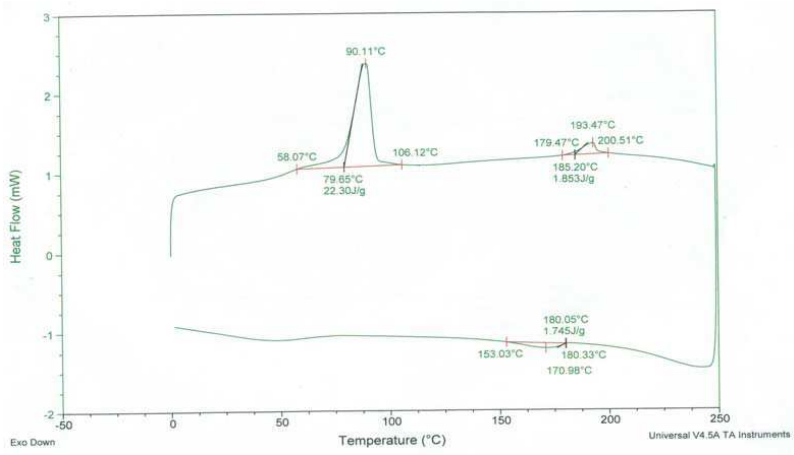

*Figure 113. The DSC curves of Pc-C_{60} dyad **44**.*

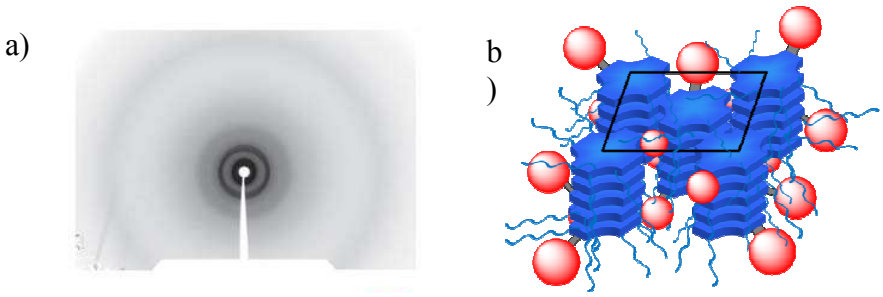

Figure 114. a) X-Ray pattern of Pc–C_{60} ***44*** *taken on its Colr mesophase at 108 ºC. b) Schematic representation of the Colr mesophase of Pc–C_{60}* ***44****.*

Similarly to Pc **38**, from these dimensions it can be deduced that there are two columns per unit cell: one at the centre of the rectangle and one at the corner (Figure 114 b). For both compounds the indexation of the X-ray reflections is consistent with a p2gg symmetry. No scattering related to the stacking distance was detected. Compared to the dimensions of the Colr phase of Pc **38**, *b* is similar and *a* is larger in Pc–C_{60} **44 (**Table 5**)**. This is probably due to the higher space demand of the fullerene and polymethylene spacers compared to the shorter hydroxy-terminated chain.

Table 4. Thermal data and structural parameters of the mesogenic compounds[a]

Compound	Transition temperatures/ ºC (ΔH = enthalpy/ kJ mol^{-1})	Mesophase Parameters measured at *T*
37	Cr 85 (30.4) Cr` 126 (29.8) Col_h ~300[b] Iso	*T*=131 ºC, *a*=31.4 Å *h*=3.6 Å
38	Cr 99 (23.7) Cr` 174 (11.8) Col_r ~300[b] Iso	*T*=190 ºC, *a*=42 Å *b*=30 Å
44	Cr 80 (58.5) Col_r 185 (4.8) Iso	*T*=108ºC, *a*=60 Å *b*=28 Å
45	Cr 70 (64.2) Col_h ~300[b] Iso	*T*=95 ºC, *a*=29.7 Å *h*=3.78 Å
48	Cr 74 (34.7) Col_h ~250[b] Iso	*T*= r.t. [d)], *a*=34.2 Å *h*=3.32 Å

[a]*Cr and Cr`: crystalline phase, Iso: isotropic liquid, Col_r : rectangular columnar mesophase, Col_h: hexagonal columnar mesophase, a and b are lattice parameters of the Col_r phase, a lattice parameter of the Col_h phase, h is the mean stacking distance.* [b] *Transition observed only POM.* [d)] *Thermally treated sample.*

Table 5. X-Ray data for the mesophase compounds Pc derivatives

Compound	Temperature (ºC)	Phase	d_{meas}(Å)	d_{calc}(Å)	h k	Lattice Constant (Å)	
37	131	Colh	27.4 16.1 13.1 10.3 4.7[b)] 3.6[b)]	27.2 15.7 13.6 10.3	1 0 1 1 2 0 2 1	a=31.4 h=3.6	
38	190	Colr (p2gg)	42.3 29.9 24.6 20.8 17.0 13.9 12.4 9.8 4.9[b)]	42.0 30.0 24.4 21.0 17.2 14.1 14.0 12.7 12.2 9.9 9.7	1 0 0 1 1 1 2 0 2 1 1 2 3 0 3 1 2 2 4 1 1 3	a=42 b=30	
44	108	Colr (p2gg)	60.4 25.4 20.0 15.8 14.1 4.7[b)]	60.0 25.4 20.0 16.3 14.0	1 0 1 1 3 0 3 1 0 2	a=60 b=28	
45	95	Col_h	25.7 14.9 12.8 9.7 4.7[b)]	25.7 14.8 12.8 19.7	1 0 1 1 2 0 2 1	a=29.7	**Estimation[c]** h=3.78 Z=0.5
48	r.t.[d]	Col_h	26.9 4.45 [b)]	29.6	1 0	a=34.2	h=3.32 Z=0.5

[a)] d_{meas} and d_{calc} are the measured and calculated diffreaction spacing: hk are the indexations of the reflections corresponding to the two-dimensional lattice of the Col_r or Col_h phase, a and b are lattice parameters of the Col_r phase, a lattice parameter of the Col_h phase, h is the mean stacking distance. [b)] diffuse maximum [c)] Estimated stacking distance (h) and number of molecules per unit cell (Z) assuming a density of 1g cm^{-3}. [d)] Thermally treated sample

Mesogenic Properties of Phthalocyanine/ C_{60} Blends

The use of blends in which a mesogenic compound induces mesomorphism to a non-mesogenic one has represented a strategy to organise Pc–C_{60} dyads into LC phases.[176] In this regard, observation of a stable columnar phase for symmetric Pc **37** and **45** suggested the potential for using phthalocyanine mesogens as a host for introducing fullerene into columnar mesophases without inducing phase separation.

The liquid crystalline properties of blends formed by evaporation of solutions of different discotic Pc-based molecules, namely Pcs **37**, **45**, and non-mesogenic C_{60} in different ratio were studied.

Symmetric Pc 37 / C_{60} Derivative Blends

a) Blends of Mesogenic Pc 37 and Non-Mesogenic Pc-C_{60} 41

A 2:1 mixture of symmetric mesogenic Pc **37** and dyad Pc–C_{60} **41** was prepared by evaporation of a THF solution of both components. This blend showed birefringence at 140 ºC in polarized optical microscopy on the cooling from the isotropic liquid. Additionally, DSC revealed broad endothermic peaks between 78 and 98 ºC on heating, and broad exothermic peaks at 101 ºC on cooling (ΔH = 5.6 kJ mol^{-1}).

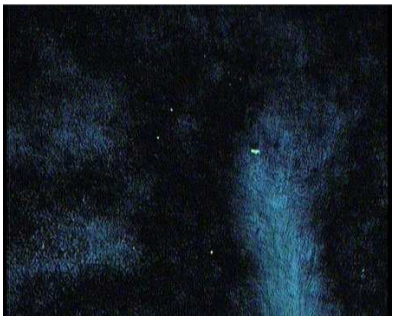

*Figure 115. Texture of a 1:2 Pc-C_{60} **41**-Pc **37** blend between crossed polarizers at 140 ºC cooling from the isotropic liquid.*

[176] A. de la Escosura, M. V. Martínez-Díaz, J. Barbera, T. Torres, *J. Org. Chem.* **2008**, *73*, 1475.

Although this experiment is not conclusive, due to absence of XRD measurements, we can deduce that mesogenic Pc induces mesomorphism into a non-mesogenic Pc-$_{C60}$ dyad made possible the organization of the Pc-C_{60} into a liquid crystalline phase.

b) Blends of Mesogenic Pc 37 and C_{60}

Mesogenic octadodecyl-substituted Pc **37** was mixed in solution with C_{60} in different ratios. The liquid crystalline properties of the resulting blends, after evaporation, were studied.

The mesomorphic properties of symmetric Pc **37** are practically unperturbed by the presence of equimolar amounts of fullerene, as inferred from the texture observed by POM and the similar crystal-to-crystal and crystal-to-mesophase transition temperatures measured by DSC for the mixture (79ºC and 128ºC, respectively, for the 1:1 Pc **37**:C_{60} blend and 85ºC and 126ºC for the mesogenic Pc **37**). The analysis of the X-ray patterns of the mixture at 150 ºC is consistent with the formation of a rectangular columnar mesophase. The rectangular lattice constants are a = 49 Å and b = 33 Å. On the other hand, the symmetry of the Pc mesophase is distorted in the presence of C_{60} causing the changed from hexagonal columnar into columnar rectangular mesophase. Additional spotty rings are detected in the middle and larges angles of the XRD patterns. These maxima are due to presence of non-mixed fullerene. As a consequence, fullerene can be incorporated into mesophase but blends are contaminated with C_{60} crystal phase segregated. These results suggest that to obtain homogenous mesophase a lower doping concentration of fullerene is required.

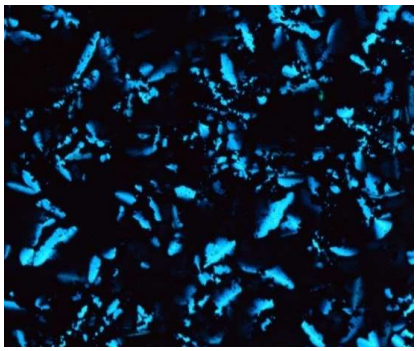

*Figure 116. Texture of a 1:1 Pc **37**-C_{60} blend between crossed polarizers at 250 ºC.*

In order to establish the maximum amount of C_{60} that can be incorporated in a homogeneus liquid crystalline Pc/C_{60} blend, additional experiments were carried, preparing blends containing smaller amounts, namely 10% and 1% of C_{60}. Thus, Pc **37:**C_{60} (90:10) and Pc **37**:C_{60} (99:1) mixtures were studied at 150 ℃. The presenc e of "extra" reflections (specifically three: 8.1 Å, 5.0 Å , 4.25 Å) due to C_{60} was observed in the Pc **37**:C_{60} (90:10) blend, whereas in Pc **37**:C_{60} (99:1) it was not. This means that at most 1% of C_{60} can be integrated without segregation into a Pc-based columnar mesophase.

Also in both cases the hexagonal symmetry of the mesophase of Pc **37** is broken to give the same annotated structure for Pc **37**:C_{60} (1:1). Interestingly, for the three mixtures Pc **37** and C_{60} containing different proportions, the same reflections mesophase gives approx. 27.4-27.7 Å, 16.5-16.8 Å, 14.6-15.0 Å, 13.0-13.4 Å, with a very slight tendency to increase with decreasing the proportion of C_{60}. That is, the distances are 27.4 Å, 16.5Å, 14.6 Å, 13.0 Å for 1:1 blend, 27.7 Å, 16.5 Å, 14.8 Å, 13.2 Å for 90:10 blend and 27.7 Å, 16.8 Å, 15.0 Å, 13.4 Å for 9:1 blend. As we mentioned earlier for 1:1 blends, the symmetry is no longer hexagonal mixtures, it is likely that the rectangular columnar mesophase for both later blends.

c) Mesogenic Bisphthalocyanine 45/C_{60} Blends

The DSC thermograms of a 1:1 mixture of bisphthalocyanine **45** and C_{60} are qualitatively similar to those of pure bisPc **45**. However, the solid-to-mesophase transition is much broader and its maximum is shifted to slightly higher temperatures. The XRD studies confirm that the mesophase is hexagonal columnar and the hexagonal lattice constant is practically identical to that measured for pure bisPc **45**. In contrast to the Pc **37**:C_{60} blends, the presence of C_{60} does not alter the symmetry and the parameters of the mesophase of pure Pc **45**, which remains the same hexagonal columnar network size (at approx. 29.7 Å) in the blend. However, in the XRD patterns of the blend additional maxima with the shape of spotty rings are recorded at middle and large angles, as the same as the previous blends. The mesophase of Pc **45** was also disordered, that is, there is not a constant distance stacking in the mixture. This lack of stacking constant distance is attributable to presence of C_{60}.

1.3.3.5. Charge Transport Properties of Pc-C_{60} 44

The charge carrier mobility of discotic liquid crystal Pc-C_{60} **44** was studied by the time-of-flight (TOF) and flash-photolysis time resolved microwave conductivities (TRMC). The TOF and TRMC measurements were conducted by Dr. Akinori Saeki in the group of Prof. Shu Seki in the Graduate School of Engineering, Osaka University, during a predoctoral stay of the candidate in Japan. These methods involves measuring the carrier transit time (τ), which is the time required for charge carriers near one of the electrodes that are photogenerated by pulsed light irradiation to travel across the sample to the other electrode under an applied electric field.

The TOF technique is the simple method, based on the definition of the mobility. In a TOF experiment, the liquid crystalline sample is held between two electrodes by introducing the melt sample into gap by capillary action. At least one of the electrodes is transparent and usually ITO. By excitation of a pulse of laser light through the ITO side, on the liquid crystalline material creates bound excitons near one of the electrodes, and free charge carriers can then be generated by dissociation of the excitons. The charge carriers either holes or electrons are collected by the contact electrode depending on the polarity of the applied electric field and the oppositely charged carrier is pulled towards the back contact to generate a transient current. As charge carriers start to drift, photocurrents can be detected until the charge carriers arrive at the other electrode.

The transit time (τ) and charge carrier mobility are calculated using the following formula: where *V* is velocity of charge carrier and d is the sample thickness.

$$\mu = \frac{d^2}{V\,\tau}$$

$$\tau = \frac{d}{V}$$

Time resolved microwave conductivities, TRMC. The charge carrier mobility as a function of temperature was measured using pulse radiolysis time-resolved microwave conductivity (PR-TRMC).

In TRMC, the sample is irradiated by a pulse of high-energy electrons to create low density of free carriers. If the charge carriers are mobile, the conductivity of the sample changes ($\Delta\sigma$) and can be monitored by a decrease in the microwave power reflected form the cell. The sum of the charge carrier mobilities of both holes and electrons can be estimated from

$$\mu_{total} = \frac{E_p}{W_{eop}}\left(\frac{\Delta\sigma}{D}\right)_{eop}$$

where Ep is the average pair-formation energy, Δσ is the change in the conductivity of the sample, D is the energy absorbed by the sample and Weop is the fraction of initially formed charge carrier pairs that survive the charge recombination/trapping process during the transient.

The TOF and TRMC measurements give “long-range” (tens of microns) and “short range” (a few molecules) charge transport properties, respectively. The TOF mobility is often lower than the TRMC value due to the disordered, multidomain or imperfectly aligned system, which give rise to a high probability to meet traps for charge carriers. In addition, in the TRMC experiment, the charge carriers migrate only between a few molecules via interactions between neighbouring aromatic rings. TRMC values depend on the degree of alignment within intracolumns but TOF values correlate with that of intercolumns and also in the intracolumn.

The short-range charge carrier properties of PcC_{60} **44** were measured by TRMC method. Upon exposure to a 355 nm laser pulse at 25 ºC, PcC_{60} **44** reveals a rapid increase of a transient conductivity, (ØΣμ) in which Ø is the quantum efficiency of charge separation and Σμ is the mobility of all the transient charge carriers, thus reaching maximum transient conductivities of 3×10^{-5} cm^2 V^{-1} s^{-1} before heating and 8.9×10^{-5} cm^2 V^{-1} s^{-1} after heating and cooling treatment (Figure 117).

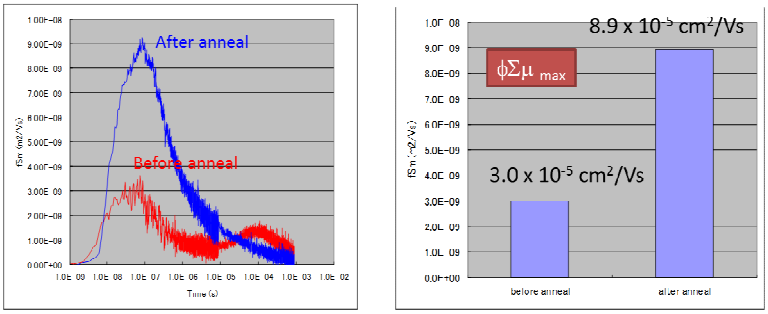

Figure 117. TRMC profiles of PcC_{60} ***44*** *before heating, at 25 ºC, the sample after heating to at 200 ºC for 10 min, then slowly cooled down to 25 ºC.*

The Ø values were determined to be 4.0 x 10^{-4} before heating and 2.0 x 10^{-4} after heating and cooling treatment. The Σμ values increased from 0.07 to 0.44 cm^2/Vs by annealing and resultant formation of columnar LC phase. Note that the total charge mobility measured after the heating and cooling treatment is 6 times higher than that before heating. These results show that after heating, the well-ordered alignment of the PcC_{60} **44** columns in the LC may facilitate intracharge transport between the PcC_{60} **44**-based columns, leading to the improvement of the macroscopic charge mobilities.

Unfortunately, we could not obtain a clear TOF transient by making sandwich-type cell with PcC_{60} **44** dyad, due to the high viscosity of the compound even though the isotropic phase at 200 ºC is still very large.

1.3.4. Summary and Conclusions

In summary

- Unsymmetrically substituted Pcs bearing both long alkyl chains and terminal hydroxyl groups were successfully obtained and purified, allowing the preparation of potentially liquid crystal phthalocyanine–fullerene derivatives in good yields.

- The liquid crystalline properties of unsymmetrically substituted phthalocyanines are difficult to predict. Actually, they have shown to be very sensitive to small changes in the substitution pattern: while Pc **39** shows mesogenic behaviour, Pc **38** resulted to be non mesogenic.

- Pc derivatives containing two mesogenic units, either two Pcs (**45**) or one Pc and one dendron (**48**) exhibit substantially lower transition temperatures (70 ºC vs. 126 ºC) than symmetrical Pc **37**), reflecting a more difficult molecular packing.

- The incorporation of a fullerene moiety is responsible for the disruption of mesomorphism in several Pc-C_{60} systems, pointing out the difficulty in accommodating the fullerene moieties without disturbing the columnar Pc arrangements of discotic liquid crystal molecules. Among the different structural parameters, the length and flexibility of the linker between the Pc core and the C_{60} has proven to be crucial to minimize the influence of C_{60}. It is also remarkable the lower isotropization temperature of mesogenic Pc–C_{60} **44** in comparison with that of Pc mesogens **37** and **38**, also indicating a decrease in the stability of the mesophase when C_{60} is covalently linked to a discotic mesogen.

- The indirect formation of non-segregated homogeneous liquid crystalline Pc/C_{60} blends has been achieved when only a small percentage, 1% or less, of C_{60} is mixed to symmetrical mesogenic Pc **37**, altering additionally the symmetry of the mesophase from hexagonal columnar to rectangular columnar.

- The organization of ZnPc-C_{60} **44** dyad within the liquid crystalline phase is improved after heating, which facilitates the charge transport properties.

General conclusion

C_{60} has proven to be an element of "distorting" not only the symmetry of discotic mesophases, but also the orderly stacking.

Phthalocyanine-fullerene based liquid crystals were obtained either by covalent concept or by the blend approach. The covalent strategy allows the incorporation of equimolar ratios of Pc and C_{60} in the mesogen, whereas only a very small amount of C_{60} should be used in Pc / C_{60} blends for achieving homogenous mesophases. However, even if the covalent concept requires tedious synthetic efforts, it resulted more useful from the applied point of view since it has been reported the benefit of using excess of fullerene for the percolated transport of the negative charges.[182]

[182] C. Winder, N. S. Sariciftci, *J. Mater. Chem.* **2004**, *14*, 1077

Chapter 1.3. Experimental Section

1.3.5. Experimental Part

Thermal behavior was investigated by using a Nikon polarizing microscope equipped with a Linkam THMS600 hot stage, and by DSC with a TA-Instruments DSC-2910 operated at a scanning rate of 10 "C min^{-1} in a nitrogen atmosphere. The apparatus was calibrated with indium (156.6 ºC, 28.4 J g^{-1}) and the transition temperatures were read at the onset of the peaks. X-Ray patterns were obtained by using a pinhole camera (Anton–Paar), operating with a point-focused Ni-filtered $Cu_{K\alpha}$ beam. The sample was held in Lindemann glass capillaries (1 mm in diameter) and heated when necessary, by means of a variable-temperature attachment. The patterns were collected on flat photographic film.

Nanosecond laser pulses from a Nd:YAG laser (Spectra Physics, INDY−HG, third harmonic generation (THG), 355 nm) with FWHM of 3-5 ns were used as excitation sources. The photon density of the laser was set at 1.6×10^{15}–3.6×10^{16} photons cm^{-2}. For the TRMC measurements, a microwave frequency of 8.6−9.4 GHz and a power of 2.1−4.6 mW were employed so that the motion of charge carriers could not be disturbed by the low electric field of the microwaves. The TRMC signal, picked up by a diode (rise time < 1 ns), was monitored by a digital oscilloscope (Tektronix, TDS3032B, rise time ∼1.2 ns). All the experiments were carried out at 25 ºC.

1.3.5.1. Synthesis of Precursor Phthalonitriles

4-[2-{4-(Hydroxymethyl)phenyl}ethynyl]phthalonitrile (**30**)

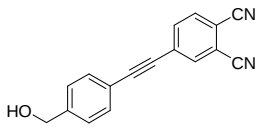

A mixture of 4-ethynylbenzyl alcohol (0.27 mg, 2.05 mmol) and 4-iodophthalonitrile (**2**) (0.5 mg, 1.96 mmol) were dissolved in freshly distilled Et_3N (10 ml). Then $[Pd(PPh_3)_2Cl_2]$ (0.14 mg, 0.02 mmol) and CuI (3.84mg, 0.02 mmol) were added. The reaction mixture was stirred for 24 h at 70 ºC under argon atmosphere. The solvent was then removed under reduced pressure and the crude product was purified by column chromatography on silica gel, (CH_2Cl_2/EtOAc, 9:1), to yield **30** (230 mg, 0.9 mmol) as a white solid. Yield: 45%.

^{1}H NMR ($CDCl_3$, 300 MHz): δ (ppm)= 7.8 (d, *J*=1,2 Hz, 1H; H-3), 7.75 (dd, *J*=8.2, *J*=1.2 Hz, 1H; H-5), 7.7 (d, *J*=8.2 Hz, 1H; H-6), 7.5 (d, *J*=8.2, 2H; H8, H12), 7.4 (d, J=8.2, 2H; H9, H11), 4.8 (s, 2H, CH_2), 1.83 (br. s, 1H, OH).

IR (KBr): v (cm^{-1}) = 3354, 3204, 3091, 2235, 2208, 1593, 1510, 1451, 1390, 1239, 1037, 897.

4-(6-Hydroxyhexyloxy)phthalonitrile (**31**)[179]

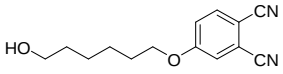

To suspension of 4-nitrophthalonitrile (2g, 11.5 mmol) and K_2CO_3 (3.20 mg, 23 mmol) in DMAC (25 ml) 1,6-hexanediol (5.47g, 46.2 mmol was added) in little portions. After the addition was complete, the reaction mixture was stirred under argon atmosphere 40 ºC for 4 days and then poured into brine (100 ml) and extracted with Et_2O. The organic phase was collected and washed with brine and dried over Na_2SO_4.

[179] J. J. Cid, *PhD thesis*, Universidad Autonoma de Madrid, Madrid, **2008**.

The solvent was evaporated under vacuum and the viscous oil was purified by column chromatography on silica gel, (diethyl ether/ hexane 1:10), to yield **31** (1.2 g, 4.9 mmol) as a green solid. Yield: 42%.

Mp: 59-61 ºC (reported:[179] 60-61 ºC).

^{1}H NMR ($CDCl_3$, 300 MHz): δ (ppm)= 7.7 (d, *J*= 8.7 Hz, 1H; H-6), 7.25 (d, *J*= 2.5 Hz, 1H; H-3), 7.2 (dd, *J* = 8.7, 2.5 Hz, 1H; H-5), 4.0 (t, J=6.3 Hz, 1H, $C\underline{H_2}O$), 3.6 (t, *J*=6.3 Hz, 1H, $HOC\underline{H_2}$), 1.9-1.8 (m, 1H, $HOCH_2C\underline{H_2}$), 1.6-1.4 (m,6H, $HOCH_2\underline{CH_2}\underline{CH_2}\underline{CH_2}$).

4,5-Didiodophthalonitrile (34)[180]

4,5-Diiodophthalimide (**32**)

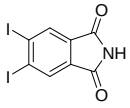

To 60 ml of 30% fuming sulfuric acid was added phthalimide (14.7 g, 0.1 mol) and iodine(25.4 g, 0.2 mol). The reaction mixture was heated to 75 ℃ overnight. This mixture was then poured onto 400 g of ice, and the precipitated solids were filtered off using a funnel with a glass frit. The solids were washed with water, a 2% solution of K_2CO_3, and a saturated solution of $Na_2S_2O_3$, and dried at room temperature. They were then extracted with acetone (1L) in a Soxhlet extractor for 48 h. The resulting precipitate which formed in the solvent vessel and consisted of 4,5-diiodophthalic acid, was filtered from the acetone, and 100 mL of water was added. This solution was concentrated to 500 mL and cooled to give 4,5-diiodophthalimide (**32**) (20 g, 0.05 mol) as a bright-yellow solid. Yield: 50%

Mp: 295-297 ºC (reported:[180] 297-299 ºC).

[180] D. S. Terekhov, K. J. M. Nolan, C. R. McArthur, C. C. Leznoff, *J. Org. Chem.* **1996**, *61*, 3034.

^{1}H NMR (DMSO-d_6, 300 MHz): δ (ppm) = 8.2 (s, 2H), 11.4 (s, 1H).

4,5-Diiodophthalamide (**33**)

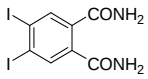

To 220 ml of concentrated aqueous ammonia was added 4,5-diiodophthalimide (**32**) (20 g, 50 mmol). The rapidly stirred mixture was heated to 50 ℃ for 1.5 h. The white solid was filtered and washed three times with ice-cold water and with methanol. The solid was dried overnight at room temperature to give intermediate **33** (17.0 g, 40 mmol) as a white powder. Yield: 80%

Mp: 296-298 ºC (reported:[180] 297-299 ºC).

^{1}H NMR (DMSO-d_6, 300 MHz,): δ (ppm) = 7.9 (s, 2H), 7.8 (br. s, 2H), 7.3 (br. s, 2H).

4,5-Diiodophthalonitrile (**34**)

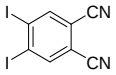

To an ice-cooled stirred suspension of of (**33**) (8.3 g, 20 mmol) in dry dioxane (80 ml) and dry pyridine (18 ml) was added trifluoroacetic anhydride (16 ml) at 0-5 ℃. After the addition was complete, the reaction mixture was warmed to room temperature, stirred overnight, and poured onto ice. The product was extracted three times with EtOAc. The organic layer was washed with water, 1 M HCl, diluted Na_2CO_3, and dried over $MgSO_4$. The solvent was removed under vacuum, and the product was purified by column chromatography on silica gel, (CH_2Cl_2/Hexane, 2:1) to give **34** (6.0 g, 15 mmol) as yellow solid. Yield: 75%

Mp: 214-216 ºC (reported:[180] 216-217 ºC).

^{1}H NMR (300 MHz, $CDCl_3$): δ (ppm) = 8.19 (s).

4,5-Didodecynylphthalonitrile (**34**)[181]

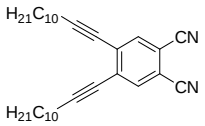

To a solution of 4,5-diiodophthalonitrile (**34**) (650 mg, 1.7 mmol) in of TEA (20 ml) and DMF (2 ml) was added $[PdCl_2(PPh_3)_2]$ (875 mg ,0.1 mmol). The reaction mixture was stirred at 100 ℃ under an inert atmosp here and 1-dodecyne (1.6 ml, 7.4 mmol) was added. The reaction was monitored by TLC (diethyl ether/hexane, 1:10) until complete consumption of starting materials. After 2 h, the reaction was cooled and filtered, and the filtrate was evaporated to dryness under reduced pressure. The resulting solid was purified by column chromatography on silica gel (diethyl ether/ hexane, 1:10), to yield **35 (**620 mg, 1.35 mmol) as a yellow solid. Yield: 79 %

^{1}H NMR ($CDCl_3$, 300 MHz): δ (ppm) = 7.7 (s, 2H), 2.5 (t, *J*=9Hz, 4H), 1.7-1.6 (m, 4H), 1.4-1.2 (m, 28H), 0.8 (t, *J*=6, 6H).

4,5-Didodecylphthalonitrile (**36**)

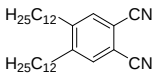

To a solution of 4,5-didodecynlphthalonitrile (**35**) (600 mg, 1.31 mmol) in TEA (50 ml) was added 10% palladium on carbon (120 mg). The suspension was stirred at room temperature, and hydrogen gas was bubbled through the reaction mixture. The reaction was monitored by TLC (diethyl ether/hexane, 1:10) until complete consumption

[181] W. M. Sharman, J. E. van Lier, *Bioconjugate Chem*. **2005**, *16*, 1166.

of starting materials. After 6 h, the reaction mixture was filtered to remove the catalyst, and the filtrate was evaporated to dryness under reduced pressure. The resulting solid was purified by column chromatography on silica gel, diethyl ether/ hexane, 1:10), to yield **6 (**450 mg, 0.96 mmol) as a yellow solid. Yield: 74%

Mp: 29-32 ºC (reported:[181] 31 ºC).

^{1}H NMR (CDCl3, 300 MHz): δ (ppm) = 7.6 (s, 2H), 2.7 (t, *J*=9 Hz, 4H), 1.6-1.5 (m, 4H), 1.4-1.2 (m, 28H), 0.9 (t, *J*=6 Hz, 6H).

1.3.1.1. Synthesis of Phthalocyanine Derivatives

Zinc (II) 2,3,9,10,16,17,23,24-octadodecylphthalocyaninato(2-)-N^{29}, N^{30}, N^{31}, N^{32} (**37**) and Zinc (II) 9,10,16,17,23,24-hexadodecyl-2-[2-(4-(hydroxymethyl)-phenyl)ethynyl]phthalocyaninato(2-)-N^{29}, N^{30}, N^{31},N^{32} (**38**)

A mixture of 4,5-didodecylphthalonitrile (**36**) (965 mg, 2.07 mmol), 4-(2-(4-(hydroxymethyl)phenyl)ethynyl)phthalonitrile (**30**) (107 mg, 0.41 mmol) and $(ZnOAc)_2$ (121.8 mg, 0.66 mmol) in DMAE (6 ml) was heated at reflux overnight with stirring under argon atmosphere. After cooling to room temperature, the solvent was removed and the residue was washed with a MeOH/H_2O (5:1) mixture. The crude product was purified by column chromatography on silica gel (toluene/THF 10:1). The symmetric Pc **37** was eluted first, obtaining as a blue solid, 470 mg (0,24mmol), 48% yield, followed by Pc **38** as a blue-greenish solid, 280 mg (0,16 mmol), 39% yield.

Pc **37**:

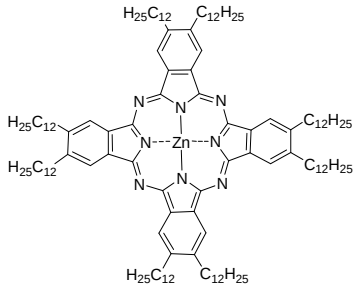

Transition temperature: Cr-Col$_h$:126 ºC, Col$_h$-Iso: ~300 ºC.

^{1}HNMR (d_8-THF, 300 MHz): δ (ppm) = 9.4 (s, 8H, ArH), 3.4-3,3 (m, 16H, alkylH), 2.3- 2.2 (m, 16H, alkylH), 1.9-1.4 (m, 144H, alkylH), 1.2-0.9 (m, 24H, alkylH).

IR (KBr): v (cm^{-1}) = 2954, 2919, 2850, 1620, 1489, 1467, 1339, 1107.

UV/Vis (THF): λ_{max} (log ε) = 677 (5.4), 613 (4.72), 351 (5.0).

HRMS (MALDI-TOF, dithranol): calc. for $C_{128}H_{208}N_8Zn$: $[M]^+$: m/z: 1921.5808, found 1921.5773.

Pc **38**:

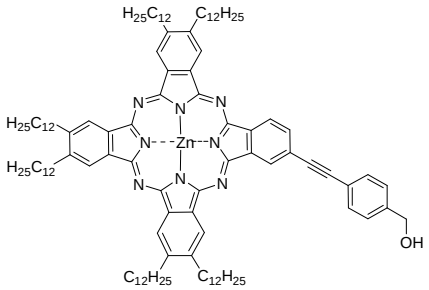

Transition temperature: Cr-Col$_r$:174ºC, Col$_r$ –Iso: ~300ºC.

^{1}HNMR (d_8-THF, 300 MHz): δ (ppm)= 9.5 (s, 1H, ArH), 9.3 (d, *J*=7.8, 1H, ArH), 9.2 (d, *J*=4.7 Hz, 2H, ArH), 9.1 (s, 1H, ArH), 9.0 (s, 1H, ArH), 8.9 (s, 1H, ArH), 8.8 (s, 1H, ArH), 8.3 (d, *J*=7.3 Hz, 1H, ArH), 7.9 (d, 2H, *J*=8 Hz, ArH), 7.7 (d, *J*=8 Hz, 2H, ,ArH), 4.9 (s, 2H, alkylH), 3.4-3,3 (m, 12H, alkylH), 2.3- 2.20 (m, 12H, alkylH), 1.9-1.3 (m, 108H, alkylH), 1.2-0.8 (m, 18H, alkylH).

IR (KBr): v (cm^{-1}) = 3448, 2955, 2922, 2851, 1617, 1514, 1488, 1465, 1338, 1093.

UV/Vis (THF): λ_{max} (log ε) = 692 (5.26), 676 (5.21), 615 (4.53), 354 (5.0).

HRMS (MALDI-TOF, dithranol): calc. for $C_{113}H_{166}N_8OZn$: $[M]^+$: m/z: 1715.2471, found 1715.2393.

Zinc (II) 9,10,16,17,23,24-hexadodecyl-2-(6`-hydroxyhexyloxy)phthalocyaninato(2-)-N^{29}, N^{30}, N^{31}, N^{32} (**39**)

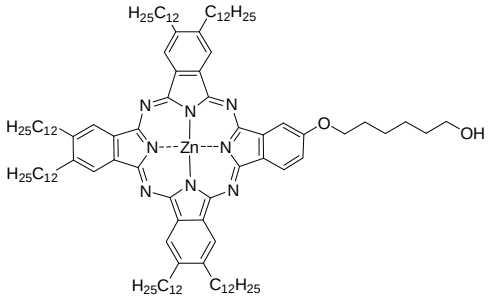

A mixture of 4, 5-didodecylphthalonitrile (**36**) (490 mg, 1.05 mmol), 4-(6-hydroxyhexyloxy)phthalonitrile (**31**) (51 mg, 0.21 mmol) and $(ZnOAc)_2$ (61 mg, 0.33 mmol) in DMAE (5 ml) was heated at reflux overnight with stirring under argon atmosphere. After cooling to room temperature, the solvent was removed, and the residue was washed with a MeOH/H_2O (5:1) mixture. The crude product was purified by column chromatography on silica gel, (toluene/THF, 10:1) as eluent to yield **39 (**100 mg, 0,06 mmol) as a green solid. Yield: 27%

Transition temperature: Cr-Iso: ~104 ºC.

^{1}HNMR (d_8-THF, 300 MHz): δ (ppm)= 9.4-9.3 (m, 3H, ArH), 9.3 (s, 1H, ArH), 9.27 (s,1H, ArH), 9.24 (s, 1H, ArH), 9.2 (s, 1H, ArH), 8.9 (s, 1H, ArH), 7.8 (dd, *J*=3Hz, 9, 1H, ArH), 4.7 (t, *J*=6Hz, 2H, OCH_2), 3.4-3,3 (m, 14H, alkylH), 2.2- 2.1 (m, 16H, alkylH), 1.9-1.3 (m, 112H, alkylH), 1.2-0.8 (m, 18H, alkylH).

IR (KBr): ν (cm^{-1}) = 3455, 3224, 2955, 2921, 2851, 1775, 1718, 1606, 1488, 1468, 1338, 1090.

UV/Vis (THF): λ_{max} (log ε) = 678 (5.2), 612 (4.5), 350 (4.8).

HRMS (MALDI-TOF, dithranol): calc. for $C_{110}H_{172}N_8O_2Zn$: $[M]^+$: m/z: 1701.2889, found 1701.2829.

1.3.1.2. Synthesis of Phthalocyanine-Fullerene Dyads

Synthesis of Phthalocyanine-C_{60} dyad (41)

Zinc (II) 9,10,16,17,23,24-hexadodecyl-2[2`-(4``-formylphenyl)ethynyl]phthalocyaninato (2-)-N^{29}, N^{30}, N^{31}, N^{32} (**40**)

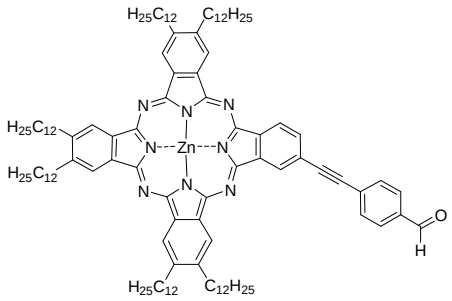

To a stirred solution of Pc **38** (40 mg, 0.023 mmol) in THF (5 ml) under argon atmosphere, a solution of IBX (14.56 mg, 0.052 mmol) in DMSO (5 ml) was added. The mixture was stirred at room temperature overnight. The reaction was monitored by TLC (hexanes/dioxane, 4:1) until all the starting phthalocyanine had reacted. Brine was then added and the mixture was extracted with ether. The combined organic layers were dried over $MgSO_4$ and concentrated in vacuum. The remaining solid was washed with methanol and water to yield Pc **40** (30 mg, 0.017 mmol) as a green solid. Yield: 75%

Mp> 250ºC.

^{1}HNMR (d_8-THF, 300 MHz): δ (ppm)= 10.3 (s, 1H, CHO), 9.4 (s, 1H, ArH), 9.18 (d, *J*=9 Hz, 2H, ArH), 9.13 (s, 2H, ArH), 8.9 (s, 2H, ArH), 8.8 (s, 1H, ArH), 8.7 (s, 1H, ArH), 8.3-8.2 (m, 5H, ArH), 3.5-3,2 (m, 12H, alkylH), 2.3- 2.1 (m, 12H, alkylH), 1.7-1.4 (m, 108H, alkylH), 1.2-0.8 (m, 18H, alkylH).

UV/Vis (THF): λmax (log ε)= 692 (5.3), 676 (5.1), 614 (4.6), 354 (5.0).

HRMS (MALDI-TOF, dithranol): calc. for $C_{113}H_{164}N_8OZn$: [M^+]: m/z: 1713.2314, found 1713.2285.

Zinc(II)9,10,16,17,23,24-hexadodecyl-2{2`-[4``-(1```-methyl-3```,4```[60]fulleropyrrolidine -2-yl)-phenyl] ethynyl} phthalocyaninato (2-)-N^{29}, N^{30}, N^{31}, N^{32} (**41**)

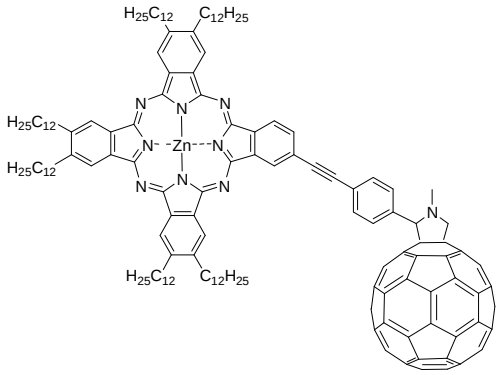

A mixture of C_{60} (36.7 mg, 0.05 mmol) and N-methylglicine (1.55 mg, 0.0175 mmol) in o-DCB (5ml) was stirred at 60 ºC under argon atmosphere. A solution of Pc **40** (30 mg, 0.0175 mmol) in o-DCB (5 ml) was then added and the mixture heated to 110 ºC overnight. After cooling to room temperature, the solvent was evaporated to dryness. Purification of the solid residue by column chromatography on silica gel (toluene and followed by toluene-THF, 10:1), and then by size-exclusion column chromatography (THF) gave pure Pc-C_{60} **41** (7 mg, 0.003 mmol) as a dark green solid. Yield: 15%

Mp> 250ºC.

^{1}**HNMR** (d_8-THF, 300 MHz): δ (ppm)= 9.6 (s, 1H, ArH), 9.5 (d, *J*=9 Hz, 1H, ArH), 9.3 (s, 2H, ArH), 9.25 (s, 1H, ArH), 9.24 (s, 1H, ArH), 9.21 (s, 1H, ArH), 9.18 (s, 1H, ArH), 8.3 (d, *J*=9 Hz, 1H, ArH), 8.1 (d, *J*=6 Hz, ArH), 8.0 (d, *J*=6 Hz, 2H, ArH), 5.3 (s,1H, pyrolidine H), 5.2 (d, *J*=9 Hz, 1H, pyrolidine H), 4.5 (d, *J*=9 Hz, 1H,pyrolidine H), 3.9 (s, 3H, ,NCH_3), 3.4-3,3 (m, 12H, alkylH), 2.3- 2.2 (m, 12H, alkylH), 1.9-1.3

(m, 108H, alkylH), 1.2-0.8 (m, 18H, alkylH).

UV/Vis (THF): λ_{max} (log ε) = 693 (5.3), 675 (5.2), 614 (4.5), 393 (5.1).

HRMS (MALDI-TOF, dithranol): calc. for $C_{175}H_{169}N_9Zn$: $[M]^+$: m/z: 2460.2787, found 2460.2771.

Synthesis of Phthalocyanine-C_{60} dyad (44)

Zinc (II) 9,10,16,17,23,24-hexadodecyl-2(6`(hexyloxy) malonic acid ester) phthalocyaninato (2-)-N^{29}, N^{30}, N^{31}, N^{32} (**42**)

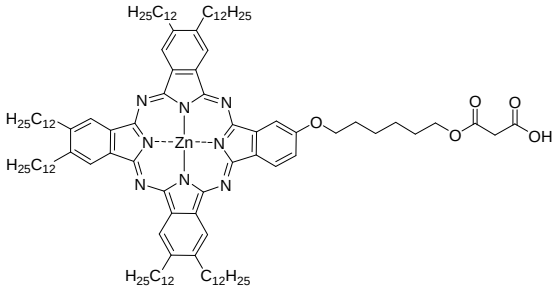

A solution of Pc **39** (100 mg, 0.058 mmol) and Meldrum acid (84.5 mg, 0.58 mmol) in toluene/THF (4:1) was stirred at 65 ℃ for 24 h and subsequently solvents were evaporated to dryness. After precipitation (solution in CH_2Cl_2 and precipitation by pouring the solution into MeOH to eliminate the unreacted Meldrum acid), pure **42** was obtained (64 mg, 0.035 mmol) as a green solid. Yield: 62%

Mp> 250ºC.

^{1}HNMR (d_8-THF, 300 MHz): δ (ppm)= 9.33-9.28 (m, 3H, ArH), 9.26 (s, 1H, ArH), 9.23 (s, 1H, ArH), 9.19 (s, 1H, ArH), 9.16 (s, 1H, ArH), 8.9 (s, 1H, ArH), 7.8 (d, J=6, 1H, ArH), 4.7 (t, *J*=6 Hz, 2H, OCH_2), 4.4 (t, *J*=6 Hz, 2H, CH_2O), 3.5 (s, 2H, $O_2CCH_2CO_2$), 3.4-3,3 (m, 12H, alkylH), 2.2- 2.1 (m, 16H, alkylH), 1.9-1.3 (m, 112H, alkylH), 1.1-0.9 (m, 18H, alkylH).

Zinc (II) 9,10,16,17,23,24-hexadodecyl-2(6`-hexyloxy,3``-octylmalonate) phthalocyaninato (2-)-N^{29}, N^{30}, N^{31}, N^{32} (**43**)

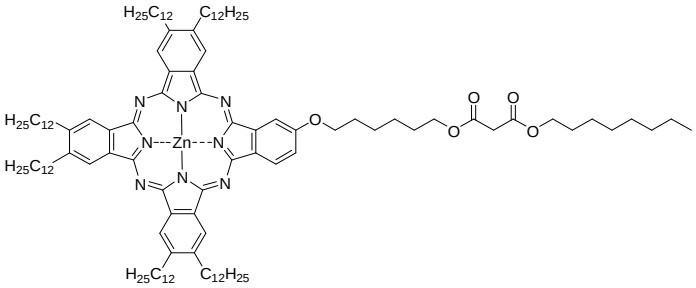

A mixture of Pc **42** (64 mg, 0.035 mmol), 1-octanol (3.79 mg, 0.029 mmol) and DCC (18 mg, 0.087 mmol) in THF (5 ml) was cooled to 0 ^{o}C under argon atmosphere. A solution of DMAP (1.77 mg, 0.014 mmol) in THF (2 mL) was then added dropwise. The mixture was stirred at 0 ºC for 1h and then warmed up to room temperature stirring was continued for 24h. The solvent was removed, and the residue was washed with MeOH. The crude product was purified by column chromatography on silica gel (toluene-THF, 10:1) to yield Pc **43** (40 mg, 0.021 mmol). Yield: 52%.

Mp> 250ºC.

^{1}HNMR (d_8-THF, 300 MHz): δ (ppm)= 9.35-9.28 (m, 3H, ArH), 9.25 (s,1H, ArH), 9.22 (s, 1H, ArH), 9.1 (s, 1H, ArH), 9.14 (s, 1H, ArH), 8.9 (s, 1H, ArH), 7.8(d, *J*=8 Hz, 1H, ArH), 4.7 (t, *J*=6 Hz, 2H, OCH_2), 4.4 (t, *J*=6 Hz, 2H, CH_2O), 4.2 (t, *J*=9 Hz, 2H, OCH_2), 3.5 (s, 2H, $O_2CCH_2CO_2$), 3.4-3,3 (m, 12H, alkylH), 2.2- 2.1 (m, 16H, alkylH), 1.9-1.3 (m, 124H, alkylH), 1.2-0.8 (m, 21H, alkylH).

HRMS (MALDI-TOF, dithranol): calc. for $C_{121}H_{190}N_8O_5Zn$: $[M]^+$: m/z: 1899.4145, found 1899.4114.

Zinc (II) 9,10, 16, 17, 23, 24- hexadodecyl -2 (6`-hexyloxy-2``-methano-[60]-fullerene 3``-octylmalonate] phthalocyaninato (2-)-N^{29}, N^{30}, N^{31}, N^{32} (**44**)

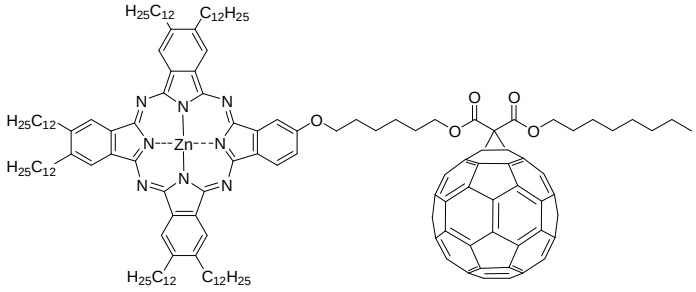

2

To a solution of C_{60} (27 mg, 0.038 mmol) in dry toluene (5 mL), a solution of Pc **43** (36 mg, 0.019 mmol) in THF (1 ml), CBr_4 (6.3 mg, 0.019 mmol), and DBU (8.5 µl, 0.056 mmol) were added. The mixture was stirred at room temperature overnight, and then evaporated to dryness. Purification of the solid residue by column chromatography (first with toluene and then with toluene/THF (10:1)), followed by size-exclusion column chromatography (THF) gave pure PcC_{60} **44** (20 mg, 0.0076 mmol). Yield: 40%.

Transition temperature: Cr-Col_r :80 ºC, Col_r-Iso:185 ºC.

^{1}HNMR (d_8-THF, 300 MHz): δ (ppm)= 9.37-9.34 (m, 3H, ArH), 9.3 (s, 1H, ArH), 9.27 (s, 2H, ArH), 9.24 (s, 1H, ArH), 8.9 (d, *J*=3 Hz, 1H, ArH), 7.8 (d, *J*=9 Hz, 1H, ArH), 4.8-4.6 (m, 6H, OCH_2), 3.4-3,3 (m, 12H, alkylH), 2.2- 2.1 (m, 16H, alkylH), 1.9-1.3 (m, 124H, alkylH), 1.2-0.8 (m, 21H, alkylH).

IR (KBr): ν (cm^{-1}) = 3448, 2955, 2921, 2850, 1745, 1608, 1408, 1465, 1338, 1097.

UV/Vis (THF): λmax (log ε) = 678 (5.3), 614 (4.6), 349 (5.0).

HRMS (MALDI-TOF, dithranol): calc. for $C_{181}H_{188}N_8O_5Zn$: $[M]^+$: m/z: 2617.3989, found 2617.3940.

Synthesis of Phthalocyanine-C_{60} 46

Zinc(II) 1`,3`–Bis-{[9,10,16,17,23,24-hexadodecyl]2(hexyloxy)phthalocyaninato} malonate (**45**)

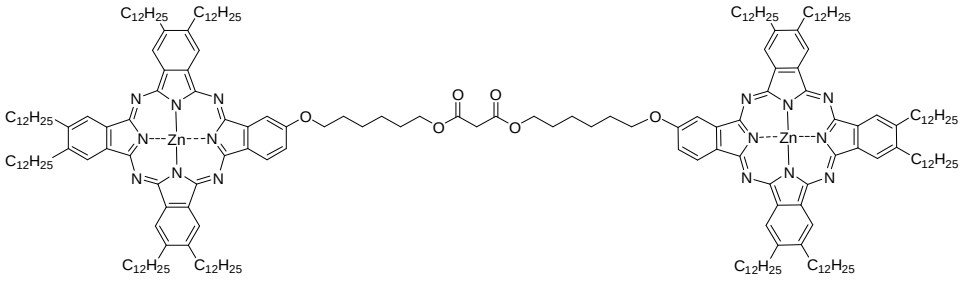

To a solution of Pc **39** (50 mg, 0.029 mmol) and malonyl chloride (1,4 µl, 0.014 mmol) in THF (5 mL), TEA (4.04 µl, 0.029 mmol) was added. The mixture was stirred at room temperature overnight, and then evaporated to dryness. Purification of the solid residue by column chromatography (toluene/THF, 10:1) gave pure Pc **45** (25 mg, 0.0072 mmol) as a green solid. Yield: 49%.

Transition temperature: Cr-Col_h:70 ºC, Col_h-Iso: ~298 ºC

^{1}HNMR (d_8-THF, 300 MHz): δ (ppm)= 9.07 (s, 2H, ArH), 9.03 (s, 2H, ArH), 8.76 (d, *J*=9 Hz, 2H, ArH), 8.68 (s, 2H, ArH), 8.61 (s, 2H, ArH), 8.5 (s, 2H, ArH), 8.4 (s, 2H, ArH), 8.3 (s, 2H, ArH), 7.5 (d, *J*=9 Hz, 2H, ArH), 4.6 (t, *J*=6 Hz, 4H, OCH_2), 4.5 (t, *J*=6 Hz, 4H, CH_2O), 3.6 (s, 2H, $O_2CCH_2CO_2$), 3.4-3,3 (m, 24H, alkylH), 2.2- 2.1 (m, 32H, alkylH), 1.9-1.3 (m, 224H, alkylH), 1.1-0.9 (m, 36H, alkylH).

IR (KBr): *v* (cm^{-1}) = 2928, 2847, 1738, 1603, 1464, 1342, 1234, 1103, 1090, 870.

UV/Vis (THF): λ_{max} (log ε) = 678 (5.28), 632 (5.03), 343 (5.15).

HRMS (MALDI-TOF, dithranol): calc. for $C_{223}H_{344}N_{16}O_6Zn_2$: $[M]^+$: m/z: 3472.5722 found 3472.5518.

Zinc(II) 1`, 3` –Bis-{ [9,10,16,17,23,24-hexadodecyl]-2(hexyloxy)phthalocyaninato-2`-methano-[60]-fullerene} malonate (**46**)

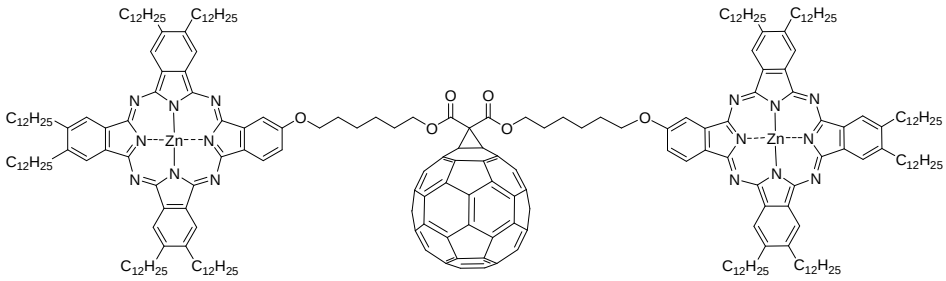

To a solution of fullerene (14.51 mg, 0.02 mmol) in dry toluene (5 mL), were added bisPc **45** (35 mg, 0.01 mmol) in THF (1 ml), I_2 (2.5 mg, 0.01 mmol), and DBU (3 µl, 0.02 mmol). The mixture was stirred at room temperature overnight and then evaporated to dryness. Purification of the solid residue by column chromatography (first with toluene and then with toluene/THF, 10:1), followed by size-exclusion column chromatography (THF) gave pure bisPc-C_{60} **46** (5 mg, 0.0012) as a green solid. Yield: 12%.

Mp> 250ºC.

^{1}HNMR (d_8-THF, 300 MHz): δ (ppm)= 9.06 (br.s, 2H, ArH), 9.02 (br.s, 2H, ArH), 8.8-8.7 (m, 4H, ArH), 8.6-8.5 (m, 4H, ArH), 8.4 (s, 2H, ArH), 8.3 (s, 2H, ArH), 7.6 (s, 2H, ArH), 4.7-4.6 (m, 8H, OCH_2), 3.4-3,3 (m, 24H, alkylH), 2.2- 2.1 (m, 32H, alkylH), 1.9-1.3 (m, 224H, alkylH), 1.1-0.9 (m, 36H, alkylH).

IR (KBr): ν (cm^{-1}) = 3442, 2956, 2920, 2851, 1750, 1646, 1609, 1466, 1432, 1339, 1105.

UV/Vis (THF): λ_{max} (log ε) = 679 (5.2), 632 (5.0), 339 (5.1).

HRMS (MALDI-TOF, dithranol): calc. for $C_{283}H_{342}N_{16}O_6Zn_2$: $[M]^+$: m/z: 4188.5526 found 4188.5649.

Synthesis of Pc-C_{60}-Dendrimer Dyad (49)

Poly(benyzy ether) malonic acid (**47**)[174f]

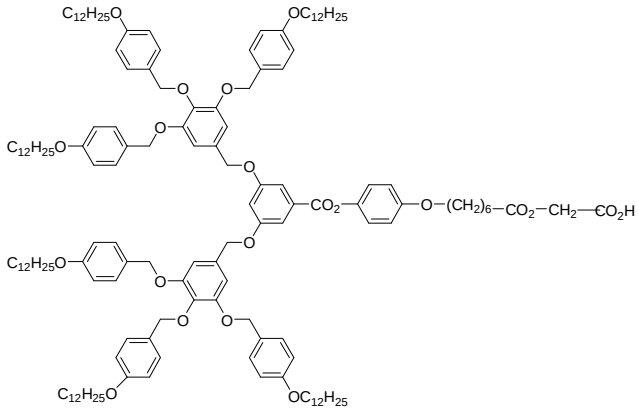

A solution of poly(benyzy ether) dendrimer (1.37g, 0.6 mmol) and meldrum acid (872mg, 6mmol) in toluene (200 ml) was stirred at 65 Cº for 24h and evaporated to dryness. After precipitation (dissolution in small volume of CH_2Cl_2 and precipitation by pouring the solution into MeOH) compound **47** (1.25 g) was obtained in a pure form as a white solid. Yield: 88%.

^{1}HNMR ($CDCl_3$, 300 MHz): δ (ppm)= 7.4 (d, *J*=3 Hz, 2H), 7.2 (d, 12H), 7.0 (d, *J*=9 Hz, 2H), 6.9-6.8 (m, 11H), 6.77-6.74 (m, 8H), 5.0-4.9 (m, 12H), 4.93 (s, 4H), 4.2 (t, *J*=9 Hz 2H), 3.9-3.8 (m, 14H), 3.4 (s, 2H), 1.7-1.6 (m, 16H), 1.4-1.2 (m, 112H), 0.8 (t, *J*=6 Hz 18H).

[174] f) N. Maringa, J. Lenoble, B. Donnio, D. Gullion, R. Deschenaux, *J. Mater. Chem.* **2008**, *18*, 1524.

1`- Poly(benzyl)ether -3`-{[9,10,16,17,23,24-hexadodecyl]2(hexyloxy)phthalocyaninato Zinc(II)}- malonate) (**48**)

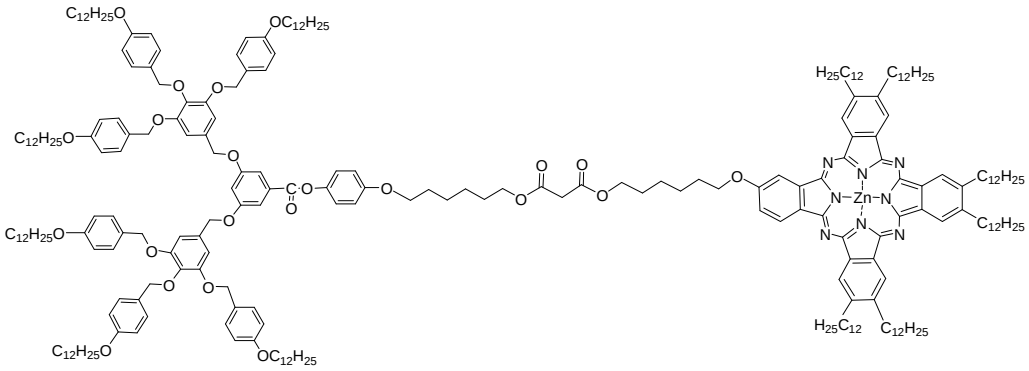

A mixture of **47** (30 mg, 0.012 mmol), Pc **39** (26 mg, 0.015 mmol), DCC (7.8 mg, 0.04 mmol), DPTS (3.7 mg, 0.012 mmol), and 4-Ppy (0.5 mg, 0.038 mmol) in CH_2Cl_2/THF (3:1) was stirred overnight under argon atmosphere at room temperature. The reaction mixture was then evaporated and the residue was purified by column chromatography on silica gel (first with CH_2Cl_2-Et_2O, 10:0.1 then by size-exclusion column chromatography (THF). Compound **48** (30 mg, 0.0074 mmol) was obtained as a green solid. Yield: 58 %.

Transition temperature: Cr-Col_h:74 ºC, Col_h- Iso: ~ 300 ºC.

^{1}HNMR (d_8-THF, 300 MHz): δ (ppm)= 9.4-9.33 (m, 3H, ArH-Pc), 9.3 (s, 1H, ArH-Pc), 9.28 (s, 1H, ArH-Pc), 9.23 (s, 1H, ArH-Pc), 9.2 (s, 1H, ArH-Pc), 9.0 (s, 1H, ArH-Pc), 7.8 (dd, *J*=3, 9 Hz, 1H, ArH-Pc),7.5-7.4 (m, 16H, ArH-Dend), 7.3 (d, *J*=9 Hz, 2H, ArH-Dend), 7.0 (d, *J*=9 Hz, 9H, ArH-Dend), 6.9 (s, 4H ArH-Dend), 6.8 (d, *J*=9 Hz, 4H, ArH-Dend), 5.1 (s, 12H, OCH_2Ph), 5.0 (s, 4H, OCH_2Ph), 4.7 (t, 2H, CH_2O) 4.4 (t, 2H, OCH_2), 4.3 (t, 2H, CH_2O) 4.2-4.0 (m, 14H, OCH_2Ph), 3.5 (s, 2H, $O_2CCH_2CO_2$), 3.4-3,2 (m, 12H, alkylH(Pc)), 2.3- 1.8 (m, 32H, alkylH), 1.7-1.3 (m, 224H, alkylH), 1.2-0.8 (m, 36H, alkylH).

IR (KBr): *v* (cm^{-1}) = 2924, 2856, 1732, 1610, 1520, 1466, 1371, 1331, 1250, 1169, 1101, 1034, 831, 725.

UV/Vis (THF): λ_{max} (log ε) = 679 (5.31), 654 (4.49), 612 (4.53), 350 (4.87).

HRMS (MALDI-TOF, ditranol): calc. for $C_{260}H_{386}N_8O_{22}Zn$: $[M]^+$: m/z: 4036.8618 found 4036.8707.

1`- poly(benzyl)ether -2`-methano-[60]-fullerene-3`-{[9,10,16,17,23,24-hexadodecyl] 2(hexyloxy) phthalocyaninato Zinc(II)}- malonate) (**49**)

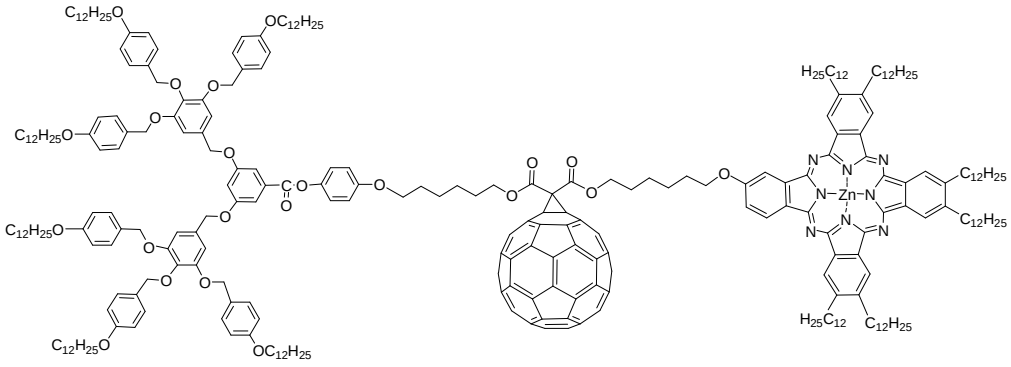

To a solution of fullerene (9 mg, 0.012 mmol) in dry toluene (5 ml), were added Pc-Dend **48** (25 mg, 0.0061 mmol) in THF (2 ml), I_2 (1.5 mg, 0.061 mmol), and DBU (3 µl, 0.02 mmol). The mixture was stirred overnight at room temperature under argon atmosphere and then evaporated to dryness. Purification of the solid residue by column (first with toluene and then with toluene/THF 10:1, followed by size-exclusion column chromatography (THF) gave pure Pc_2-C_{60} **49** (8 mg, 0.0016 mmol). Yield: %27.

Mp> 250ºC.

^{1}HNMR (d_8-THF, 300 MHz): δ (ppm)= 9.4-9.3 (m, 9H, ArH-Pc) ,7.5-7.3 (m, 15H, ArH-Dend), 7.0-6.9 (m, 20H, ArH-Dend), 5.1-4.9 (m, 16H), 4.0-3.8 (m, 20H), 3.4-3.3 (m, 12H), 2.0-1.1 (m, 256H), 1.2-0.8 (m, 36H).

IR (KBr): ν (cm^{-1}) = 2926, 2858, 1740, 1605, 1510, 1470, 1375, 1335, 1240, 1173, 1105, 822, 727.

UV/Vis (THF): λmax (log ε) = 680 (5.19), 654 (4.57), 615 (4.51), 346 (5.02).

MALDI-TOF MS (DCTB): m/z 4755.2 $(M+H)^+$.

Chapter 2. Porphyrinoids for Dye Sensitized Solar Cells

2.1. Introduction

As stated in the general introduction, dyes like porphyrinoids which have a high molar extinction coefficient in the red/near infrared region have recently received much attention for their application in the field of DSSCs. Among them, a very high efficiency up to 11 % has been achieved by rational design of the push–pull porphyrin dye (YD2, Figure 118) bearing an electron-donating diarylamino group at one meso position opposite to the binding 4-ethynylbenzoic acid moiety. Bulky substituents are located in the two remaining meso positions.[94] A record power conversion efficiency of 12.3% in this family of porphyrin sensitizers has been recently reported by the same authors using a related dye (YD2-o-C8) and an organic dye as cosensitizer.[183] These results demonstrate that a careful choice of the appropriate substituted porphyrins may yet offer a feasible alternative the most commonly used ruthenium dyes. Unfortunately, the photophysical stability of these porphyrin dyes is not very high, but these results are the most important proof of concept for future applications of porphyrinoids in DSSCs.

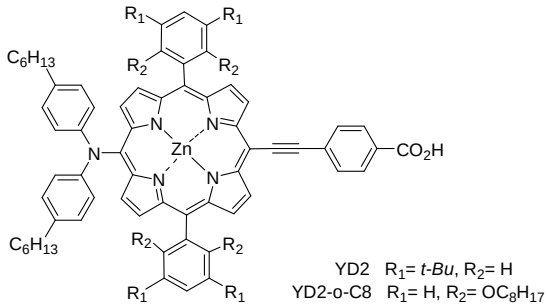

Figure 118. Molecular structure of high efficient porphyrin sensitizers YD2 and YD2-o-C8.

The introduction of different substituents at the peripheral or non-peripheral positions of phthalocyanines produces, among others, important changes in the Q-band absorption and the aggregation properties of these macrocycles, and modification in the HOMO-LUMO levels. Up to very recently, *tert*-butyl peripheral groups have proved to

94 T. Bessho, S. M. Zakeeruddin, C. Y. Yeh, E. W. G. Diau, M. Grätzel, *Angew. Chem. Int. Ed.* **2010**, *49*, 6646.

183 A. Yella, H. W. Lee, H. N. Tsao, C. Yi, A. K. Chandiran, M. K. Nazeeruddin, E. W. G. Diau, C. Y. Yeh, S. M Zakeeruddin, M. Grätzel, *Science*, **2011**, *334*, 629.

be the best compromise to get good Pc dye solubility, low aggregation tendency, and a "push-pull" character to induce directionality in the Pc excited state. Indeed, there are only few reports studying the influence of the peripheral substituents on the photovoltaic performance of Pc-sensitized solar cells, and still a rational trend has not been found.[184] For instance, the introduction of six strong electron-donor α-butoxy groups in Pcs leads to remarkably low overall devices efficiencies (ca. 1 %)[184a] (Figure 119a). Since this Pc sensitizer does not show any particular strong tendency to form aggregates, a possible explanation to these results might be a low electron-injection yield consequence of the modification of the dye HOMO-LUMO levels. On the other hand, recently, phthalocyanine-based DSSCs have reached efficiency values of 4.6% by employing a Pc derivative carrying bulky 2,6-diphenylphenoxy peripheral substituents (Figure 119b), which completely suppresses macrocycle aggregation when anchored to the TiO_2 film. This Pc derivative also bears a phenylene spacer to connect the macrocycle with the carboxylic anchoring group[185a] For the first time, Pc-based solar cells have achieved high efficiency without using CHENO as coadsorbent. In this case, the peripheral bulky groups avoid macrocycle aggregation and contribute to block the interactions between the Pc aromatic surface and the I_3^- electrolyte, thus reducing the dark current. The same authors have recently reported an improvement of the efficiency (5.3%) by using a related dye.[185b]

As mentioned in the general introduction, the use of conjugated spacers with the anchoring group results in important changes in the overall conversion efficiency for both porphyrin and phthalocyanine sensitizers. In particular, ethynyl bridges have proved to be very effective for connecting the Pc or Por π-system with the carboxylic anchoring group. In this regard, by using ZnPc substituted with peripheral diphenylphenoxy groups and an ethynyl bridge between the anchoring carboxy group and the Pc macrocycle (TT40 in Fig 119c), our group has reported very recently the highest efficiency - 6.1% - ever described for a Pc-based solar cell.[186] This high

[184] a) L. Giribabu, Ch. Vijaykumar, V. G. Reddy, P. Y. Reddy, Ch. S. Rao, S-R. Jang, J. H. Yum, M. K. Nazeeruddin, M. Grätzel, *Sol. Energy Mater. Sol. Cells* **2007**, *91*, 1611. b) S. Eu, T. Katoh, T. Umeyama, Y. Matano, H. Imahori, *Dalton Trans.* **2008**, 5476.

[185] a) S. Mori, M. Nagata, Y. Nakahata, K. Yasuta, R. Goto, M. Kimura, M. Taya, *J. Am. Soc,* **2010**, *132*, 4054. b) M. Kimura, H. Nomoto, N. Masaki, S. Mori, Angew. *Chem. Int. Ed***. 2012,** *51*, 4371.

[186] M. E. Ragoussi, J. J. Cid, J. H. Yum, G. de la Torre, D. Di Censo, M. Grätzel, M. K. Nazeeruddin, T. Torres, *Angew. Chem. Int. Ed*. **2012**, *51*, 4375.

efficiency can be attributed to benefits of the ethynyl moiety as a bridge for optimal electronic coupling between the ZnPc and TiO_2. The compound is highly stable under light.

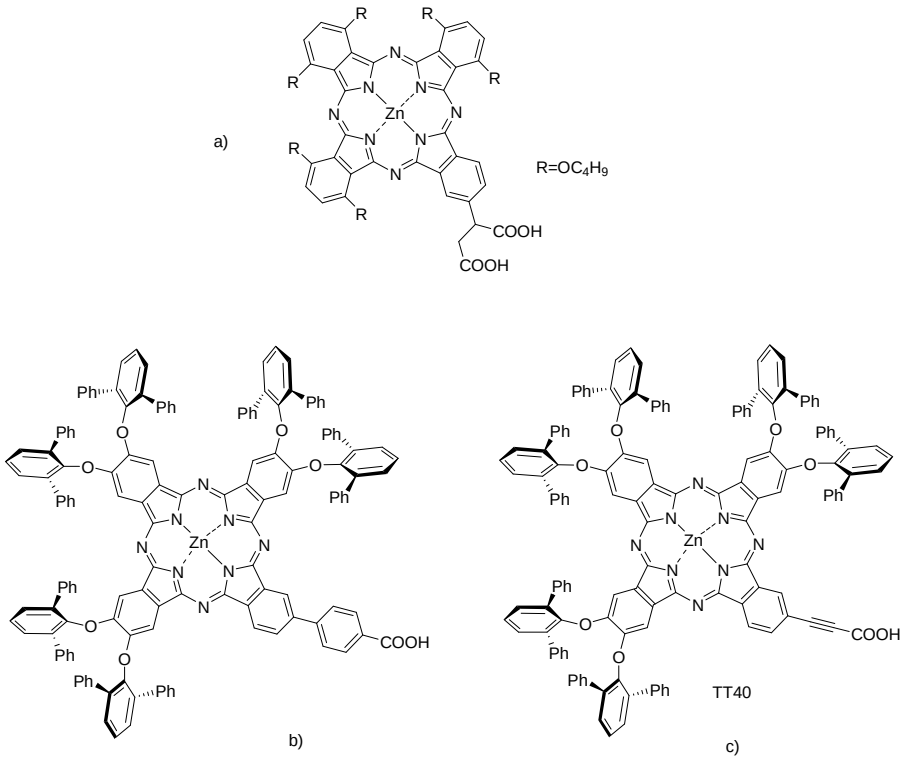

Figure.119. Molecular structure of Pc sensitizers bearing a) α-alkoxy and b, c) bulky β-aryloxy substituents.

2.2. Objectives

NIR-IR dyes are gaining popularity in the field of photovoltaics. Since photocurrent density is directly related to the absorption ability of organic materials, a higher short circuit current should be achieved if the absorption of the dye is extended to the near infrared. As already mentioned, phthalocyanine derivatives constitute ideal structures as absorbers in a wide region of the electromagnetic spectrum. The past decade has seen increasing attention being paid to the synthesis of novel Pc derivatives, with the aim of both studying in detail the structure-property relationship

and fulfilling the essential requirements of efficient sensitizers for DSSCs. In order to achieve this goal, our group has been focused toward designing novel Pc dyes with the following features:

- Increasing the light harvesting ability
- Preventing aggregation onto the TiO_2 surface
- Lowering the HOMO level (slightly below the redox potential of the electrolyte) to minimize the recombination between the sensitizer and electrolyte and to maximize the photovoltage

On this connection, two main objectives (A and B) were defined for this work:

A. Preparation of novel peripherally substituted Pcs

Although many Pc derivatives peripherally substituted with *ter*t-butyl groups have been prepared, there are only a few reports on the influence of the other electron donating and electron accepting groups on the photovoltaic performance of Pc sensitized solar cells as mentioned before. Novel Pc derivatives which either bear triarylamine-terminated bisthiophene or hexylbisthiophene, or electron deficient alkylsulfonyl units were designed as targets of our work (Figure 120). Moreover, electron deficient Pcs could be possible candidates as electroactive units in p-type DSSCs.

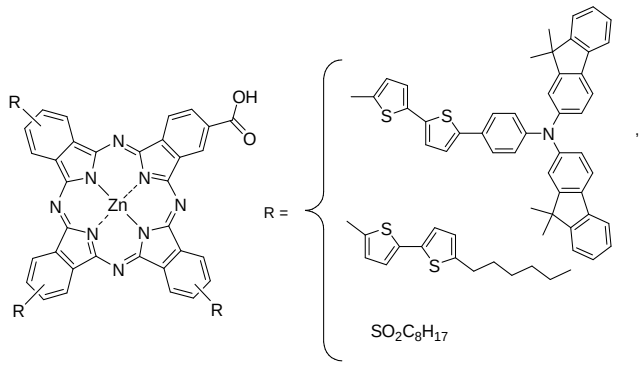

Figure 120. Molecular structure of electron-deficient and electron-donating Pcs.

B. Stuctural modification of the Pc ring system

The chemical flexibility of Pcs from the structural point of view allows the formal replacement of one or more of their isoindol units by other hetero- or carbocycles. This fact has been exploited in the preparation of novel Pc derivatives, with different absorption properties in order to match with the terrestrial solar emission spectrum. For instance, as mentioned in Chapter 1.2, the replacement of the four benzene rings in a Pc by azulene units greatly alters the electronic structure, as proved by the dramatic difference between the absorption spectra of Pc and azulenocyanine. Azulenocyanine exhibits absorption which extends into the near-IR due to the small HOMO-LUMO band gap. Such properties may allow its application as a sensitizer for dye sensitized solar cells. Since one of the main purposes of this work is to increase the light harvesting ability in the NIR, a series of azulenocyanine-phthalocyanine mixed compounds having a carboxyl group either directly linked to the macrocycle ring or through π-conjugated bridges were designed. The initial synthetic targets were the azulenocyanines shown in Figure 121.

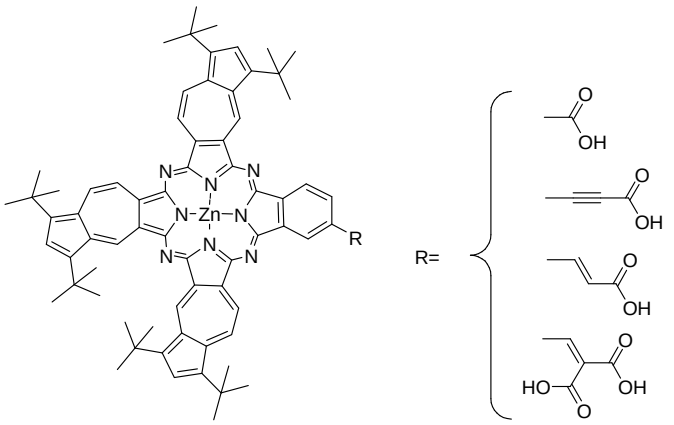

Figure 121. Molecular structure of carboxyazulenocyanine derivatives proposed

On the other hand, as already discussed in the general introduction, the formal removal of one isoindol unit from the Pc skeleton leads to the SubPc analogues. This change causes a hypsochromic shift in the Q- band in the electronic spectra to around 550-600 nm, leading to purple colored macrocycles. In addition, the aggregation

problems always associated with Pcs are suppressed, due to the non-planar aromatic structures of SubPs. Even though SubPcs have proven to be promising candidates as donor material for small molecule organic solar cells due to their lower oxidation potential, there has been no report on the immobilization of SubPc on nanocrystalline TiO_2 up to now. Therefore, the characteristic features of SubPcs encouraged us to investigate dye sensitized solar cells using SubPcs as a light harvesting material. Two derivatives were designed to incorporate into DSSC devices (Figure 122).

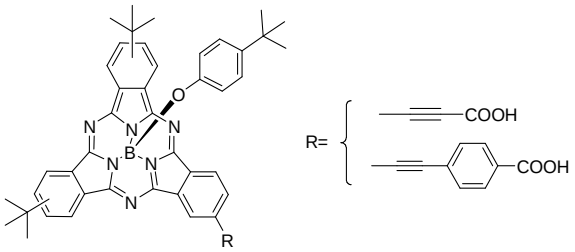

Figure 122. Molecular structure of Subphthalocyanines designed for DSSCs.

2.3. Peripherally Substituted Pcs for DSSCs

2.3.1. Synthesis of Electron-Donor Phthalocyanines

ZnPc **53** and **54** were synthesized by a new convergent approach, based on the key preparation a carboxytriiodo-ZnPc **52**, and subsequent introduction of the peripheral π-conjugated substituents by Suzuki cross-coupling reactions.

The statistical cross condensation of 4-iodophthalonitrile[111](**2**) and 4-hydroxymethylphthalonitrile[141](**20**) in the presence of $Zn(OAc)_2$ in DMAE yielded the unsymmetrically substituted ZnPc **50** in 23% yield.

[111] a) H. Lam, S. M. Marcuccio, P. I. Svirskaya. S. Greenberg, A. B. P. Lever, C. C. Leznoff, R. L. Cerny, Can. J. Chem. **1989**, *67*, 1087. b) J. G. Young, W. Onyebuagu, *J. Org. Chem.* **1990**, *55*, 2155.

[141] R. F. Enes, J. J. Cid, A. Hausmann, O.Trukhina, A. Gouloumis, P. Vazquez, J. A. S. Cavaleiro, A. C. Tomé, D. M. Guldi, T.Torres, *Chem. Eur. J*. **2012**, *18*, 1727.

After purification by column chromatography, ZnPc **50** was subjected to oxidation in the presence of the periodinane derivative IBX in DMSO to yield formyl ZnPc **51** in 64% yield. Using sodium chlorite in the presence of sulfamic acid, as hypochlorite scavenger, ZnPc **51** was converted to ZnPc **52** in 60% yield (Scheme 25).

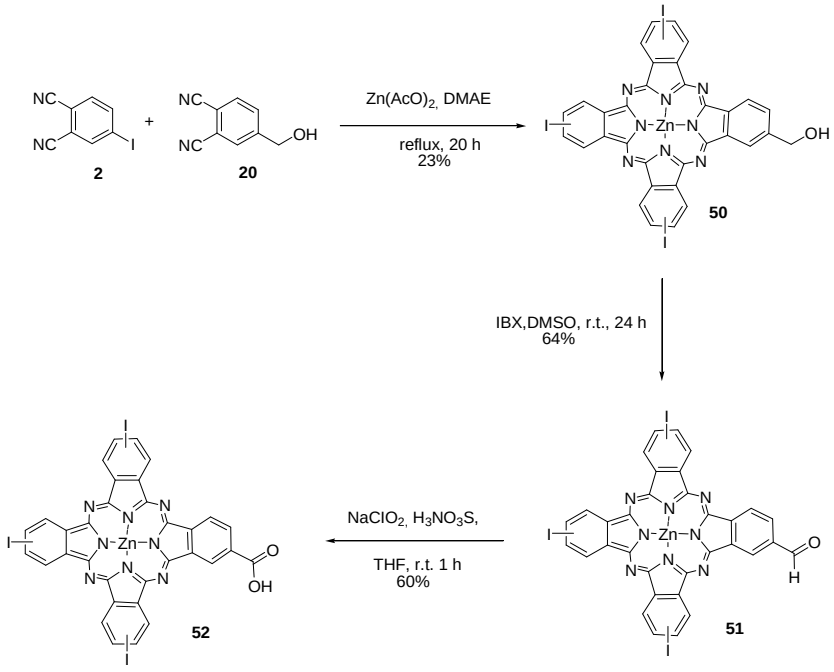

*Scheme 25. Synthesis of triiodocarboxylZnPc (**52**).*

Tetrasubstituted Pcs obtained by the statistical method starting from two different phthalonitriles substituted in position 4, as it is the case above, are constituted by a maximum of eight regioisomers in a ratio that strongly depends on the stoichiometry of the reactants. Therefore, Pc **50**, and consequently **51** and **52** are indeed mixtures of eight regioisomers that could not be separated by chromatography.

The triarylamine-terminated bisthiophene boronic acid pinacol ester **53a** was synthesized in our laboratory according to literature procedures[187] whereas

[187] a) S. Kim, K. Song, S. Kang, J. Ko, *Chem. Commun*. **2004**, 68. b) M. Ince, F. Cardinali, J. H. Yum, M. V. Martínez-Díaz, M. K. Nazeeruddin, M. Grätzel, T. Torres, *Chem. Eur. J.* **2012**, *18*, 6343.

hexylbisthiophene boronic acid **53b** was commercially available. The Suzuki cross-coupling reactions between ZnPc **52** and the corresponding boronates, were performed in the presence of [$Pd(PPh_3)_4$] as catalyst in DME (Scheme 26). ZnPcs **54** and **55** were obtained in 36 % and 43 % yields, respectively, after final purification by size exclusion chromatography.

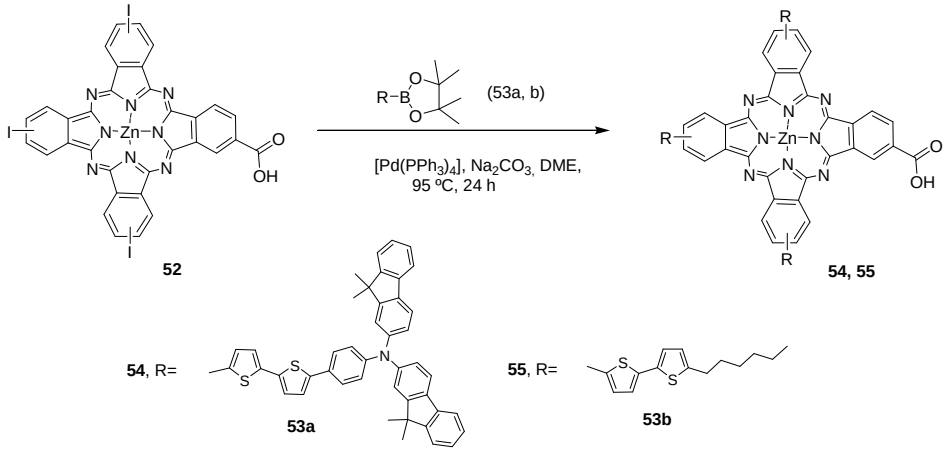

*Scheme 26. Synthesis of phthalocyanines **54** and **55**.*

The structures of all new Pcs were confirmed by IR, UV-Vis and MALDI-TOF spectroscopies.^{1}H-NMR spectra of triiodoPcs **50-52** in d_8-THF gave well-resolved peaks between 8.5 and 9.7 ppm for the Pc aromatic macrocycle. Figure 123 shows the ^{1}H-NMR spectrum of compound **52** as an example. However, the strong aggregation of ZnPcs **54** and **55** in common organic solvents such as $CHCl_3$ and THF caused very broad and uninformative resonances. Nevertheless, the integration of the assignable signals is consistent with the expected values.

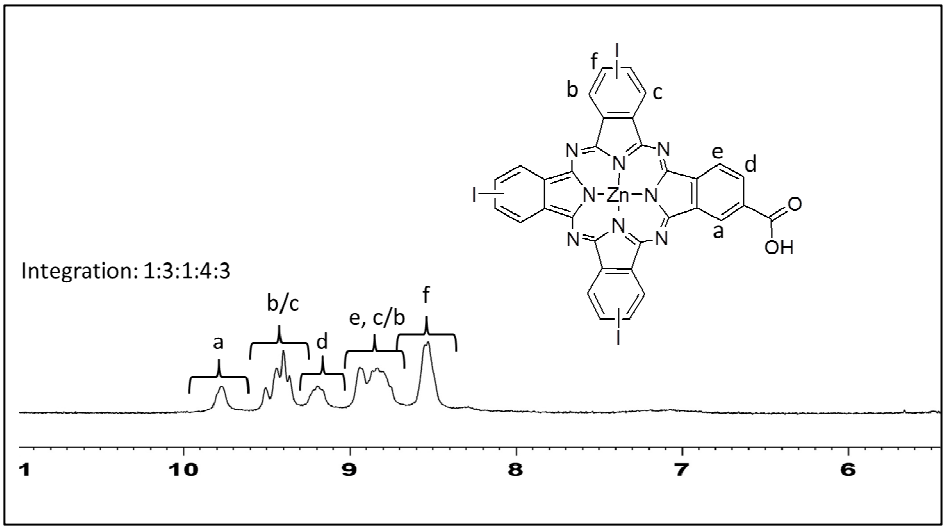

*Figure 123. Aromatic part of the ^{1}H-NMR spectrum of compound **52** in d_8-THF.*

The new ZnPcs **54** and **55** show an extended π-conjugated system which produces an important red shift in the absorption maximum of ca. 30 nm, in comparison to that of TT1 (Figure 124). The UV/Vis spectrum of TT1 shows a Q-band at 679 nm, while compounds **54** and **55** show a maximum absorbance at 707 and 702 nm, respectively. Both Pcs, **54** and **55**, additionally present a broad absorption around 400-500 nm, which is assigned to the π-conjugated bisthiophene peripheral substituent. This absorption becomes more intense in the case of derivative **54**. Aggregation of **54** is easily detected from optical absorption studies, which result in a broad absorption and a decrease of the extinction coefficient of the Q-band. The tail of the absorption extends to 850 nm and **54** covers a broad range in the Vis/NIR region, in which conventional Pcs do not exhibit absorption. This behaviour could infer important advantages to these new Pc dyes, which could lead to increasing the photocurrent for the application of these compounds in photovoltaic devices.

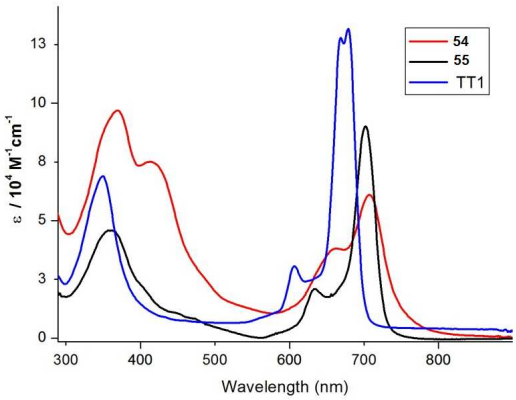

*Figure 124. UV/Vis spectra in THF (1 x 10^{-5} M) of Pcs **54** and **55** compared to that of TT1.*

As mentioned before, Pc **52** could be a mixture of up to eight regioisomers, since it comes from **50**. Therefore, **54** and **55** could be constituted by several regioisomers. Different regioisomers could have, in principle, different properties as DSSC sensitizers.

2.3.2. Photovoltaic Studies of Pc 54 and 55

Dye sensitized solar cells based on Pc **54** and **55** dyads were prepared in collaboration with Prof. Michael Grätzel *(EPFL,* Switzerland*)* during a predoctoral stay of the candidate.

Tables 6, 7 and 8 summarize the I-V [short-circuit currents (Jsc), open-circuit voltages (Voc), fill factors (FF) and conversion efficiencies (η)] of the DSSCs in various conditions. Table 6 shows the photovoltaic performance of dyes **54** and **55** in DSSC devices using standard mesoporous double TiO_2 films (6 μm thick transparent films) and a volatile acetonitrile-based electrolyte. Pcs dye solutions were prepared in THF at a concentration of 0.1 mM without coadsorbent, CDCA (chenodeoxyclic acid), and with 2 mM and 10 mM CDCA. The films were immersed into a dye solution for 5 h at room temperature. The short-circuit photocurrent density (J_{sc}) (from 3.26 to 5.25 mA/cm^2 for **54** and from 3.65 to 4.96 mA/cm^2 for **55**) and the open circuit voltage (V_{oc}) both for **54** and **55** Pc-sensitized cells increased with a concentration of 2mM of CDCA in

comparison to that of no CDCA. The highest power conversion efficiencies, 2.07% and 1.98%, for **54** and **55**, respectively, were achieved with 2 mM CDCA. When the concentration of CDCA in the dye solution increased to 10 mM, the cells gave a lower short circuit photocurrent density (J_{sc}) (4.17 mA/cm^2 for **54** and 4.46 mA/cm^2 for **55**), resulting in a decrease of the overall efficiency, even though the open circuit voltage (V_{oc}) increased.

Table 6. Effect of a coadsorbent on Pc-sensitized DSSCs[a]

Dye	CDCA (mM)	*Jsc* (mA/cm^2)	*Voc* (mV)	*FF*	η (%)
54	0	3.26	503	0.68	1.11
	2	5.25	541	0.73	2.07
	10	4.17	554	0.75	1.72
55	0	3.65	525	0.71	1.36
	2	4.96	543	0.74	1.98
	10	4.46	549	0.74	1.82

[a] *TiO_2 thickness: 6 μm, Dye concentration: 0.1mM , Dipping time: 5h, Electrolyte: M1*

The low photocurrent in high concentration of CDCA could result from fewer adsorbed dye molecules, due to CDCA's competitive adsorption with dyes. Figure 125 shows the photocurrent–voltage curves of compound **53** and compound **54** sensitized solar cells.

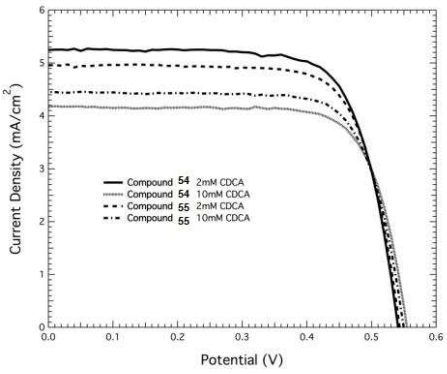

*Figure 125. Photocurrent density-voltage (J-V) characteristics of ZnPcs **54** and **55** sensitized DSSCs in the presence of CDCA.*

To test the effect of electrolyte, devices at 0.1 mM concentration of **54** and **55** solutions and 2mM concentration of CDCA in THF were prepared. Table 7 shows the photovoltaic performance of **54** and **55** sensitized solar cells in the presence of either M1 or A6986 electrolytes. The electrolytes compositions were follows:

M1: 0.6 M methyl-*N*-butylimidazolium iodide, 0.04 M iodine, 0.025 M LiI, 0.05 M guanidinium thiocyianate, and 0.28 M tert-butylpyridine in a 15/85 (v/v) mixture of valeronitrile and acetonitrile.

A6986: 0.6 M *N*-butyl *N*-butylimidazolium iodide, 0.05 M iodine, 0.1 M LiI, and 0.05 M *tert*-butylpyridine in a 15:85 (v/v) mixture of valeronitrile and acetonitrile.

The devices, employing A6986, gave a higher short circuit photocurrent density (J_{sc}) of 7.35 and 7.05 mA/cm^2 for **54** and **55**, respectively, leading to a higher power conversion efficiency (from 2.07 to 2.49% for **54** and from 1.98 to 2.45% for **55**) while the open circuit voltage was relatively low. This lower V_{oc} and higher J_{sc} may explain by the presence of more Li^+ cations in the case of A6986. As discussed in the general introduction, the addition of more Li^+ cations in the electrolyte can provoke a positive shift of the TiO_2 conduction band potential because of the Li^+ cations adsorbed on the TiO_2 surface during the dye loading which induces the potential drop.

Table 7. Effect of the electrolyte on Pc-sensitized DSSCs[a]

Dye	Electrolyte	*Jsc* (mA/cm^2)	*Voc* (mV)	*FF*	η (%)
54	M1	5.25	541	0.73	2.07
	A6986	7.35	483	0.70	2.49
55	M1	4.96	543	0.74	1.98
	A6986	7.05	498	0.70	2.45

[a] TiO_2 thickness: 6 µm, Dye concentration: 0.1mM + 2mM CDCA, Dipping time: 5h.

In order to push the power conversion efficiency further, the scattering layer composed of bigger particles was incorporated on nano-TiO_2 layer. In DSSCs, the

energy conversion efficiency depends on the morphology and structure of the dye-adsorbed TiO_2 film. The high surface area of nanocrystalline TiO_2 shows better light harvesting due to the high quantity of the adsorbed dye. However, increasing the TiO_2 film thickness would cause more recombination of photo-injected electrons. Instead of using only nanocrystalline TiO_2 particle film, a bilayer structure consisting of a light scattering layer and a nanocrystalline semitransparent TiO_2 layer can improve photocurrent density due to the detention of incident light by light scattering particles resulting in the enhancement of the overall power conversion efficiency. With the bilayer having 6.8 + 5 (scattering) µm thickness, the short circuit current increased to 8.32 mA/cm^2 for **54** and 8.34 mA/cm^2 for **55**.

Table 8**.** Effect of a scattering layer on Pc-sensitized DSSCs[a]

Dye	CDCA (mM)	*Jsc* (mA/cm^2)	*Voc* (mV)	*FF*	η (%)
54	2	8.32	471	0.69	2.65
	10	8.18	490	0.71	2.85
55	2	8.34	466	0.69	2.70
	10	7.05	487	0.72	2.47

[a] TiO_2 thickness: 6.8 +5 (sc) µm, Dye concentration: 0.1 mM, Dipping time: 15h, Electrolyte: A6986

The power conversion efficiencies of the **54** and **55** sensitized-cells are improved to 2.65% and 2.70%, respectively. The current density-voltage curves and the incident photon-to-current efficiency (IPCE) spectra of **54** and **55** DSSCs are represented in Figure 126. The IPCEs show considerable high-energy photons absorption contribution, which is in agreement with absorption spectra in solution.

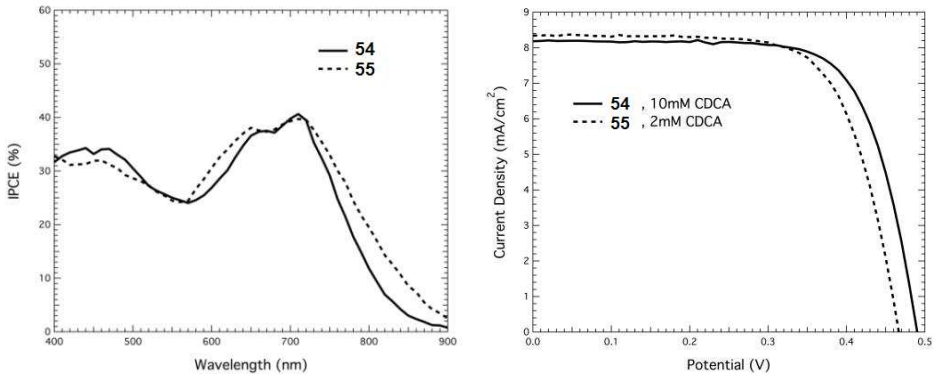

*Figure 126. IPCE spectrum and I-V curves for devices of **54** and **55** sensitized DSSCs.*

2.3.3. Synthesis and Electrochemical Properties of Electron-Deficient Phthalocyanines

The preparation of the tri(octylsulfonyl)carboxyZnPc (**58**) was attempted in two different ways (Scheme 27). The first strategy consisted of three steps. First, tri(octylsulfonyl)iodo ZnPc **17** was subjected to a Sonogashira coupling reaction with propargylic alcohol in the presence of triphenylarsine and [$Pd_2(dba)_3$], to give compound **56** in 65% yield. Then, compound **56** was treated with IBX in DMSO, giving rise to aldehyde derivative **57** in 75% yield. Compound **57** was transformed in the last step to carboxyl-Pc **58** by treating with $NaClO_2$/sulfamic acid in 48% yield (Scheme 27). Even though this strategy afforded compound **58** in good yield, is quite time-consuming and require multiple purification steps. A second direct route was therefore developed.

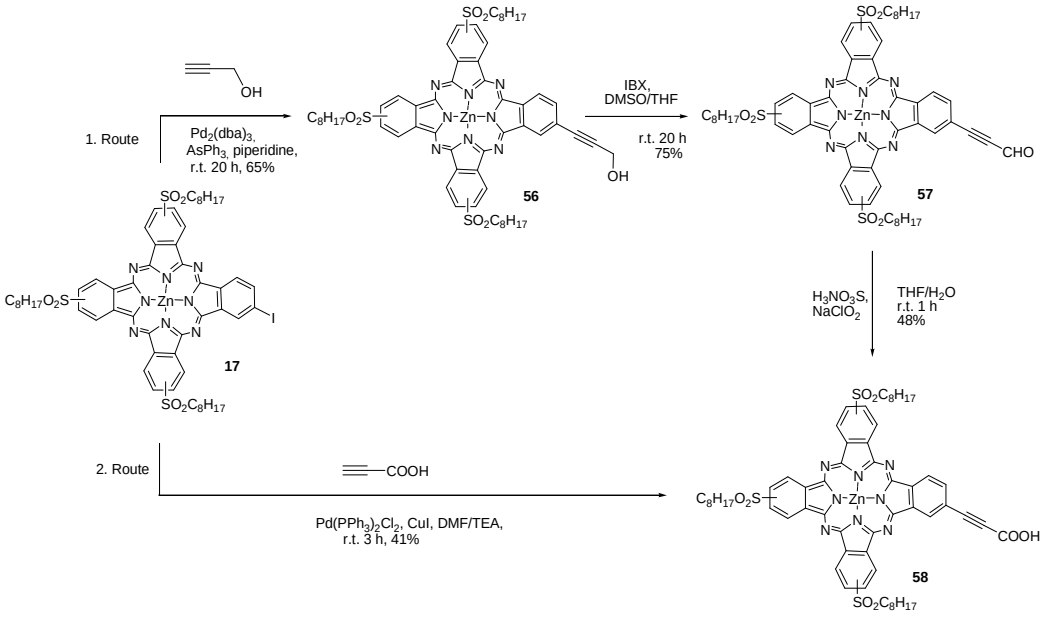

*Scheme 27. Synthesis of carboxytri(octylsulfonyl)ZnPc **58**.*

Thus, the one-pot Sonagashira coupling between tri(octylsulfonyl)iodoZnPc **17** and propargylic acid[188] was performed in the presence of $Pd(PPh_3)_2Cl_2$ and CuI in DMF at room temperature. Compound **58** was indeed obtained, however a significant amount of starting material was recovered. The polarity difference of the target compound and starting Pc allows an easy separation by column chromatography, which leads to 41% yield of ZnPc **58** (based on recovered starting tri(octylsulfonyl)iodo ZnPc **17**). For the same reason mentioned before for other tetrasubstituted Pcs, compound **58** could be a mixture of up to eight regioisomers, which could not be separated.

All new compounds were fully characterized by ^{1}H-NMR, UV-Vis, FT-IR and MALDI-TOF spectroscopies. The ^{1}H-NMR spectra of compound **58** in d_8-THF shows broad signals in the aromatic region as a consequence of the presence of many regioisomers and of strong aggregation.

[188] a) C. W. Lee, H. P. Lu, C. M. Lan, Y. L. Huang, Y. R. Liang, W. N. Yen, Y. C. Liu, Y. S. Lin, E. W. G. Diau, C. Y. Yeh, *Chem. Eur. J.* **2009**, *15*, 1403. b) C. F. Lo, S. J. Hsu, C. L. Wang, Y. H. Cheng, H. P. Lu, E. W. G. Diau, C. Y. Lin, *J. Phys. Chem. C.* **2010**, *114*, 12018.

The UV-Vis spectrum of compound **58** is depicted in Figure 127, and shows the Q-band centered at 676 nm.

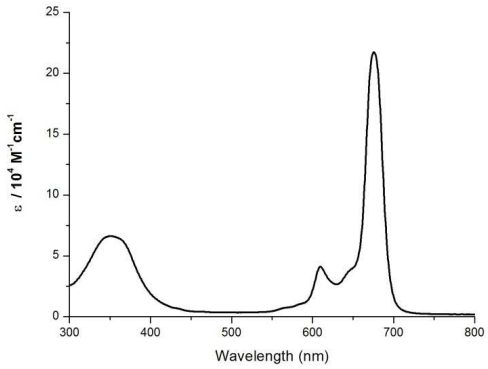

*Figure 127. UV-Vis spectrum of Pc **58** in THF~1x10^{-5}M.*

The redox behavior of the Pc **58** was studied by cyclic voltammetry (CV) using a platinum electrode in 0.1 M tetra (n-butyl)ammonium hexafluorophosphate ($TBAPF_6$) in dry CH_2Cl_2. The potentials were referred to Fc/Fc^+ as the internal reference. The electrochemical data of Pc **58** are summarized in Table 9. As shown in Figure 128, Pc **58** exhibits one reversible oxidation potential at 0.68 V. On the other hand, one reversible reduction wave at -1.19 and a quasi reversible wave at -1.59 V were observed in the cathodic potential regime. The HOMO and LUMO energy levels were calculated to be -5.4 and -3.6 on the basis of the oxidation potential and the first reduction potential, according to the following equations

$$E_{LUMO} = -(E^{red}_{Fc/Fc+}) - 4.8$$
$$E_{HOMO} = -(E^{ox}_{Fc/Fc+}) - 4.8$$

Table. 9. Cyclic voltammetry of Pc **58** (V) [a]

Compound	$E^1_{½,\,ox}$	$E^1_{½,\,red}$	E^2_{red}	HOMO	LUMO
58	0.68	-1.19	-1.59	-5.48	-3.60

[a] Measured in dichloromethane/tetrabutylammonium hexafluorophosphate ($TBAPF_6$) (0.1M), c=1x10^{-4} M, 295 K, scan rate=100 mVs^{-1}, vs. Fc/Fc+.

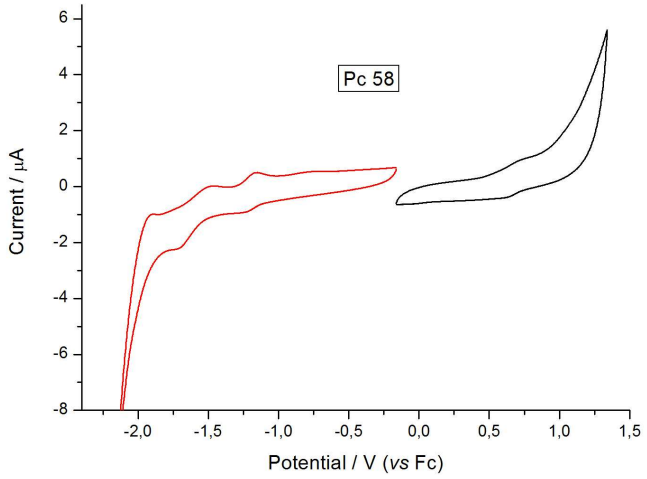

Figure 128. *Cylic voltammogram of the Pc **58** measured in a CH_2Cl_2 solution containing 0.1 M $TBAPF_6$ using a platinum as a working electrode and a Pt counter electrode with scan rate of 100 mV s^{-1}.*

The reduction of compound **58** is facilitated by the presence of strong acceptor sulfonyl groups. The LUMO level of **58** was measured to be approximately - 3.6 eV, quite similar[107b] to that of tri-*tert*butylcarboxy Pc **TT1** (Figure 30). On the other hand, the formal replacement of the *tert*-butyl groups in **TT1** with stronger electron withdrawing sulfonyl groups in **58** resulted in a HOMO level of – 5.48 dropping by 0.1 eV. This only a moderate stabilization in accordance with similar values found in Chapter 1.1.

The properties of Pc **58** as sensitizer in DSSCs are now under study.

2.4. Subphthalocyanine and Azulenocyanine Derivatives for DSSCs

2.4.1. Synthesis of Subphthalocyanine Derivatives

This section have been carried out in collaboration with Prof. Christian Claessens *(UAM, Spain)*.

Subphthalocyanines are formed by cyclotrimerization of phthalonitriles in the presence of boron reagents in a high boiling point solvent such as p-xylene.[51] Among the different boron reagents, BCl_3 has been the more widely used. When only one mono-substituted phthalonitrile is used as starting material, SubPcs with the composition of A_3 are formed as a mixture of C_1 and C_3 regioisomers. If a mixture of two different phthalonitriles is used, the cyclotrimerization produces a mixture of four SubPcs of compositions A_3, A_2B, AB_2 and B_3. The relative yield of each SubPc depends on the molar ratio of the reactants. The lower tendency of these molecules to aggregate in solution, when compared to Pcs, facilitates the chromatographic separation of different reaction compounds. However in the case of monosubstituted phthalonitriles SubPcs A_2B or AB_2 are constituted by a mixture of up to three regioisomers, which in many cases are not easy to separate. Tricoordinated boron compounds are known to react with nucleophiles by an addition-elimination type mechanism in which a halogen ligand is exchanged. In this kind of reactions, the vacant p orbital of sp^2 boron efficiently coordinates the incoming nucleophile, forming a tetracoordinated intermediate species, which may then eliminate the weakest-bound ligand. In general, the axial functionalization of Subcs with nucleophiles such as phenol derivatives not only facilitates the separation, but also prevents hydrolysis during the chromatographic work up in silica-gel, as was the case of bromo- or chlorosubstituted SubPcs. On the other hand, functionalization of the peripheral benzene ring of the SubPc is somewhat difficult due to its chemical stability. Indeed, the SubPc ring is frequently destroyed in the presence of a nucleophile at high temperatures or in acidic or basic media.

[51] a) A. Meller, A. Ossko, *Monatsh. Chem.* **1972**, *103*, 150. b) B. del Rey, U. Keller, T. Torres, G. Rojo, F. Agullo-Lopez, S. Nonell, C. Marti, S. Brasselet, I. Ledoux, J. Zyss. *J. Am. Chem. Soc*. **1998**, *120*, 12808. c) C. G. Claessens, T. Torres, *Chem. Eur. J.* **2000**, *6*, 2168. d) C. G. Claessens, D. González-Rodríguez, T. Torres, *Chem. Rev.* **2002**, *102*, 835. e) T. Torres, *Angew. Chem. Int. Ed.* **2006**, *45*, 2834.

Nevertheless, several metal-catalyzed reactions have been reported by our group on the coupling of halogen substituted SubPc with terminal alkynes.[51d,e,52b-g]

The synthesis of SubPcs **61** and **62,** peripherally functionalized with carboxy groups, was, thus, carried out in two steps. First, iodoSubPc **59** was synthesized and then the corresponding acid derivatives were formed by means of a Sonogashira catalytic cross-coupling reaction. Two different carboxylic acids were used, namely, propargylic acid and 4-ethynylbenzoic acid.

More specifically, di-*tert*-butyliodoSubPc **59** was prepared by a statistical condensation reaction of 4-iodophthalonitrile (**2**) and 4-*tert*-butylphthalonitrile (1:2 molar ratio) in the presence of BCl_3 in *p*-xylene following a procedure developed in our group.[189] The reaction was followed by substitution of the axial chlorine atom with 4-*tert*-butylphenol in toluene in the presence of stoichiometric amounts of TEA. After purification by column chromatography, compound **59** was obtained in 12% yield, (Scheme 28). In this particular case **59** is constituted by a mixture of three regioisomers that could not be separated.

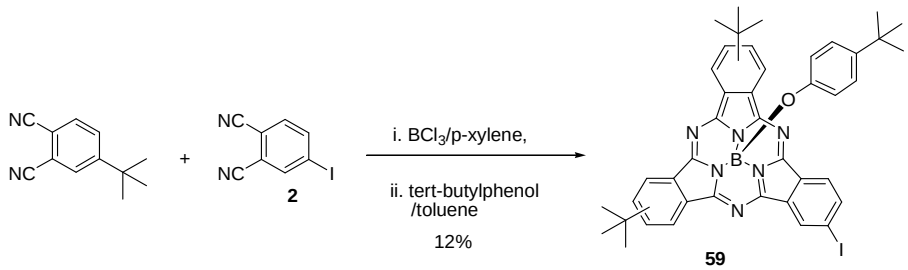

*Scheme 28. Synthesis of SubPc **59**.*

With the iodo-derivative in hand, we proceeded to the Sonogashira coupling of **59** with the corresponding carboxylic acid derivative (Scheme 30). In the case of 4-ethynylbenzoic acid, a deprotection of the commercially available 4-

[52] b) C. G. Claessens, T. Torres, *Chem Commun.* **2004**, *7*, 1298. c) D. Rodriguez, T. Torres, D. M. Guldi, J. Rivera, M. A. Herranz, L. Echegoyen, *J. Am. Chem. Soc*, **2004**, *126*, 6301. d) D. González-Rodríguez, C. G. Claessens, T. Torres, S. Liu, L. Echegoyen, N. Vila, S. Nonell, *Chem. Eur. J.* **2005***, 11,* 3881. g) D. González-Rodríguez, E. Carbonell, G. De Miguel Rojas, C. Atienza Castellanos, D. M. Guldi, T. Torres, *J. Am. Chem. Soc.* **2010**, *132*, 16488.

[189] C. G. Claessens, unpublished results.

[(trimethylsilyl)ethynyl]benzoic acid was firstly performed to obtain the free alkyne derivative (**60**) (Scheme 29).

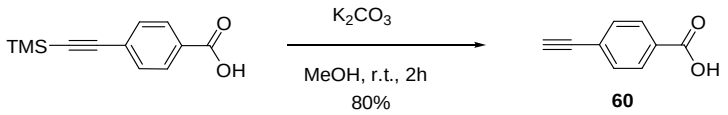

*Scheme 29. Deprotection of TMS group of 4-(ethynyl)benzoic acid (**60**).*

The Sonogashira coupling was carried out in the presence of $PdCl_2(PPh_3)_2$, CuI, in TEA/DMF, thus affording SubPcs **61** and **62**. The carboxylic acid derivative was added to the reaction mixture at 0 ºC, which was then allowed to warm up to room temperature. The reaction was left stirring for 3 h but consumption of the starting material was not complete. The purification of the crude material by column chromatography using a mixture of CH_2Cl_2/MeOH(10:1) allowed the isolation of carboxySubPcs from the remaining iodoSubPc. SubPc **61** and **62** were obtained in 43% and 48% yields, respectively, based on the recovered SubPc **59**, as mixtures of three regioisomers.

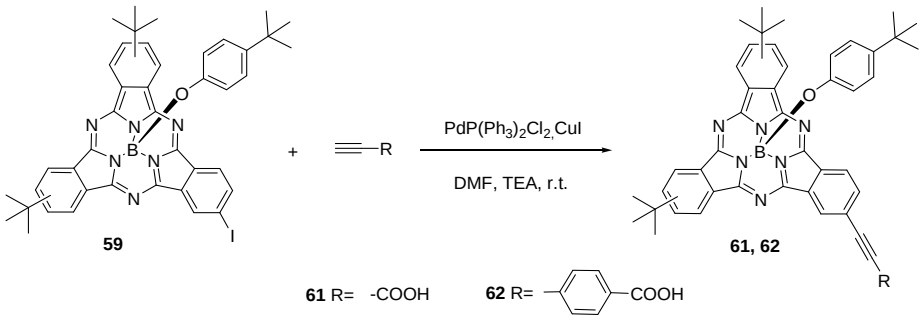

*Scheme 30. Synthesis of SubPc **61** and **62**.*

All compounds were characterized by MALDI-TOF, ^{1}H-NMR, UV-Vis and IR spectroscopies.

Unlike typical broadened peaks observed in the ^{1}H-NMR spectra of phthalocyanines due to the tendency of their π-system to form aggregates, SubPcs gave rise to well-resolved spectra in $CDCl_3$. All aromatic protons appear between 9.5-7.0 ppm, with the exception of the axial phenoxy ligand, whose signals are shielded at 5.6 ppm, due to the strong ring current produced by the aromatic core. The ^{1}H-NMR spectrum of compound **62** is shown in Figure 129 as an example.

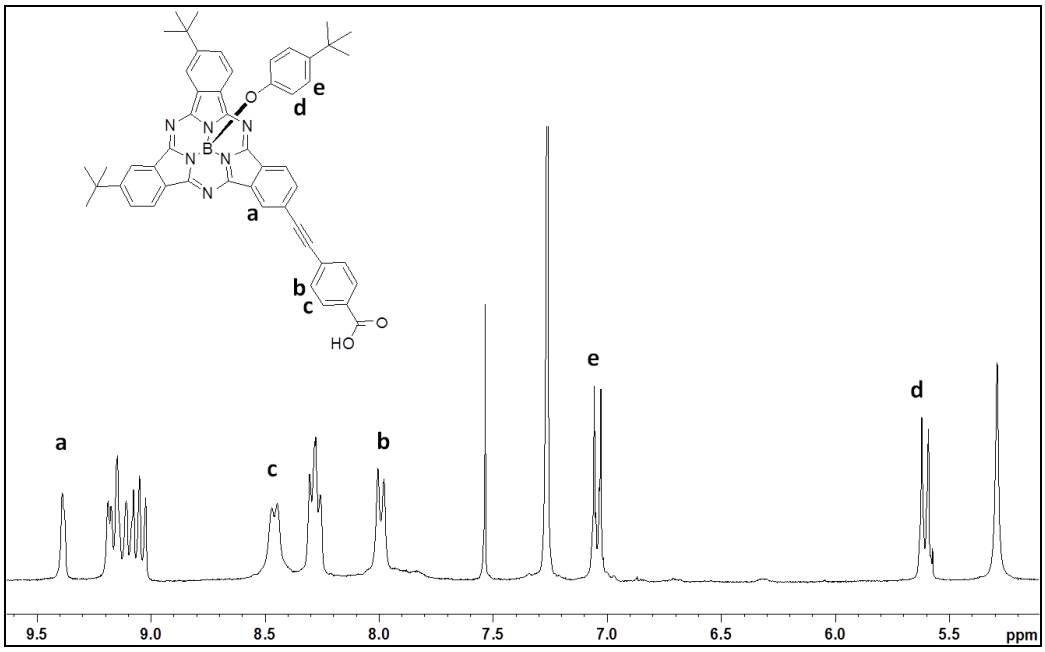

*Figure 129. Aromatic part of the ^{1}H-NMR spectrum of compound **62** in $CDCl_3$.*

As mentioned in the general introduction, SubPc present the Q band and Soret band blue-shifted compared to those of Pcs owing to the smaller conjugated system. Figure 130 displays the electronic absorption spectra of SubPc **61** and **62**, which are very similar, showing the B band at 270 nm and the Q band at 580 nm, together with a shoulder of vibronic origin at 505-570 nm. Moreover, SubPc **61** shows a decrease in the extinction coefficient of the Q-band in comparison to that of SubPc **62** which could be due to higher aggregation tendency.

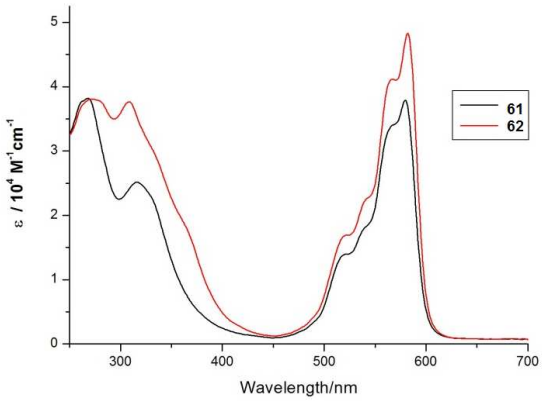

*Figure 130. UV-vis spectra of SubPc **61** and **62** in $CHCl_3$ ~ 1x10^{-5} M*

2.4.2. Photovoltaic Studies of SubPcs

Cyclic voltammetry (CV) was performed to determine the HOMO and the LUMO energy levels of the SubPcs. Figure 131 shows the cyclic voltammograms of the SubPc **61** and **62** using a glassy carbon working electrode in 0.1 mol/L $TBAPF_6$, CH_2Cl_2 solution. Both dyes exhibited a reversible oxidation potential at 0.5 V. When scanning toward negative potentials, the two sensitizers showed a reversible wave at 1.57 V. The electrochemical data and the HOMO and the LUMO levels are summarized in Table 10. The HOMO and the LUMO levels of the two dyes are sufficient for efficient electron injection into TiO_2 and dye regeneration.

Table. 10. Cyclic voltammetry results of SubPc **61** and **62** (V)[a]

Compounds	$E^1_{½, OX}$	$E^1_{½, red}$	E^2_{red}	HOMO	LUMO
61	0.52	1.55	2.08	-5.32	-3.25
62	0.55	1.51	1.94	-5.35	-3.29

[a] Measured in dichloromethane/tetrabutylammonium hexafluorophosphate ($TBAPF_6$*) (0.1M), c=1x10^{-4} M, 295 K, scan rate=100 mVs^{-1}, vs. Fc/Fc+.*

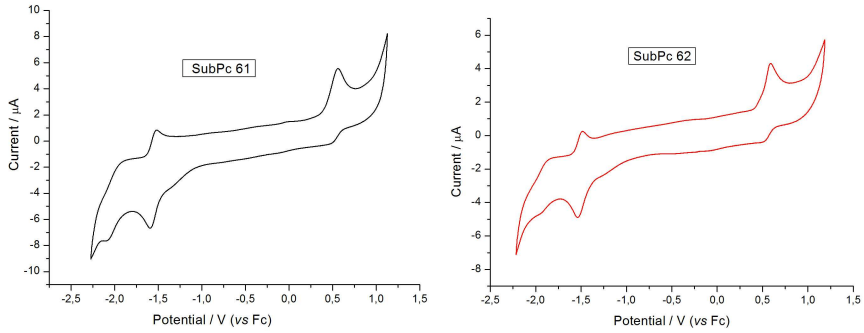

*Figure 131. Cylic voltammogram of the SubPc **61** and **62** measured in a CH_2Cl_2 solution containing 0.1 M $TBAPF_6$ using a glassy carbon as a working and a Pt counter electrode with scan rate of 100 mV s^{-1}.*

To gain further insight into the electron density distribution within the frontier orbitals, quantum chemical calculations on SubPc **61** and **62** using semi-empirical AM1 calculations were performed. It has been shown that this level of calculations is sufficient to describe properly the HOMO and LUMO levels in the case of SubPc.[190] The calculations show that the HOMOs are localized at the donor part, around the macrocycle for both dyes, which are far away from the attaching group. In contrast, LUMOs are distributed over the carboxylic acid ethyne bridge (Figure 132). The calculations suggest that in order to minimize back transfer from the TiO_2 to the oxidized dye, the HOMO should be located at the donating part of the molecules, far away from the anchoring group and/or the TiO_2 surface.

[190] V. R. Ferro, J. M. García de la Vega, R. H. González-Jonte, L. A. Poveda, *J. Mol. Struct. Theochem* **2001**, *537*, 223

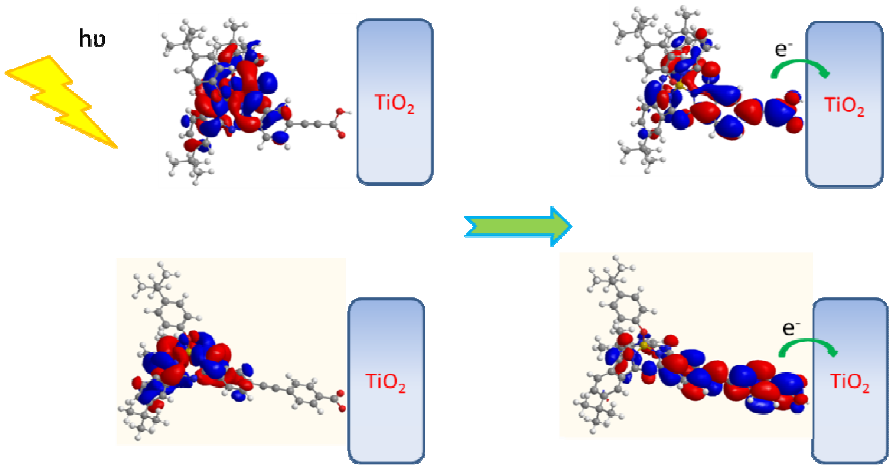

*Figure 132. Frontier molecular orbitals of SubPc **61** (above) and **62**(below) calculated using AM1 semi-empirical method.*

Dye sensitized solar cells based on SubPc **61** and **62** were made in collaboration with Prof. Michael Grätzel *(EPFL,* Switzerland*)* by using TiO_2 electrodes with a film thickness of 12+5 µm and different electrolytes. The TiO_2 electrodes were immersed into the SubPc **61** and **62** solutions (0.1 mM in ethanol), and kept at room temperature for 5 h.

The compositions of electrolytes were:

AY2: 0.165M 1,3-dimethylimidazolium iodide, 0.045M iodine, 0.8M tert-butyl pyridine (TBP) and 0.1M $LiClO_4$ in acetonitrile.

959: (1.0 M 1,3-dimethylimidazolium iodide (DMII), 0.03M iodine, 0.1M guanidinium thiocyanate and 0.5M *tert*-butylpyridine in a mixture of valeronitrile/ acetonitrile (15:85 v/v)).

960: 1.0 M 1,3-dimethylimidazolium iodide (DMII), 50 mM LiI, 30 mM I2, 0.5 M ter-butylpyridine, and 0.1 M guanidinium thiocyanate (GNCS) in the mixed solvent of acetonitrile and valeronitrile (v/v, 85/15).

AY3:

As already mentioned, the cone-shaped geometry of SubPcs, which contrasts with the flat structure of Pcs, lower their tendency to aggregate, therefore, the addition

of coadsorbant is not essential. Table 11 shows the photovoltaic performance of **61** and **62** sensitized solar cells.

The devices using electrolyte 959 gave Voc around 547 mV for both dyes. However, very low short-circuit photocurrent densities (Jsc), and as a consequence lower efficiencies, were obtained. On the other hand, by using electrolyte 960, the efficiencies obtained were three times higher than in the previous cells for both SubPcs due to the increased Jsc. This can be attributed to the presence of Li+ in electrolyte 960, which caused a drop in the photovoltage and an increase in the Jsc. Additionally, the devices employing AY2 electrolyte gave a higher short-circuit photocurrent density of 5.5 and 5.3 mA/cm2 for SubPc **61** and **62** respectively, whereas the Voc was slightly lower for both dyes. This lower Voc could result from the presence of $LiClO_4$ additive in the AY2 electrolyte, since it has been reported that the TiO_2 acceptor states shifted to more positive potential, up to 1.0V upon addition of 0.1 M $LiClO_4$, $NaClO_4$ or $Mg(ClO_4)_2$ to the electrolyte.[68b] Finally, by using AY3 electrolyte, the power conversion efficiency of the SubPc **61** and **62** sensitized cells reached 1.3% and 1.08%, respectively.

Table 11. DSSC performance of SubPc **61** and **62** in the presence of different electrolyte.

Dye	Electrolyte	Jsc (mA/cm^2)	Voc (mV)	FF	$\eta\,(\%)$
61	959	0.32	542.0	0.647	0.11
	960	0.94	532.1	0.715	0.36
	AY2	5.36	347.6	0.550	1.03
	AY3	6.17	357.8	0.599	1.32
62	959	0.19	547.0	0.639	0.07
	960	0.55	519.1	0.727	0.21
	AY2	5.5	343.7	0.585	1.12
	AY3	4.9	347.7	0.622	1.08

[68] b) D. F. Watson, G. J. Meyer, *Coord. Chem. Rev.* **2004**, *248*, 1391.

2.4.3. Synthesis of Azulenocyanine Derivatives

The synthetic route for compound **63** is shown in Scheme 31. Starting compound, formylazulenocyanine **27,** was already described in Chapter 1.

Several carboxyPc derivatives were successfully synthesized by our group in good yield by treating their corresponding aldehyde with $NaClO_2$ in water, in the presence of sulfamic acid as a chlorine atom scavenger. Using a similar oxidation reaction, it was expected that the aldehyde derivative **27** would yield carboxy-azulenocyanine **63**.

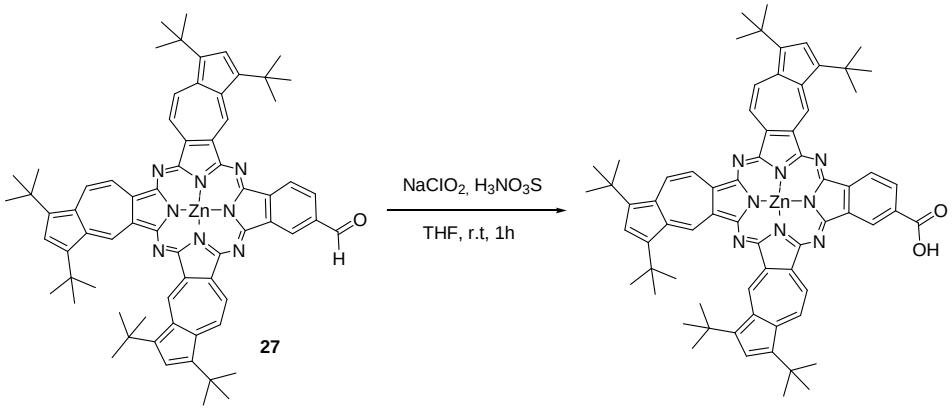

Scheme 31. *An unsuccessful attempt for the synthesis of* carboxyazulenocyanine **63***.*

Monitoring the reaction by TLC indicated that consumption of compound **27** was completed after 1 h. MALDI-TOF mass spectrum of the final compound after purification by column chromatography showed a mixture of products, one of which was identified as the desired azulenocyanine **63.** However, peaks assigned to side products corresponding to chlorinated and hydroxylated derivatives of azulenocyanine **63** were also identified. Although sodium chlorite reacts with aldehydes under mild conditions to form carboxylic acids, the main drawback of this reaction is the formation as a by-product, hypochlorous acid (HClO), which is a good electrophile and react with the activated azulene ring. Unfortunately, in our case, even using an excess of sulfamic acid, to capture this intermediate, carboxyazulenocyanine **63** could not be obtained as

a pure compound. Figure 133 shows the MALDI-TOF spectrum of the mixture of the compounds obtained.

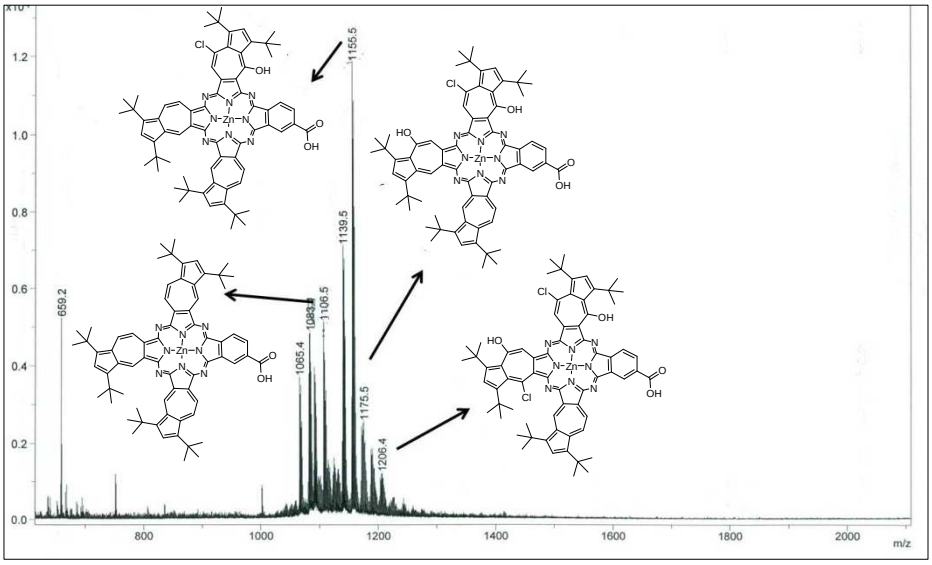

*Figure 133. MALDI-TOF mass spectrum of compound **63**.*

Concerning azulenocyanine **65**, the synthetic pathway involves first the cyclotetramerization of 4-iodophthalonitrile (**2**) and 1,3-di-*tert*-butyl-5,6-dicyanoazulene (**24**) in the presence of $Zn(OAc)_2$ to obtain the iodo-derivative **65** in 11% yield, followed by a palladium-catalyzed Sonagashira reaction with propargylic acid in the presence of $Pd(PPh_3)_4$ and catalytic amount of CuI in THF (Figure 134). The desired compound **65** was obtained in 45% yield based on recovered compound **64**.

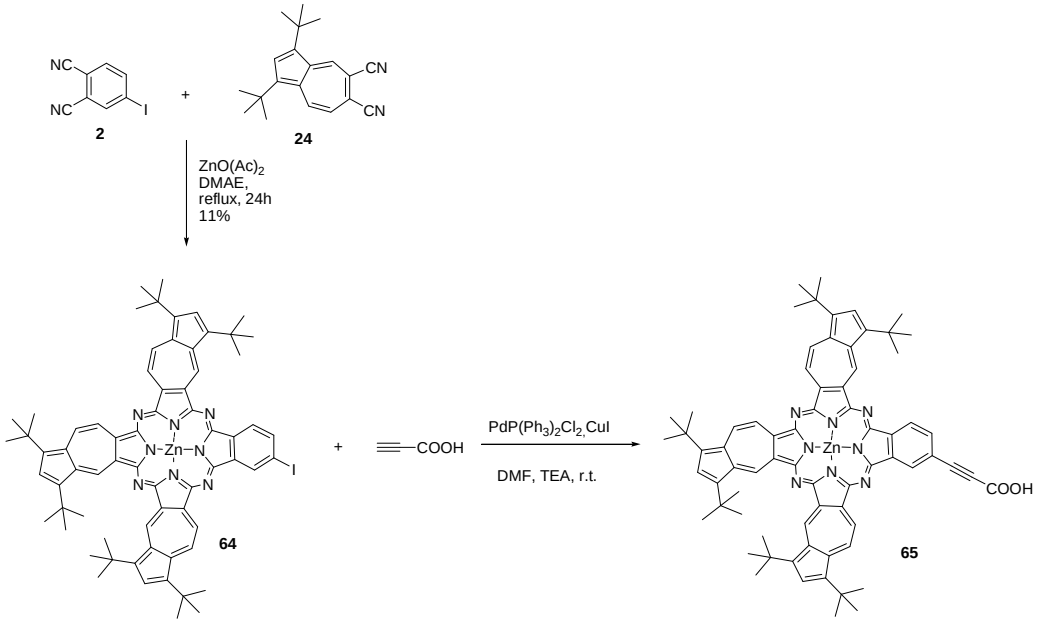

*Figure 134. Synthesis of azulenocyanine derivatives **64** and **65**.*

For the same reason mentioned above in the case of tetrasubstituted phthalocyanines, compound **65**, obtained in a statistical reaction of unsymmetrically substituted phthalonitriles, could be a mixture of up to eight regioisomers, which could not be separated. We do not expect that this fact might be relevant for the performance of the compound in DSSCs.

On the other hand, the synthesis of azulenocyanine **66** was attempted under a Knoevenagel condensation reaction of aldehyde **27** with malonic acid using piperidine as a catalyst, following a procedure similar to the one that followed in our group for Pcs.[104] However, the reaction in methanol at reflux temperature for 5h failed to produce the desired compound **66**.

In order to increase the reactivity of compound **27** towards malonic acid, the reaction was carried out in a higher boiling point solvent like acetonitrile at reflux for 5 h. Under these conditions, decarboxylation took place yielding compound **67**, which was

[104] M. García-Iglesias, J. J. Cid, J. H. Yum, A. Forneli, P. Vázquez, M. K. Nazeeruddin, E. Palomares, M. Grätzel, T. Torres, *Energy Environ. Sci*. **2011**, *4*, 189.

identified by MALDI-TOF mass spectrometry. This result is not unexpected, since it has been reported that the Knoevenagel condensation with carboxylic acid in the presence of pyridine or piperidine as a base, leads in some cases to decarboxylation and elimination occurs spontaneously during the reaction. This is also known as Doebner modification.[191] To avoid this problem, Kwon *et*. *al*. reported the Knoevenagel condensation using microwave irradiation under solvent-free conditions.[192] Thus, further work for the synthesis of compound **66** will be carried out under these conditions after the completion of this work.

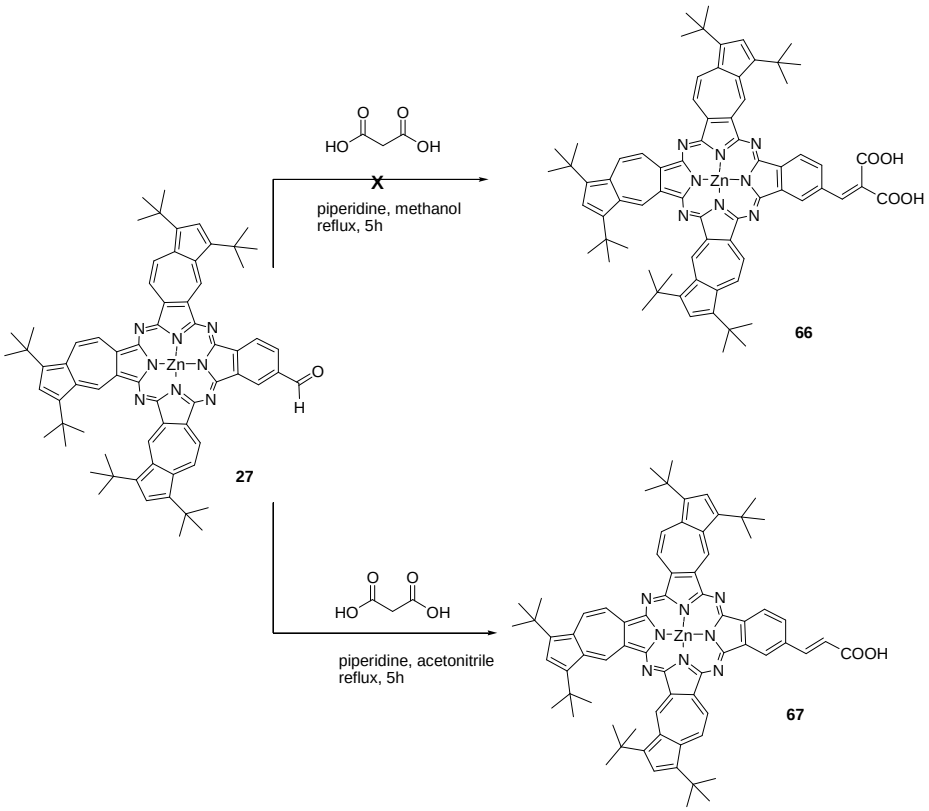

*Figure 135. Attemped Knoevanagel reaction of compound **27** for the synthesis of **66** and **67**.*

[191] a) C. J. Simpson, M. J. Fitzhenrya, N. Patrick, J. Stamford, *Tetrahedron Lett.* **2005**, *46*, 6893. b) E. Bermudez, O. N. Ventura, P. S. Mendez, *J. Phys. Chem. A.* **2010**, *114*, 13086.

[192] P. S. Kwon, Y. M. Kim, C. J. Kang, T. W. Kwon, S. K. Chung, Y. T. Chang, *Syn. Commun.* **1997**, *27*, 4091.

All compounds were characterized by ^{1}H-NMR, UV-Vis, IR and MALDI-TOF spectroscopy.

Figure 136 shows the electronic absorption spectrum of compound **65**. As already discussed in Chapter 1, azulenocyanine derivatives exhibit a broad absorption spectrum in the near-IR regions from 270 to 1120 nm with maxima at 302, 399, 566, 900 and a shoulder at 1005 nm.

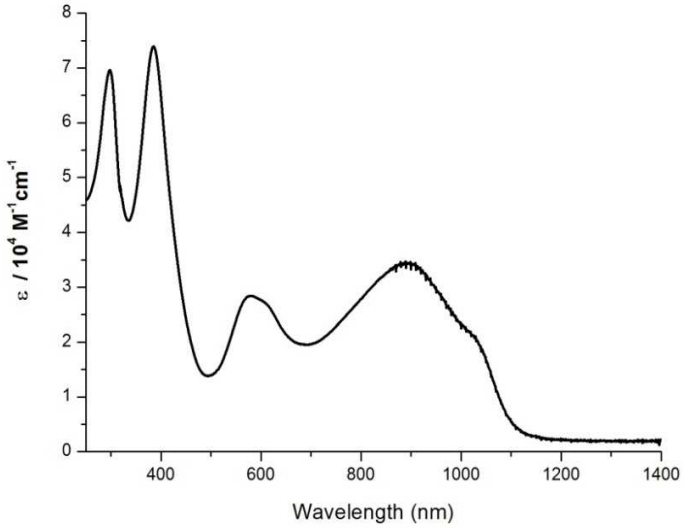

*Figure 136. UV-vis spectra of **65** in $CHCl_3$ ~ 1.10^{-5} M*

The ^{1}H NMR spectra of azulenocyanine derivatives were poorly resolved due to aggregation. ^{1}H NMR spectra of **64, 65** and **67** gave typical multiplets in ratios of 3:8:4 between 11.5 and 8 ppm for three sets of azulenocyanine ring protons as seen for other azulenocyanine derivatives in Section 1.2.

The properties of azulenocyanines **65** and **67** as sensitizers in DSSC are currently under study.

2.5. Summary and Conclusions

- A key compound, carboxytriiodoZnPc **53**, has been synthesized and used in a convergent strategy for preparing highly conjugated panchromatic sensitizers **54** and **55**. This synthetic approach might represent a general method to prepare other carboxyZnPc dyes bearing elaborated π-conjugated peripheral substituents.

- These dyes have been used as sensitizers in dye-sensitized solar cells, which exhibit a panchromatic response and moderate power conversion efficiencies close to 3%.
- The panchromatic response of dyes **54** and **55** is because of the complementary absorption in the visible region caused by the π-conjugated bisthiophene peripheral substituents and the ZnPc near infrared absorption. However, aggregation phenomena may explain the overall efficiencies achieved. Our group is currently investigating the preparation of other substituted carboxyZnPc dyes by this method in which aggregation phenomena are suppressed.

- We have successfully synthesized unsymmetrically substituted SubPcs **61** and **62** bearing a carboxylic acid group at the peripheral positions.

- The DSSC based on SubPc **61** exhibits a power conversion efficiency of *ca*. 1.32%. SubPc **62** showed a relatively lower efficiency than that observed with SubPc **61** which could be due to presence of an additional phenyl ring spacer, which reduces the charge injection yield. Similar results have been found in Pc series studied in our group. These results are promising and should encourage further studies on DSSCs using peripherally anchored SubPc compounds.

- Tris(octylsulfonyl)carboxyphthalocyanine **58** and carboxy-azulenocyanine derivatives **65** and **67** have synthesized as Red and NIR-IR dyes, respectively, for DSSC applications. Investigations on their performance in devices are in progress.

Chapter 2. Experimental Section

2.6. Experimental Section

Electrochemical measurements were performed at room temperature in a potentiostate/galvanostate Autolab PGSTAT30. Measurements were carried out in a home-built one-compartment cell with a three-electrode configuration, containing 0.1m tetrabutylammonium hexafluorophosphate ($TBAPF_6$) as supporting electrolyte. $TBAPF_6$ purchased from Fluka (<99%). A glassy carbon (GCE) or platinum was used as the working electrode, a platinum wire as the counter electrode and, a $Ag/AgNO_3$ non-aqueous electrode was used as reference. Prior to each voltammetric measurement the cell was degassed under an argon atmosphere for about 20 min. The electrochemical measurements were performed by using a concentration of approximately 0.2 mM of the corresponding compound, and ferrocene was added as an internal reference

A screen-printed double layer film of interconnected TiO_2 particles was used as photoanode. A paste composed of 20 nm anatase TiO_2 particles for the transparent nanocrystalline layer was coated on the FTO glass plates (Nippon Sheet Glass, 4 mm thickness) by repetitive screen printing. The TiO_2 electrodes were treated by $TiCl_4$ (40 mM in H_2O) at 70 ℃ for 30 min and sintered again at 500 ℃ for 30 min before they were dipped into the dye solution. The TiO_2 electrodes were immersed into the dye solutions (either 0.1 mM or 0.2 mM in THF or ethanol with different concentration of coadsorbent), and kept at room temperature for 5 or 15 h. The dye-adsorbed TiO_2 electrode and thermally platinized counter electrode were assembled into a sealed sandwich type cell with a gap of a hot-melt ionomer film (Surlyn 1702, 25 μm thickness, Du Pont).

2.6.1. Synthesis of Electron-Donor Pcs

2.6.1.1. Synthesis of triiodocarboxyphthalocyanine (**52)**

Zinc(II) 9(10),16(17),23(24)-triiodo-2-hydroxymethyl-phthalocyaninato(2-)-N^{29}, N^{30}, N^{31}, N^{32} (**50**) (mixture of regioisomers)

A mixture of 4-iodophthalonitrile[111] (**2**) (525 mg, 2.07 mmol), 4-(hydroxymethyl)phthalonitrile[141] (**20**) (64 mg, 0.41 mmol) and $Zn(OAc)_2$ (121 mg, 0.66 mmol) in DMAE (6 ml) was heated at reflux for 20 h with stirring under argon atmosphere. After cooling to room temperature, the solvent was removed and the residue was washed with a MeOH-H_2O (5:1) mixture. The crude product was purified by column chromatography on silica gel (Toluene/THF (10:1), Hexanes/dioxane (3:2)) to yield Pc **50** (93 mg, 0.09 mmol) as a blue solid. Yield: 23%.

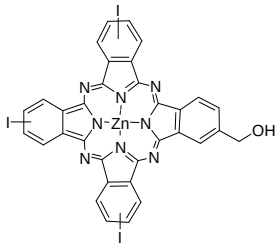

Mp>250 ºC

^{1}H NMR (d_8-THF, 300 MHz): δ (ppm)=9.4-9.3 (m, 3H), 9.2-8.9 (m, 2H), 8.9-8.6 (m, 3H), 8.6-8.4 (m, 3H), 8.3-8.1 (m, 1H), 5.5 (s, 2H), 5.1-4.9 ppm (br, 1H).

FT-IR (KBr): *v* (cm^{-1}) = 3503, 2957, 2922, 2401, 1603, 1589, 1381, 1304, 1264, 1140, 1097, 1057, 901, 816, 741.

---

111 a) H. Lam, S. M. Marcuccio, P. I. Svirskaya. S. Greenberg, A. B. P. Lever, C. C. Leznoff, R. L. Cerny, Can. J. Chem. **1989**, *67*, 1087. b) J. G. Young, W. Onyebuagu, *J. Org. Chem.* **1990**, *55*, 2155.

141 R. F. Enes, J. J. Cid, A. Hausmann, O.Trukhina, A. Gouloumis, P. Vazquez, J. A. S. Cavaleiro, A. C. Tomé, D. M. Guldi, T.Torres, *Chem. Eur. J.* **2012**, *18*, 1727.

UV/Vis (THF): λ_{max} (log ε) = 673 (5.08), 608 (sh) (4.37), 357 nm (4.69).

HRMS (MALDI-TOF, dithranol): calc. for $C_{33}H_{15}I_3N_8OZn$: [M^+]: m/z: 983.7794, found 983.7823.

Anal. Calc for $C_{33}H_{15}I_3N_8OZn$ (%): C, 40.21; H, 1.53; N, 11.37. Found: C, 40,38; H, 1.67 ; N, 11.16.

Zinc(II) 9(10),16(17),23(24)-triiodo-2- formyl -phthalocyaninato(2-)-N^{29}, N^{30}, N^{31}, N^{32} (**51**) (mixture of regioisomers)

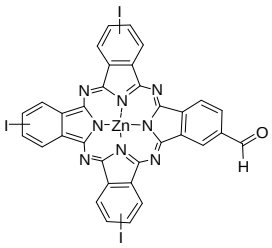

To a stirred solution of Pc **50** (90 mg, 0.09 mmol) in THF (2 ml) under argon atmosphere, a solution of IBX (128 mg, 0.45 mmol) in DMSO (5 ml) was added. The mixture was stirred at room temperature for 24h. The reaction was monitored by TLC (toluene-THF, 10:1) until all the starting phthalocyanine had reacted. Brine was then added and the mixture was extracted with THF. The combined organic layers were dried over $MgSO_4$ and evaporated *in vacuo*. The solid residue was purified by column chromatography on silica gel (toluene-THF, 10:1) to give **51** (57 mg, 0.06 mmol) as a blue solid. Yield: 64%.

Mp>250 ºC

^{1}H NMR (d_8-THF, 300 MHz): δ (ppm) =10.85 (s, 1H, CHO), 9.6-9.31 (m, 4H), 9.30-9.05 (m, 1H), 8.9-8.68 (m, 4H), 8.5-8.4 ppm (m, 3H).

FT-IR (KBr): ν (cm^{-1}) = 2954, 2923, 2854, 1691, 1594, 1484, 1456, 1431, 1378, 1304, 1139, 1091, 1053, 1033, 894, 755.

UV/Vis (THF): λ_{max} (log ε) = 673 (5.19), 653 (sh) (4.48), 608 (sh) (4.46), 354 nm (4.76).

HRMS (MALDI-TOF, dithranol): calc. for $C_{33}H_{13}I_3N_8OZn$: [M^+]: m/z: 981.7638, found 981.7603.

Anal. Calc. for $C_{33}H_{13}I_3N_8OZn$ (%): C, 40.30; H, 1.33; N, 11.39.Found: C, 40,52; H, 1.62 ; N, 11.08.

Zinc(II) 9(10),16(17),23(24)-triiodo-2- carboxy--phthalocyaninato(2-)-N^{29}, N^{30}, N^{31}, N^{32} (**52**) (mixture of regioisomers)

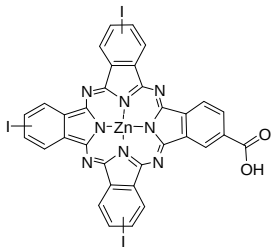

To solution of phthalocyanine **51** (25 mg, 0.025 mmol) in THF (3 ml), a solution of H_3NO_3S (9.7 mg, 0.1mmol) in H_2O (1 ml) was added at 0 ºC. A solution of $NaClO_2$ (4.6 mg, 0.050 mmol) in H_2O (1 mL) was added dropwise while the temperature was kept at 0 ºC. After the addition was complete, the mixture was further stirred for a 1h at room temperature. Brine was then added and the mixture was extracted with THF. The combined organic layers were dried over $MgSO_4$ and evaporated *in vacuo*. The solid residue was purified by short column chromatography on silica gel (THF) to give Pc **52** (15 mg, 0.015 mmol) as a blue solid. Yield: 60%.

Mp>250 ºC

^{1}H NMR (d_8-THF, 300 MHz): δ (ppm)=9.93-9.68 (m, 1H), 9.6-9.30 (m, 3H), 9.27-9.0 (m, 1H), 8.9-8.7 (m, 4H), 8.6-8.4 ppm (m, 3H).

FT-IR (KBr):*v* (cm^{-1}) = 3437, 2953, 2922, 2857, 1687, 1612, 1454, 1383, 1305, 1264, 1140, 1096, 1045, 923, 887, 812, 747.

UV/Vis (THF): λ_{max} (log ε) = 675 (4.97), 641 (sh) (4.48), 611 (sh) (4.41), 349 nm (4.70).

HRMS (MALDI-TOF, dithranol**):** calc. for $C_{33}H_{13}I_3N_8O_2Zn$: [M^+]: m/z: 997.7587, found 997.7589.

Anal Calc. for $C_{33}H_{13}I_3N_8O_2Zn$ (%): C, 39.65; H, 1.31; N, 11.21. Found: C, 39.99; H, 1.60 ; N, 11.02.

2.6.2.2. Synthesis of Pcs 54 and 55

Zinc(II)9(10),16(17),23(24)-tris-[2-(*N,N*-bis-(9,9-dimethylfluoren-2-yl)-4-aminophenyl)-5,5'-bithiophene] 2-Carboxy-phthalocyaninato(2-)-N^{29}, N^{30}, N^{31}, N^{32} (**54**) (mixture of regioisomers)

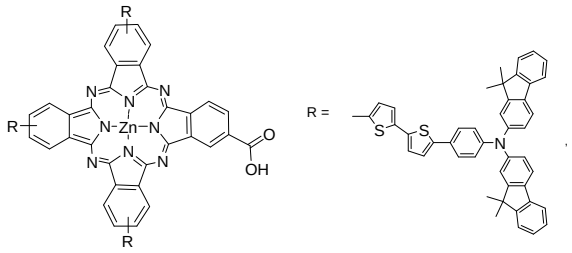

A suspension of ZnPc **52** (33 mg, 0.033 mmol), bisthiophene-boronic acid pinacol ester (**53**)[187] (102 mg, 0.13 mmol), [$Pd(PPh_3)_4$] (3.5 mg, 0.003 mmol) and a solution of Na_2CO_3 (34 mg, 0.33 mmol) in H_2O (1 ml) in dimethoxyethane (5 ml) was stirred at 95 ℃ under argon atmosphere for 24 h. T he suspension was then cooled to

[187] a) S. Kim, K. Song, S. Kang, J. Ko, *Chem. Commun*. **2004**, 68. b) M. Ince, F. Cardinali, J. H. Yum, M. V. Martínez-Díaz, M. K. Nazeeruddin, M. Grätzel, T. Torres *Chem. Eur. J.* **2012**, *18*, 6343.

room temperature and poured onto a 1M NH_4Cl solution (50 ml). The mixture was extracted with ethyl acetate (2 × 50 ml) and the combined organic extracts were washed with brine (10 ml), dried over $MgSO_4$ and evaporated *in vacuo*. The crude product was purified by preparative size exclusion chromatography (Biobeads SX-1 in THF) to yield ZnPc **54** (30 mg, 0.01 mmol) as a dark green solid. Yield: 36%

Mp>250 ºC

^{1}H NMR (d_8-THF, 300 MHz): δ (ppm)=10.4-6.3 (m, 78H, ArH), 1.8-0.9 ppm (m, 36H, alkylH).

FT-IR (KBr): υ (cm^{-1}) = 3435, 2957, 2920, 2860, 1724, 1604, 1535, 1488, 1452, 1390, 1308, 1183, 1141, 1055, 822, 789.

UV/Vis (THF): λ_{max} (log ε) = 707 (4.78), 662 (4.58), 413 (4.87), 369 nm (4.98).

HRMS (MALDI, DCTB): calc. for $C_{165}H_{115}N_{11}O_2S_6Zn$ [M^+]: m/z: 2537.685, found 2537.695.

Zinc(II) 9(10),16(17),23(24)-tris[5'-hexyl-2,2'-bithiophene]- 2-carboxy-phthalocyaninato (2-)-N^{29}, N^{30}, N^{31}, N^{32} (**55**) (mixture of regioisomers)

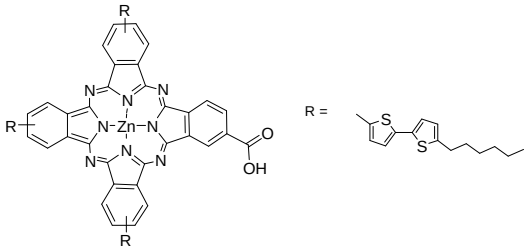

ZnPc **55** was prepared as for compound **54**, using ZnPc **52** (20 mg, 0.02 mmol), 5'-hexyl-2,2'-bithiophene-5-boronic acid pinacol ester (22.5 mg, 0.06 mmol), $[Pd(PPh_3)_4]$(2.3 mg, 0.002 mmol) and Na_2CO_3 (1 ml of a 1M aqueous solution). The

crude product was purified by preparative size exclusion chromatography (Biobeads SX-1 in THF) to yield ZnPc **55** (12 mg, 0.008 mmol) as a green solid. Yield: 43%

Mp>250 ºC

^{1}H NMR (d_8-THF, 300 MHz): δ (ppm)=10.3-6.3 (m, 24H, ArH), 1.8-0.9 ppm (m, 39H, alkyl).
FT-IR (KBr): ν (cm^{-1}) = 3432, 2954, 2923, 2853, 1656, 1608, 1491, 1455, 1380, 1337, 1285, 1261, 1144, 1096, 1049, 1026, 885, 793.

UV/Vis (THF): λ_{max} (log ε) = 702 (4.9), 634 (4.3), 361 (4.6).

HRMS (MALDI-TOF, dithranol): calc. for $C_{75}H_{64}N_8O_2S_6Zn$: [M^+]: m/z: 1364.277, found 1364.271.

2.6.2. Synthesis of tri(octylsulfonyl)-carboxy-phthalocyanines (58)

Zinc(II) 9(10),16(17),23(24)- tri(octylsulfonyl)- 2- hydroxyethynyl -phthalocyaninato (2-)- N^{29}, N^{30}, N^{31}, N^{32} (**56**) (mixture of regioisomers)

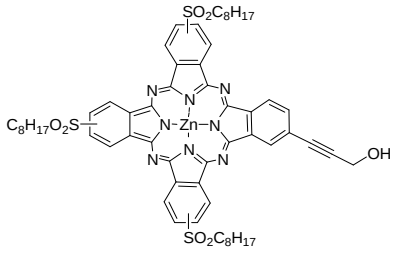

A mixture of tri-octylsulfonyliodoZnPc **17** (127 mg, 0.1 mmol), [$Pd_2(dba)_3$] (16.5 mg, 0.018 mmol) and $AsPh_3$ (11 mg, 0.03 mmol) was stirred in freshly distilled and deaerated piperidine (3 ml). Propargylic alcohol (12µl, 0.2 mmol) was then added and the reaction was stirred under argon at room temperature for 20 h. The solvent was removed under reduced pressure and the green solid was extracted with CH_2Cl_2. The organic layer was washed with water, dried over Na_2SO_4 and the solvent evaporated.

The compound was purified by column chromatography on silica gel (CH_2Cl_2/THF, [100:2] to yield compound **57** (75 mg, 0.06 mmol) as a green solid. Yield: 65%.

Mp>250 ºC

^{1}HNMR (d_8-THF, 300 MHz): δ (ppm)= 9.7-9.4 (m, 3H; ArH), 9.3-8.6 (m, 8H; ArH), 8.3-8.1 (m, 1H; ArH), 4.8-4.7 (m, 2H, CH_2OH), 3.8-3.8 (m, 6H, Alkyl-H), 2.3-2.2 (m, 12H, Alkyl H), 1.5-1.2 (m, 24H, Alkyl H), 0.80 (s, 9H, CH_3).

FT-IR (KBr) ν (cm^{-1}): 3487, 2914, 2858, 2426, 1917, 1601, 1574, 1466, 1398, 1385, 1304, 1149, 1101, 908, 841, 746

HRMS (MALDI-TOF, dithranol): calc. for $C_{59}H_{66}N_8O_7S_3Zn$: [M^+]: m/z: 1158.3503 found 1158.3458

Zinc(II) 9(10),16(17),23(24)- tri(octylsulfonyl)- 2- formylethynyl -phthalocyaninato (2-)- N^{29}, N^{30}, N^{31}, N^{32} (**57**) (mixture of regioisomers)

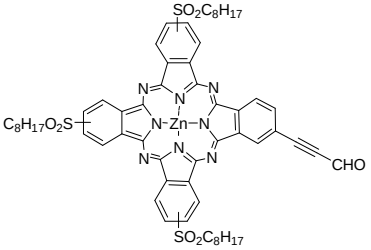

A solution of IBX (28 mg, 0.1 mmol) in DMSO (5 ml) was added to a stirred solution of Pc **56** (40 mg, 0.034 mmol) in THF (2 ml) under argon atmosphere. The mixture was stirred at room temperature for 24h. Brine was then added and the mixture was extracted with THF. The combined organic layers were dried over $MgSO_4$ and evaporated *in vacuo*. The solid residue was purified by column chromatography on silica gel (CH_2Cl_2/THF, 9:1) to give **57** (0.025 mmol, 30 mg) as a green solid. Yield: 75%.

Mp>250 ºC

^{1}HNMR (d_8-THF, 300 MHz): δ (ppm)= 9.9-9.5 (m, 3H; ArH), 9.4-8.7 (m, 8H; ArH), 8.5-8.4 (m, 1H; ArH), 3.8-3.7 (m, 6H, Alkyl-H), 2.2-2.1 (m, 12H, Alkyl H), 1.5-1.2 (m, 24H, Alkyl H), 0.8 (s, 9H, CH_3).

FT-IR (KBr) ν (cm^{-1}): 2934, 2835, 2191, 1709, 1690, 1603, 1501, 1393, 1149, 1095, 914, 839, 741.

MS (MALDI, dithranol), *m/z*: 1157.4 [M^+].

Zinc(II) 9(10),16(17),23(24)- tri(octylsulfonyl)- 2- carboxyethynylphthalocyaninato (2-)- N^{29}, N^{30}, N^{31}, N^{32} (**58**) (mixture of regioisomers)

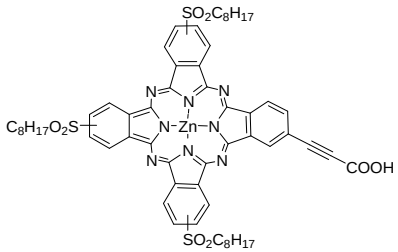

Method A:

Compound **17** (50 mg, 0.04 mmol), [$PdP(Ph_3)_2$] (2.8 mg, 0.004 mmol) and CuI (0.5 mg, 0.002 mmol) were stirred in a mixture of DMF/TEA (6:1l) (3.5 ml) under argon. Propargylic acid (7.5 µl, 0.12 mmol) was added while the temperature was kept at 0 ºC. The reaction was then stirred at room temperature for 3 h. Water was then added and the mixture was extracted with EtOAc. The combined organic layers were dried over $MgSO_4$ and evaporated *in vacuo*. Purification by column chromatography on silica gel (CH_2Cl_2-MeOH, 10:1) gave Pc **58** (14 mg, 0.012 mmol) as a blue solid. Yield: 41% based on recovered starting material.

Mp>250 ºC

^{1}HNMR (d_8-THF, 300 MHz): δ (ppm)= 9.7-8.3 (m, 12H; ArH), 3.9-3.7 (m, 6H, Alkyl-H), 2.2-2.1 (m, 12H, Alkyl H), 1.4-1.2 (m, 24H, Alkyl H), 0.8 (s, 9H, CH_3).

FT-IR (KBr) ν (cm^{-1}): 3379, 2934, 2853, 2218, 1709, 1601, 1493, 1466, 1398, 1305, 1142, 1090, 914, 874, 746.
UV-Vis (THF), λ_{max} (nm) (log ε) : 676 (5.33), 609 (sh), (4.61), 350(4.82).

HRMS (MALDI-TOF, dithranol): calc. for $C_{59}H_{64}N_8O_8S_3Zn$: [M^+]: m/z: 1172.3295 found 1172.3281.

Method B

To a solution of compound **57** (33 mg, 0.03 mmol) in THF (3 ml), a solution of H_3NO_3S (11 mg, 0.12 mmol) in H_2O (1 ml) was added at 0 ºC in an ice-water bath. A solution of $NaClO_2$ (5.2 mg, 0.6 mmol) in H_2O (1 ml) was added dropwise while the temperature was kept at 0 ºC. After the addition was complete, the mixture as further stirred for a 1h at room temperature. Brine was then added and the mixture was extracted with THF. The combined organic layers were dried over $MgSO_4$, filtered and evaporated *in vacuo*. The solid residue was purified by *short* column chromatography on silica gel using a mixture of CH_2Cl_2/MeOH (9:1) to yield compound **58** (17 mg, 0.014 mmol) as a blue solid. Yield: 48%.

2.6.3. Synthesis of Subphthalocyanines Derivatives

4'-*Tert*-butylphenoxy(-2(3),16(17)-di(*tert*-butyl)-2-iodosubphthalocyaninato)boron(III) (mixture of regioisomers) (**59**)[189]

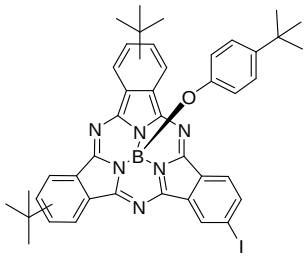

To mixture of 4-*tert*-butylphthalonitrile (578 mg, 3.14 mmol) and 4-iodophthalonitrile (**2**) (400 mg, 1.57 mmol), BCl_3 (7.5 ml, 1 M solution in *p*-xylene) was added under argon atmosphere. The reaction mixture was refluxed at 150℃ for 2 h. After cooling down to room temperature the unreacted BCl_3 and solvent were quickly removed *in vacuo*. 4-*tert*-butylphenol (943 mg, 6.28 mmol), dry toluene (4ml) and then TEA (0.2 ml, 1.6 mmol) were added to the crude mixture and stirring was continued at 110℃ for 3 h. The solvent was removed by vacuum di stillation and the solid was washed with a mixture of methanol/water (4:1). The compound was purified by column chromatography on silica gel (Hexane/Dioxane (8:1)) as eluent to yield **59** (186 mg, 0.18mmol) as a reddish solid. Yield: 12%

Mp>250 ºC

^{1}H NMR ($CDCl_3$, 300 MHz): 9.2 (d, *J*=9 Hz, 1H), 8.87 (d, *J*=9 Hz,2H), 8.78-8.72 (m, 2H), 8.5 (t, *J*=9 Hz, 1H), 8.1 (d, *J*=9 Hz, 1 H), 7.9 (d, *J*= 9, 2H) 6.7 (d, *J*=9 Hz, 2H), 5.2 (d, *J*=9 Hz, 2H), 1.5 (s, 18H), 1.07 (s, 9H).

FT-IR (film) υ (cm^{-1}): 2961, 2866, 1618, 1605, 1510, 1456, 1177, 1068, 885, 762.

[189] C.G. Claessens, unpublished results.

UV/Vis ($CHCl_3$): 571 (4.64), 513 (4,08), 315 (4,34), 268 (4.46).

HRMS (MALDI-TOF, dithranol): calc. for $C_{42}H_{40}BIN_6O$: [M^+]: m/z: 782.2403, found 782.2419.

4-(Ethynyl)benzoic acid (**60**)[188]

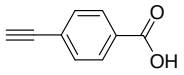

59

To a solution of 4-(trimethylsilyl)ethynylbenzoic acid (50 mg, 0.22 mmol) in THF-MeOH (5 ml) mixture was added K_2CO_3 (56 mg, 0.41 mmol). The reaction mixture was stirred for 2 h at room temperature. Then the solvent was evaporated under reduced pressure and the crude product was purified by column chromatography on silica gel (CH_2Cl_2-MeOH (5:1)) yielding **60** (26 mg, 0.17 mmol) as a white solid. Yield: 79 %

^{1}H NMR (300 MHz, DMSO-d_6): 8.04 (d, *J*=8.2, 2H), 7.6 (d, *J*=8.2, 2H), 4.4 (s, 1H).

4'-*tert*-Butylphenoxy[2(3),16(17)-di(*tert*-butyl)-2-carboxyethynylsubphthalocyaninato)] boron(III) (**61**) (mixture of regioisomers) and 4`-*tert*-butylphenoxy[2(3),16(17)-di(*tert*-butyl)-2-(4``-ethynylbenzoicacid)subphthalocyaninato] boron(III) (**62**) (mixture of regioisomers)

General procedure: A mixture of SubPc **59** (50 mg, 0.064 mmol), [$PdP(Ph_3)_2$] (4.5 mg, 0.006 mmol) and CuI (0.6 mg, 0.003mmol) was stirred in the mixture of DMF/TEA (6:1) (3.5 ml) under argon. The corresponding alkynyl carboxylic acid derivative (0.2 mmol) was added while the temperature was kept at 0 ºC. The reaction was then stirred at room temperature for 2 h. Water was then added and the mixture was extracted with EtOAc. The combined organic layers were dried over $MgSO_4$ and

[188] a) C.W. Lee,H.P. Lu,C.M. Lan,Y.L. Huang,Y.R. Liang, W.N. Yen, Y.C. Liu,Y.S. Lin,E.W.G. Diau, C.Y. Yeh, *Chem. Eur. J.***2009**, *15*, 1403. b) C.F. Lo, S.J. Hsu, C.L. Wang, Y.H. Cheng, H.P. Lu, E.W.G. Diau, C.Y.Lin, J. Phys. Chem. C, 2010, 114, 12018.

evaporated *in vacuo*. The solid residue was purified by column chromatography on silica gel (CH_2Cl_2-MeOH, 10:1).

SubPc **61** (12 mg, 0.016 mmol) was obtained as a reddish solid. Yield: 43% (based on the recovered starting material).

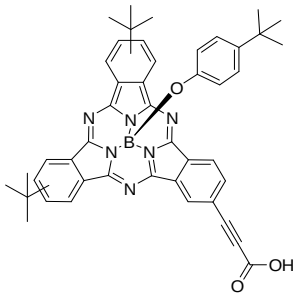

Mp>250 ºC

^{1}H-NMR (300 MHz, CDCI3), δ (ppm): 9.3 (s, 1H), 9.2 (s, 2H), 9.1- 8.9 (m, 3H), 8.4-8.2 (m, 3H), 6.9 (d, *J*=9 Hz, 2H), 5.6 (d, *J*=9 Hz, 2H), 1.74 (s, 18H), 1.38 (s, 9H).

FT-IR (film) υ (cm^{-1}): 3298, 2961, 2921, 2853, 2218, 1730, 1609, 1474, 1366, 1258, 1177, 1055, 812, 798, 758.

UV-Vis ($CHCl_3$), λ_{max} (nm) (log ε) : = 580 (4.57), 570 (4,49), 542 (4.26), 515 (4.11), 316 (4,40), 268 (4.58).

HRMS (MALDI-TOF, dithranol): calc. for $C_{45}H_{41}BN_6O_3$: [M^+]: m/z: 723.3364 found 723.3401.

SubPc **62** (17 mg, 0.021 mmol) was obtained as a reddish solid. Yield: 48 % (based on the recovered starting material).

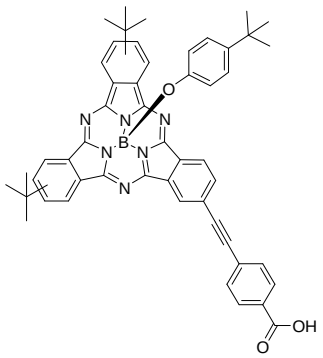

Mp>250 ºC

^{1}H-NMR (300 MHz, CDCl3), δ (ppm): 9.4 (s, 1H), 9.2-9.0 (m, 5H), 8.4 (d, *J*=9 Hz, 2H), 8.3-8.2 (m, 3H), 7.9 (d, *J*=9 Hz, 2H), 6.9 (d, *J*=9 Hz, 2H), 5.5 (d, *J*=9 Hz, 2H), 1.43 (s, 18H), 1.08 (s, 9H).

FT-IR (film) υ (cm^{-1}): 3379, 2961, 2934, 2893, 1726, 1699, 1618, 1510, 1470, 1267, 1254, 1124, 1097, 806, 760.

UV-Vis ($CHCl_3$), λ_{max} (nm) (log ε) : =583 (4.68), 568 (4,61), 543 (4.35), 523 (4.22), 310 (4,57), 271 (4.58).

HRMS (MALDI-TOF, dithranol): calc. for $C_{51}H_{45}BN_6O_3$: [M^+]: m/z: 799.3677 found 799.3664.

2.6.4. Synthesis of Azulenocyanine derivatives

1,3,9(10,11),11(12,13),18(19,20),20(21,22)-hexa-tert-butyl-27(28,29)-iodo-triazuleno [6,5(5,6)-a:5',6'-(6',5')f:5'',6''(6'',5'')k]-benzo[2''',3'''p]-porphyrazinato Zn(II) (**64**) (mixture of regioisomers)

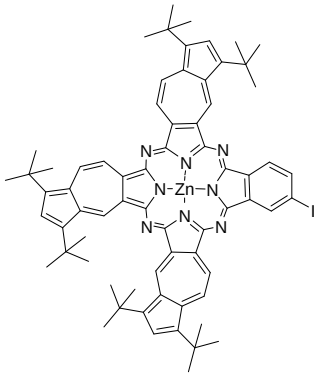

A mixture of 1,3-di-tert-butyl-5,6-dicyanoazulene (**24**) (120 mg, 0.41 mmol), 4-iodophthalonitrile (**2**) (26.2 mg, 0.10 mmol) and $Zn(OAc)_2$ (30 mg, 0.16 mmol) in DMAE (6 mL) was heated at reflux for 24 h with stirring under argon atmosphere. After cooling to room temperature, the solvent was removed. The crude product was purified by column chromatography on silica gel (hexanes-dioxane, 3:1) to yield compound **63** (20 mg, 0.016 mmol) as a dark-grayish solid. Yield: 16%.

Mp>250 ºC

^{1}H-NMR (300 MHz, d_8-THF), δ (ppm): 11.2-10.4 (m, 3H, ArH), 9.3-9.0 (m, 8H, ArH), 8.3- 8.0 (m, 4H, ArH), 2.1-1.5 (m, 54H, alkylH).

FT-IR (film) υ (cm^{-1}): 2956, 2938, 2870, 1567, 1426, 1363, 1209, 1165, 1047, 956, 893, 714, 664.

UV-Vis ($CHCl_3$), λ_{max} (nm) (log ε) : 1025 (4.3), 880 (4.6), 595 (4.5), 385 (4.8), 291 (4.7).

HRMS (MALDI-TOF, dithranol): calc. for $C_{68}H_{69}IN_8Zn$: [M^+]: m/z: 1188.3976 found 1188.4009.

1, 3, 9 (10,11), 11 (12,13),18(19,20),20 (21,22)-hexa-tert-butyl-27 (28,29) – carboxyethynyl-triazuleno[6,5(5,6)-a:5',6'-(6',5')f:5'',6''(6'',5'')k]benzo[2''',3'''p] porphyrazinato Zn(II) (**65**) (mixture of regioisomers)

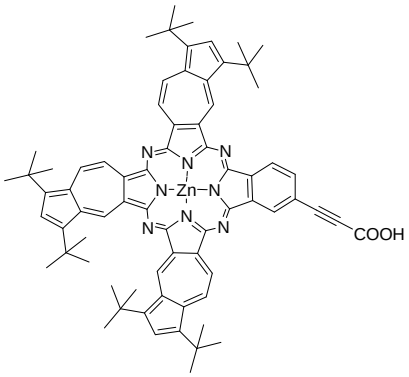

To a freshly distilled and deaerated THF/ Et_3N (6:2) solution (8 ml) containing compound **63** (50 mg, 0.04 mmol), CuI (0.5 mg, 0.002mmol) and $Pd[P(Ph_3)_2]_2Cl_2$ (3 mg, 0.004 mmol), propargylic acid (7.5µL, 0.12 mmol) was added. The mixture was stirred at room temperature under an argon atmosphere for 2h. The solution was then washed with brine, dried over Mg_2SO_4, filtered and evaporated in vacuo. The black solid was purified by column chromatography on silica gel (CH_2Cl_2/MeOH, 10:1) to yield **65** (15 mg, 0.013mmol) as a black-grayish solid. Yield: 45% (based on the recovered starting material).

Mp>250 ºC

^{1}H-NMR (300 MHz, d_8-THF), δ (ppm): 11.3-10.5 (m, 3H), 9.4-8.7 (m, 8H), 8.4- 7.8 (m, 4H), 2.1-1.3 (m, 54H, alkylH).

FT-IR (film) υ (cm^{-1}): 3474, 2951, 2924, 2870, 2218, 1589, 1456, 1362, 1204, 1163, 1041,891, 716, 689.

UV-Vis ($CHCl_3$), λ_{max} (nm) (log ε) : 1032 (4.3), 869 (4.5), 581 (4.45), 385 (4.8), 297 (4.8).

HRMS (MALDI-TOF, dithranol): calc. for $C_{71}H_{70}N_8O_2Zn$: [M^+]: m/z: 1130.4908 found 1130.4873.

1,3,9(10,11),11(12,13),18(19,20),20(21,22)-hexa-tert-butyl-27(28,29) –carboxy ethenyl-triazuleno[6,5(5,6)-a:5',6'(6',5')f:5'',6''(6'',5'')k]benzo[2''',3'''p]-porphyrazinato Zn(II) (**67**) (mixture of regioisomers)

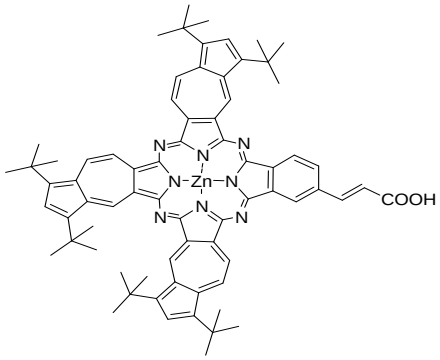

A solution of compound **27** (20 mg, 0.018 mmol), malonic acid (9.6 mg, 0.09 mmol) and piperidine (0.042 ml, 0.42mmol) in acetonitrile (10 ml) was heated under reflux for 5h. After being cooled to room temperature, solvent was removed under vacuum. The solid was extracted with THF, washed with brine and acidified (pH~2) with 2M H_3PO_4 (2 ml). The solvent was removed by vacuum distillation and the remaining dark solid was purified by column chromatography on silica gel (CH_2Cl_2/MeOH, 9:1) to give compound **67** (10 mg, 0.008 mmol) as a dark-grayish solid. Yield: 46%.

Mp>250 ºC

^{1}H-NMR (300 MHz, d_8-THF), δ (ppm): 11.9-10.3 (m, 3H), 9.8-8.7 (m, 8H), 8.4- 7.8 (m, 6H), 2.1-1.5 (m, 54H, alkylH).

FT-IR (film) υ (cm^{-1}): 3648, 2956, 2924, 2882, 1695, 1568, 1431, 1363, 1314, 1231, 1158, 1120, 1046, 956, 893, 860, 774.

MS (MALDI, dithranol), *m/z*: 1132.5 [$(M)^+$]